Synthesis, Characterization and Redox Properties of “Hyper S-Confused Porphyrinoids” and “Porphyrinoids with Thiophenes and Phenanthroline”

विद्या वाचस्पति की
उपाधि की अपेक्षाओं की आंशिक पूर्ति में प्रस्तुत शोध प्रबंध

A thesis submitted in partial fulfillment of the requirements for the Degree of Doctor of Philosophy

द्वारा / By

Vishnu Mishra

पंजीकरण सं. / Registration No.

20183572

शोध प्रबंध पर्यवेक्षक / Thesis Supervisor:

Prof. V. G. Anand

IISER PUNE

भारतीय विज्ञान शिक्षा एवं अनुसंधान संस्थान पुणे

Indian Institute of Science Education and Research (IISER), Pune

2024

Dedicated to my Parents...

Late. Mr. Govind Mishra and Mrs. Savitri Mishra

My Sisters...

Mrs. Shweta and Mrs. Swati

My Wife and my Daughter.

Mrs. Shivani and Vaanya

भारतीय विज्ञान शिक्षा एवं अनुसंधान संस्थान, पुणे
INDIAN INSTITUTE OF SCIENCE EDUCATION AND RESEARCH (IISER), PUNE
Mendeleeve Block, Dr. Homi Bhabha Road, Pune – 411 008, Maharashtra, India

Dr. V. G. Anand
Professor

CERTIFICATE

Certified that the work incorporated in the thesis entitled " **Synthesis, Characterization and Redox Properties of "Hyper S-Confused Porphyrinoids" and "Porphyrinoids with Thiophenes and Phenanthroline**" Submitted by **Vishnu Mishra** was carried out by the candidate, under my supervision. The work presented here or any part of it has not been included in any other thesis submitted previously for the award of any degree or diploma from any other University or institution.

(Supervisor)

Date: 15/08/2024

Ph: +91-20-25908091 | Fax: +91-20-25899790 *Email: vg.anand@iiserpune.ac.in*

INDIAN INSTITUTE OF SCIENCE EDUCATION AND RESEARCH PUNE
(An Autonomous Institution under Ministry of HRD, Govt. of India)

Declaration by Student

Name of Student: Vishnu Mishra

Reg. No.: 20183572

Thesis Supervisor(s): Prof. V. G. Anand

Department: Chemistry Department

Date of joining program: 1st January 2018

Date of Pre-Synopsis Seminar : 5th September 2023

Title of Thesis : **Synthesis, Characterization and Redox Properties of "Hyper S-Confused Porphyrinoids" and "Porphyrinoids with Thiophenes and Phenanthroline".**

I declare that this written submission represents my idea in my own words and where others' ideas have been included; I have adequately cited and referenced the original sources. I declare that I have acknowledged collaborative work and discussions wherever such work has been included. I also declare that I have adhered to all principles of academic honesty and integrity and have not misrepresented or fabricated or falsified any idea/data/fact/source in my submission. I understand that violation of the above will be cause for disciplinary action by the Institute and can also evoke penal action from the sources which have thus not been properly cited or from whom proper permission has not been taken when needed.

The work reported in this thesis is the original work done by me under the guidance of

Dr./Prof. V. G. Anand.

Date: 15/08/2024

Signature of the student

Acknowledgements

"The successful completion of this doctoral dissertation would not have been possible without the support of many individuals, to whom I express my heartfelt gratitude."

I would like to express my deepest gratitude to my thesis supervisor, **Prof. V. G. Anand**, for his unwavering guidance, continuous support, and invaluable encouragement throughout my Ph.D. journey. His immense knowledge, insightful ideas, and belief in my abilities have been instrumental in shaping this research. I am especially grateful for the academic freedom he provided and for his care and mentorship, which extended beyond academics. His support has been like that of a parent, and I truly appreciate his kindness. I also extend my heartfelt thanks to **Mrs. Padmapriya Anand** for her warmth and affection and to **Samarth and Savi** for their joyful presence.

I am deeply grateful to **Dr. Jayant Udgaonkar** (Former Director, IISER Pune) and **Dr. Sunil S. Bhagwat** (Current Director, IISER Pune) for providing excellent research facilities and fostering an inspiring academic environment.

I sincerely appreciate the valuable guidance and suggestions from my Research Advisory Committee members, **Dr. Pramod Pillai** (IISER Pune) and **Dr. Kumar Vanka** (NCL Pune), which have greatly enriched my research.

My heartfelt thanks go to **Dr. R. G. Bhat**, **Dr. R. Boomishankar**, **Dr. R. Vaidyanathan**, **Dr. Nirmalya Ballav**, **Dr. M. Jayakannan**, **Dr. Shabana Khan**, and **Dr. Jeetender Chugh** for their valuable assistance and insightful discussions during my research. I am also grateful to all the faculty members at IISER Pune for their encouragement and support.

I extend my sincere thanks to my lab members **Dr. T. Y. Gopalakrishna, Dr. Santosh G., Dr. Kiran, Dr. Sujit, Dr. Rashami, Dr. Brijesh, Dr. Tarun, Dr. Santosh P., Dr. Sunita, Dr. Rakesh, Dr. Ashok, Dr. Madan, Dr. Uday, Dr. Prachi, Dr. Pragati, Mr. Markose, and Dr. Ramesh, Mr. Rakesh Mr. Saurav raj**, for fostering a collaborative and friendly research environment. Their constant support and camaraderie have made this journey truly memorable.

I thank **Mr. Shiva Shankar Mahato** (Assistant librarian) and **Ms. Sneha** for library support. I thank IISER, Pune administrative staff members especially Mayuresh, Nayana, Tushar, Sayali, Aloke, Mahesh, Ganesh, Sanjay, Yatish and Megha for their generous support. I thank **Goldi Misra**(Chief Technology Officer and Chief Information Security Officer), **Neeta Deo**(Senior Technical Officer), **Parveen Nasa**(Senior Technical Officer (Instrumentation) and **Nisha Kurkure** (Senior Technical Officer (High Performance Computing) for IT support.

I sincerely acknowledge the support of **Praveen Nasa(SCXRD), Ravindra, Chinmay (NMR), Sandeep (HRMS), and Suresh (MALDI)** for their instrumental assistance.

I am also thankful to my friends and batch-mates of IISER Pune especially **Jabed, Akanksha, Pooja, Madhushudan, Surjeet, Rishu, Umashish, Deepak, Nahid, Ruksana, Sourabh, Brij, Supriya** and **Sanchaita** for their enormous support. It is indeed difficult to name all of them.

I am also deeply grateful to my school teachers, for guiding me in the right direction and shaping my early education. Additionally, I extend my heartfelt thanks to my college teachers, for inspiring my interest in chemistry and laying the foundation for my academic journey.

I am forever indebted to my family for their unwavering love and support. No words can truly express my deep gratitude to my parents, **Late Mr. Govind Mishra and Mrs. Savitri Mishra**, whose guidance and sacrifices have shaped my journey. I am also profoundly grateful to my sisters, **Mrs. Shweta, Mrs. Swati,** and **my wife Mrs. Shivani**, for their constant encouragement and belief in me.

Finally, I extend my sincere gratitude to **IISER Pune** for providing the fellowship and the excellent academic environment that has been instrumental in my research journey.

I also wish to acknowledge and express my heartfelt appreciation to all those who have supported me in various ways over the past five years. Despite my best efforts, if any names have been unintentionally omitted, I extend my sincere gratitude to them as well for their unconditional help, encouragement, and kindness throughout this journey.

Contents

Synopsis

The thesis entitled “Synthesis, Characterization and Redox Properties of “Tetra S-Confused Porphyrinoids” and “Porphyrinoids with Thiophenes and Phenanthroline” investigates various properties of porphyrinoids, with a particular focus on confused porphyrinoids mainly in porphycenes and expanded porphyrinoids. The primary objective is to understand the concept of aromaticity in confused porphyrinoids and expanded porphyrinoids. To achieve this, the thesis describes efficient and straightforward methods for synthesizing nearly planar confused porphycenes and expanded porphyrinoids that incorporate different types of heterocyclic rings. The synthetic routes for producing confused porphycenes and expanded porphyrinoids are detailed. Spectroscopic techniques, including UV-Vis absorption spectroscopy and Nuclear Magnetic Resonance (NMR) spectroscopy, are employed to propose the solution-state structures of the synthesized compounds. Single crystal X-ray diffraction studies confirm the solid-state geometries and conformational dynamics of the macrocycles. Cyclic Voltammetry (CV) and variable temperature Electron Paramagnetic Resonance spectroscopy (VT-EPR) establish the redox and magnetic properties of the macrocycles. Quantum mechanical calculations support the electronic and redox properties of the macrocycles, providing deeper insight into their behavior and potential applications.

The first chapter provides a detailed overview of the evolution of the concept of "confused systems" in porphyrins, discussing the concepts of aromaticity and antiaromaticity in porphyrins and their expanded derivatives. It highlights the unique redox properties and the significance of these macrocycles in stabilizing stable organic radical as well as diradical species. Incorporating pyridine, bipyridine, and 1,10-phenanthroline into the core of macrocyclic systems facilitates the exploration of chirality transfer in expanded porphyrinoids. This advancement opens new avenues in asymmetric catalysis and chirality sensing, while also providing additional binding sites for metal ions and other ions.

The second chapter explores the structural isomers of porphyrin, particularly focusing on 18π-isoelectronic macrocycles obtained by rearranging tetrapyrroles cyclically. The isomers include porphycene (**II.2**), N-confused porphyrin (**II.3**), and neo-confused porphyrin (**II.4**), which exhibit different electronic and redox properties due to their altered π-networks and aromaticity, despite maintaining an 18π-electron count. N-confused porphyrin (**II.3**) forms organometallic complexes by replacing nitrogen with an activated β-CH to form metal–carbon bonds. Core-modified NCPs have been synthesized by substituting pyrrole with other heterocyclic units like furan or thiophene. S-confused porphyrin features an exocyclic keto moiety, inducing aromaticity. O-confused porphyrin,

like NCP, forms complexes with metals such as Ni(II), Pd(II), and Ag(III). Advanced synthesis methods have produced porphyrinoids with multiple confused pyrrole rings, including doubly N-confused porphyrin and expanded porphyrins like the 22π core-modified sapphyrin and hexaphyrins with multiple confused pyrrole units. Octaphyrins adopt unique conformations to bind metal ions. The 20π tetrathiaisophlorin (**II.5**) is a notable non-pyrrolic confused porphyrinoid, stabilized as an 18π monocationic species.

This chapter presents the first synthesis of tetrathia porphycene (20π) and its expanded 28π and 30π hexathia porphycene, each featuring four confused thiophene rings. The 20π tetrathia porphycene stands out as the first entirely confused porphycene. Expanding the core enhances the planarity of the macrocycle. Tetrathia porphycene (20π) shows a co-crystal with C_{60} fullerene which displayed a weak supramolecular interaction.

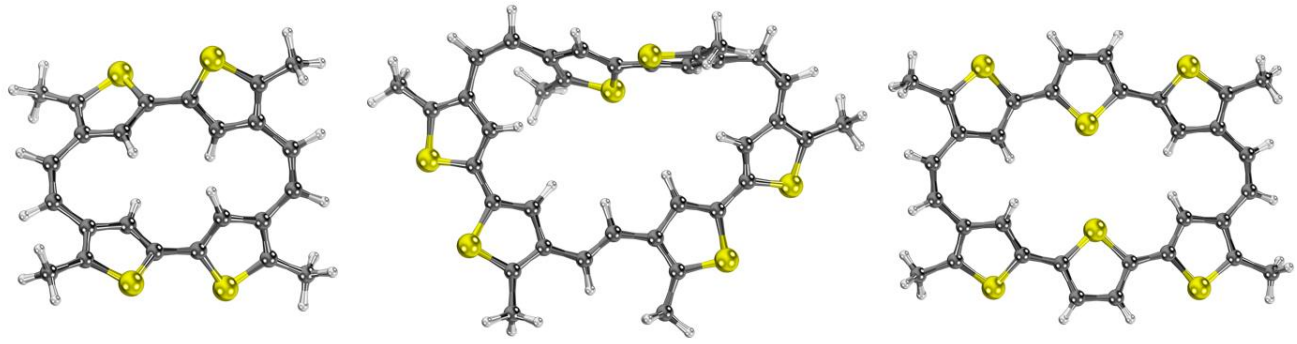

20π **30π** **28π**

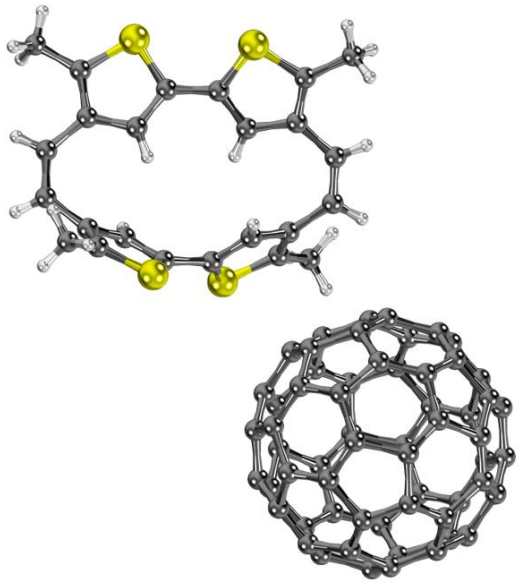

Co-crystal of Tetra S-Confused Porphycene (20π) with C_{60}

The third chapter highlights the integration of 1,10-phenanthroline into macrocyclic systems, showcasing its potential to create unique molecular architectures with diverse applications. This

pursuit is driven by the distinctive properties of 1,10-phenanthroline, a bidentate ligand known for its stable coordination interactions with various metal ions. The planar, aromatic nature of 1,10-phenanthroline and its capacity to chelate metal ions selectively and specifically have made it a focal point in numerous applications, from analytical techniques to catalyst and material design. Incorporating 1,10-phenanthroline into macrocyclic systems aims to leverage these unique characteristics while exploring the emergent properties resulting from combining macrocyclic frameworks with metal-coordinating functionalities. Macrocycles, large ring structures known for their remarkable properties such as molecular recognition, host-guest chemistry, and catalysis, offer a versatile platform when combined with 1,10-phenanthroline. This integration introduces an additional layer of complexity and utility, enhancing the potential for applications in molecular sensing, catalysis, and supramolecular chemistry. The synthesis and characterization of these hybrid macrocyclic architectures reveal their modular nature, allowing for the fine-tuning of properties to design molecules with tailored functions for specific applications. Exploring metal coordination within these frameworks expands the scope, providing opportunities for catalytic transformations and novel material design. The combination of macrocyclic frameworks with metal-coordinating 1,10-phenanthroline moieties prompts a deeper understanding of the structure-property relationships within these compounds. Researchers investigate how the spatial arrangement of the macrocycle and the metal coordination environment influence reactivity, stability, and selectivity.

This chapter presents the synthesis and structural characterization of phenanthroline-embedded isoamethyrin, a novel compound where the bipyrrole unit is replaced by phenanthroline and the other pyrrole units are substituted with thiophene. This innovative molecular architecture was synthesized through the oxidative coupling of 2,9-bis(5-(phenyl(thiophen-2-yl)methyl)thiophen-2-yl)-1,10-phenanthroline. In the second part of this chapter, a radical molecule is synthesized using a modified synthetic strategy. Instead of the traditional coupling reaction, the approach involves MacDonald's condensation. Specifically, 2,9-bis(5-(phenyl(thiophen-2-yl)methyl)thiophen-2-yl)-1,10-phenanthroline is subjected to MacDonald's condensation with benzaldehyde. This results in the formation of a radical species, demonstrating a unique pathway in the synthesis of radical molecules through strategic modifications in synthetic approaches. This method leverages the reactivity of the phenanthroline core and the versatile condensation reaction to yield the desired radical compound.

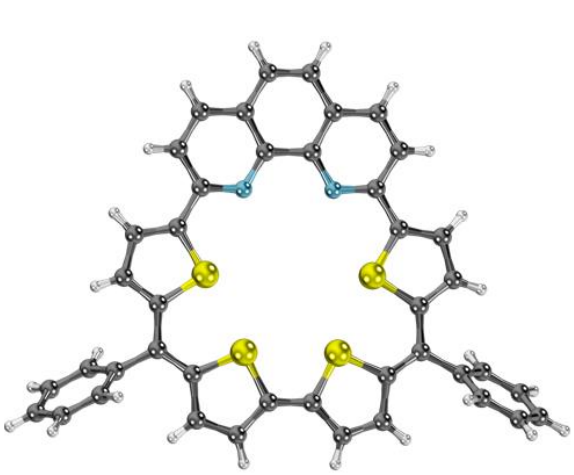

24π
Isoamethyrin

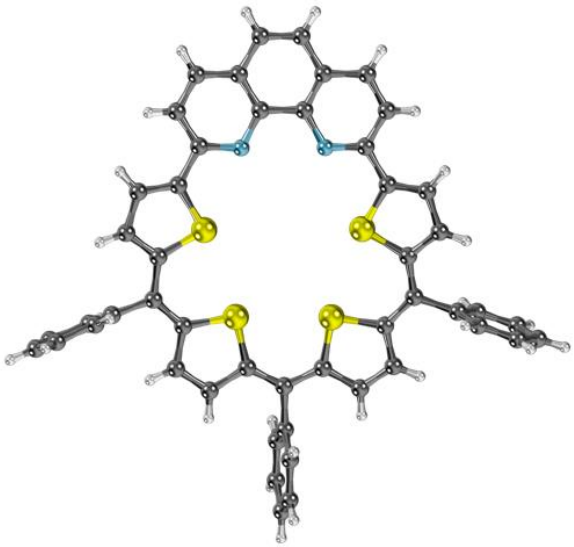

25π
Radical molecule

The fourth chapter provides a comprehensive overview of aromatic expanded porphyrinoids, covering their synthesis, structural characterization, physical and chemical properties, and emerging applications. The influence of core modification in expanded porphyrinoids mainly in hexaphyrin was also evaluated by replacing nitrogen with various chalcogens. The macrocycle can adopt two distinct geometries: a rectangular shape, where the diol condenses with thiophene and selenophene, and a triangular configuration, where the diol condenses with furan. This structural diversity highlights the significant impact of core modification on the properties and potential applications of expanded porphyrinoids. In this chapter, we focus on the synthesis of β-substituted hexaphyrin incorporating thiophene as the heterocyclic units.

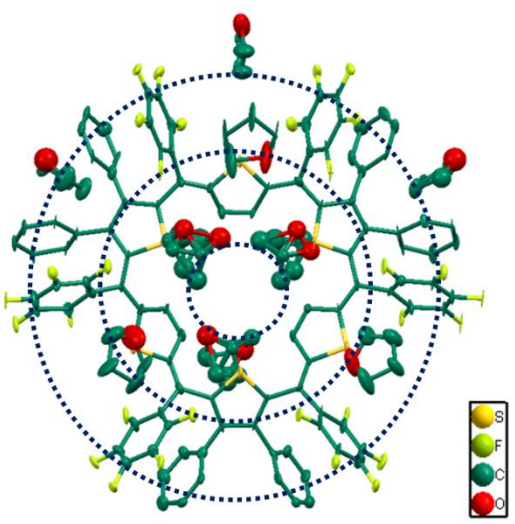

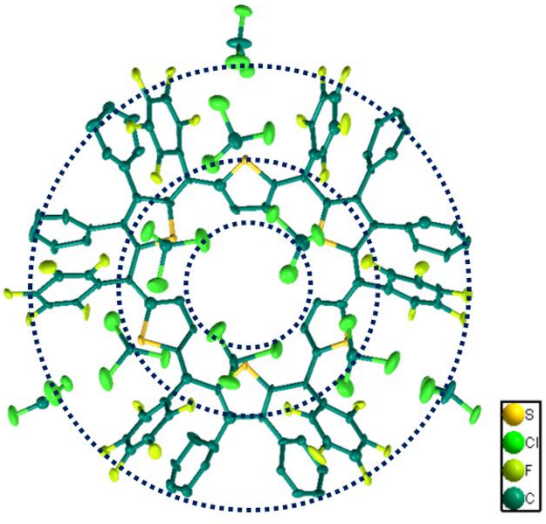

This structural modification introduces significant diversity compared to conventional hexaphyrins with thiophene. Notably, these β-substituted thiophene-containing hexaphyrin exhibit unique property, acting as molecular sponges. This property is characterized by their capability to absorb and release guest molecules, which can be attributed to the increased porosity and adaptability of the macrocyclic structure. This unique behavior opens up potential applications.

List of Publications

1) Tetra S-Confused Porphyrinoids; Vishnu Mishra, Hosahalli S. Udaya and Venkataramanrao G. Anand; DOI 10.1039/D3OB01270K.

2) Topological Diversity in Electrochemically Active Core-Modified Expanded Porphyrinoids; Hosahalli S. Udaya, Vishnu Mishra, and Venkataramanrao G. Anand; DOI.org/10.1021/acs.orglett.3c02328.

Chapter 1

I.1 Introduction:

The concept of "confused systems" has been a topic of intrigue and extensive research within the scientific community, particularly in the field of chemistry. Confused systems involve differences in bonding structures that lead to the generation of isomeric forms. This concept has roots in the foundational work of Linus Pauling,[1] who extensively studied the bonding structures and isomeric forms of porphyrins. His research notebook entries, as illustrated in Figure 1, reveal his primary interest in the electronic structure of porphyrin isomers. Pauling's notes from that period highlight his thoughts on the "determination of numbers of unexcited electronic structures for porphyrin," laying the groundwork for future studies on confused systems.

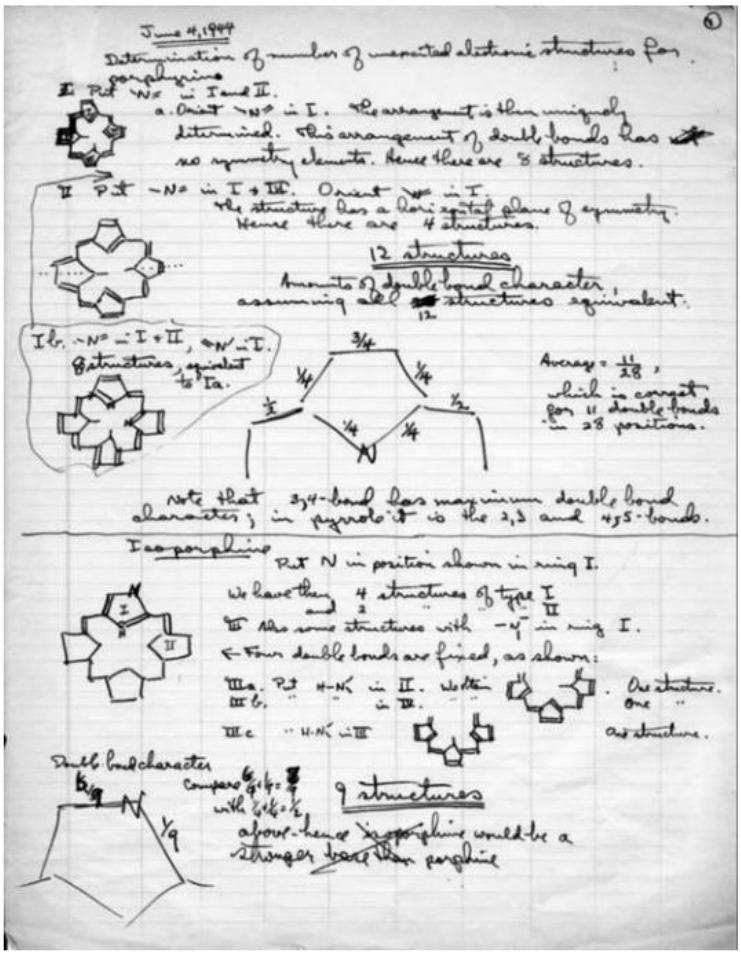

Figure 1. A page from the June 4, 1944 entries in Linus Pauling'snotebook. Ava Helen and Linus Pauling Papers, Oregon State University Special Collections.

The exploration of confused systems gained significant momentum in the mid-20th century and was further propelled by key studies in the 1990s. Piotr J. Chmielewski et al. (1994) demonstrated novel behaviors in certain porphyrin structures that exhibited unconventional bonding and electronic properties.[2] The typical pyrrole-aryl aldehyde condensation provides convenient access to a new family of core-modified porphyrins. A notable example of these compounds is tetra-p-tolylporphyrin(**I.2**), which features an inverted pyrrole ring. This core-modified porphyrin, known as a "carbaporphyrin," has a unique structural configuration that distinguishes it from other isomers, such as porphycene. Unlike carbaporphyrins, porphycenes have a different arrangement of pyrrole units, resulting in distinct electronic and photophysical properties. The work by Chmielewski et al. underscored the potential of these modified systems to reveal new aspects of molecular behavior and reactivity.

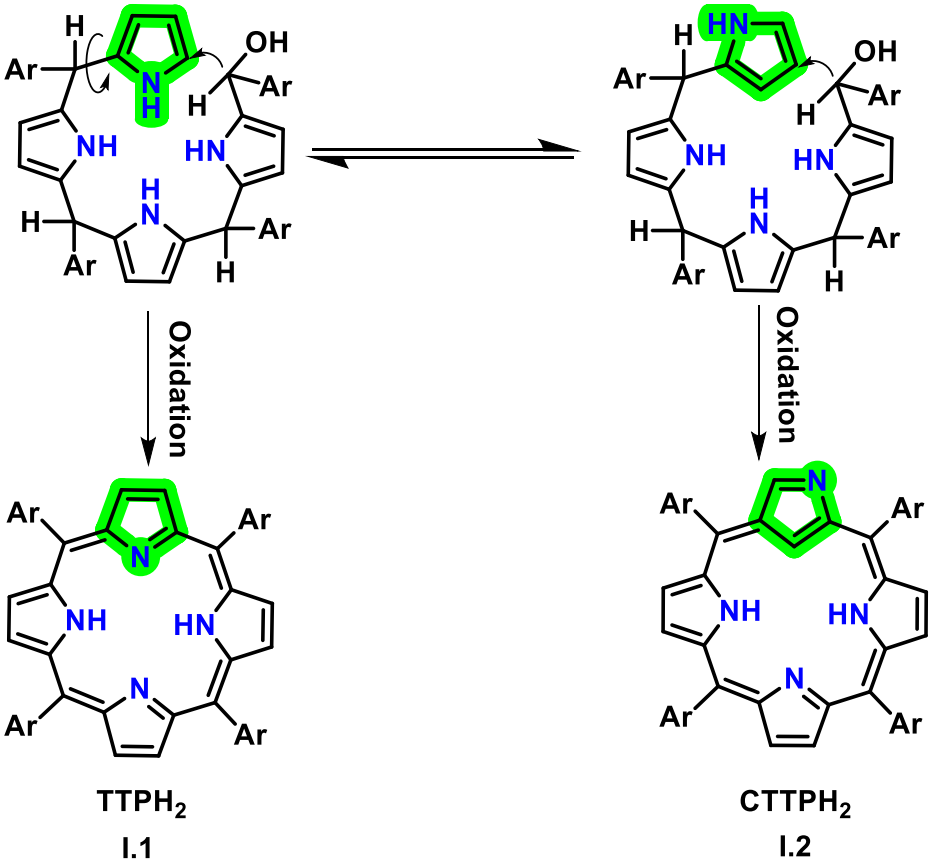

Figure 2 Synthesis of $TTPH_2$(I.1) and $CTTPH_2$(**I.2**).

Hiroyuki Furuta et al. advanced the field with their research.[3] They synthesized and characterized N-confused tetraphenylporphyrin (**I.2**), a novel isomeric porphyrin derivative. This compound was produced using a modified TPP synthesis involving benzaldehyde and pyrrole under unique conditions. The structural analysis confirmed the presence of a "confused pyrrole" ring, deviating significantly from planarity due to steric repulsion among inner hydrogens. Spectroscopic studies

revealed characteristic red-shifted and broadened absorption spectra, particularly upon protonation, indicating severe distortion from planarity. The stepwise protonation process, inferred from NMR shifts, highlights distinct protonation sites and substantial resonance stabilization loss in protonated forms. The formation of NCTPP under specific templating anions suggests a unique anion template effect. NCTPP's stability and unique properties propose its potential as a substitute in porphyrin applications, including metal ligation, photosensitization, and anion binding.

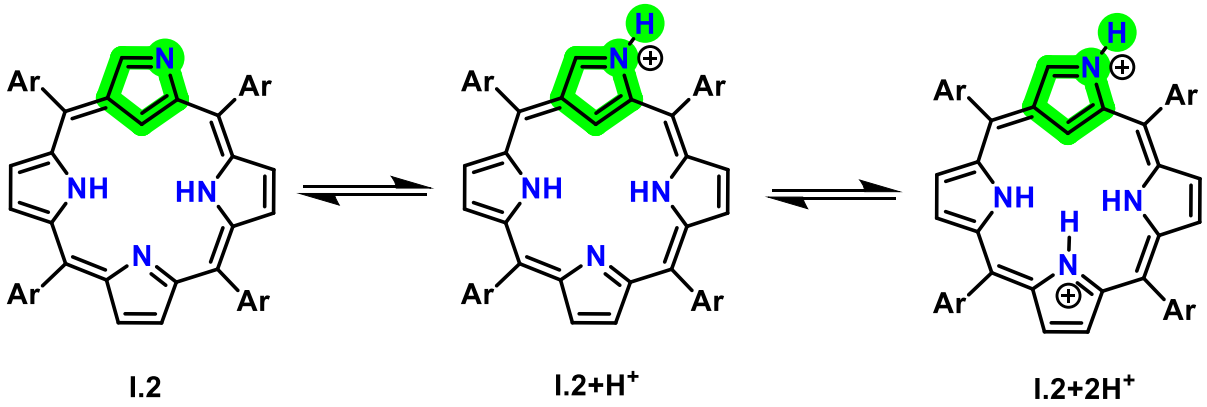

Figure 3 Step wise protonation of $CTTPH_2$(**I.2**).

The early 21st century saw further advancements in the study of confused systems. Ewa Pacholska et al., explored the synthesis and characterization of a new macrocyclic compound,[4] 5,10-diphenyl-15,20-bis(p-tolyl)-2-aza-21-carba-22-selenaporphyrin (SeC-DPDTPH), derived via a [3 + 1] condensation strategy involving 2,5-bis(phenylhydroxymethyl)selenophene and 5,10-bis(p-tolyl)tripyrrane. The formation of SeC-DPDTPH, an isomer of 21-selenaporphyrin with an inverted pyrrole ring, suggests a potential mechanistic pathway involving β-condensation instead of the usual α-condensation. Characterization of SeC-DPDTPH was confirmed through X-ray crystallography, high-resolution mass spectrometry, and ^{1}H NMR spectroscopy. The study revealed significant disorder in the molecule's crystal structure and provided detailed insights into its aromaticity and tautomeric equilibrium in different solvents. Spectroscopic analysis indicated that SeC-DPDTPH retains aromatic characteristics similar to its parent compound, Se-DPDTPH, but with distinct ^{1}H NMR shifts indicative of the macrocycle's unique electronic environment. The findings highlight the complexity of macrocycle formation and the influence of substituents and solvent conditions on the resulting porphyrinoid structures.

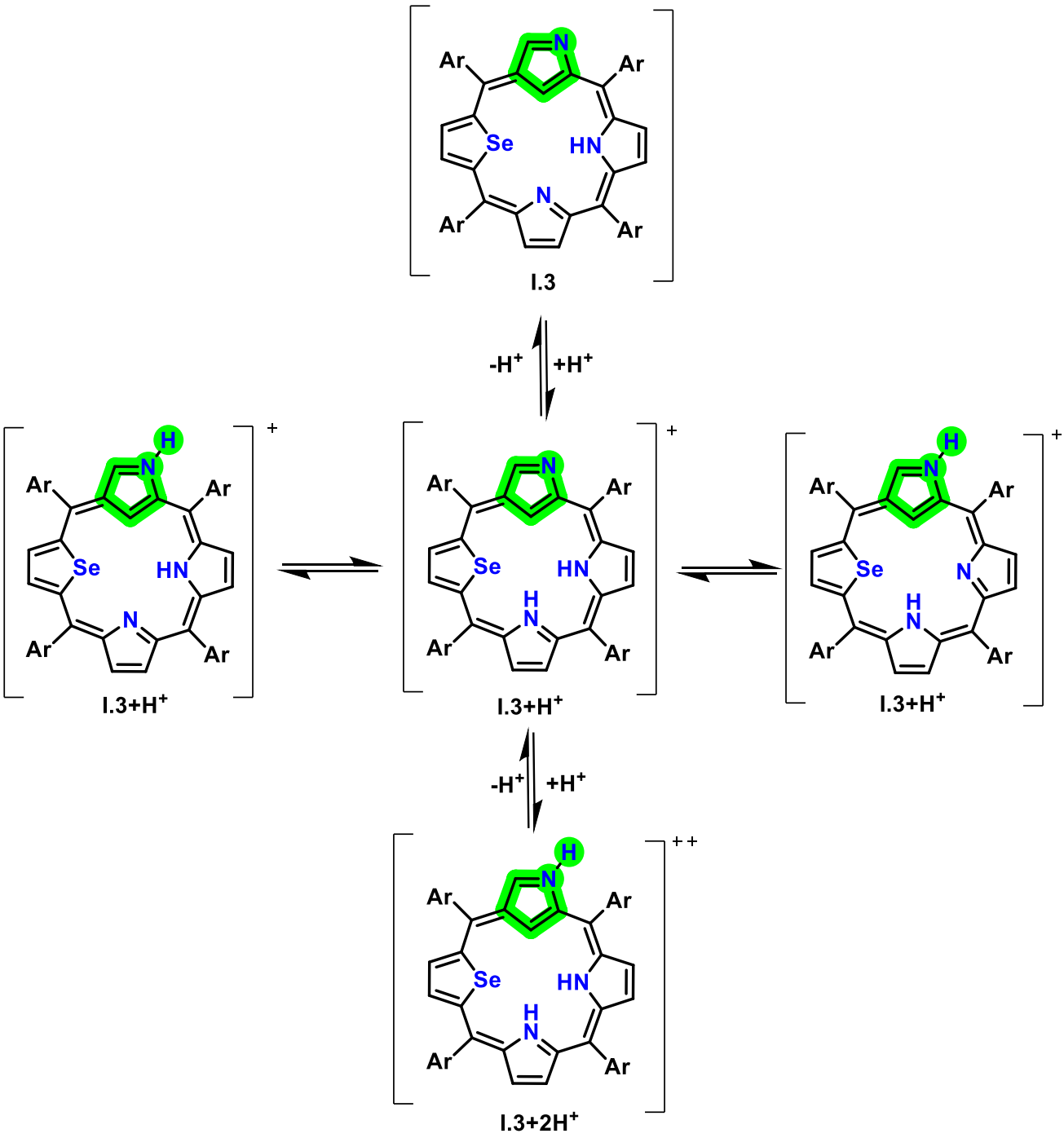

Figure 4 Monoprotonation and Diprotonation of $CTTPH_2$.

Building on these foundations, Simi K. Pushpan et al. in 2001 investigated the synthesis and characterization of core-modified N-confused porphyrins[5] incorporating heteroatoms such as sulfur, selenium, and oxygen have been successfully achieved through an efficient 3+1 MacDonald-type condensation method. This approach yielded the desired porphyrins in significantly higher quantities compared to previous methods, facilitating easier separation and further exploration of their unique properties. Detailed NMR studies revealed the presence of multiple tautomers in solution and provided insight into the structural dynamics and protonation behavior of these compounds. The unique

structural features and coordination chemistry of these modified porphyrins, especially their ability to form metal-carbon bonds and stabilize higher oxidation states of metals, hold promising potential for the development of novel organometallic complexes with diverse applications in materials science and catalysis. Overall, this work expands the toolbox for porphyrin chemistry, offering new avenues for the synthesis and functionalization of porphyrin-based systems.

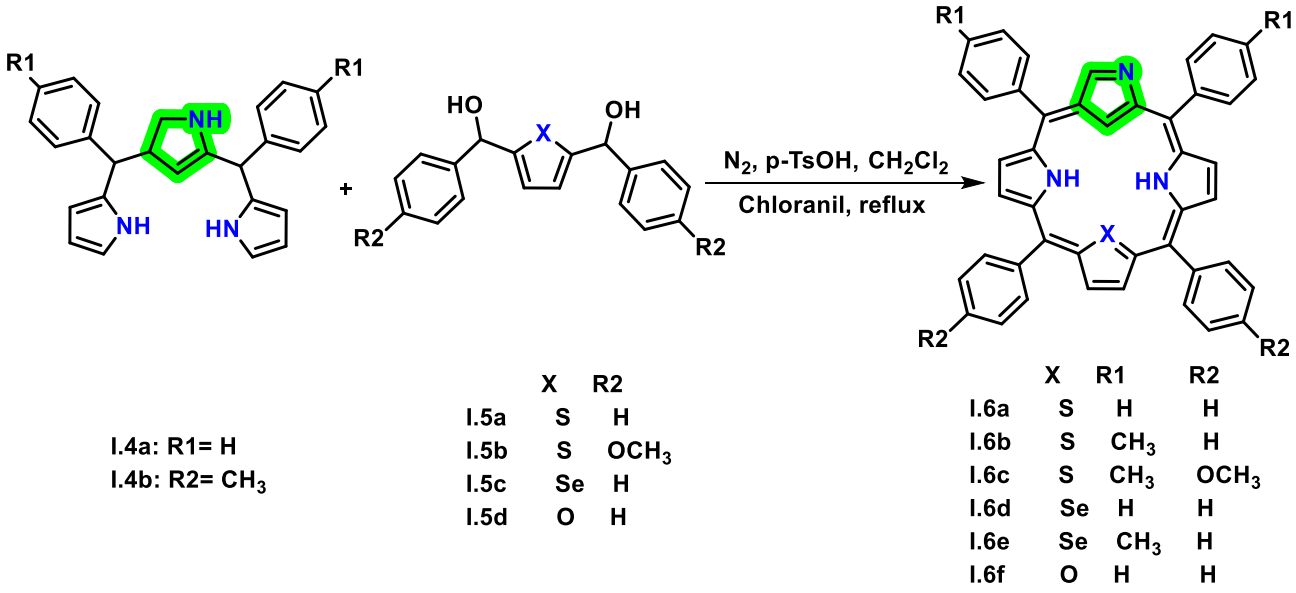

Figure 5 Synthesis of CTTPH2 through 3+1 MacDonald-type condensation method.

Natasza sprutta et al. investigated the acid-catalyzed condensation of pyrrole (**I.7**) and 2,5-bis(p-tolylhydroxymethyl)thiophene (**I.8**) successfully produced the first diheteroporphyrin featuring an inverted pyrrole ring, along with the known 21,23-dithiaporphyrin.[6] The resulting novel compound, 5,10,15,20-tetra(p-tolyl)-2-aza-21-carba-22,24-dithiaporphyrin (**I.9**), exhibited distinct spectroscopic properties indicative of its unique structure and aromaticity.

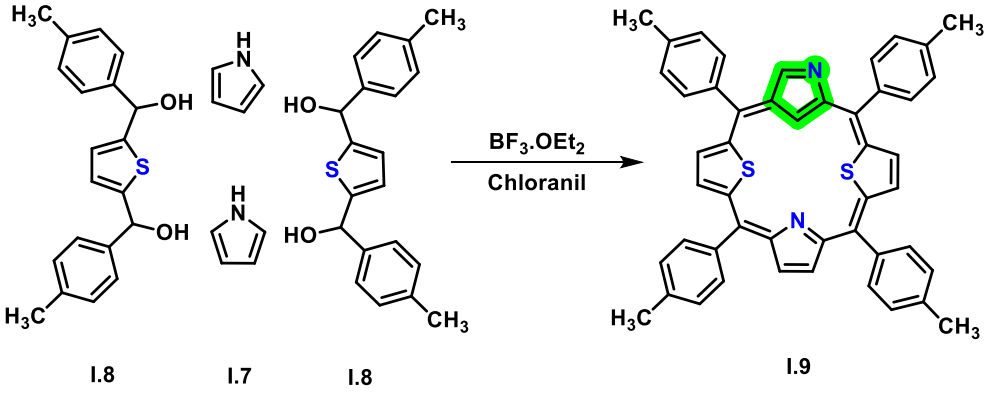

Figure 6 Synthesis of first confused diheteroporphyrin.

This study provides valuable insights into the mechanisms of core-modified porphyrin synthesis, particularly emphasizing the possibility of generating inverted diheteroporphyrins through established

synthetic pathways. The identification and characterization of these compounds expand the understanding of porphyrin chemistry and suggest further exploration of their coordination properties and potential applications.

Miłosz Pawlick, et al detail the synthesis, characterization, and reactivity of "true" O-confused oxaporphyrin (**I.10**) and its derivatives using the heteroatom confusion concept.[7] By interchanging an oxygen atom with a β-methine group in furan, 5,10,15,20-tetraaryl-21-oxaporphyrin is transformed into 2-oxa-5,10,15,20-tetraaryl-21-carbaporphyrin (**I.10**). This process stabilizes the targeted O-confused oxaporphyrin in its dicationic form, as confirmed by ^{1}H NMR spectroscopy. The reactive nature of the furan ring allows for the stabilization of O-confused oxaporphyrin derivatives at the C(3) position. These findings reveal the significant potential of O-confused oxaporphyrin (**I.10**) as a fundamental intermediate for constructing stable, finely-tuned organometallic compounds. This study advances the understanding of carbaporphyrinoid chemistry and opens new pathways for creating innovative macrocyclic compounds with unique electronic and coordination properties.

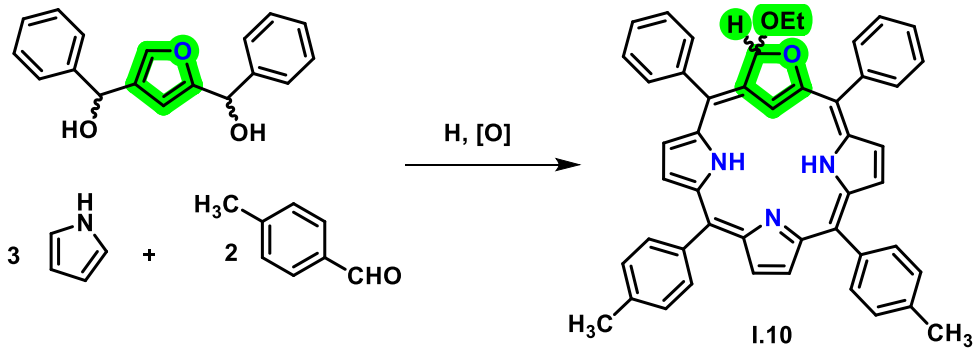

Figure 7 Synthesis of first O-confused porphyrin (I.10).

Unlike porphyrin, these N-confused and S-confused porphyrin systems demonstrate the ability to form metal complexes, which result in the formation of distinct metal-carbon bonds.[2,8,9] This unique characteristic is attributed to the presence of the "confused pyrrole" ring, which introduces new binding sites and alters the electronic environment of the macrocycle. These metal complexes exhibit clear spectroscopic signatures and enhanced stability compared to traditional porphyrin-metal complexes. The metal-carbon bond formation in CTPP and its derivatives opens new avenues for exploring catalytic applications, coordination chemistry, and the development of advanced materials. This expanded reactivity underscores the versatility and potential of confused porphyrins.

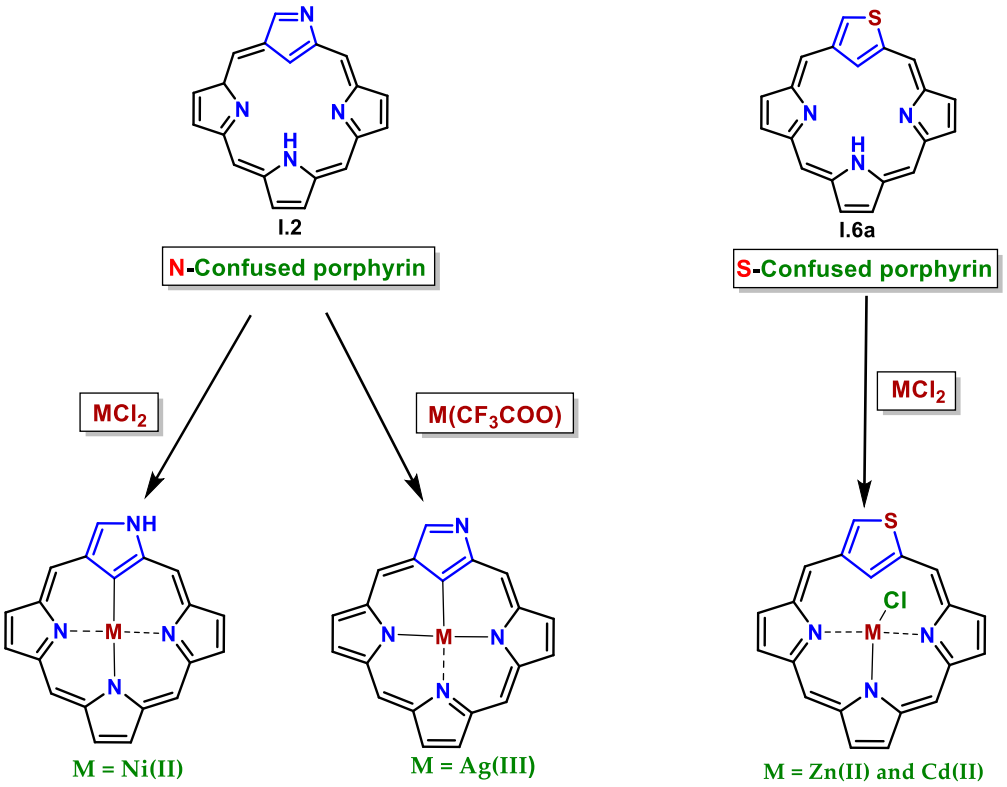

Figure 8 Metal complexes of Confused porphyrins.

Panchal et al explored the successful synthesis of the first S-confused tetrathia isophlorin (**I.12**) has revealed its unique redox properties and behavior.[10] Unlike its parent isophlorin, the 20π confused isophlorin does not simply oxidize to its corresponding dication. Instead, it undergoes an unusual pathway, forming a chlorinated derivative upon oxidation. The oxidation process, catalyzed by Meerwein salt, unexpectedly produces a monocationic species (**I.13**) through a radical intermediate rather than the anticipated dication. Structural and spectroscopic analyses confirm this transformation, with the exocyclic C=O group on the confused thiophene ring indicating a significant deviation from typical porphyrin chemistry. The methyl-substituted analogue (**I.12b**) exhibits similar properties but shows resistance to further oxidation, underscoring the unique stability and reactivity of these macrocycles. These findings highlight the distinct redox behavior and structural complexity of antiaromatic macrocycles, offering new insights into their potential applications in porphyrinoid organometallic complexes. The study paves the way for further exploration of the redox chemistry and functional properties of S-confused isophlorins and related compounds.

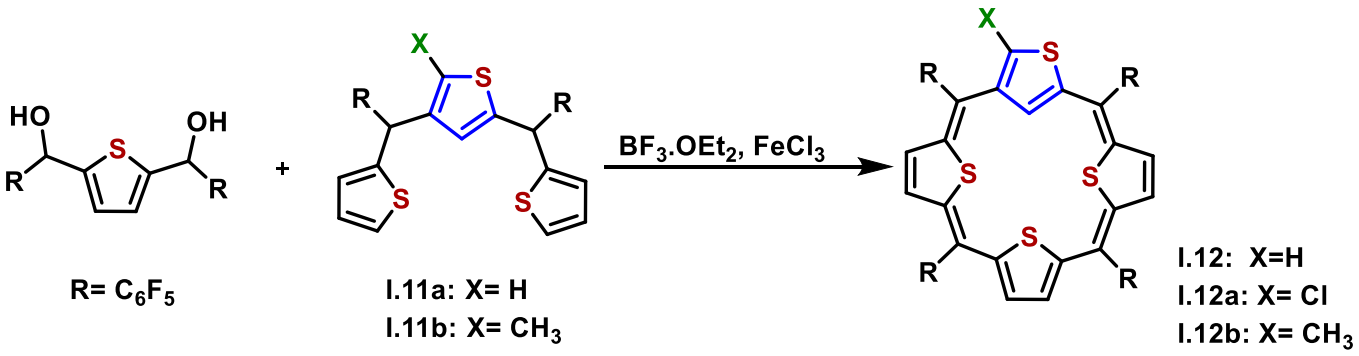

Figure 9 Synthesis of first S-confused tetrathia isophlorin.

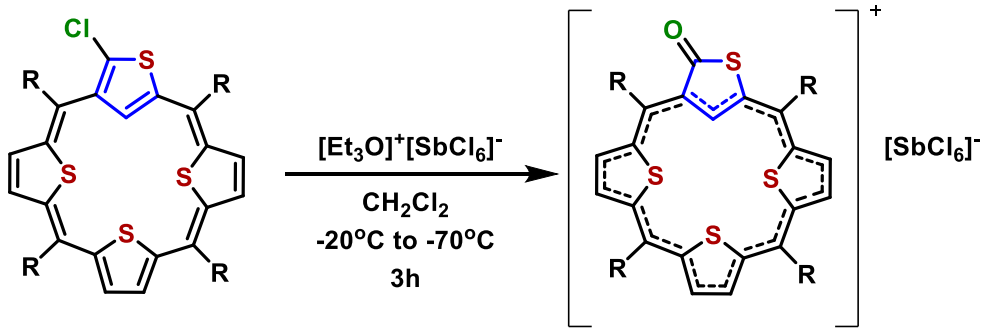

Figure 10 Synthesis of first S-confused tetrathia isophlorin and its monocationic species.

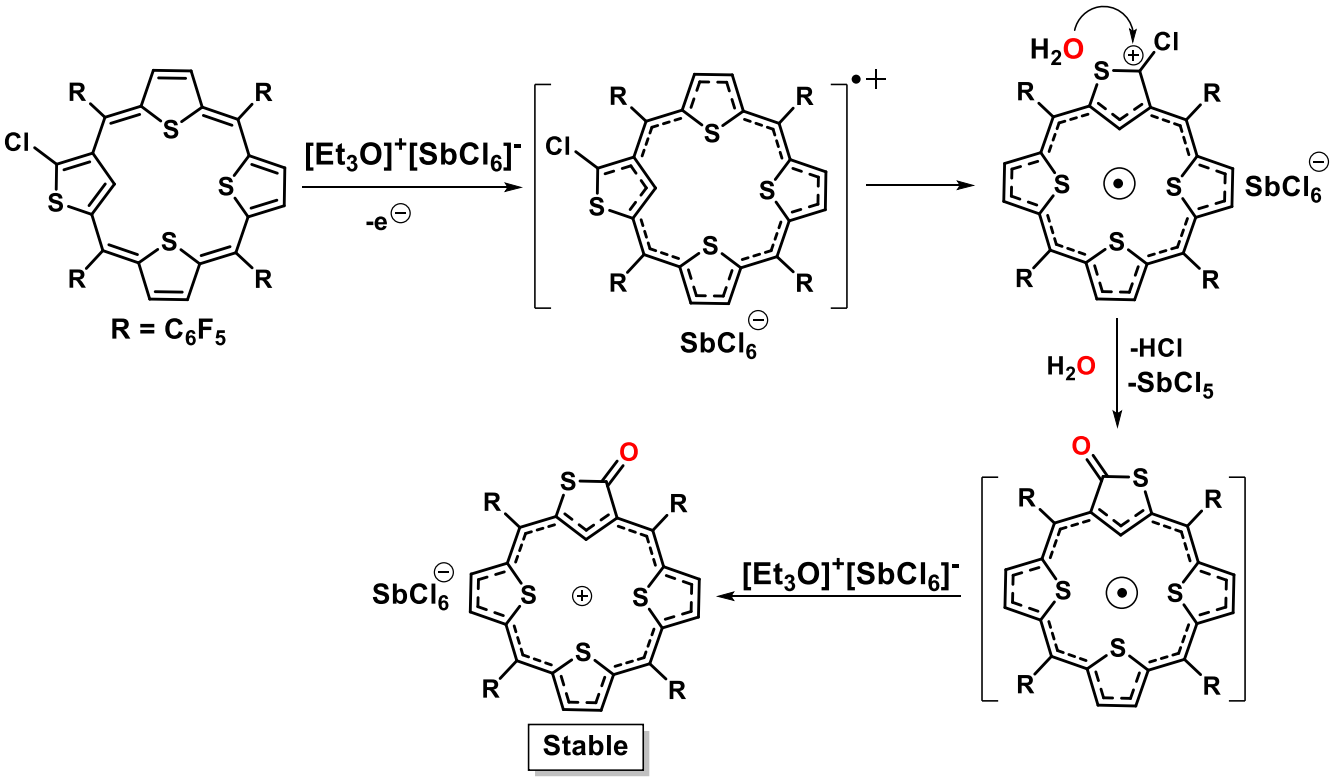

Figure 11 Plausible mechanism for the formation of monocationic species.

The mechanism reveals that compound **I.12** undergoes one-electron oxidation in the presence of Meerwein's salt, producing a radical cationic species. This species reacts with moisture, generating a radical species that features an exocyclic C=O group on the confused thiophene ring. Due to its

instability, this radical species undergoes another one-electron oxidation, resulting in the formation of a stable monocationic species (**I.13**). This process illustrates the complex reactivity of compound **1**, highlighting the formation of unique intermediates and the involvement of the confused thiophene ring in these transformations.

This observation does not necessarily conclude that the macrocyclic radical species is unstable. Tullimilli Y. Gopalakrishna et al. has already reported stable macrocyclic radicals (**I.14**) at room temperature,[11] akin to organic, benzo-fused triangular radical molecules.[12,13,14,15] This implies that, despite the formation of a transient intermediate in our case, it is possible for similar macrocyclic radicals to exhibit stability under appropriate conditions. Therefore, the instability of the radical species observed here could be attributed to specific structural or environmental factors rather than an inherent property of macrocyclic radicals. This radical exhibits remarkable stability, as it does not undergo pi-dimerization and consistently retains its paramagnetic behaviour, demonstrating its robustness under various conditions.

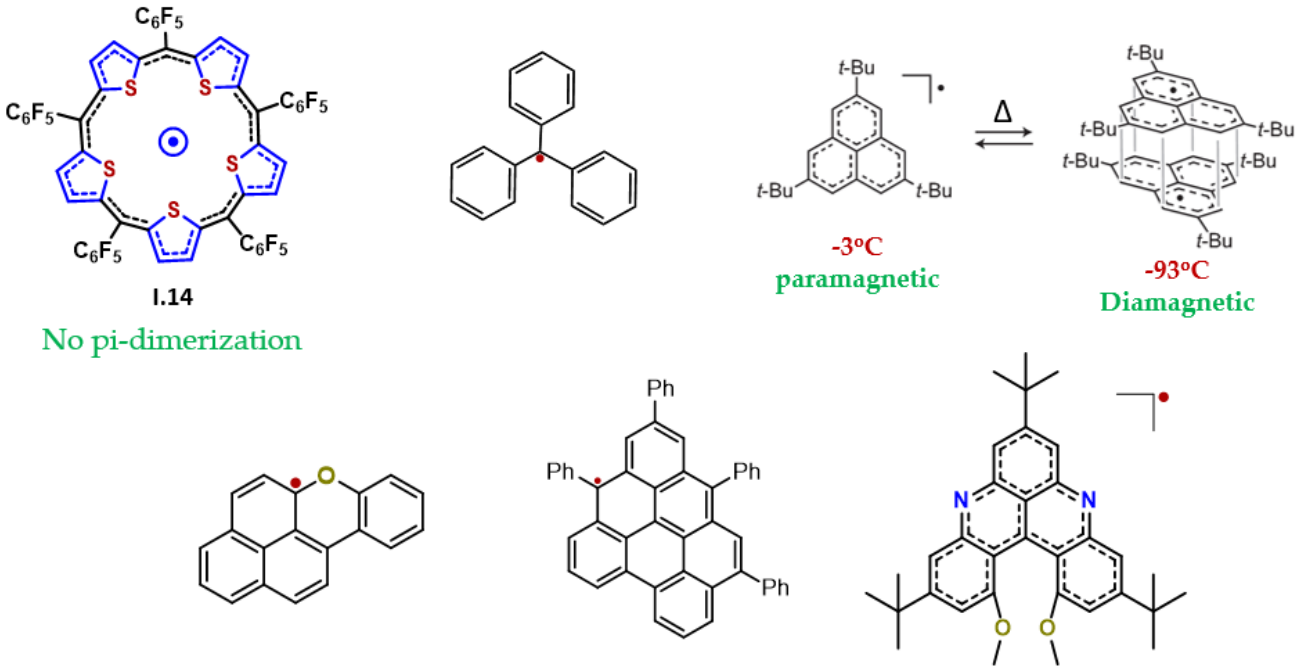

Figure 12 Stable radical species.

P. Bäuerle, et al. explored the synthesis of stable α-cyclo[n]thiophenes (α-C[n]T) with up to 76 members, exhibiting unique self-organization and significant internal cavities.[16] These macrocycles form well-defined planar structures, confirmed by spectroscopy and X-ray analysis, and create stable monolayers as observed by STM. They have successfully synthesized expanded pi-conjugated cyclo[10]thiophene (**I.15**). The exclusive syn-conformation of all thiophene units in **I.15** leads to significant ring strain, influencing its unique optoelectronic properties. Their study of **I.15** in various

oxidation states reveals distinct optical and electronic behaviors, including the formation of radical cations and dications.[17] Notably, the ESR and absorption spectra support the existence of a polaron-pair structure in the doubly oxidized **I.15**. These findings advance the understanding of cyclic oligothiophenes, highlighting their potential for future applications in organic (semi)conductors and molecular electronics.

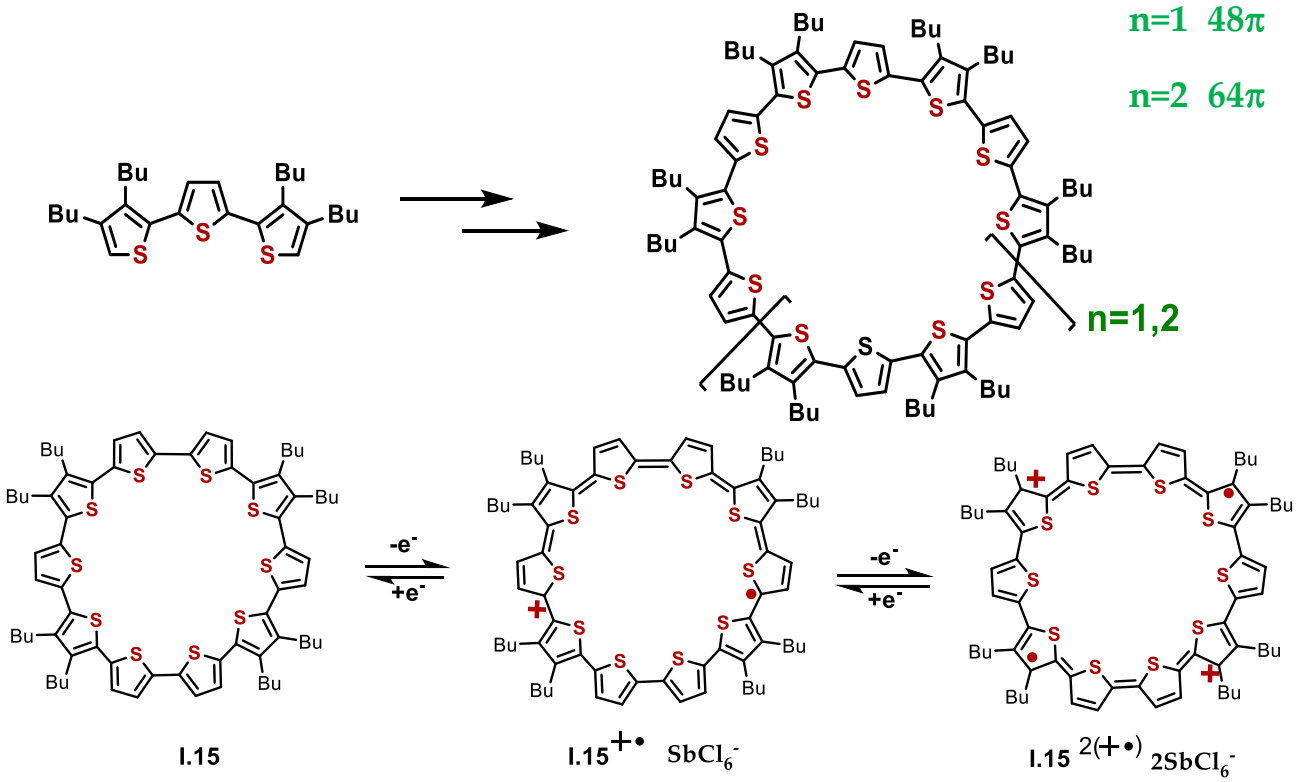

Figure 13 Synthesis of stable radical cations and dications.

The replacement of pyrrole with thiophene leads to notable changes in the electronic properties of the macrocyclic system. This has inspired other research groups to investigate the incorporation of different heterocyclic units, such as pyridine, bipyridine, and phenanthroline, into the core of the macrocycle. These modifications are aimed at tailoring the electronic, optoelectronic, and structural properties of the resulting macrocycles.

Incorporating pyridine, for instance, can introduce nitrogen atoms into the macrocycle, potentially enhancing its electron-withdrawing properties and affecting its aromaticity. Bipyridine units could offer additional coordination sites for metal ions, thus expanding the application range of these macrocycles in fields like catalysis and materials science. Phenanthroline, with its rigid and planar structure, could provide further insights into the effects of conjugation and steric hindrance within the macrocyclic framework.

These structural variations are not merely academic exercises; they have practical implications. By modifying the heterocyclic core, researchers can fine-tune the properties of macrocycles for specific applications, such as in organic semiconductors, photovoltaic materials, and molecular electronics. The systematic exploration of these heterocyclic substitutions opens up new avenues for designing advanced materials with customized properties.

Jun-ichiro Setsune, et al,[18] and Harrison D. Root, et al,[19] present a new method for altering the electronic properties of expanded porphyrins through protonation. They showed that free-base pyriamethyrin (**I.18**) and dipyriamethyrin (**I.21**), initially non-aromatic, can be transformed into anti-aromatic systems by protonating with methane sulfonic acid (**I.19**). This change is supported by UV-Vis and NMR spectroscopic data and DFT calculations. Protonation extends π-conjugation across the macrocycle, resulting in significant spectral shifts and downfield NH resonance shifts indicative of anti-aromaticity. Theoretical models, including electron density plots and NICS values, corroborate these findings, demonstrating a shift from local aromaticity to global anti-aromaticity. This work introduces a new approach for switching between electronic states in porphyrinoids using protonation, with potential applications in materials science and biomedical research. This method provides a novel tool for designing and functionalizing macrocyclic systems with adjustable electronic properties.

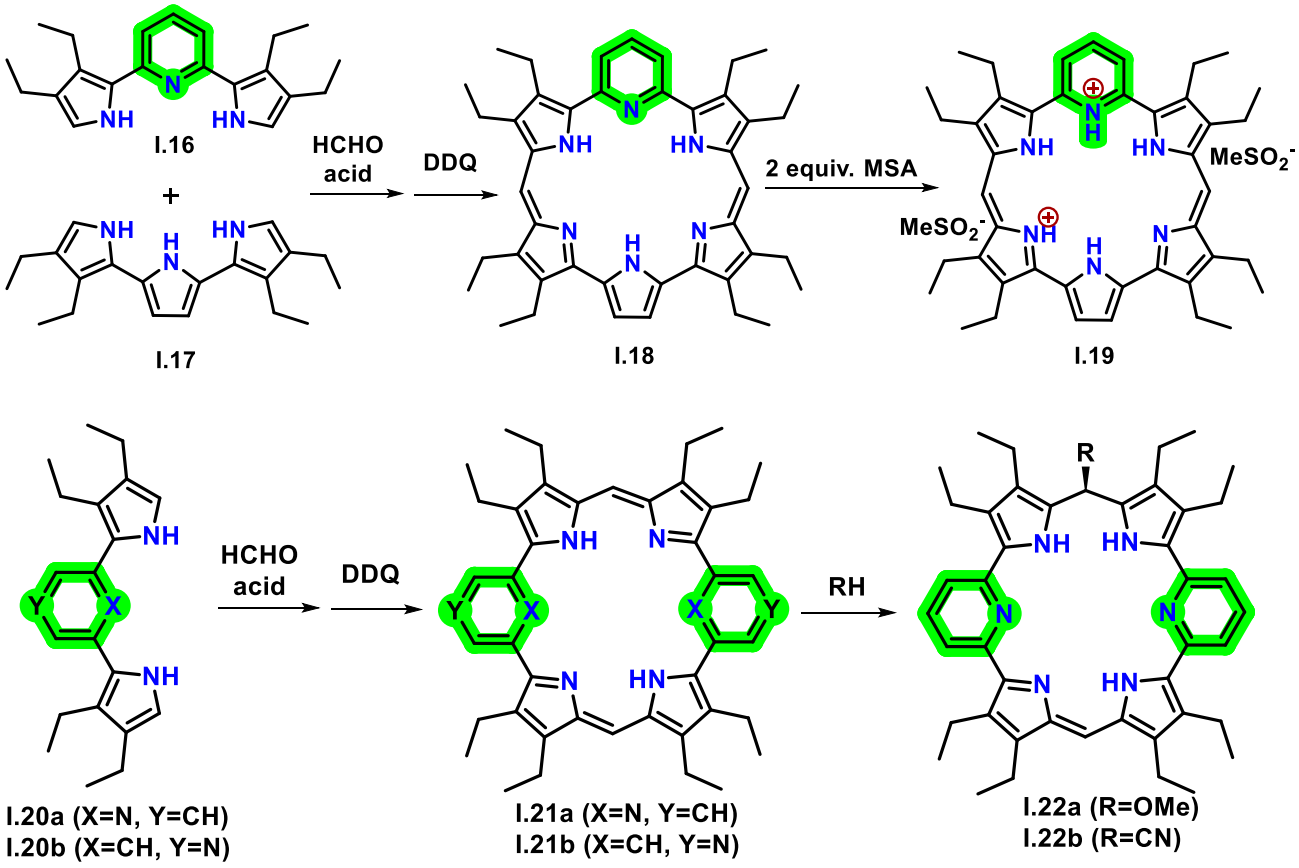

Figure 14 Synthesis of pyriamethyrin and dipyriamethyrin.

The exploration of chirality transfer in expanded porphyrinoids opens up new avenues in asymmetric catalysis and chirality sensing. This study focused on the helical chirality of large-sized porphyrinoids, particularly cyclooctapyrroles, which adopt a unique figure-eight loop conformation. Jun-ichiro Setsune, et al, demonstrated that the helical chirality of cyclooctapyrrole metal complexes can be manipulated through reversible ligand substitution.[20] The key findings include the successful synthesis of a novel substitution-labile binuclear CoII complex of an expanded pyriporphyrin analogue (**I.23**) and the induced helical chirality change through ligand exchange reactions. The structural analysis via X-ray crystallography revealed critical interactions, such as hydrogen bonding and weak Co-N(pyridine) coordination, essential for helicity changes. The study highlighted that homochiral ligands, such as mandelate and threonine, can induce significant diastereoselectivity and Cotton effects in circular dichroism spectra, demonstrating precise chirality sensing capabilities. The dynamic coordination behavior of these complexes not only advances our understanding of helical chirality in porphyrinoids but also suggests potential applications in the development of new chiral materials and catalysts. Further research into the dynamic metal complexes of cyclooctapyrroles is warranted to fully exploit their chirality transfer properties in various chemical applications.

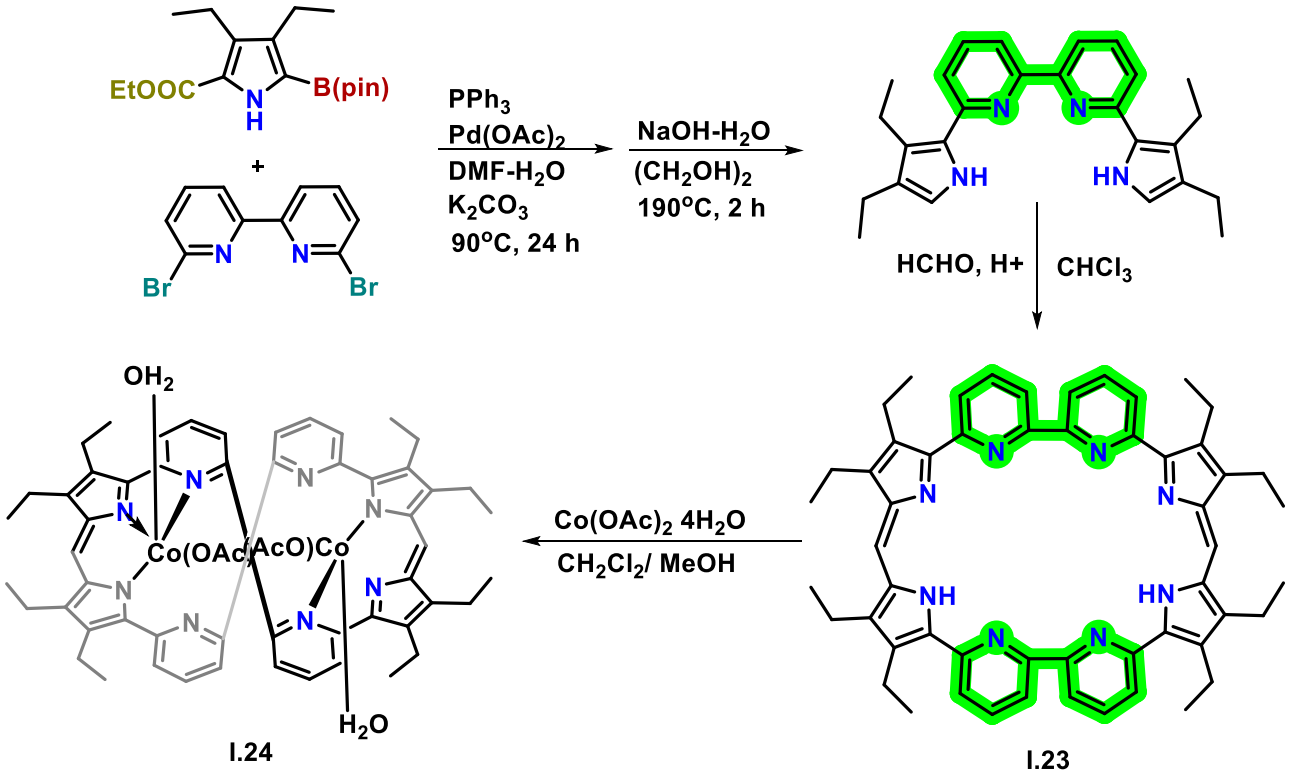

Figure 15 Synthesis of expanded pyriporphyrin analogue.

Masatoshi Ishida, et al, successfully synthesized a novel porphyrin analogue, **I.25**, incorporating a 1,10-phenanthroline moiety designed to facilitate selective and efficient Mg^{2+} complexation.[21] The unique structural features of **I.25**, such as its gable-type nonplanar macrocyclic structure and relatively

small monoanionic coordination sphere, enable rapid and facile Mg^{2+} binding. This complexation is accompanied by significant fluorescence enhancement and red-shift, making **I.25** an effective Mg^{2+}-responsive fluorescent sensor. Importantly, **I.25** demonstrates a high degree of selectivity for Mg^{2+} over other physiologically relevant cations such as Na^{+}, K^{+}, and Ca^{2+}, ensuring minimal interference in biological applications.

The compound's ability to emit far-red fluorescence above 600 nm, coupled with its ratiometric detection capabilities, offers a substantial advantage for real-time monitoring of intracellular Mg^{2+} levels. Additionally, the robustness of **I.25** in semi-aqueous solutions further underscores its potential utility in biological environments. This study highlighted the promising applications of **I.25** as a cell-permeable fluorescent sensor for Mg^{2+}, providing a valuable tool for assessing total cellular Mg^{2+} content and contributing to a deeper understanding of Mg^{2+}'s role in cellular physiology.

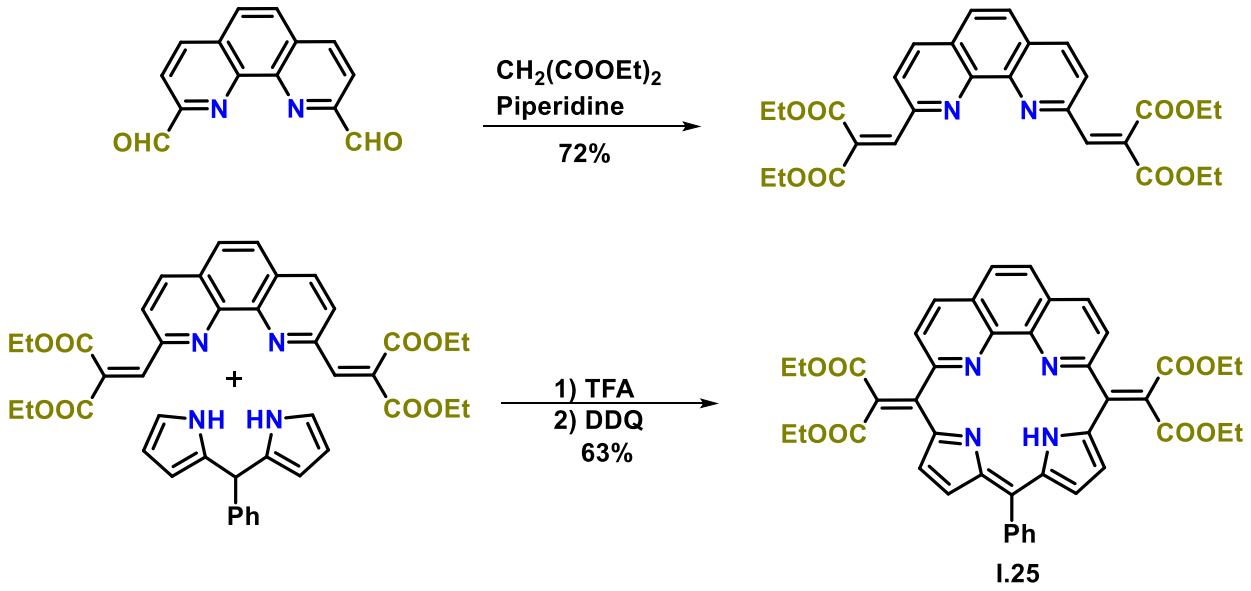

Figure 16 Synthesis of novel porphyrin analogue, incorporating 1,10-phenanthroline moiety.

Masatoshi Ishida, et al, synthesized and characterized a novel 1,10-phenanthroline-embedded sapphyrin analogue (**I.28**) with meso alkylidenyl double bonds.[22] Upon protonation, this compound uniquely forms a stable singlet biradicaloid species. This transformation, confirmed through various spectroscopic methods, alters the macrocyclic π-conjugation and induces high-spin states, providing new insights into protonation-induced magnetization. The formation of compound 1 involved a "4+1" condensation strategy. Protonation was shown to result in significant changes in UV/Vis-NIR absorption, ESR spectra, and magnetic susceptibility, indicating the presence of a singlet biradicaloid with strong antiferromagnetic coupling.

Electrochemical analysis revealed a smaller HOMO-LUMO energy gap for the protonated form compared to the original compound, further confirming the electronic alteration upon protonation. The

mechanism involves protonation at the α-carbon of the diethyl malonyl groups, leading to a stable tricationic biradicaloid (**I.29**). These findings demonstrate the potential of protonation-induced switching in designing novel functional materials with unique magnetic properties, advancing the development of molecular devices and switches.

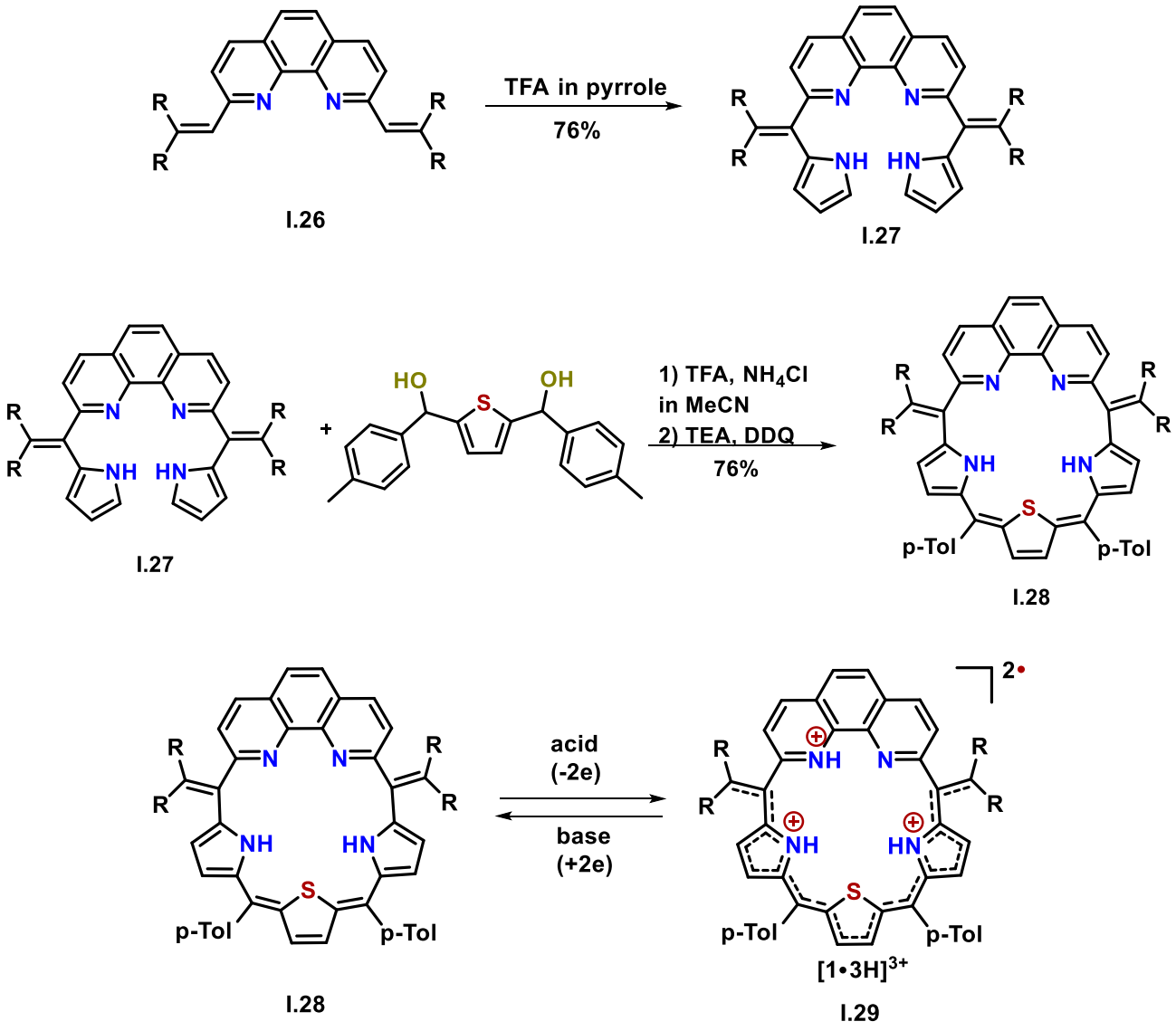

Figure 17 Synthesis of 1,10-phenanthroline-embedded sapphyrin analogue.

In summary, the concept of "confused systems" regarding porphyrins explores differences in bonding structures leading to isomeric forms. Initial foundational work on porphyrin isomers paved the way for future studies. Key advancements include the discovery of core-modified porphyrins, such as carbaporphyrins and porphycenes, which exhibit unique electronic and photophysical properties. Further research synthesized N-confused tetraphenylporphyrin, revealing distinct structural and electronic characteristics, and explored a new macrocyclic compound, SeC-DPDTPH, offering

insights into macrocycle formation and aromaticity. Investigations into core-modified N-confused porphyrins with heteroatoms enhanced their stability and coordination chemistry.

Additional studies introduced stable macrocyclic radicals, expanded porphyrins, and unique macrocyclic compounds with varying electronic properties. Notable contributions include the synthesis of stable α-cyclo[n]thiophenes and new methods for altering electronic properties through protonation. Research on chirality transfer in expanded porphyrinoids and Mg^{2+}-responsive fluorescent sensors highlighted potential applications in asymmetric catalysis and biological environments. The synthesis of a 1,10-phenanthroline-embedded sapphyrin analogue demonstrated protonation-induced magnetization, advancing molecular devices and switches. These studies collectively expand the understanding and applications of macrocyclic systems in various scientific fields.

References

(1) M. O. Senge, *Angew. Chem., Int. Ed. Engl.*,2011, **50**, 4272–4277.

(2) P. J. Chmielewski, L. Latos-Grażyński, K. Rachlewicz and T. Glowiak, *Angew. Chem., Int. Ed. Engl.*, 1994, **33**, 779–781.

(3) T. Hiroyuki Furuta, T. Asano and T. Ogawa, *J. Am. Chem. Soc.*, 1994, **116**, 767-768.

(4) E. Pacholska, L. Latos-Grazynski, L. Szterenberg and Z. Ciunik, *J. Org. Chem.*, 2000, **65**, 8188–8196.

(5) S. K. Pushpan, A. Srinivasan, V. R. G. Anand, T. K. Chandrashekar, A. Subramanian, R. Roy, K. Sugiura and Y. Sakata, *J. Org. Chem.*, 2001, **66**, 153–161.

(6) N. Sprutta and L. Latos-Grazyński, *Org. Lett.*, 2001, **3**, 1933–1936.

(7) M. Pawlicki and L. Latos-Grazyński, *J. Org. Chem.*, 2005, **70**, 9123–9130.

(8) H. Furuta, Inorg Chem, 1999, 38, 2676–2682.

(9) M. J. Chmielewski, M. Pawlicki, N. Sprutta, L. Szterenberg and L. Latos-Grazyński, *Inorg. Chem.*, 2006, **45**, 8664–8671.

(10) S. P. Panchal and V. G. Anand, *Org. Lett.*, 2017, **19**, 4854–4857.

(11) T. Y. Gopalakrishna, J. S. Reddy and V. G. Anand, *Angew. Chem.*, 2014, **126**, 11164–11167.

(12) M. Gomberg-2002-an-instance-of-trivalent-carbon-triphenylmethyl.

(13) S. Suzuki, Y. Morita, K. Fukui, K. Sato, D. Shiomi, T. Takui and K. Nakasuji, *J. Am. Chem. Soc.*, 2006, **128**, 2530–2531.

(14) P. Ravat, O. Blacque and M. Juríček, *J. Org. Chem.*, 2020, **85**, 92–100.

(15) A. Ueda, H. Wasa, S. Suzuki, K. Okada, K. Sato, T. Takui and Y. Morita, *Angew. Chem., Int. Ed. Engl.*, 2012, **51**, 6691–6695.

(16) F. Zhang, G. Götz, E. Mena-Osteritz, M. Weil, B. Sarkar, W. Kaim and P. Bäuerle, *Chem. Sci.*, 2011, **2**, 781–784.

(17) F. Zhang, G. Götz, E. Mena-Osteritz, M. Weil, B. Sarkar, W. Kaim and P. Bäuerle, *Chem. Sci.*, 2011, **2**, 781–784.

(18) J. I. Setsune and K. Yamato, *Chem. Comm.*, 2012, **48**, 4447–4449.

(19) H. D. Root, D. N. Mangel, J. T. Brewster, H. Zafar, A. Samia, G. Henkelman and J. L. Sessler, *Chem. Comm.*, 2020, **56**, 9994–9997.

(20) J. I. Setsune, M. Kawama and T. Nishinaka, *Tetrahedron Lett.*, 2011, **52**, 1773–1777.

(21) M. Ishida, Y. Naruta and F. Tani, *Angew. Chem., Int. Ed. Engl.*, 2010, **49**, 91–94.

(22) M. Ishida, S. Karasawa, H. Uno, F. Tani and Y. Naruta, *Angew. Chem.*, 2010, **122**, 6042–6045.

Aim of Thesis

Porphyrins, characterized by their macrocyclic structure of four interconnected pyrrole subunits, are crucial organic compounds found in many biological systems such as hemoglobin and chlorophyll. These molecules are notable for their unique electronic properties and ability to coordinate metal ions, adhering to the 18π-electron rule that grants them aromaticity and stability. Recent advancements in synthetic chemistry have paved the way for the development of structural isomers of porphyrins, known as confused porphyrins, which exhibit altered properties while maintaining the 18π-electron count, as well as confused porphycenes, which also possess unique properties.

The structural isomers of porphyrin, such as porphycene (**II.2**), N-confused porphyrin (**II.3**), and neo-confused porphyrin (**II.4**), are created by rearranging the tetrapyrroles in a cyclic fashion. This rearrangement alters the skeletal framework, leading to a modified π-network and altered aromaticity. Despite retaining the 18π-electron count, these isomers display distinct electronic and redox properties. Among them, N-confused porphyrin (NCP) is particularly notable for its ability to form organometallic complexes when a metal binds in the central cavity, owing to the α, β-connectivity of the pyrrole, which replaces the central nitrogen with an activated β-CH, enabling the formation of a metal-carbon bond.

Core-modified NCPs have been synthesized by substituting a regular or confused pyrrole with another heterocyclic unit, such as furan or thiophene. In S-confused porphyrin, the alpha carbon of the confused thiophene is oxidized to an exocyclic keto moiety, inducing aromaticity in the π-network. Similarly, O-confused porphyrin forms organometallic complexes with metal ions like Ni(II), Pd(II), and Ag(III). These core modifications significantly enhance the versatility and functionality of NCPs, making them suitable for a range of applications in catalysis, materials science, and molecular devices.

Further advancements have been made by incorporating an extended π-conjugated network through the addition of more heterocyclic units to the core of porphyrins and integrating aromatic rings such as 1,10-phenanthroline and bipyridine. This results in the formation of expanded porphyrinoids. These structural modifications significantly enhance their redox properties and metal coordination abilities. Expanded porphyrinoids exhibit unique electronic and photophysical characteristics, making them highly promising for various advanced applications, including organic electronics, non-linear optics, and energy storage devices. The expanded π system allows for better charge transport and increased stability, while the additional aromatic rings facilitate diverse metal coordination, further broadening their functional versatility and potential in cutting-edge technological applications.

After studying extensive literature in these fields, it has been found that confusion in porphycenes can give rise to new kinds of macrocyclic systems with unique properties. Additionally, expanding the core of these macrocycles can lead to the formation of unique molecules with distinctive characteristics. Therefore, in this thesis, the initial focus was on the synthesis of completely confused porphycene systems to investigate whether these modifications can lead to significant enhancements in the versatility and functionality of these systems. Subsequently, it was aimed to synthesize phenanthroline-incorporated expanded porphyrinoids, analogous to amethyrin and open-shell molecules. These novel compounds are anticipated to exhibit unique coordination properties due to the incorporation of the phenanthroline cavity, potentially enhancing their functionality and broadening their application in fields such as catalysis, materials science, and molecular devices.

Moreover, 30π aromatic expanded isophlorin analogues featuring diverse structural characteristics were synthesized by substituting heterocyclic rings such as furan, thiophene, and selenophene. Inspired by these findings, a modified synthetic scheme was adopted by substituting the β-position of the heterocyclic rings instead of changing the entire heterocyclic unit. This strategy aims to explore and observe the structural diversity and potential novel properties arising from β-position substitutions, further expanding the versatility and functionality of these macrocyclic systems.

Chapter 2:- Tetra S-Confused Porphyrinoids

II.1 Introduction:

The structural isomers of porphyrin **II.1** are 18π-isoelectronic macrocycles obtained by rearranging the tetrapyrroles in a cyclic fashion. Porphycene (**II.2**),[1] N-confused porphyrin (**II.3**) [2a], and neo-confused porphyrin (**II.4**) [3] are well-studied isomers of the parent 18π porphyrin (**Fig. 1**). Experimental and computational studies attest that an altered skeletal framework leads to a modified π-network and the accompanying aromaticity.[4] Consequently, these isomers differ in their electronic and redox properties in spite of adhering to the 18π-electron count. N-confused porphyrin (NCP) **II.3** is known to form organometallic complexes when a metal binds in the central cavity of the porphyrin.[2b,c] Due to the α,β-connectivity of the pyrrole, nitrogen in the centre is replaced by an activated β-CH to form a metal–carbon bond.[5] Core-modified NCPs have been successfully synthesized by replacing either a regular or a confused pyrrole with another heterocyclic unit such as furan or thiophene.[6a,b,c] In an S-confused porphyrin, the alpha carbon of the confused thiophene is oxidized to an exocyclic keto moiety which induces aromaticity in the π network.[7] Similar to the parent NCP, O-confused porphyrin has been identified to form organometallic complexes with various metal ions such as Ni(II), Pd(II) and Ag(III).[8a,b] Modified processes have been developed to synthesize porphyrinoids with more than one confused pyrrole ring. In particular, doubly N-confused porphyrin has been synthesized in which two nitrogens of a parent porphyrin in the macrocyclic core are replaced by the β-CH of inverted pyrrole rings.[9] The availability of two β-CHs in the core of the doubly N-confused porphyrin offers a unique advantage to access the higher oxidation state of a metal ion such as Cu(III).[10]

A confused pyrrole ring is also easily incorporated into the π network of expanded porphyrins. A 22π core-modified sapphyrin is the first example of an N-confused expanded porphyrin.[11] To date, a much larger hexaphyrin is known to accommodate two or more confused pyrrole rings. Specifically, a hexaphyrin with two confused pyrrole units is known to undergo oxidation at the unsubstituted alpha position of pyrrole to yield an exocyclic keto group. The oxygen of this keto group acts as an excellent donor atom to complex metal ions such as Cu(II) and Ni(II) in the macrocyclic cavity.[12] Furthermore, to date, hexaphyrins with three N-confused pyrrole units represent a porphyrinoid with the maximum number of confused heterocyclic rings.[13] A larger macrocycle, octaphyrin, with two confused pyrrole rings was found to adopt a figure-of-eight conformation. The orientation of the confused pyrrole nitrogen was much similar to that of a regular octaphyrin, yielding four nitrogens in the porphyrin like

cavity to bind metal ions.[14] A 20π tetrathiaisophlorin **II.5** is the solitary example of a non-pyrrolic confused porphyrinoid. Unlike NCP **II.3**, the confused thiophene in **II.5** leads to an unstable 19π radical species which is stabilized as an 18π monocationic species.[15a] To date, it has remained a synthetic challenge to synthesize a porphyrinoid composed of only confused heterocycles. This chapter describes the first synthesis of a tetrathia porphycene and its expanded congener 30π hexathia porphycene with four and six confused thiophene rings, respectively.

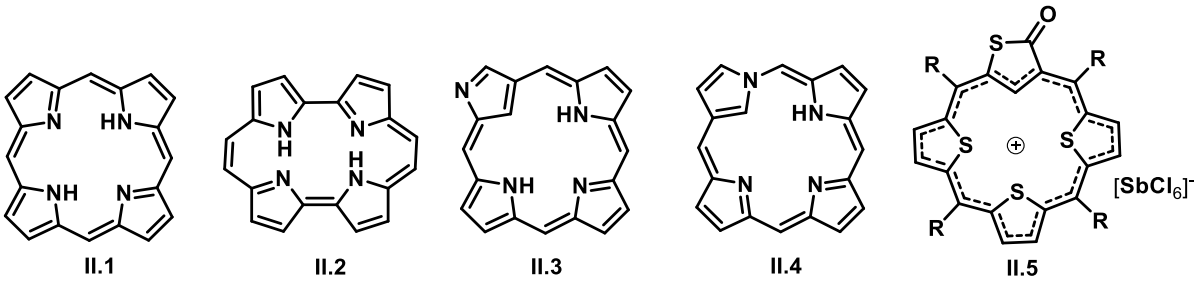

Figure 1. 18□ isoelectronic isomers (**II.2-II.5**) of porphyrin, **II.1**.

Vogel and co-workers synthesized the first porphycene by McMurry coupling of a bipyrrole dialdehyde.[15b] A similar strategy with either bifuran or bithiophene dialdehyde was employed to synthesize core-modified tetra-oxa and tetrathia porphycenes. In contrast to the parent 18π porphycene **II.2**, the tetraoxa and tetrathia porphycenes **II.6a** and **II.6b** account for 20π-electrons and are susceptible to two-electron redox reactions to yield the 18π dicationic species **II.7a** and the 22π dianionic species **II.7b,** respectively (**Fig. 2**).[16,17] A similar synthetic methodology with the dialdehyde of bithiophene and terthiophene was employed by Cava and workers to yield hexathiophene expanded porphycenes.[18]

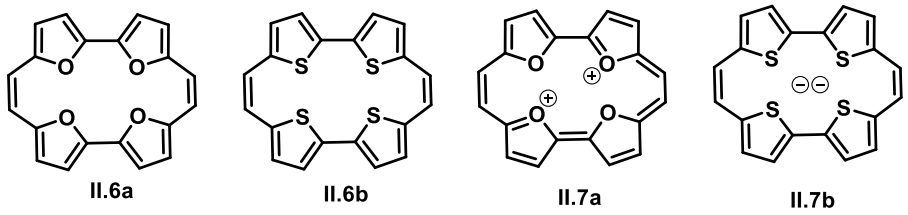

Figure 2 Tetraoxa and tetrathia porphycenes, **II.6a** and **II.6b**, and aromatic 18***π*** dicationic species, **II.7a** and 22***π*** dianionic species, **II.7b**.

II.2 Synthesis and characterization of 'Tetra S-Confused Porphyrinoids' II.8 and II.9.

Synthesis of 'Tetra S-Confused Porphyrinoids' II.8 and II.9.

Porphycenes as first example of a porphyrinoid containing only confused heterocyclic units was synthesized by McMurry coupling of 4',4"-diformyl thiophene. Selective lithiation of either 3-bromothiophene or 5,5'-dibromobithiophene was employed to synthesize the methyl substituted diformyl bithiophene, **II.10**. It was further subjected to McMurry coupling to yield the targeted porphycene **II.8** in 30% yields (scheme 1). Along with this macrocycle, its expanded congener bearing six thiophenes with three ethylene bridges, **II.9**, was also isolated in 3% yields.

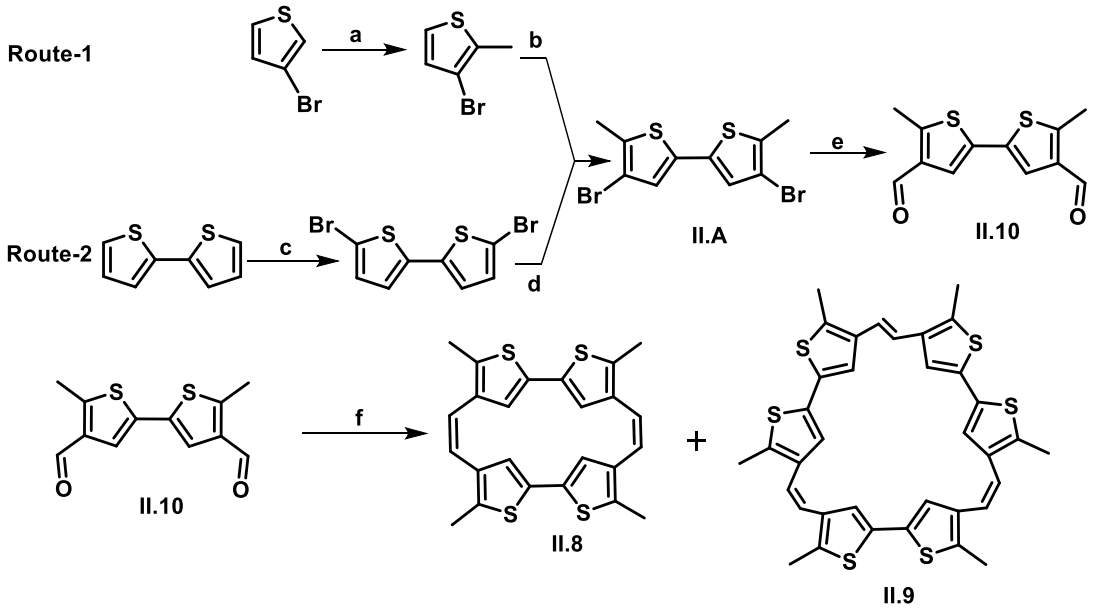

a: LDA, CH_3I in Dry THF, **b**: LDA, $CuCl_2$ in Dry THF, **c**: NBS in CH_3COOH and $CHCl_3$(1:1), **d**: LDA in Dry THF, CH_3I in Dry THF, **e**: n-BuLi, DMF in Dry THF, **f**: Zn, $TiCl_4$, CuCl, pyridine, Dry THF, Reflux

Scheme 1 Synthesis of Tetra S-Confused Porphycenes, **II.8** and **II.9.**

Structural Characterization of Tetra S-Confused Porphycenes:

The Tetra S-Confused Porphycenes, **II.8** and **II.9** were analyzed through high-resolution mass spectrometry (figure-II.1), UV-Vis, NMR Spectroscopy, X-ray crystallography, and cyclic volumetric studies.

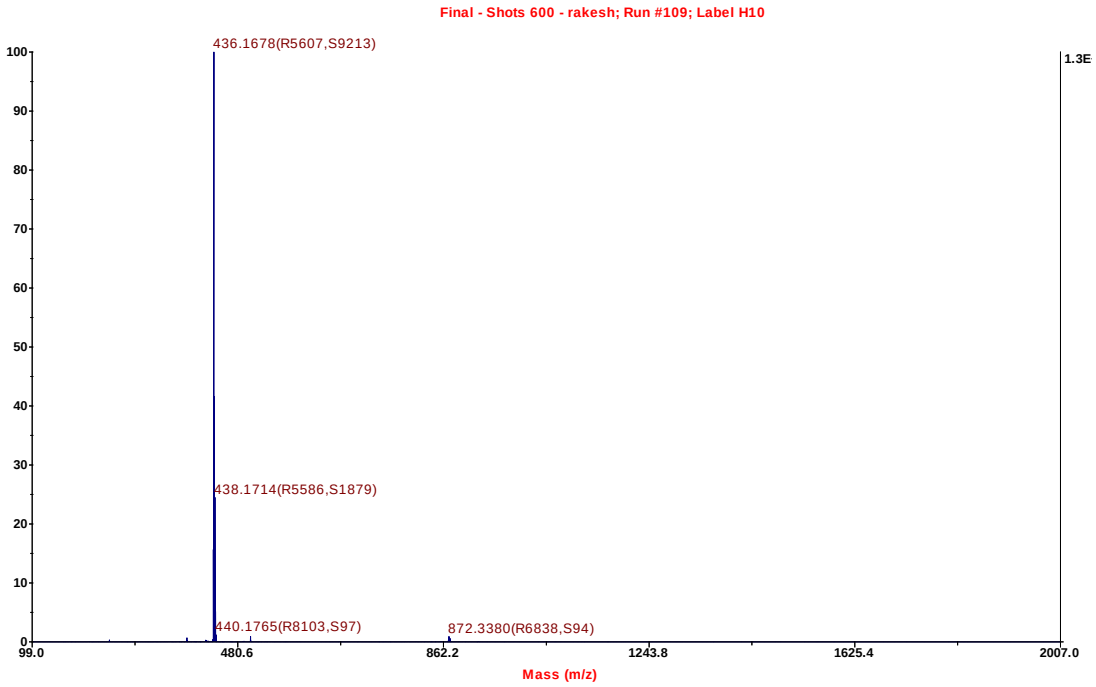

Figure 3 MALDI TOF/TOF mass spectrum of **II.8 (** Calculated mass for $C_{24}H_{20}S_4$ is 436.0448.)

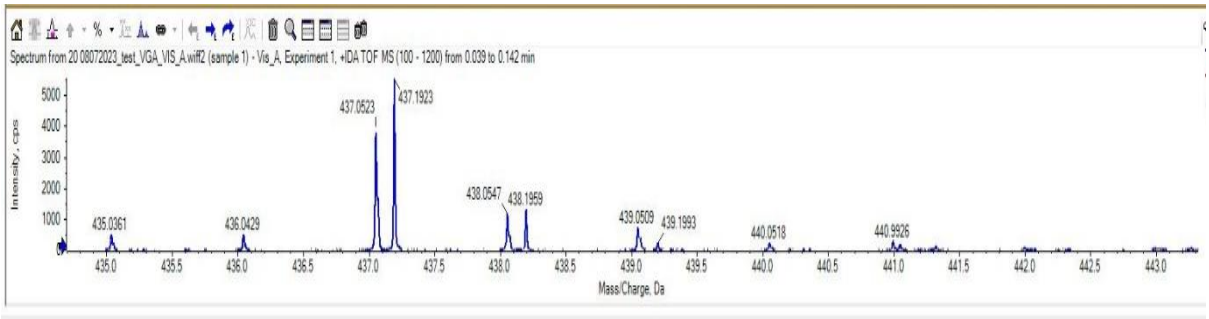

Figure 4 +IDA TOF mass spectrum of **II.8 (**Calculated mass for $C_{24}H_{20}S_4$ is 436.0448.).

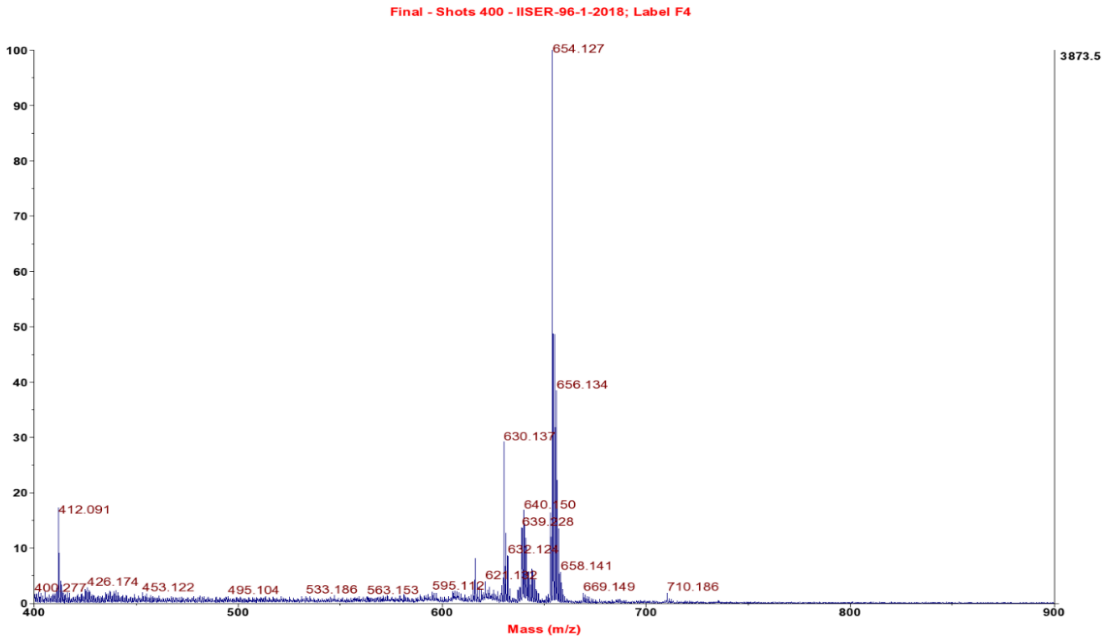

Figure 5 MALDI TOF/TOF mass spectrum of **II.9** (Calculated mass for $C_{36}H_{30}S_6$ is 654.0786.).

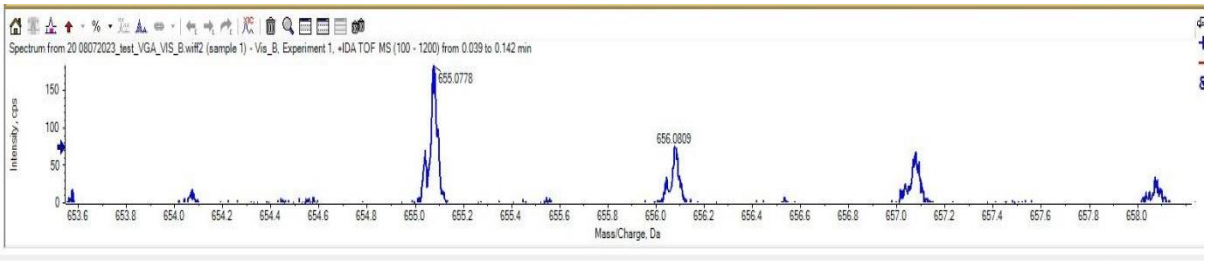

Figure 6 +IDA TOF mass spectrum of **II.9**(Calculated mass for $C_{36}H_{30}S_6$ is 654.0786.)

Based on the successful synthesis of these macrocycles, another strategy was designed to synthesize a hexathia porphycene with four confused thiophene units (**Scheme 2**). It is well established that lithiated halo thiophenes undergo "halogen dance" (HD) under basic conditions.[19] By utilizing HD conditions, the requisite precursor 4,4'-diformyl terthiophene, **II.11**, was synthesized from 5,5'-dibromoterthiophene in 65% yields. McMurry coupling of this dialdehyde, **II.11**, yielded the expected hexathia porphycene **II.12** in 13% yields (**Scheme 2**). The composition of all the macrocyclic products, **II.8**, **II.9,** and **II.12** were confirmed by mass spectrometry, which exhibited the expected molecular ion peak.

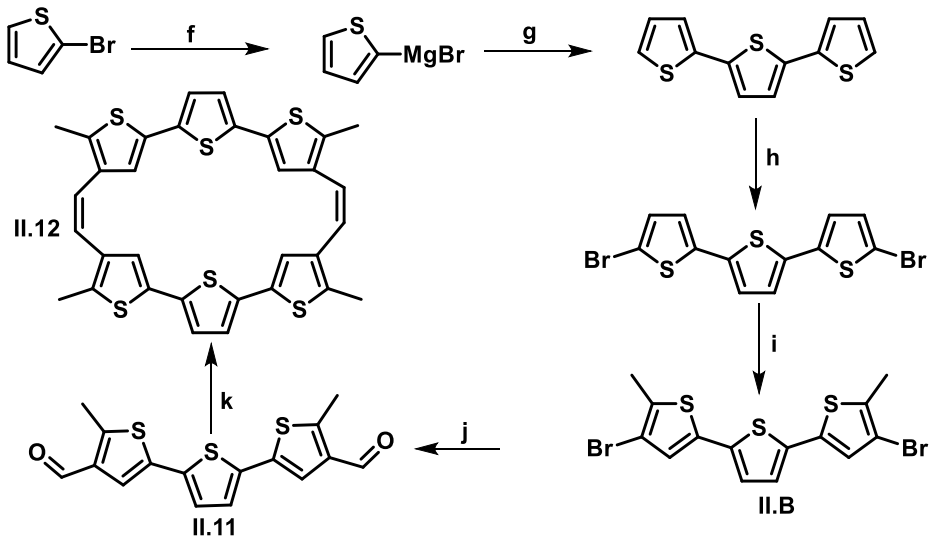

f = Mg, I_2 in Diethyl ether, **g** = 2,5-Dibromothiophene, $Ni(dppp)Cl_2$, **h** = NBS in CH_3COOH and $CHCl_3$ (1:1),reflux 45min, **i** = LDA, Dry THF, CH_3I, **j** = n-BuLi, DMF in Dry THF, **k** = Zn, $TiCl_4$, CuCl, pyridine in Dry THF.

Scheme 2 Synthesis of tetra S-Confused expanded porphycene, **II.12**.

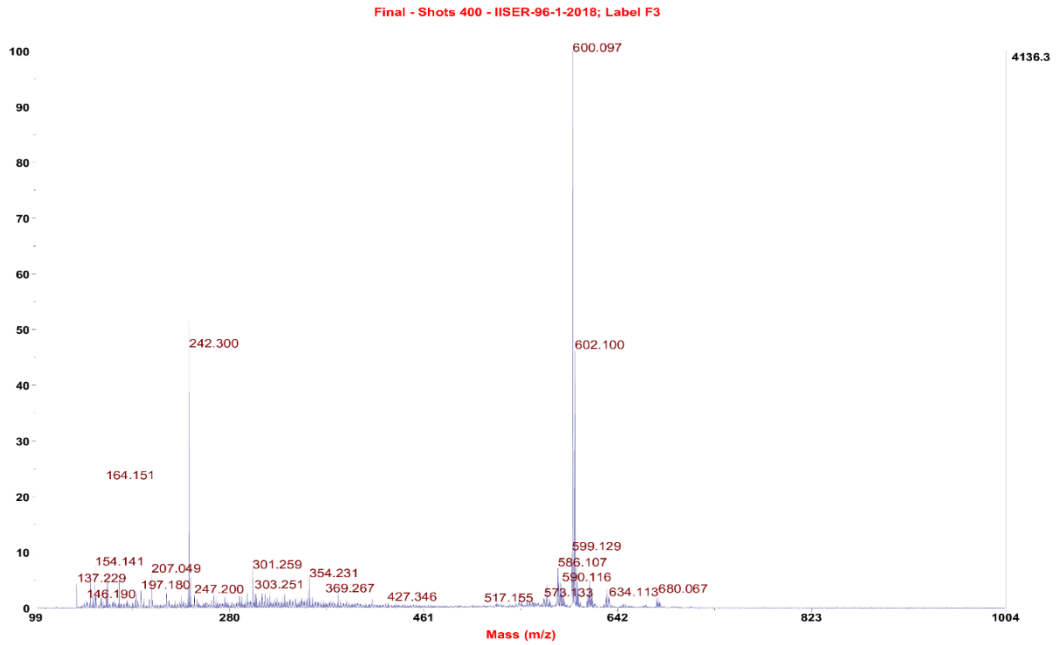

Figure 7 MALDI TOF/TOF mass spectrum of **II.12** (Calculated mass for $C_{32}H_{24}S_6$ is 600.0248).

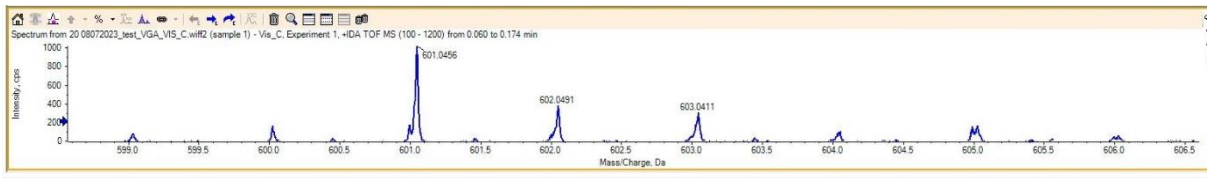

Figure 8 +IDA TOF mass spectrum of II.**12**(Calculated mass for $C_{32}H_{24}S_6$ is 600.0248).

Electronic absorption studies

The UV-Vis absorption spectrum of **II.8** displayed an uncharacteristic and high energy absorption at 300 nm (72100). In contrast to the parent 20π porphycene, the observed λ_{max} is blue-shifted by more than 30 nm, suggesting a weak overlap of the π orbitals. **II.9** and **II.12** also exhibited only a single absorption at 314 (56500) and 300 (40800), respectively, suggesting a feeble conjugation between the heterocyclic units.

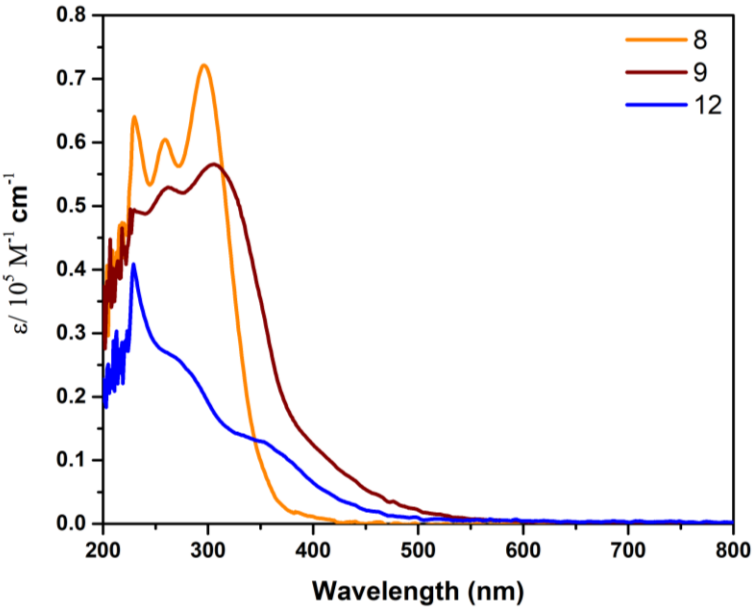

Figure 9 UV/vis absorption spectrum of **II.8**, **II.9,** and **II.12** in CH_2Cl_2.

NMR characterization

In contrast to the symmetrical ^{1}H NMR spectrum of **II.8**, the hexathia expanded porphycene **II.9** showed a ^{1}H NMR spectrum supporting its unsymmetrical molecular structure. Three sets of methyl protons were identified as singlets at δ 2.12, 2.48 and 2.50 ppm. Similarly, three different sets of β-CH of thiophenes were found to resonate as singlets at δ 6.91, 6.94 and 7.01 ppm. Two different conformations for the ethylene bridges were observed as a singlet at δ 6.72 ppm and as two doublets at δ 6.35 and 6.52 ppm. A coupling constant of 15 Hz further confirmed the *E* conformation of ethylene bridge protons. Based on the molecular structure, the ^{1}H NMR spectrum further confirmed two different ethylene bridges due to the *E* and *Z* conformation. In principle, **II.9** is a structural isomer and π-isoelectronic with the planar and aromatic 30π hexathia hexaphyrin. However, the chemical shift values observed for **II.9** do not comprehend a diatropic ring current expected of (4n +2)π systems.

This can be chiefly attributed to the structure-induced loss of planarity. In comparison with **II.9**, the other hexathia expanded porphycene **II.12** displayed a symmetrical ^{1}H NMR spectrum supporting the observed molecular structure. A singlet at δ 2.44 ppm was observed for the methyl protons. Three different singlets corresponding to the β-CH of the confused thiophenes, central thiophenes, and ethylene bridges were observed at δ 6.36, 6.88, and 7.11 ppm. These chemical shift values do not support the ring current effect for the formal 28π-electrons that can be counted for **II.12**. In tune with the molecular structure determined from X-ray crystallography, these chemical shift values did not reflect the paratropic ring current effect expected of 4nπ systems. An estimated Nucleus Independent Chemical Shift (NICS)[21] value of +1.4 ppm for **II.8** supports the diminished ring current due to loss of planarity and possibly due to the cross conjugation induced by confused thiophene rings. In fact, similar low NICS values of +0.25 and −1.25 ppm were estimated for hexathia porphycenes **II.9** and **II.12**.

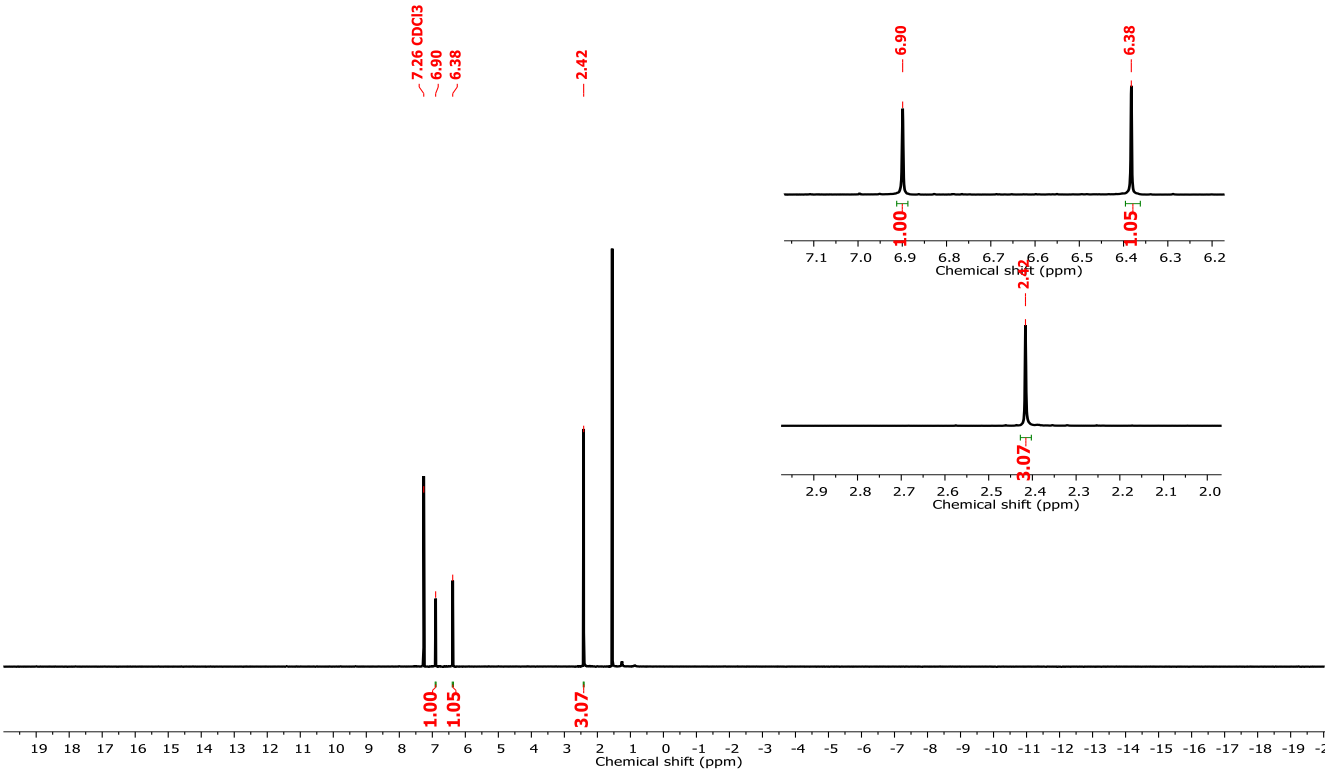

Figure 10 ^{1}H NMR Spectrum of **II.8** in $CDCl_3$.

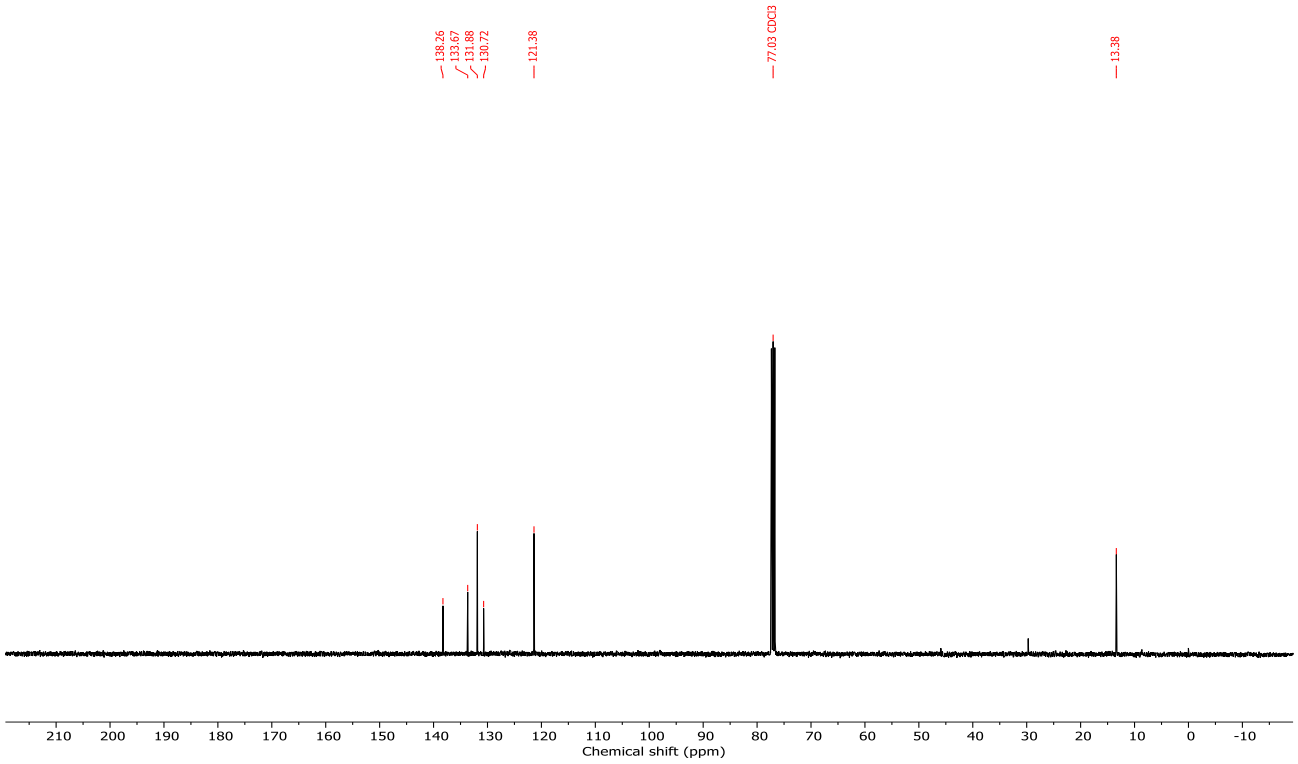

Figure 11 $^{13}C\{^{1}H\}$ NMR Spectrum of **II.8** in $CDCl_3$.

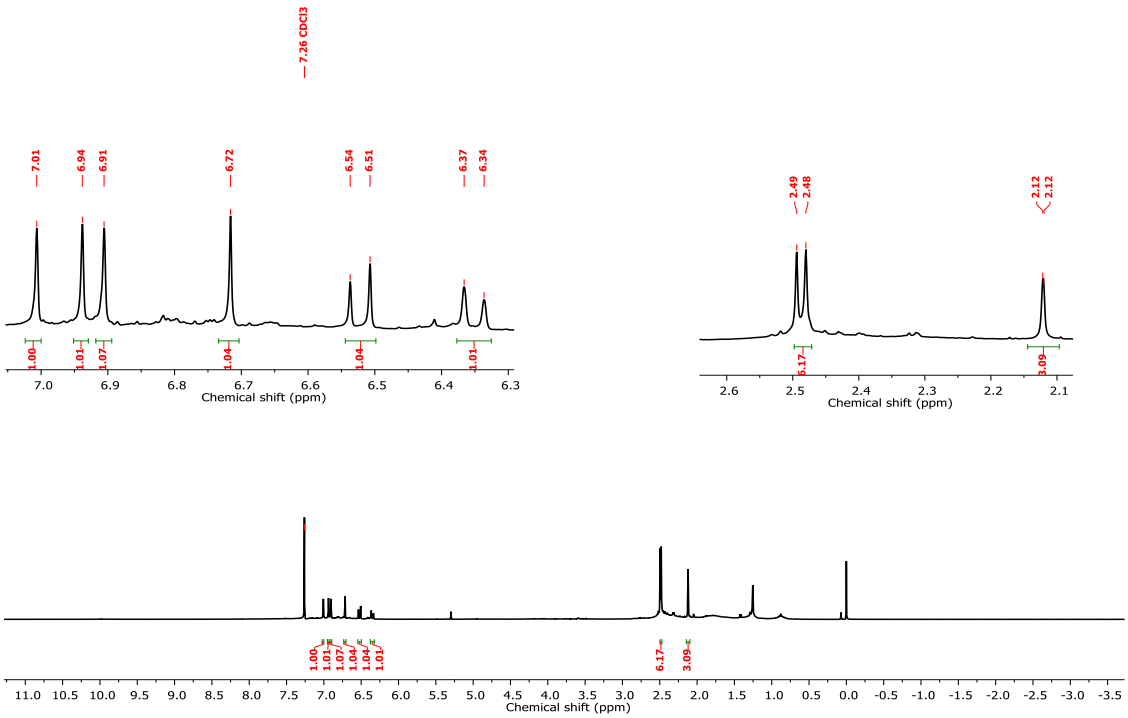

Figure 12 ^{1}H NMR Spectrum of **II.9** in $CDCl_3$.

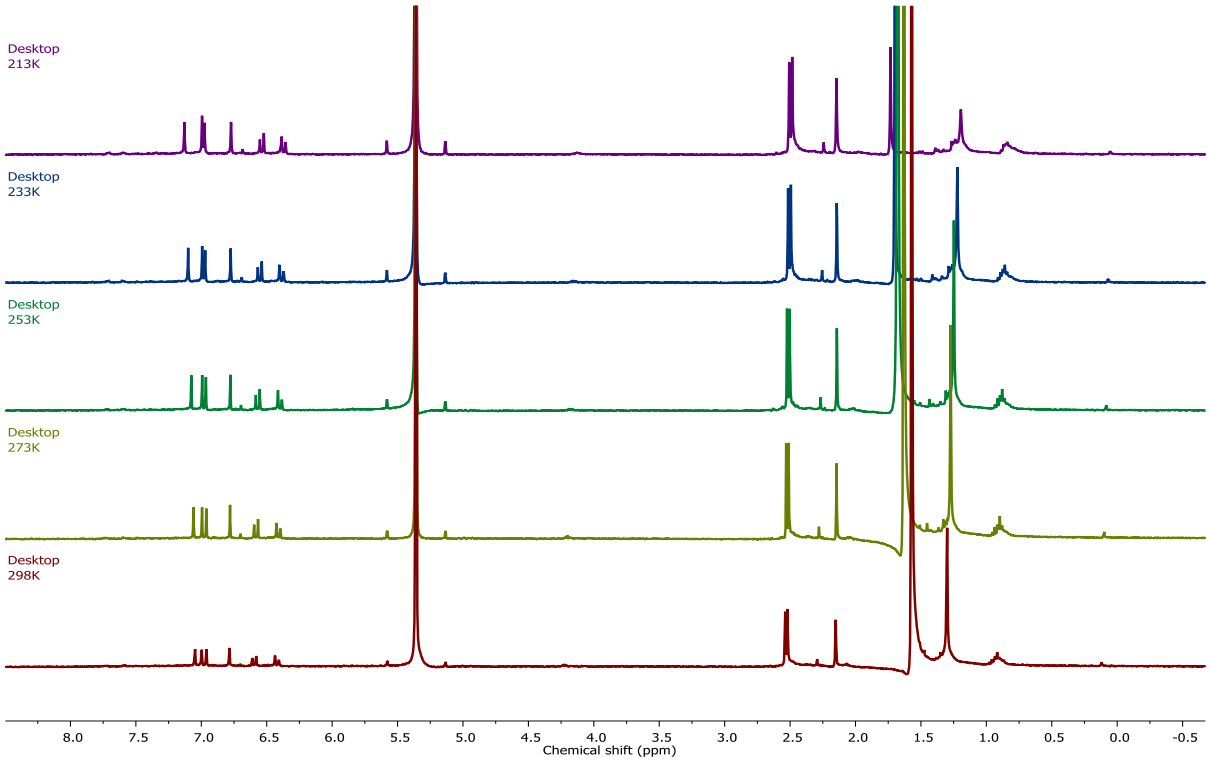

Figure 13 Variable Temperature ^{1}H NMR Spectra of **II.9** in Methanol-d_4.

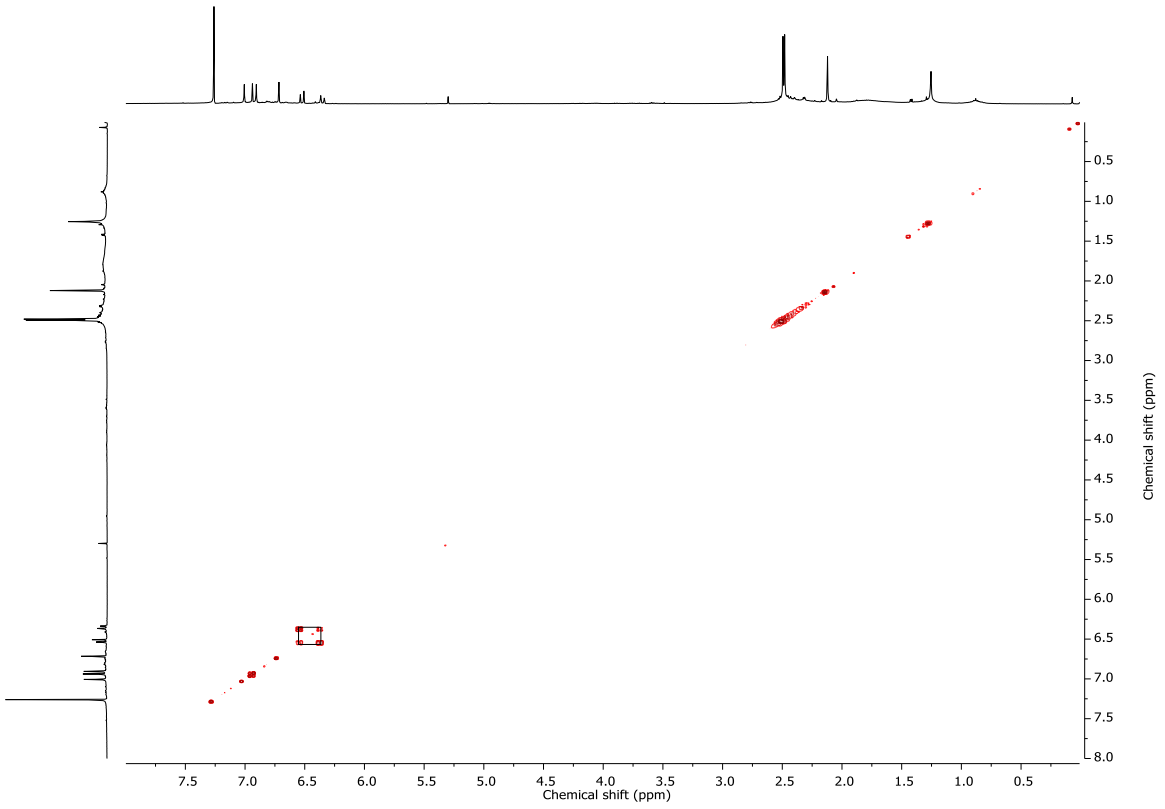

Figure 14 ^{1}H-^{1}H COSY Spectrum of **II.9** in $CDCl_3$.

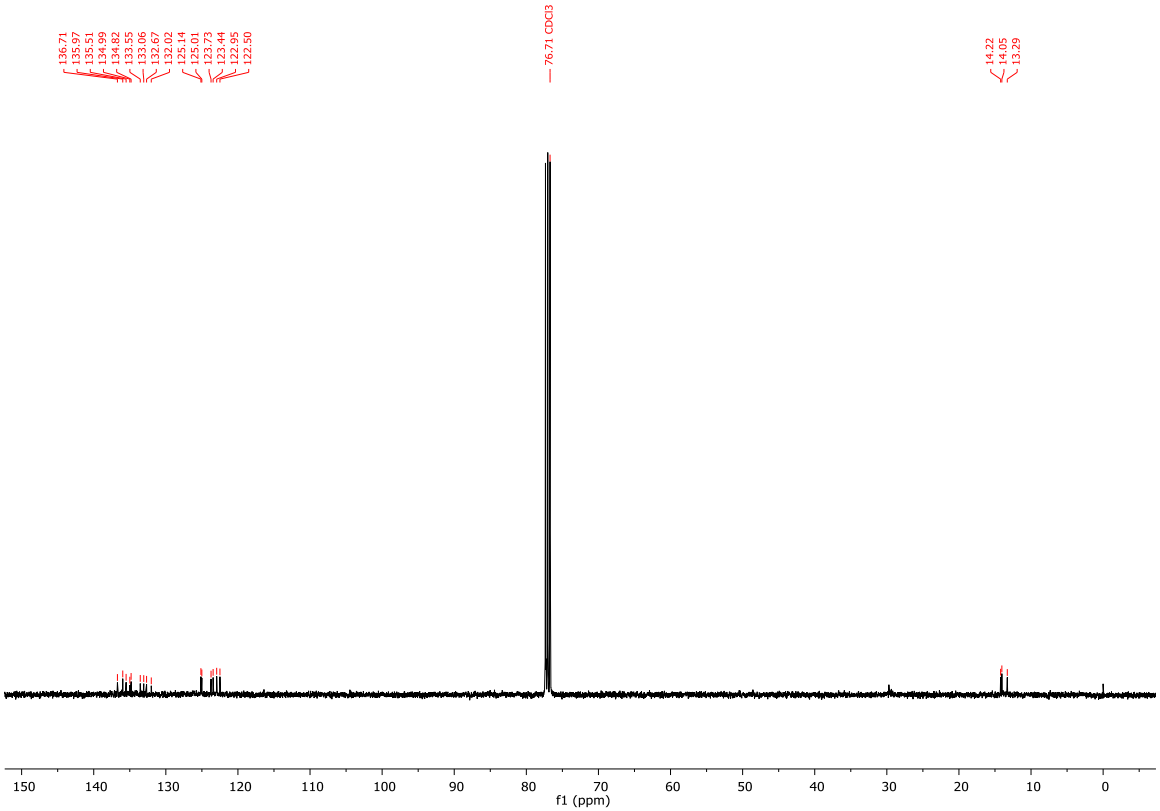

Figure 15 $^{13}C\{^{1}H\}$ NMR Spectrum of **II.9** in $CDCl_3$.

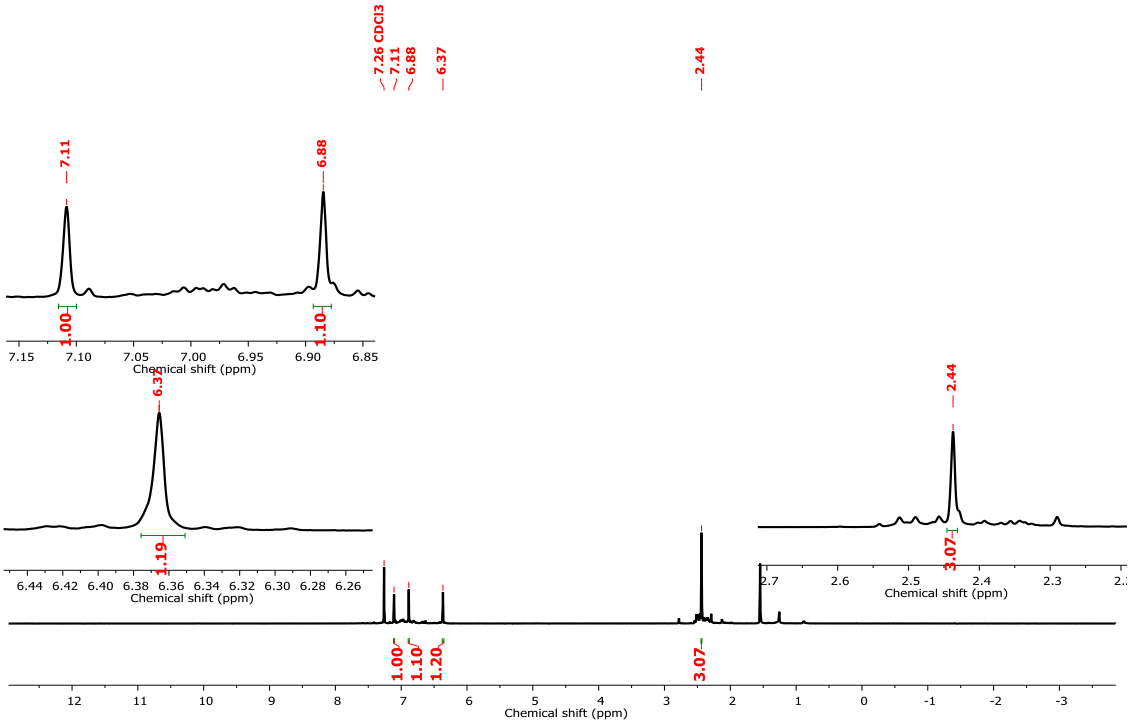

Figure 16 ^{1}H NMR Spectrum of **II.12** in $CDCl_3$.

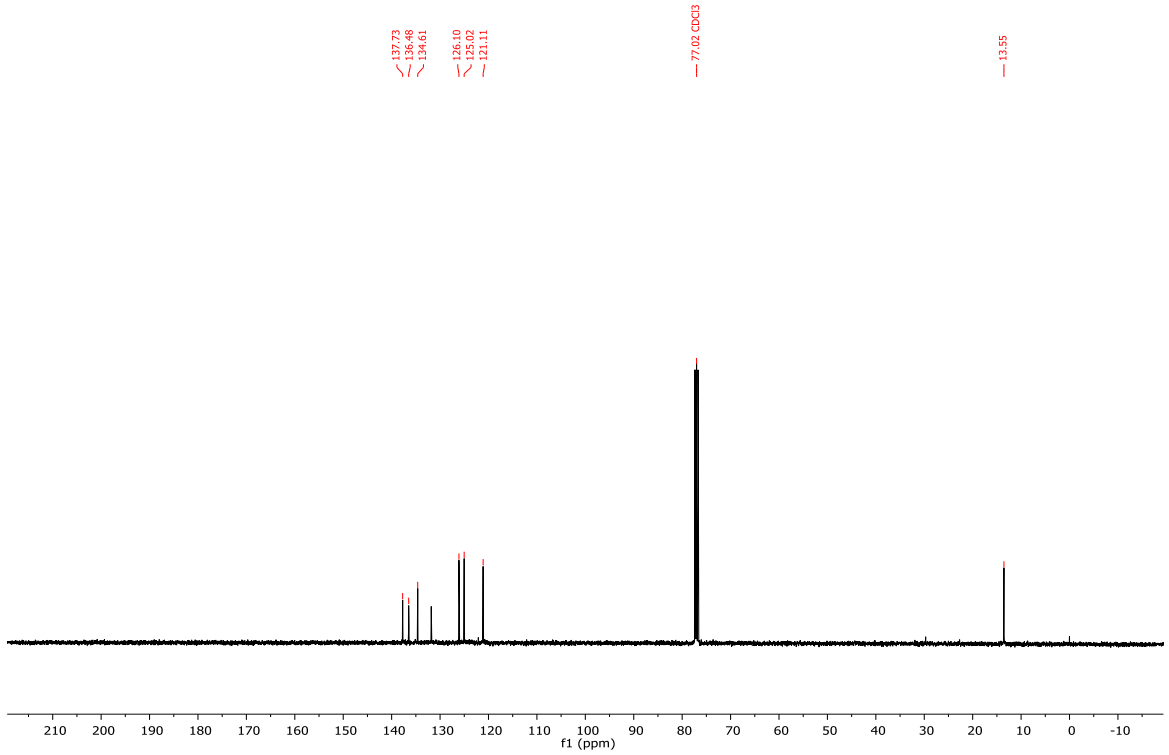

Figure 17 $^{13}C\{^{1}H\}$ NMR Spectrum of **II.12** in $CDCl_3$.

Single crystal X-ray diffraction analysis of Tetra S-Confused Porphycenes II.8, II.9, and II.12:

Furthermore, they were successfully characterized by single crystal X-ray diffraction analysis (**Fig.18**). Good quality crystals were grown by vapor diffusion of either hexane or methanol into a solution of the respective macrocycles in dichloromethane/chloroform. Tetra S-confused porphycene **II.8** revealed a non-planar structure for the macrocycle in which the core of the macrocycle has four β-CHs due to the 2,4-connectivity of the thiophene units (**Fig.18a** and **b**). Owing to the crowding of the cavity by four hydrogens, the macrocycle adopts a ruffled geometry. Both the ethylene bridges were found to be in the *Z* conformation and all the sulphur atoms were facing away from the macrocyclic cavity. A similar unsubstituted tetrathia porphycene was found to adopt a bowl-like conformation in the solid state.[17] In contrast to the symmetrical structure of **II.8**, the hexathia expanded porphycene **II.9** revealed severe distortions from a planar geometry (**Fig.18c** and **d**). In particular, one of the ethylene bridges adopted the *E* conformation while the other two resembled the *Z* conformation. However, in contrast to many expanded porphyrins,[20a,b] the hexathia porphycene **II.9** did not exhibit ring inverted structures. At least two thiophene rings adopted an orientation perpendicular to the macrocyclic plane which further results in the loss of the planar geometry for the macrocycle. The observed structure significantly differs from a similarly unsubstituted hexathia porphycene, which displayed only the *Z*

conformation for all the ethylene bridges.[17,18] By decreasing one of the ethylene bridges, the hexathia porphycene **II.12** adopts a near-planar geometry in the solid state (**Fig.18e** and **f**). Unlike **II.9**, the ethylene bridges of **II.12** adopt the *Z* conformation and the terminal thiophenes of the terthiophene retain the confused orientation, leading to four β-CHs in the center of the macrocycle. Similar to many terthiophene units, the central thiophene unit is oriented such that the S atom of the heterocycle is at the center of the macrocycle.

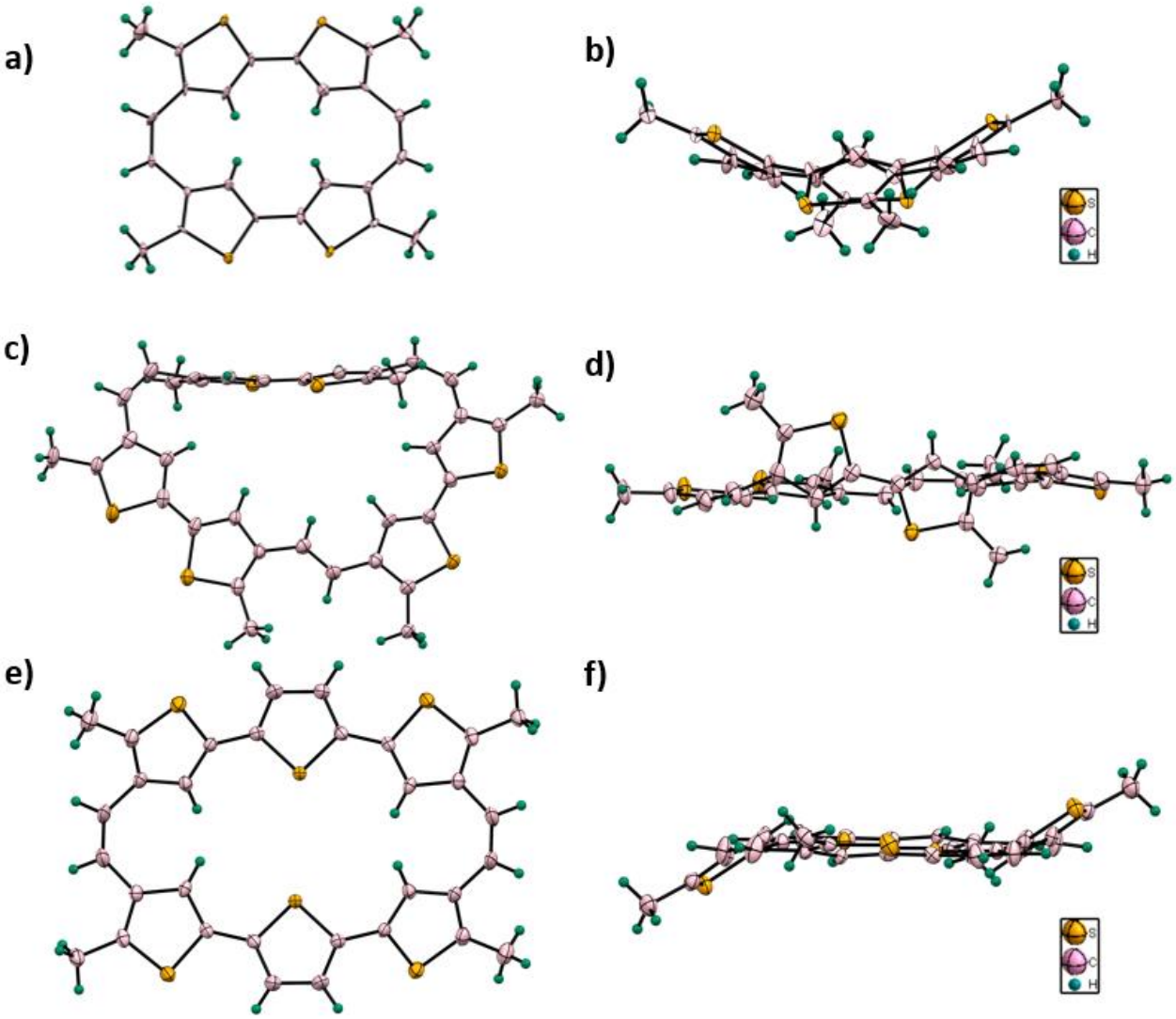

Figure 18. ORTEP plot of **II.8** (**a** and **b**), **II.9** (**c** and **d**) and **II.12** (**e** and **f**). Top view (**a, c** and **e**) and side view (**b, d** and **f**). Solvent molecules are omitted for clarity**.**

Cyclic voltammetry studies

Both anti-aromatic and non-aromatic porphyrinoids are known to undergo reversible two-electron ring oxidation. Consequently, it was anticipated that the synthesized Tetra S-confused porphycenes could be oxidized to yield dicationic species. However, cyclic voltammetric studies unveiled predominantly irreversible redox processes for compound **II.8**, **II.9**, and **II.12**. Specifically, the tetrathia S-confused porphycene **II.8** displayed only one oxidation peak at +1.10 V. Similarly, hexathia porphycene **II.9** exhibited two signals at +0.77 and -0.42 V. Even the near-planar hexathia porphycene **II.12** displayed three peaks at +0.78, -0.31, and -1.40 V. These cyclic voltammograms were found to be uncharacteristic of typical porphyrinoids.

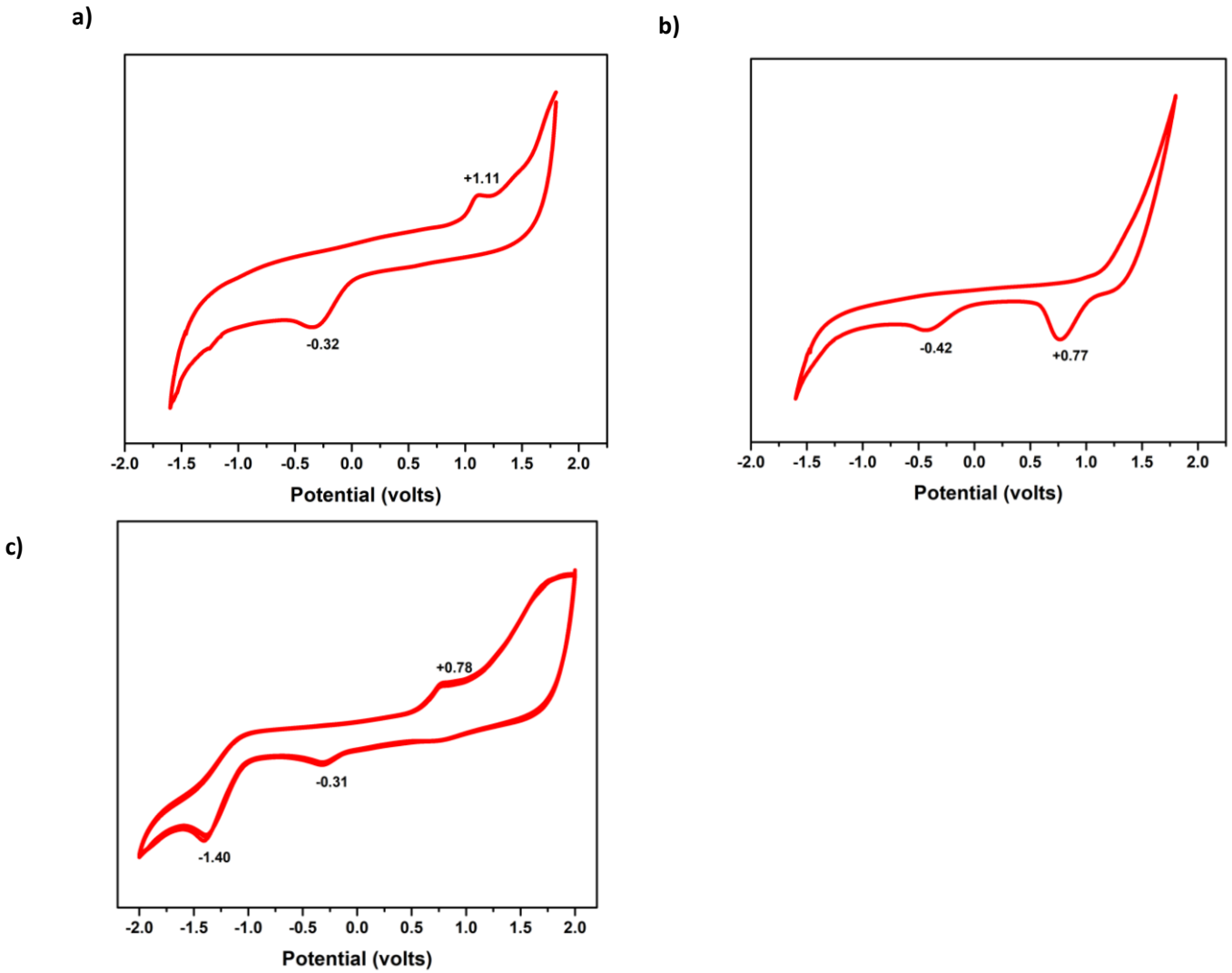

Figure 19 Cyclic voltammogram (CV) of **II.8**(a), **II.9**(b) and **II.12**(c) in CH_2Cl_2 (with 0.1 M $(Bu)_4NPF_6$ as the supporting electrolyte).

The observed electrochemical behavior suggests unique redox properties for these Tetra S-confused porphycenes, deviating from the expected reversible two-electron ring oxidation commonly associated

with 4n□ porphyrinoids. Further investigations into these distinctive redox processes will be crucial for a comprehensive understanding of their electronic properties and potential applications.

II.3 Synthesis and characterization of α-free 'Tetra S-Confused Porphyrinoids' II.14 and II.15.

Synthesis of α-free 'Tetra S-Confused Porphyrinoids' II.14 and II.15.

Similar to the above mentioned methodology, synthesis of α-free confused porphycenes was attempted via McMurry coupling of 4',4"-diformyl thiophene. The process involved the selective lithiation of either 3-bromothiophene or 5,5'-dibromobithiophene to obtain diformyl bithiophene, denoted as **II.13**. Subsequent McMurry coupling of dialdehyde, **II.13**, lead to the formation of the targeted porphycene **II.14** in 10% yields (**see Scheme 3**). Notably, in this reaction, an expanded congener bearing six thiophenes with three ethylene bridges, identified as **II.15**, was also isolated, albeit in less than 1% yields. This synthetic route showcases the versatility of the McMurry coupling and highlights the potential for obtaining structurally diverse porphycenes.

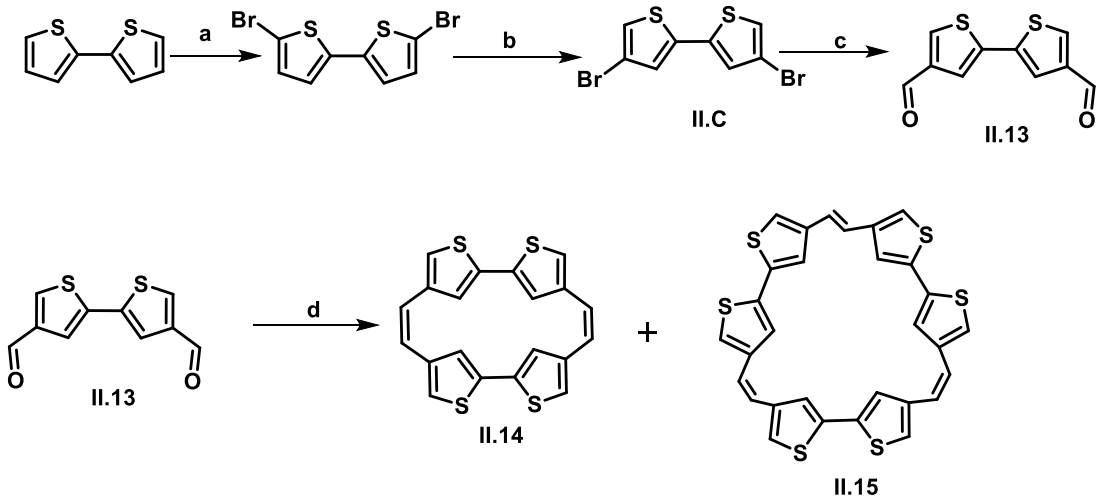

a: NBS in CH_3COOH and $CHCl_3$(1:1), **b**: LDA in Dry THF, CH_3OH in Dry THF, **c**: n-BuLi, DMF in Dry THF, **d**: Zn, $TiCl_4$, CuCl, pyridine, Dry THF, Reflux

Scheme 3 Synthesis of α-free Tetra S-Confused Porphycenes, **II.14** and **II.15.**

Single crystal X-ray diffraction analysis of α-free Tetra S-Confused Porphycenes, II.14 and II.15:

Furthermore, these compounds were successfully characterized through single crystal X-ray diffraction analysis (Fig.20). High-quality crystals were obtained through vapor diffusion of either hexane or methanol into the solution of the respective macrocycles in dichloromethane/chloroform. However, it was noted that in the case of α-free Tetra S-confused porphycene, the crystal data quality was not as optimal as observed for Tetra S-confused porphycenes. Despite this, the α-free Tetra S-confused porphycenes exhibited a similar non-planar structure to their methyl-substituted counterparts. The ethylene bridges were observed to adopt the same conformation as in the case of the methyl-substituted macrocycles **II.8** and **II.9**.

It is worth noting that, due to challenges in the purification process, the characterization of these two macrocycles using additional spectroscopic techniques such as NMR, UV-Vis, etc., was not feasible. The crystallographic analysis, however, provided valuable insights into the structural features of these compounds.

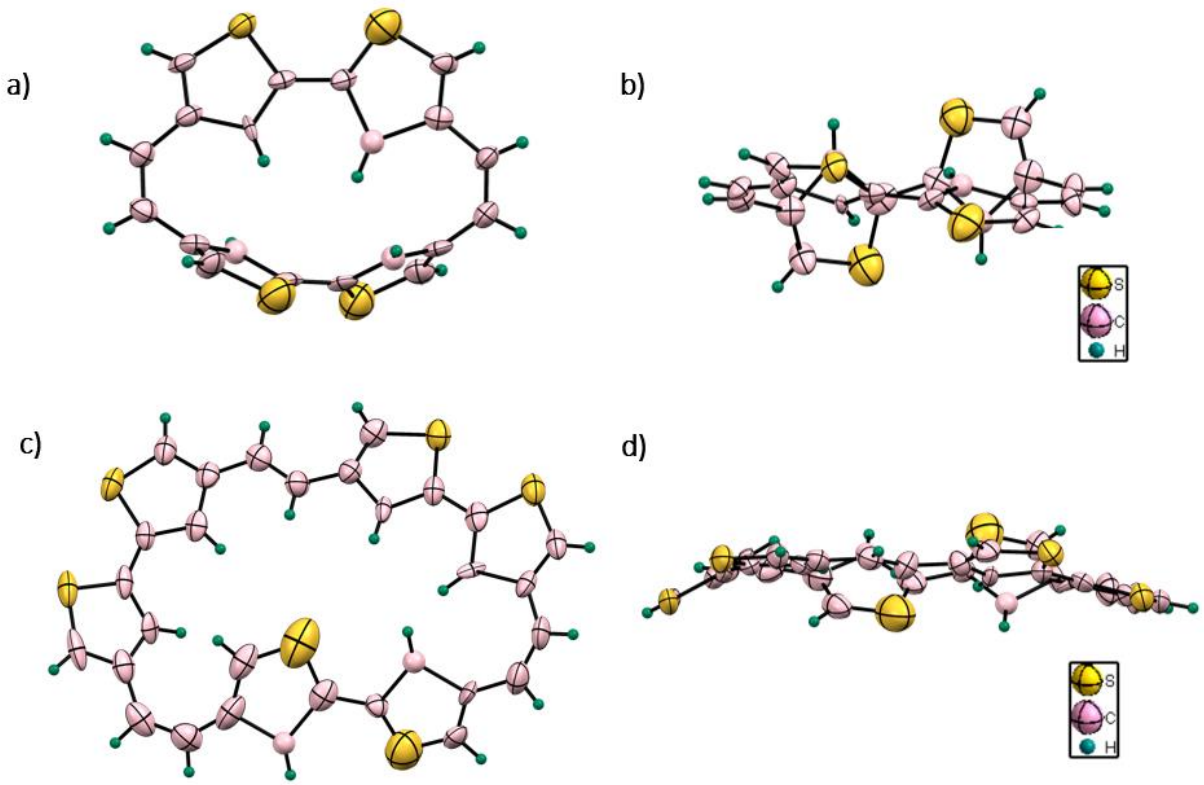

Figure 20 ORTEP plot of **II.14** (a and b) and **II.15** (c and d). Top view (a and c) and side view (b and d). Solvent molecules are omitted for clarity.

II.4 Quantum mechanical calculations:

Nucleus Independent Chemical Shift (NICS)

The aromaticity and anti-aromaticity of macrocycles **II.8**, **II.9**, **II.12**, **II.14**, and **II.15** were evaluated through quantum mechanical calculations using the Gaussian09 rev D program. Density Functional Theory (DFT) with Becke's three-parameter hybrid exchange functional (B3LYP) and a 6-31G (d, p) basis set for all atoms was employed. The optimized geometry structures were derived from single-crystal X-ray diffraction analysis. To measure aromaticity/anti-aromaticity, the negative of the calculated magnetic shielding at the center, known as "Nucleus Independent Chemical Shift" (NICS), was utilized. A negative NICS indicates aromatic characteristics, while a positive NICS suggests anti-aromatic features (refer to **Table II.1** for details). The NICS approach, introduced by Schleyer et al., provides a simple magnetic criterion for assessing cyclic conjugated systems when exposed to a magnetic field.

Macrocycle	NICS (0) ppm
8	**+1.4**
9	**+0.25**
12	**-1.25**
14	**+0.95**
15	**-1.65**

Table II.1: Estimated NICS values for macrocycles **II.8** to **II.15**.

Anisotropy of induced current density (ACID)

The Anisotropy of Induced-Current Density (ACID) emerges as a valuable criterion for assessing ring current effects within aromatic and anti-aromatic systems. This method proves effective in visualizing the ring current induced by the delocalized π electrons within the molecular structure. The ACID plots not only provide insights into the magnitude but also the direction of the ring current. These plots are generated when an external magnetic field is applied orthogonally to the mean macrocyclic plane. Utilizing the Continuously Applying Set of Gauge Transformation (CGST) methods, current density plots are obtained and then visualized using POVRAY 3.7 software for Windows. The ACID plot, depicting the flow of induced current, serves as a powerful tool for representing aromatic and anti-

aromatic characteristics. Specifically, a clockwise ring current within the ACID plot signifies the aromatic nature of the molecule, while anti-aromatic ring currents indicate the anti-aromatic nature of the given molecules (**Figure 21**).

Moreover, the ACID plot serves a dual purpose by offering a practical means to discern the pathway of delocalized π electrons within a cyclic conjugated system. The incorporation of arrows in the plot facilitates the determination of the direction in which these π electrons are distributed, adding an additional layer of interpretability to the analysis. This approach, combining theoretical calculations with visual representation, enhances our understanding of the electronic structure and aromaticity/anti-aromaticity in cyclic conjugated systems.

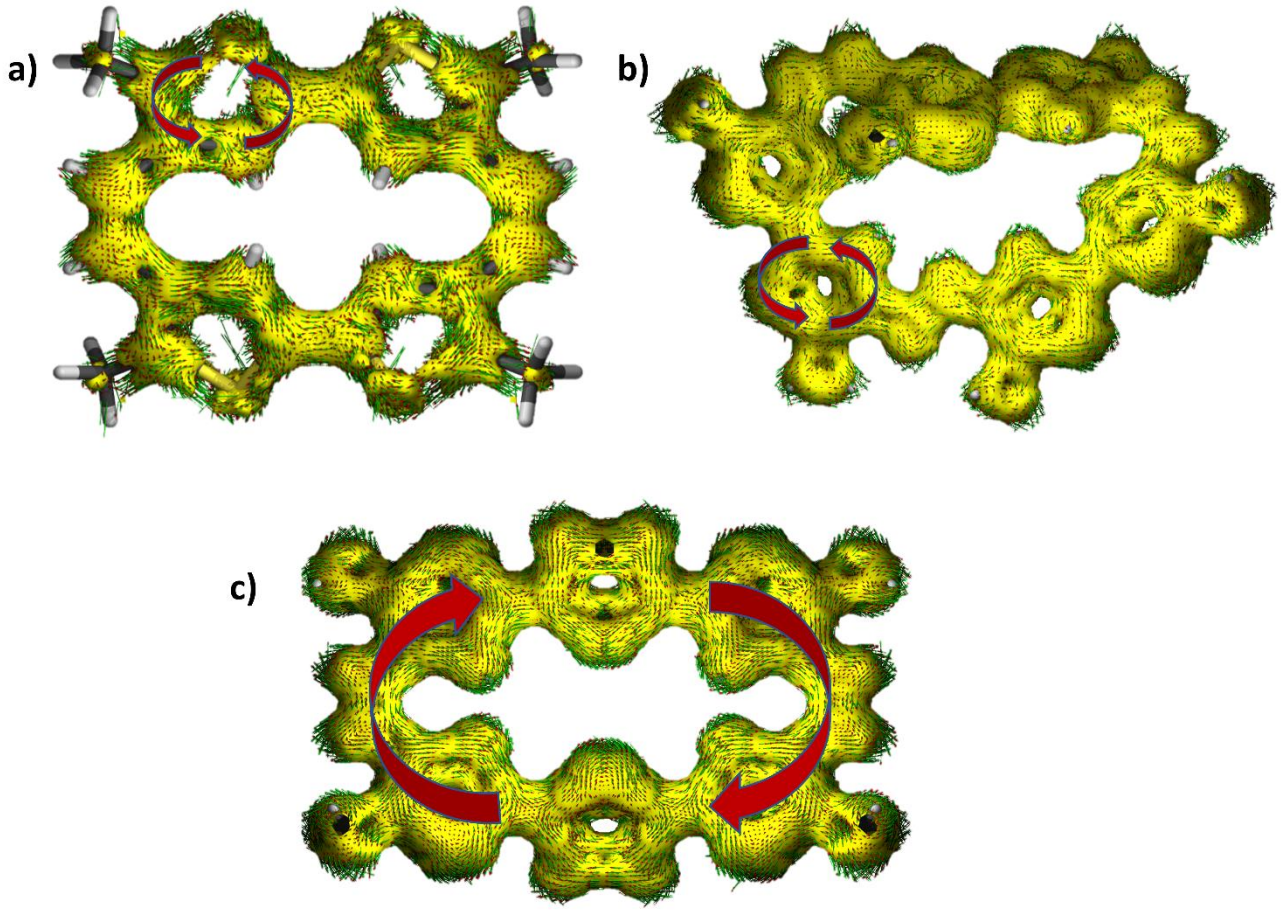

Fig.21A ACID plot for **II.8** (a), **II.9** (b) and **II.12** (c). At iso value 0.02, an external magnetic field is applied orthogonal to the macrocycle plane.

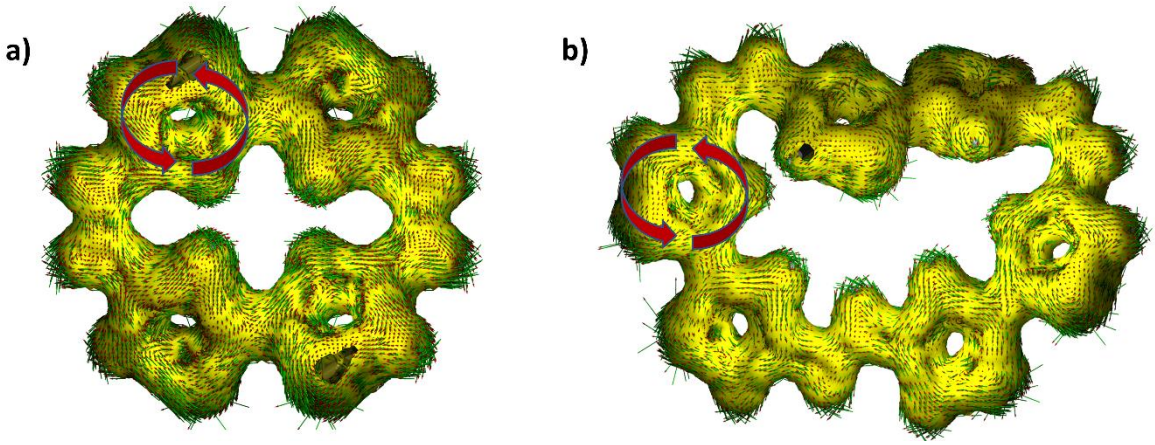

Fig.21B ACID plot for **II.14** (a), and **II.15** (b). At iso value 0.02, an external magnetic field is applied orthogonal to the macrocycle plane.

II.5 Cocrystallization of Isophlorin (II.8) with C60

Further support for the poor π-conjugation in 20π HCP **II.8** was obtained by co-crystallization with a C_{60} fullerene. Planar porphyrinoids are known to interact through π–π interactions without altering their topology.[25,26] An attempt was made to attain planarity by host–guest chemistry based on non-covalent interaction. A co-crystal of **II.8** with C_{60} fullerene was obtained which displayed a weak π- π interaction, as observed by the inter-planar distance of 3.657 Å at an angle of 22.87° between one thiophene unit of a macrocycle and C_{60} (Fig.23).

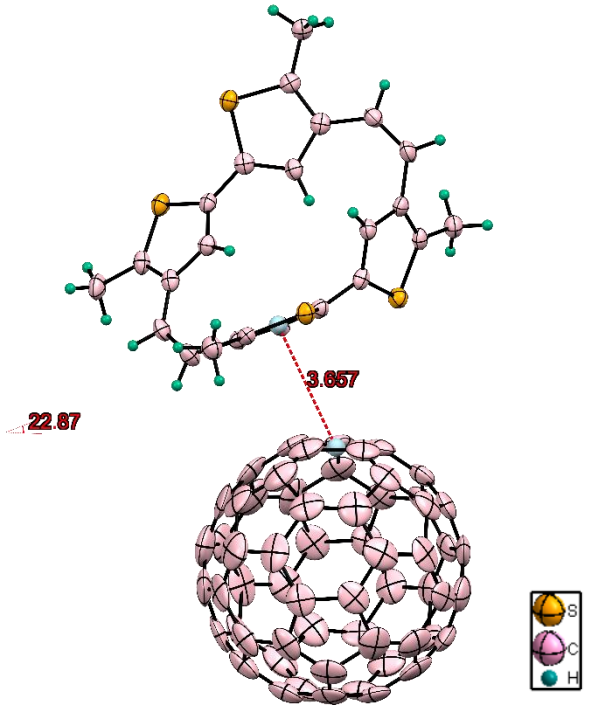

Figure 22 Co-crystal of **II.8** with C_{60}.

Crystal data: C_{60}, C_{24} H_{20} S_4, Monoclinic, space group P 21/n, a = 15.595(6), b = 17.734(7),c = 17.811(7)Å, α = 90, β = 108.212(9), γ = 90. V = 4679(3)Å3, Z = 4, T = 150(2) K, D_{calcd} = 1.643 g cm^{-3}, R_1 = 0.0938 (3542), R_w (all data) = 0.2646(10721), GOF = 0.971.

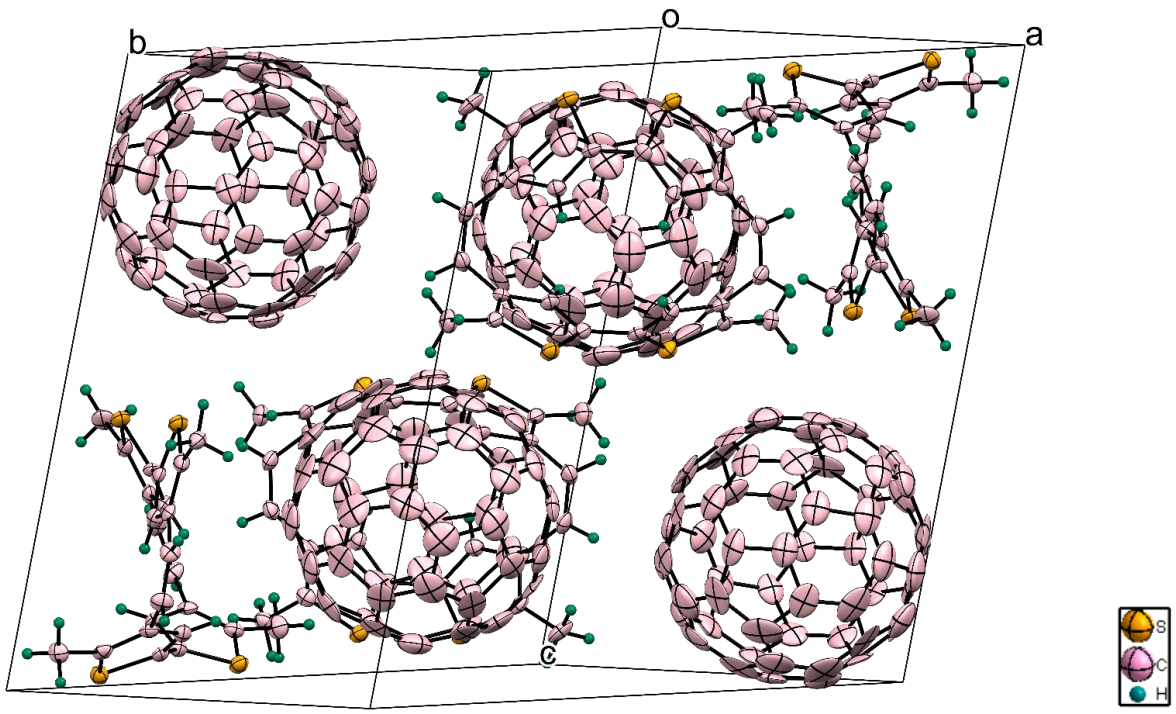

Figure 23 Crystal packing Co-crystal of **II.8** with C_{60}.

Conclusions

In conclusion, this study presents a pioneering example of a porphycene and expanded porphycenes comprised exclusively of confused heterocyclic units. Comprehensive analytical investigations affirm that tetra S-confused porphyrinoids exhibit a lack of aromaticity, potentially attributed to cross conjugation resulting from the 2,4-connectivity of the heterocyclic units. The introduction of alpha substitution on the confused thiophene effectively prevents the formation of an exocyclic keto group, thus sustaining the cross-conjugated π-network. Quantum chemical calculations provide additional support for the presence of a cross-conjugated π-network in the studied porphycene.

Remarkably, these macrocycles demonstrate that π-isoelectronic species can display modified electronic and redox properties. This groundbreaking finding opens new avenues for exploring the synthesis of porphyrinoids with distinct electronic characteristics. Notably, the study hints at the potential synthesis of the hypothetical hyper-confused tetra-pyrrolic porphyrin, a macrocycle that remains elusive but holds promise for future investigation.

Looking ahead, ongoing efforts are dedicated towards realizing the synthesis of the elusive hyper-confused tetra-pyrrolic porphyrin, building upon the insights gained from this research. It is anticipated that these findings will contribute significantly to the understanding of porphycene chemistry and inspire further advancements in the field of macrocyclic porphyrinoids.

Experimental Section

Experimental procedures involved the use of basic alumina and silica in glass columns for column chromatography. NMR analyses were conducted on a Bruker 400 MHz spectrometer, and chemical shifts were reported in ppm on the delta scale relative to $CHCl_3$ (7.28) or CD_2Cl_2 ($\delta = 5.51$). Electronic spectra were captured using a Perkin-Elmer λ-35 UV-Vis spectrophotometer and Shimadzu UV3600 UV/Vis/NIR spectrophotometer in an optical quartz cuvette with a 10 mm path length. High-Resolution Mass spectra (HRMS) were acquired through a WATERS G2 Synapt Mass Spectrometer.

For single-crystal diffraction analysis, a BRUKER KAPPA APEX II CCD Duo diffractometer with graphite monochromatic Mo Kα radiation ($\lambda = 0.71073$ Å) was utilized at 100K. In cases of disordered solvent molecules, the SQUEEZE utility in the PLATON software package was applied to eliminate contributions to scattering from these solvents. Crystallographic data can be accessed at the Cambridge Crystallographic Data Centre (CCDC) under deposition numbers 2255866 (**II.8**), 2255867 (**II.9**), 2256478 (**II.12**).

Cyclic voltammetry (CV) and Differential pulse voltammetry (DPV) measurements were carried out on a BAS electrochemical system in a three-electrode cell with dry CH_2Cl_2, and tetrabutylammonium perchlorate served as the supporting electrolyte. Measurements were conducted under an Argon atmosphere using a glassy carbon (working electrode), a platinum wire (counter electrode), and a saturated calomel (reference electrode). Calibration was performed using the ferrocene/ferrocenium couple.

Quantum mechanical calculations were executed using the Gaussian09 rev D program suite on the High-Performance Computing Cluster facility of IISER PUNE. Density Functional Theory (DFT) with Becke's three-parameter hybrid exchange functional and the Lee-Yang-Parr correlation functional (B3LYP) were employed, with a 6-31G(d, p) basis set for all atoms. Molecular structures from single-crystal analysis were employed for geometry optimization. Time-dependent TD-DFT calculations simulated steady-state absorption spectra, and molecular orbital contributions were analyzed using the GaussSum 2.2 program package. The global ring centers for NICS (0) values were determined at the non-weighted mean centers of the macrocycles, and NICS (0) values were obtained using the gauge-independent atomic orbital (GIAO) method based on optimized geometries.

Materials Synthesis methods:

All reactions involving air- or moisture-sensitive reagents were conducted in glassware thoroughly dried in a heating oven and under a nitrogen atmosphere unless specified otherwise. Anhydrous tetrahydrofuran (THF) was distilled from sodium-benzophenone to ensure its anhydrous state.

Reagents, procured at the highest commercial quality, were employed without additional purification unless explicitly mentioned. The reactions were carried out under magnetic stirring and monitored using thin-layer chromatography (TLC) with 0.15–0.2 mm pre-coated silica gel plates (10–40 μm), employing UV light or DNP solution (an aqueous solution of 2,4-Dinitrophenyl hydrazine, also known as Brady's reagent) with heating as visualizing and developing agents, respectively.

Dichloromethane (CH_2Cl_2) underwent a purification process by refluxing and distillation over P2O5 to remove impurities. The commercially available pyrrole and thiophene were subjected to fresh distillation prior to use to ensure their purity. All other reagents and solvents utilized in this study were of commercial reagent grade and were employed without additional purification steps. This approach maintains the quality and purity of the materials used in the experimental procedures.

Column chromatography, utilizing silica gel (100-200 mesh and 230–340 mesh), was employed for the purification of both precursor and target molecules (Macrocycles). NMR spectra were recorded on Bruker 400 spectrometers and calibrated using residual undeuterated solvent as an internal reference ($CDCl_3$ ^1H NMR δ = 7.26 ppm). The following abbreviations were used to denote multiplicities: s = singlet, d = doublet, t = triplet, q = quartet, m = multiplet, br = broad.

Synthesis of 4,4'-dibromo-5,5'-dimethyl-2,2'-bithiophene(II.A)

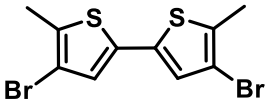

Route-1

Lithium diisopropylamide (LDA) was prepared by the addition of n-BuLi (1.6 M in hexanes, 0.017 mol, 10.7 mL) to a solution of diisopropylamine (0.02 mol, 2.07 g) in 25 mL of anhydrous THF (-78°C to room temperature). 3-Bromo-2-methyl thiophene (32.6 g, 200 mmol) was dissolved in dry THF and LDA (100 mL, 17.045 mmol) was added dropwise at −78 °C under an inert atmosphere. The solution was then stirred for 1.5 h at −78 °C. $CuCl_2$ (2.52 g, 18.75 mmol) was added and the reaction mixture was stirred overnight at room temperature. The reaction was quenched with a 1 M HCl solution, dichloromethane was added and the organic phase was washed with water (2×), dried over anhydrous $MgSO_4$, and filtered. The solvent was removed under reduced pressure and the crude product was purified by Column

chromatography (silica, *n*-hexane : dichloromethane, 4:1). After recrystallization from ethanol, 4,4'-dibromo-5,5'-dimethyl-2,2'-bithiophene was obtained as white crystals (85%).

Route-2 (via Halogen Dance reaction)

Took THF (50 ml) in a 2-necked RB and took it up to 0˚C followed by the addition of diisopropylamine (13.37 mmol) and n-BuLi(1.6 M in Hexane, 7.74ml) at 0˚C. Stirred it at the same temp for ½ hr then raised it to room temp for another ½ hr then decreased the temp to -78˚C and added 5,5'-dibromo-2,2'-bithiophene(4.9 mmol) dissolved in THF(150 ml), the solution becomes turbid then stirred it for additional 2 hr at the same temperature. Then raised the temp to -40˚C and stirred it for 4 hrs at this temp. After that added CH_3I (2.5 eq.) and then raised the temp up to room temp. and quenched the reaction with water and extracted with diethyl ether and dried over Na_2SO_4 and after evaporation under reduced pressure recrystallized with MeOH which gives a brown color solid of 4,4'-dibromo-5,5'-dimethyl-2,2',-bithiophene(95%).

^{1}H NMR (400 MHz, $CDCl_3$), δ (ppm): 6.89 (s, 2H), 2.38 (s, 6H).

^{13}C{^{1}H} NMR (101 MHz, $CDCl_3$) δ 133.6, 133.5, 125.9, 109.6, 14.8.

Synthesis of 4,4'-dialdehyde-5,5'-dimethyl-2,2'-bithiophene (II.10)

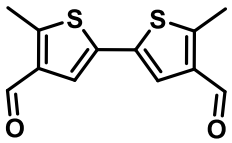

In a two-neck 250 ml RB flask with 60 ml to THF was cooled to -78˚C then n-BuLi (18 mmol, 1.6 M in Hexane) was added to the RB. 4,4'-dibromo-5,5'-dimethyl-2,2'-bithiophene (8 mmol, 3 g) dissolved in THF(100 ml) was added dropwise over a course of time approximately 1 hr. The mixture was then stirred for an additional 3 hours at -78˚C, followed by the addition of N, N-Dimethyl formamide (30 mmol, 2.5 g) in one portion after which the reaction mixture was stirred at the same temperature for 1 hr then allowed to reach the room temperature. A saturated solution of $NaHCO_3$ (100 ml) was then added followed by the addition of conc. HCl in ice until bubbles started to form. The

organic layer was evaporated and recrystallized with toluene to give a brown solid as a pure product (60%).

^{1}H NMR (400 MHz, $CDCl_3$), δ (ppm): 9.99 (s, 2H), 7.37 (s, 2H), 2.78 (s, 6H).

^{13}C{^{1}H} NMR (101 MHz, $CDCl_3$) δ 184.1, 151.5, 137.7, 133.2, 123.2, 13.6.

Synthesis of Tetrathiaporphycene (II.8) and Hexathiaporphycene (II.9).

A solution of $TiCl_4$ (20 mmol, 3.8 g) was added in THF at 0˚C temperature followed by Zn/CuCl mixture under nitrogen with reflux over a period of 2 hrs. It was followed by addition of pyridine with reflux over a period of 2.30 hrs. To the above gently refluxing suspension was added by syringe a solution of 4,4'-dialdehyde-5,5'-dimethyl-2,2'-bithiophene (500 mg, 2 mmol) in 150 mL of THF. After refluxing for 50-54 h, the reaction mixture was cooled to room temperature. Then a quenching solution of K_2CO_3 (10%) was carefully introduced with stirring. The reaction mixture was filtered and the filtrate was concentrated under reduced pressure. The residue was extracted with CH_2C1_2 (300 mL), and the extract was washed with water (twice, 100 mL each) and dried over anhydrous Na_2S0_4, and the solvent was removed in vacuo. The residue was subjected to column chromatography (silica, CH_2Cl_2) and the front running band give yellow crystalline tetrathiaporphycene (**II.8**) as the first fraction;(30%);

^{1}H NMR (400 MHz, $CDCl_3$), δ (ppm): 6.90 (s, 4H), 6.38 (s, 4H), 2.42 (s, 12H);

^{13}C{^{1}H} NMR (101 MHz, $CDCl_3$) δ 138.3, 133.7, 131.9, 130.7, 121.4, 13.4; UV-vis λ_{max} (nm) (ε) $Lmol^{-1}cm^{-1}$ (in CH_2C1_2) 300(72100);

MALDI TOF/TOF mass spectra calculated for $C_{24}H_{20}S_4$ is 436.0448, found 436.1976.

HR-MS (IDF-TOF: m/z = 437.0523(found [M]+H) (Calculated mass for $C_{24}H_{20}S_4$ is 436.0448.)

Crystal data: $C_{24}H_{20}S_4$, Monoclinic, space group C 2/c, a = 23.035(4), b = 4.0257(6), c = 23.664(4)Å, α=90, β= 114.896(4), γ=90. V = 1990.6(5) $Å^3$, Z = 4, T=150(2) K, D_{calcd} = 1.457 g cm^{-3}, R_1 = 0.0401 (1836), Rw (all data) = 0.0989(2520), GOF = 1.022.

The second fraction afforded light red crystalline annulene **(II.9)** (3.6%);

^{1}H NMR (400 MHz, $CDCl_3$), δ (ppm): 7.01 (s, 2H), 6.94(s, 2H), 6.91 (s, 2H), 6.72 (s, 2H), 6.54-6.51 (d, 2H, *J*=12Hz), 6.37-6.34 (d, 2H, *J*=12Hz), 2.50 (s, 6H), 2.48 (s, 6H), 2.12 (s, 6H);

^{13}C{^{1}H} NMR (101 MHz, $CDCl_3$) δ 136.7, 135.9, 135.5, 134.9, 134.8, 133.5, 133.1, 132.7, 132.0, 125.1, 125.0, 123.7, 123.4, 122.9, 122.5, 14.2, 14.1, 13.3;

UV-vis λ_{max} (nm)(ε) $Lmol^{-1}cm^{-1}$ (in CH_2C1_2) 314(56500);

MALDI TOF/TOF mass spectra calculated for $C_{36}H_{30}S_6$ is 654.0786, found 654.2856.

HR-MS (IDF-TOF: m/z = 655.0778(found [M]+H) (Calculated mass for $C_{36}H_{30}S_6$ is 654.0786.)

Crystal data: $C_{36}H_{30}S_6$, Triclinic, space group P -1, a = 5.446(3), b = 12.775(6), c = 22.985(10)Å, α = 76.667(15), β = 88.760(15), γ= 81.168(15). V = 1537.4(13)$Å^3$, Z = 2, T=150(2) K, D_{calcd} = 1.415 g cm^{-3}, R_1 = 0.0800 (2993), Rw (all data) = 0.2278(7543), GOF = 0.885.

Synthesis of 4,4''-dibromo-5,5''-dimethyl-2,2',-terthiophene (II.B) (via Halogen Dancing reaction)

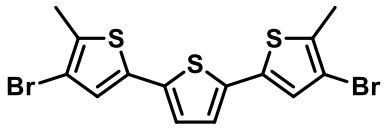

Took THF (50 ml) in a 2-necked RB and took it up to 0˚C followed by the addition of diisopropylamine (1.363 g, 13.37 mmol) and n-BuLi (1.6 M in Hexane, 7.74ml) at 0˚ C. Stirred it at the same temp for half an hour and then raised to room temp for another half an hour. The temperature was further decreased the temp to -78˚ C and added 5,5''-dibromo-2,2',-terthiophene(2 g, 4.9 mmol) dissolved in THF(150 ml). The solution turned turbid and stirring continued for additional 2 hrs at the same temperature. Temperature was then raised to -40° C and stirred it for 4 hrs at this temp. Then, CH_3I (2.5 equiv.) was added followed by warming the reaction mixture to room temp. The reaction was then quenched with water and extracted with diethyl ether and dried over Na_2SO_4. The resulting organic

layer was evaporation under reduced pressure to obtain a solid, which was recrystallized with MeOH to yield a brown colored solid of 4,4''-dibromo-5,5''-dimethyl-2,2',-terthiophene(94%).

^{1}H NMR (400 MHz, $CDCl_3$), δ (ppm): 6.98 (s, 2H), 6.96 (s, 2H), 2.39 (s, 6H).

^{13}C{^{1}H} NMR (101 MHz, $CDCl_3$) δ 135.5, 133.9, 133.5, 126.0, 124.2, 109.7, 14.8.

Synthesis of 4,4''-dialdehyde-5,5''-dimethyl-2,2',-terthiophene(II.11)

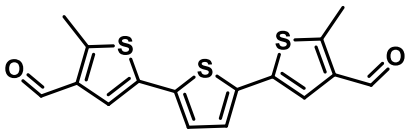

THF (50 ml) in a 2-necked RB flask was cooled to -78˚C to which n-BuLi (15.42 mmol, 1.6 M in Hexane) was added followed by 4,4''-dibromo-5,5''-dimethyl-2,2',-terthiophene (4.6 mmol, 2 g) dissolved in THF. The solution turns turbid and was stirred for 2 hrs at the same temperature. Then DMF (1.308 g) was added dropwise over a period of half an hour and continued stirring at the same temp. for another 1 hour. The reaction mixture was warmed up to room temperature, to which a saturated solution of $NaHCO_3$(100 ml) was then added followed by the addition of conc. HCl in ice until bubbles started to form. The organic layer was evaporated and recrystallized with toluene to give a brown solid as the pure product (65%).

^{1}H NMR (400 MHz, $CDCl_3$), δ (ppm): 9.99 (s, 2H), 7.40 (s, 2H), 7.03 (s, 2H), 2.78 (s, 6H).

^{13}C{^{1}H} NMR (101 MHz, $CDCl_3$) δ 184.2, 151.1, 137.7, 135.5, 133.9, 124.9, 122.7, 13.6.

Synthesis of Hexathiahomoporphycene (II.12)

A solution of $TiCl_4$ (15.06mmol, 2.8 g) was added in THF at 0˚C temperature followed by Zn/CuCl mixture (1.96/0.298 g) under nitrogen with reflux over a period of 2 hrs. Pyridine (1.2 ml) was then added to the reaction mixture with reflux over a period of 2.30 hrs. To the above gently refluxing suspension was added by syringe a solution of 4,4'-dialdehyde-5,5'-dimethyl-2,2'-bithiophene (500

mg, 1.5 mmol) and in 150 mL of THF. After refluxing for 50-54 h, the reaction mixture was cooled to room temperature. The reaction was carefully quenched by slow addition of aqueous K_2CO_3 (10%) with continuous stirring. The reaction mixture was then filtered and the filtrate was concentrated under reduced pressure. The residue was extracted with CH_2C1_2 (300 mL), and the extract was washed with water (twice, 100 mL each) and dried over anhydrous Na_2S0_4, and the solvent was removed in vacuo. The residue was subjected to column chromatography (silica, CH_2CI_2) and the front running band give orange color crystalline Hexathiahomoporphycene (**12**) as the first fraction;(30%);

^{1}H NMR (400 MHz, $CDCl_3$), δ (ppm): 7.11 (s, 4H), 6.88 (s, 4H), 6.37 (s, 4H), 2.44 (s, 12H);

^{13}C{^{1}H} NMR (101 MHz, $CDCl_3$) δ 137.7, 136.5, 134.6, 126.1, 125.0, 121.1, 13.6;

UV-vis λ_{max} (nm) (ε) $Lmol^{-1}cm^{-1}$ (in CH_2C1_2) 300 (40800);

MALDI TOF/TOF mass spectra calculated for $C_{32}H_{24}S_6$ is 600.0248, found 600.1548.

HR-MS (IDF-TOF: m/z = 601.0456{found [M]+H}(Calculated mass for $C_{32}H_{24}S_6$ is 600.0248).

Crystal data: $C_{32}H_{24}S_6$, Triclinic, space group P 21/c, a = 7.3422(16), b = 14.469(3), c = 13.051(3)Å, α = 90, β = 102.207(7), γ= 90. V = 1355.1(5)Å3, Z = 2, T=150(2) K, D_{calcd} = 1.473 g cm^{-3}, R_1 = 0.0551 (2240), Rw (all data) = 0.1724(3388), GOF = 1.025.

Synthesis of II.C, II.13, II.14, and II.15.

A comparable synthetic approach was employed for the synthesis of another precursor, denoted as II.C, utilizing a halogen-dancing strategy. In contrast to the use of a methylating agent (CH_3I), this method involved the use of methanol (CH_3OH). The II.C underwent a formylation reaction, resulting in the formation of precursor II.13. Subsequent to this, a McMurry coupling reaction was carried out (similar to the synthesis of **II.8** and **II.9**), leading to the generation of α-free Tetra S-Confused Porphycenes, specifically II.14 and II.15. This synthetic strategy demonstrates versatility in achieving diverse molecular structures through strategic modifications in the reaction pathways.

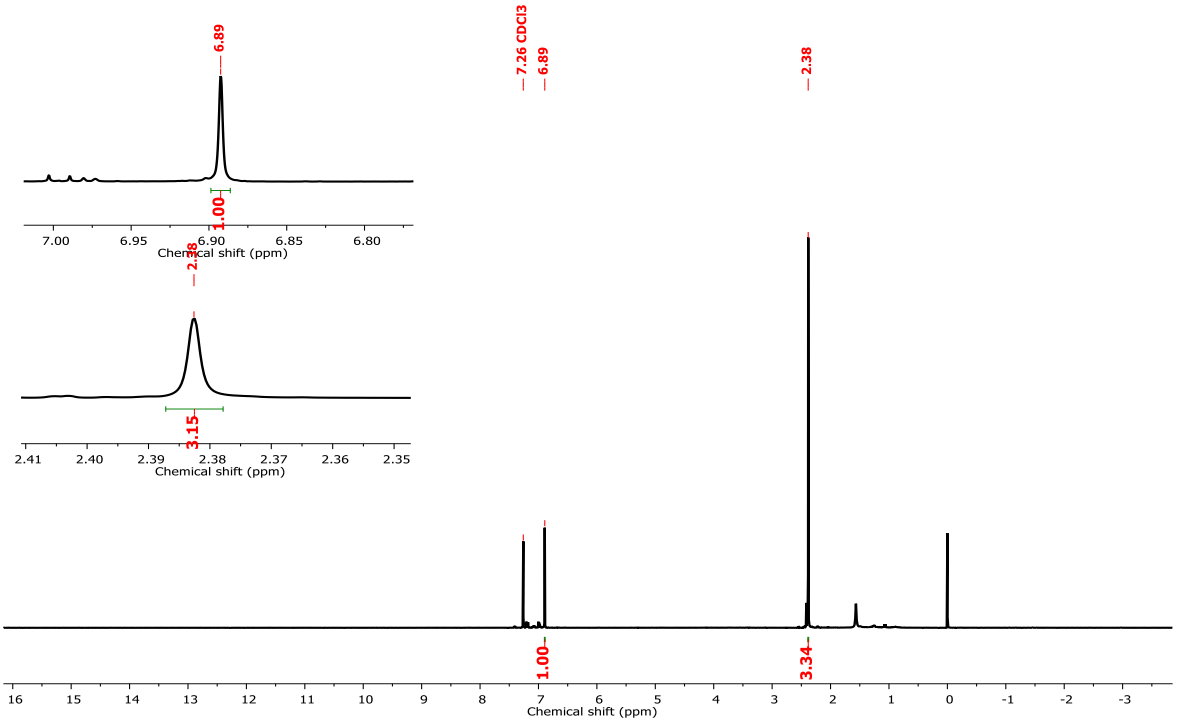

S8: ^{1}H NMR spectrum of **A** in $CDCl_3$.

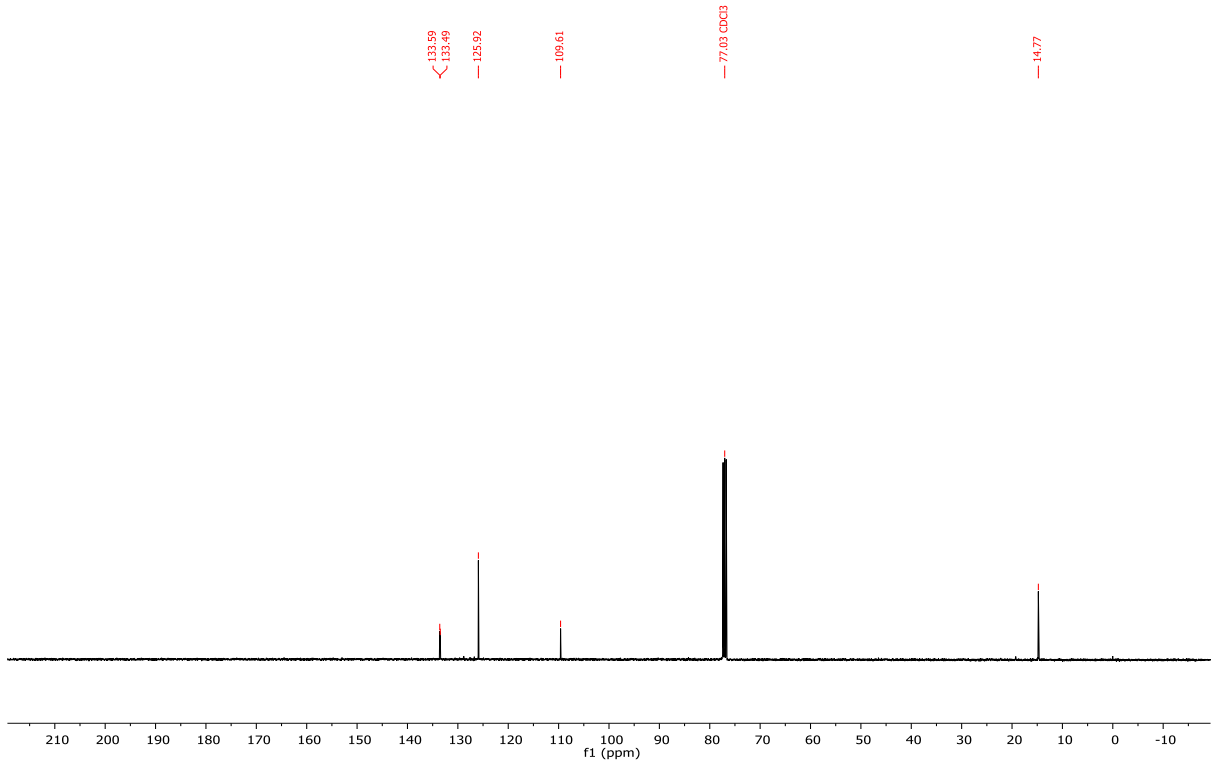

S9: $^{13}C\{^{1}H\}$ NMR Spectrum of **II.A** in $CDCl_3$.

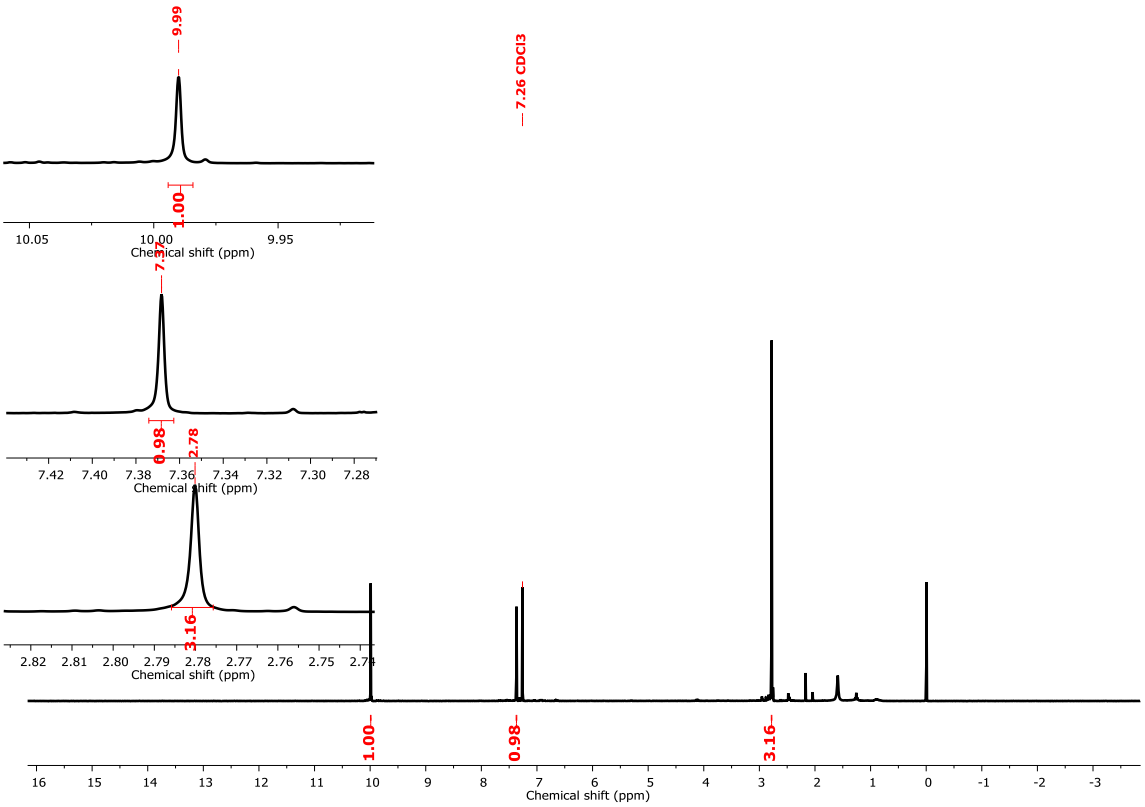

S10: ^{1}H NMR Spectrum of **10** in $CDCl_3$.

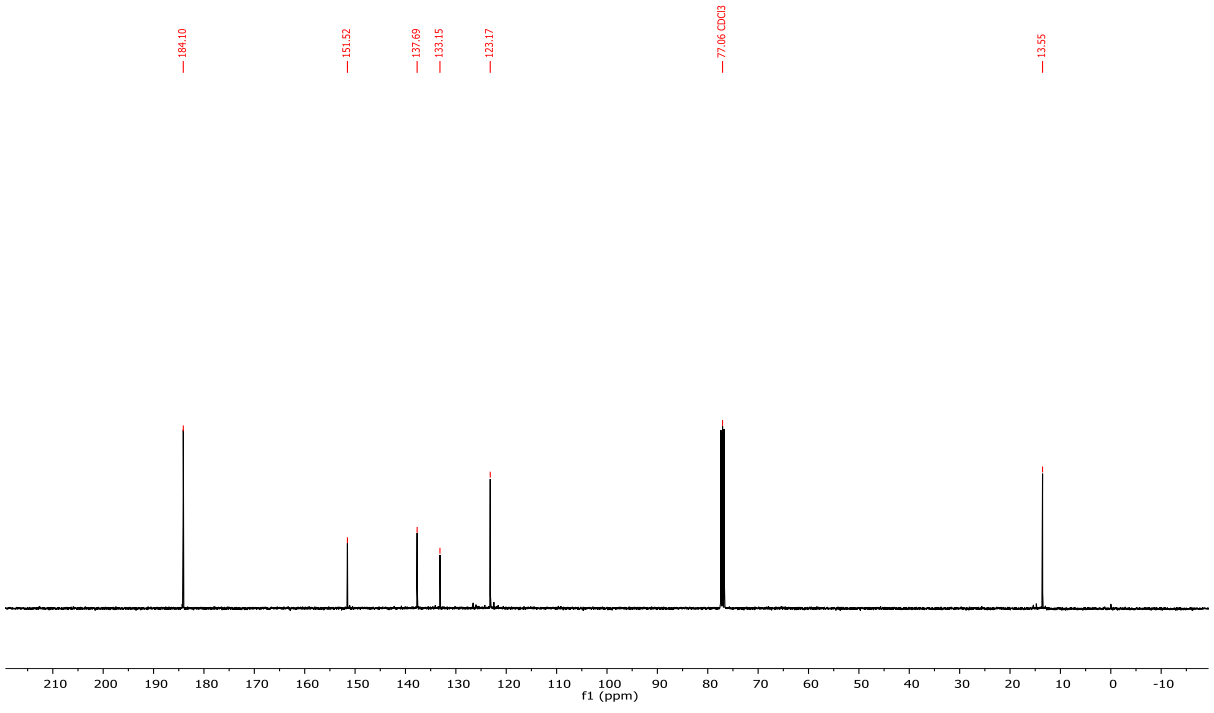

S11: $^{13}C\{^{1}H\}$ NMR Spectrum of **II.10** in $CDCl_3$.

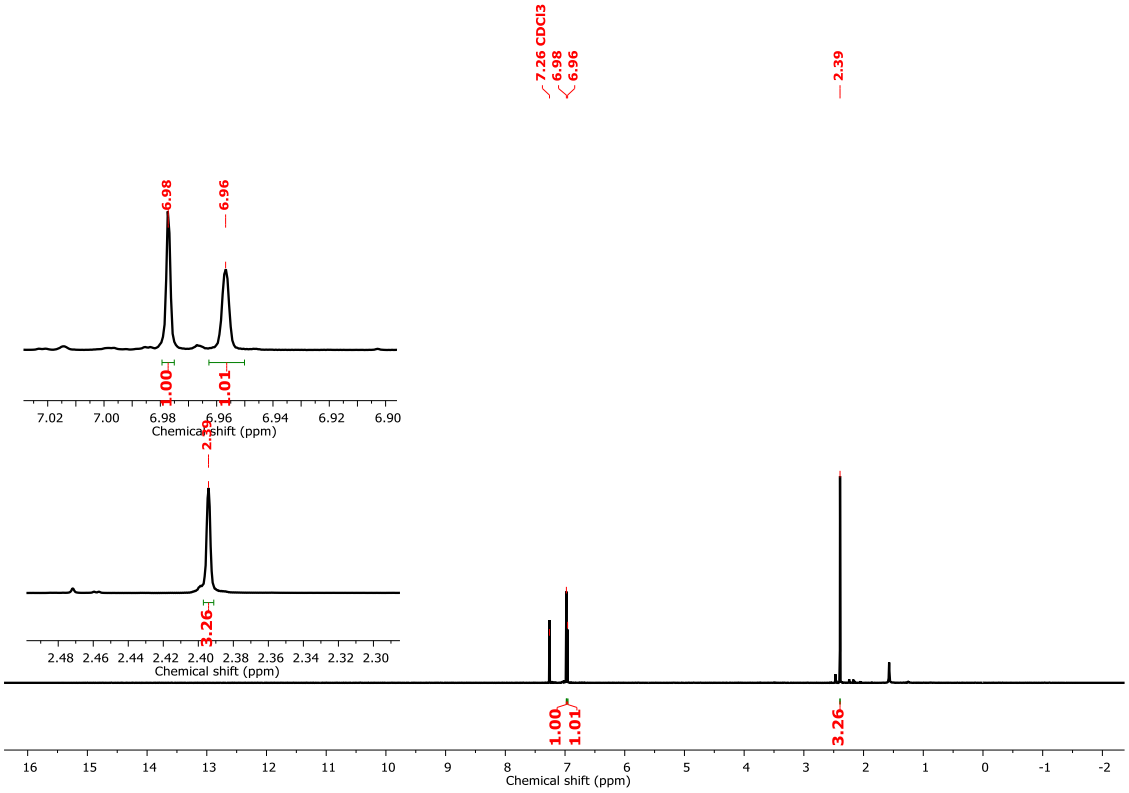

S18: ^{1}H NMR Spectrum of **B** in $CDCl_3$.

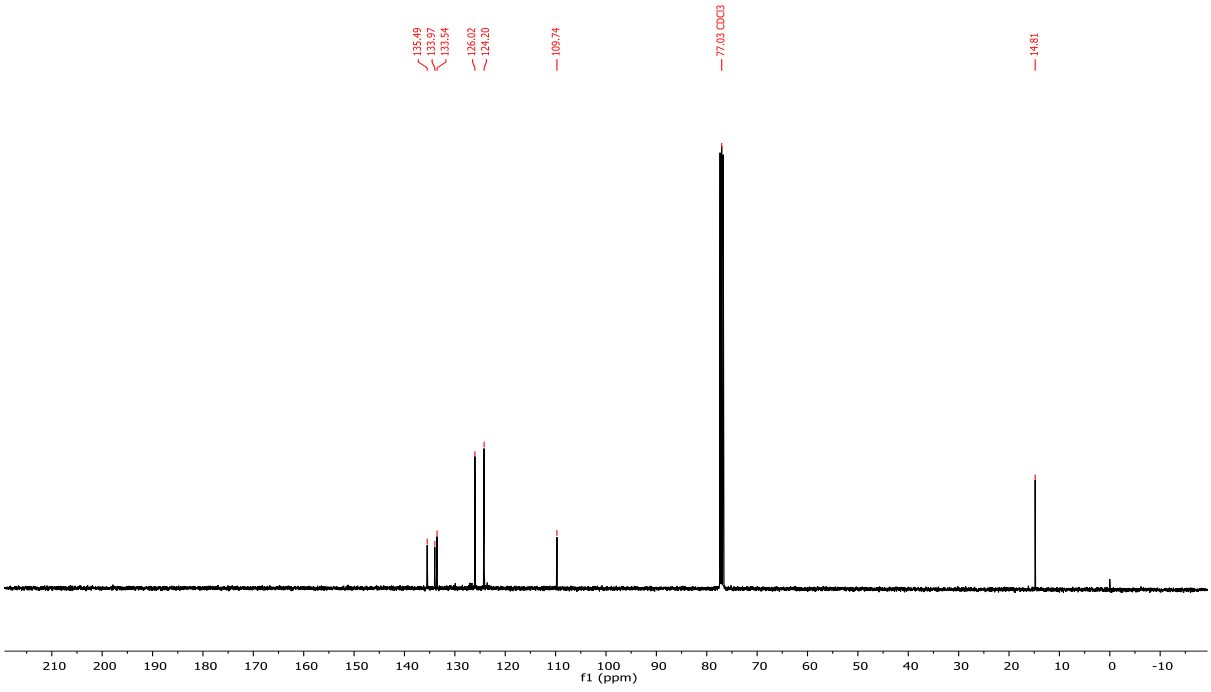

S19: $^{13}C\{^{1}H\}$ NMR Spectrum of **II.B** in $CDCl_3$.

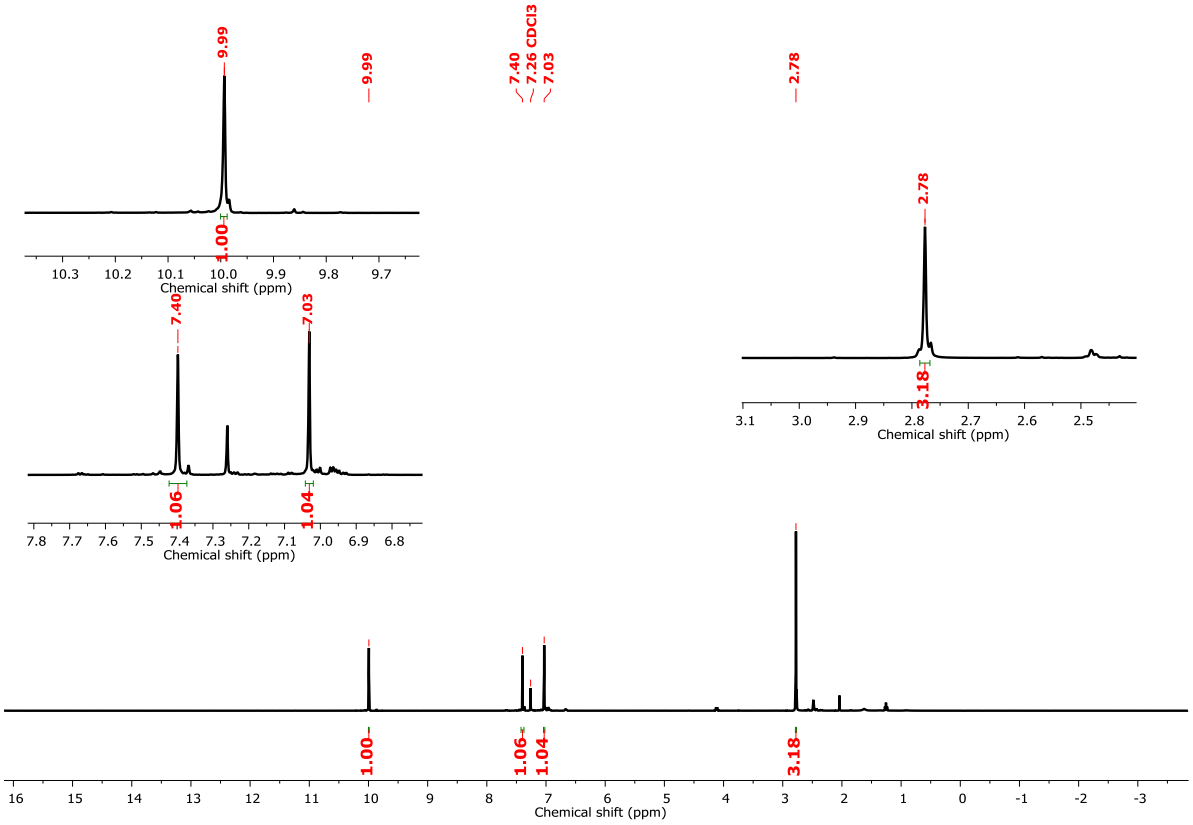

S20: ^{1}H NMR Spectrum of **11** in $CDCl_3$.

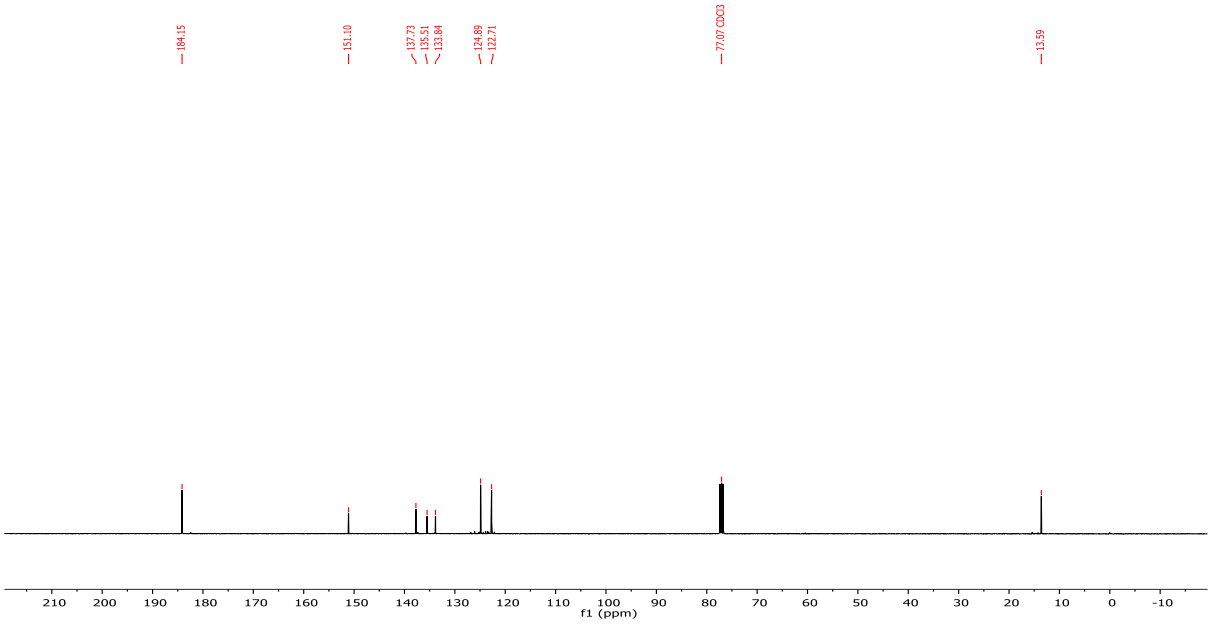

S21: $^{13}C\{^{1}H\}$ NMR Spectrum of **II.11** in $CDCl_3$.

References

(1) E. Vogel, M. Köcher, H. Schmickler and J. Lex, *Angew.Chem., Int. Ed. Engl.,* 1986, **25**(3), 257–259.

(2) (a) H. Furuta, T. Asano and T. Ogawa, *J. Am. Chem. Soc.*, 1994,**116**, 767–768; (b) P. J. Chmielewski, L. Latos–Grażyński,K. Rachlewicz and T. Glowiak, *Angew. Chem., Int. Ed. Engl.*, 1994, **33**(7), 779–781; (c) R. Li, A. D. Lammer, G. M. Ferrence and T. D. Lash, *J. Org. Chem.*, 2014, **79**, 4078–4093.

(3) T. D. Lash, A. D. Lammer and G. M. Ferrence, *Angew. Chem., Int. Ed.*, 2011, **50**, 9718–9721.

(4) M. Toganoh and H. Furuta, *Chem. Commun.*, 2012, **48**(7), 937–954.

(5) M. Toganoh and H. Furuta, *Chem. Rev.*, 2022, **122**, 8313–8437.

(6) (a) P.-Y. Heo, K. Shin and C.-H. Lee, *Tetrahedron Lett.*, 1996, **37**(2), 197–200; (b) E. Pacholska, L. Latos-Grazynski,L. Szterenberg and Z. Ciunik, *J. Org. Chem.*, 2000, **65**, 8188–8196; (c) S. K. Pushpan, A. Srinivasan, V. R. G. Anand,T. K. Chandrashekar, A. Subramanian, R. Roy, K. Sugiura and Y. Sakata, *J. Org. Chem.*, 2001, **66**(1), 153–161.

(7) M. J. Chmielewski, M. Pawlicki, N. Sprutta, L. Szterenbergand L. Latos-Grazyński, *Inorg. Chem.*, 2006, **45**(21), 8664–8671.

(8) (a) N. Sprutta and L. Latos-Grazyński, *Tetrahedron Lett.*, 1999, **40,** 8457–8460; (b) M. Pawlicki and L. Latos- Grazyński, *J. Org. Chem.*, 2005, **70**(23), 9123–9130.

(9) H. Furuta, H. Maeda and A. Osuka, *J. Am. Chem. Soc.*, 2000, **122**(5), 803–807.

(10) H. Maeda, A. Osuka and H. Furuta, *J. Am. Chem. Soc.*, 2003,**125**(51), 15690–15691.

(11) S. K. Pushpan, A. Srinivasan, V. G. Anand, S. Venkatraman, T. K. Chandrashekar, B. S. Joshi, R. Roy and H. Furuta, *J. Am. Chem. Soc.*, 2001, **123**, 5138–5139.

(12) M. Suzuki, M. C. Yoon, D. Y. Kim, J. H. Kwon, H. Furuta,D. Kim and A. Osuka, *Chem. – Eur. J.*, 2006, **12**(6), 1754–1759.

(13) Y. S. Xie, K. Yamaguchi, M. Toganoh, H. Uno, M. Suzuki, S. Mori, S. Saito, A. Osuka and H. Furuta, *Angew. Chem., Int. Ed.*, 2009, **48**(30), 5496–5499.

(14) K. Mitsuno, T. Yoshino, I. Gupta, S. Mori, S. Karasawa, M. Ishida and H. Furuta, *Angew. Chem.*, 2017, **129**(45), 14440–14444.

(15) S. P. Panchal and V. G. Anand, *Org. Lett.*, 2017, **19**(18), 4854–4857.

(16) E. Vogel, M. Sicken, P. Röhrig, H. Schmickler, J. Lex and O. Ermer, *Angew. Chem., Int. Ed. Engl.*, 1988, **27**(3), 411–414.

(17) F. Ellinger, A. Gieren, T. Hiibner, J. Lex, F. Lucchesini, A. Merz, R. Neidlein and J. Salbeck, *Monatsh. Chem.*, 1993, **124**, 931–943.

(18) Z. Hu, J. L. Atwood and M. P. Cava, *J. Org. Chem.*, 1994, **59**, 8071–8075.

(19) 19 R. Bobrovsky, C. Hametner, W. Kalt and J. Fröhlich, *Heterocycles*, 2008, **76**, 1249–1259.

(20) (a) T. Tanaka and A. Osuka, *Chem. Rev.*, 2017, **117**(4), 2584–2640; (b) R. Misra and T. K. Chandrashekar, *Acc. Chem. Res.*, 2008, **41**(2), 265–279.

(21) P. Von, R. Schleyer, C. Maerker, A. Dransfeld, H. Jiao, N. J. R. Van and E. Hommes, *J. Am. Chem. Soc.*, 1996, **118**, 6317.

(22) M. Kon-No, J. MacK, N. Kobayashi, M. Suenaga, K. Yoza and T. Shinmyozu, *Chem. – Eur. J.*, 2012, **18**(42), 13361–13371.

(23) J. S. Reddy and V. G. Anand, *J. Am. Chem. Soc.*, 2009, **131**(42), 15433–15439.

(24) M. J. Frisch, et al., Gaussian 03, Revision C.02, Gaussian, Inc., Wall-ingford CT, 2004. (Full reference provided in the ESI†).

(25) J. C. Ma, D. A. Dougherty and M. Beckman, *Chem. Rev.*, 1997, **97**, 1303–1324.

(26) B. K. Reddy, S. C. Gadekar and V. G. Anand, *Chem. Commun.*, 2015, **51**(39), 8276–8279.

(27) S. P. Panchal, S. C. Gadekar and V. G. Anand, *Angew. Chem.*, 2016, **128**(27), 7928–7931.

Chapter 3:- Phenanthroline Appended Porphyrinoids

Section-A

Synthesis and characterization of 'phenanthroline-embedded isoamethyrin'

III.A.1 Introduction:

The integration of 1,10-phenanthroline into macrocyclic systems represents a compelling frontier in contemporary synthetic chemistry, offering a rich tapestry of opportunities for the creation of unique molecular architectures with diverse applications. This endeavor stems from the distinctive features of 1,10-phenanthroline, a bidentate ligand renowned for its ability to engage in stable coordination interactions with various metal ions.[1] As researchers embark on the journey to seamlessly weave 1,10-phenanthroline moieties into the fabric of macrocyclic structures, the ensuing molecular hybrids exhibit enhanced functionalities, opening avenues for advancements in catalysis, sensing, and supramolecular chemistry.

The fascination with 1,10-phenanthroline lies in its planar, aromatic nature and the capacity to chelate metal ions with a high degree of selectivity and specificity. This property has been exploited in myriad applications, ranging from analytical techniques to the design of catalysts and materials with tailored properties. By integrating 1,10-phenanthroline into macrocyclic systems, researchers aim not only to harness the unique characteristics of this ligand but also to explore the emergent properties arising from the marriage of macrocyclic frameworks and metal-coordinating functionalities.

Macrocycles, defined by their large ring structures, have captivated the scientific community for decades due to their diverse and often remarkable properties. These compounds exhibit a wide range of functionalities, including molecular recognition, host-guest chemistry, and catalysis. The integration of 1,10-phenanthroline into macrocycles introduces an additional layer of complexity and utility, as the resulting compounds can serve as versatile platforms for addressing challenges in areas such as molecular sensing and catalysis.

As we navigate through the synthesis and characterization of these hybrid macrocyclic architectures, the implications for their utility become increasingly apparent. The inherent modularity of 1,10-phenanthroline-containing macrocycles allows for fine-tuning of properties, enabling the design of

molecules with tailored functions for specific applications. The exploration of metal coordination within these frameworks further expands the scope, providing avenues for catalytic transformations and novel material design.

This two-fold integration – the macrocyclic framework and the metal-coordinating 1,10-phenanthroline moiety – prompts a deeper understanding of the structure-property relationships within these compounds. Researchers delve into elucidating how the spatial arrangement of the macrocycle and the metal coordination environment influence reactivity, stability, and selectivity. Such insights not only enrich our fundamental understanding of chemical systems but also pave the way for the rational design of molecules with enhanced performance in targeted applications.

In 1995, Maxwell J. Crossley and co-workers have used the sequential condensation of porphyrin-2,3-diones with 1,2,4,5-benzenetetramine and 1,10-phenanthroline-5,6-dione constitutes a sophisticated and strategically significant synthetic route. The resulting conjugated phenanthroline appended porphyrin systems offer a versatile platform for connecting porphyrin π-systems to external redox centers **III.1**.[2]

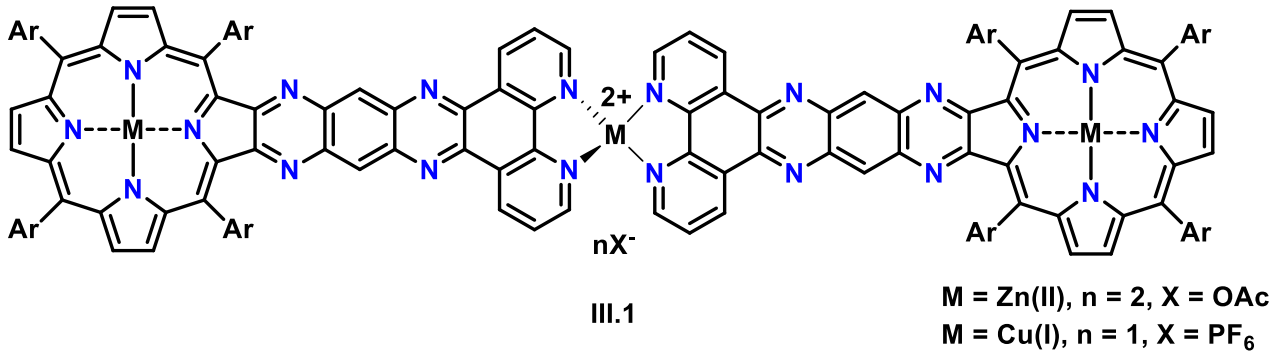

Figure 1 Conjugated phenanthroline appended porphyrin system, **III.1**.

With Christiane Dietrich-Buchecker, who would become his long-term collaborator in this field, Sauvage introduced phenanthroline moiety inside the macrocyclic core, for which they employed phenanthroline ligands featuring hydroxyl groups attached to the phenyl moiety of the ligand(**III.2**). These hydroxyl-functionalized ligands undergo intracomponent Williamson ether macrocyclization, leading to the formation of interlocked products (**III.3**).[3]

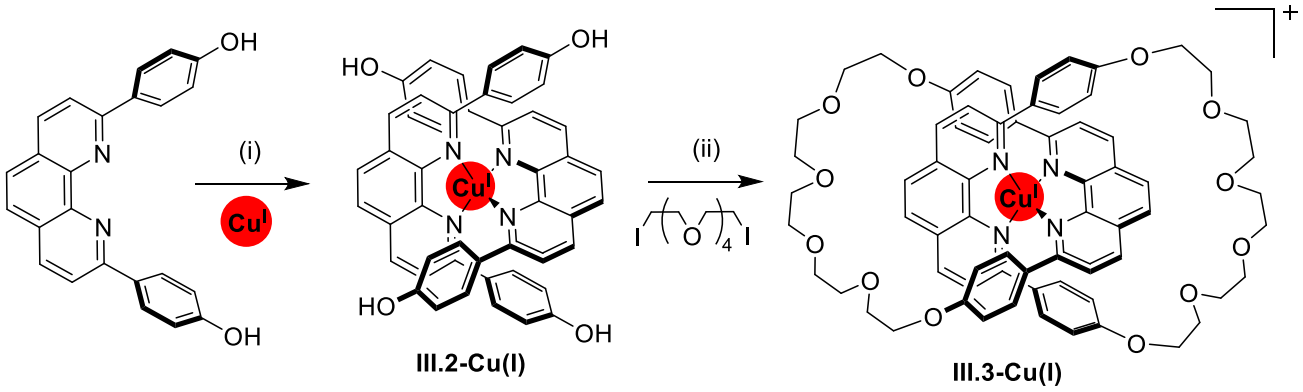

Figure 2 Phenanthroline incorporated interlocked macrocyclic system, **III.3**

Ishida and co-workers have proficiently synthesized the innovative porphyrin analogue **III.4** incorporating an embedded 1,10-phenanthroline moiety which could be exploited as an Mg^{2+}-responsive fluorescent sensor, that provides a ratiometric detection of Mg^{2+} by far-red fluorescent emission above 600 nm.[4] Klaus Mullen reported the first mesomorphic macrocycles **III.5a–c**, opening up a wide variety of possibilities for synthesizing new systems based on the 1,10-phenanthroline unit and their metal complexes.[5]

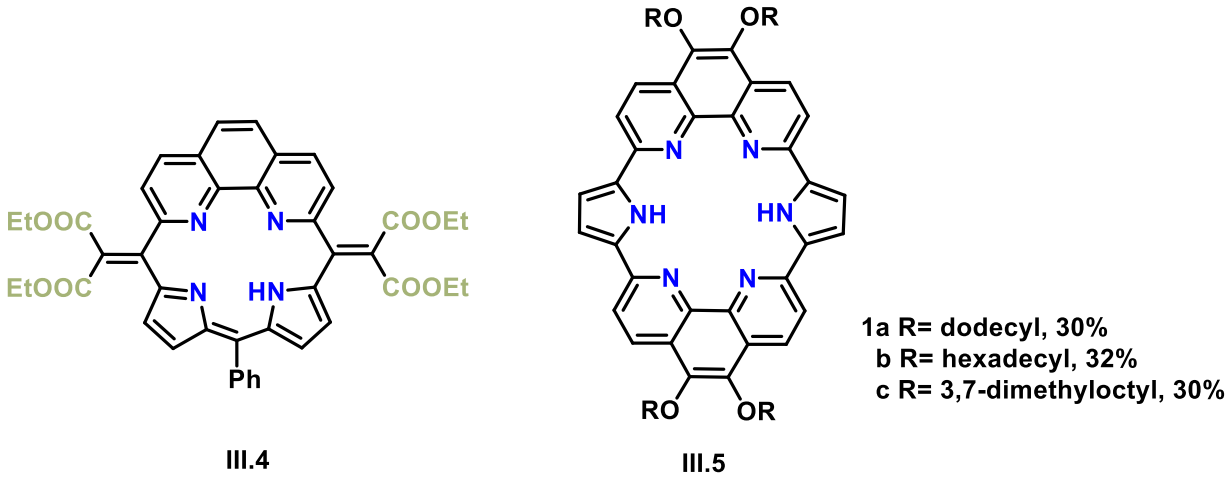

Figure 3 Phenanthroline incorporated macrocyclic systems, **III.4** and **III.5**.

III.A.2 Synthesis and characterization of 'phenanthroline-embedded isoamethyrin' III.7.

Synthesis of 'Phenanthroline-embedded isoamethyrin' III.7.

We endeavored to synthesize isoamethyrin, wherein the bipyrrole unit was replaced by phenanthroline and other pyrrole units were substituted with thiophene. The phenanthroline-embedded isoamethyrin was synthesized through the oxidative coupling of 2,9-bis(5-(phenyl(thiophen-2-yl)methyl)thiophen-

2-yl)-1,10-phenanthroline. The process involved the selective lithiation of 2,2'-(phenylmethylene)dithiophene to produce the monoborylated derivative **III.A**. This monoborylated derivative **III.A** was subsequently subjected to Suzuki coupling with 2,9-dibromo-1,10-phenanthroline, resulting in the formation of 2,9-bis(5-(phenyl(thiophen-2-yl)methyl)thiophen-2-yl)-1,10-phenanthroline (**III.6**) with a yields of <5%.

This synthetic strategy enabled the construction of a novel molecular architecture, incorporating phenanthroline and thiophene units in place of traditional pyrrole moieties. The careful selection of synthetic steps and reagents ensured precise control over the molecular structure, paving the way for the exploration of new functional materials and their potential applications.

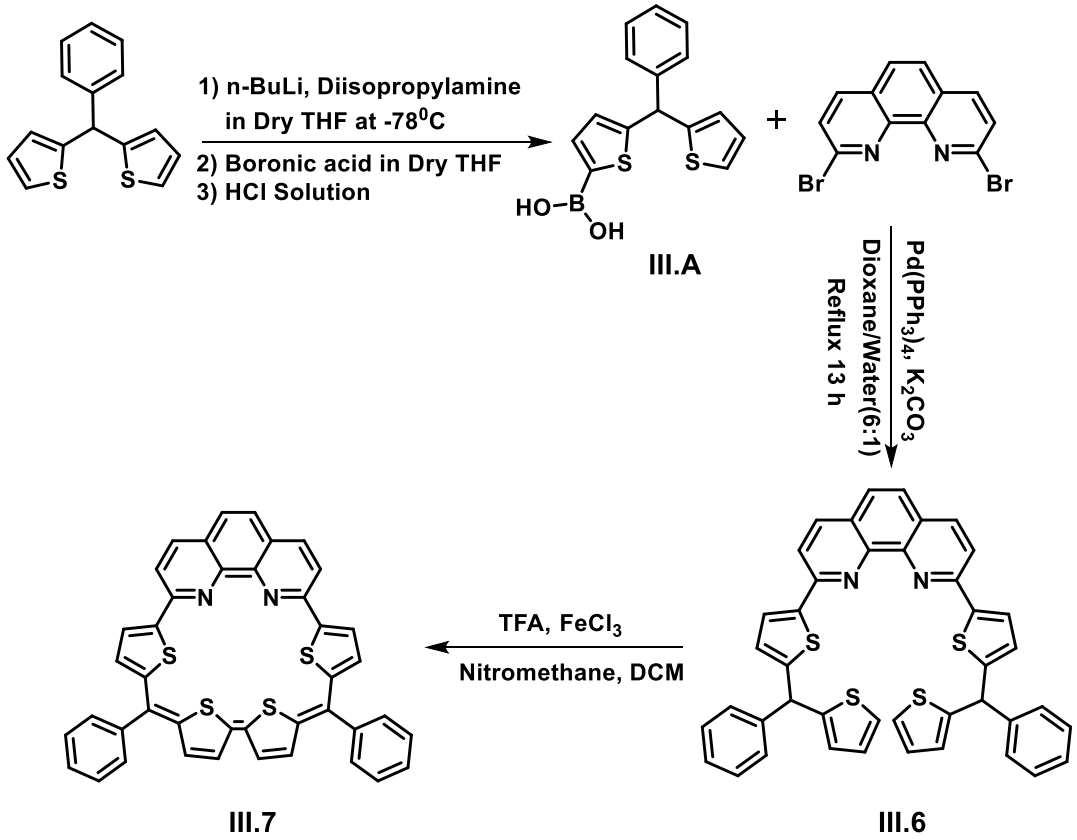

Scheme 1 Synthesis of phenanthroline-embedded isoamethyrin(**III.7**).

Structural characterization of 'Phenanthroline-embedded isoamethyrin' III.7.

Phenanthroline-embedded isoamethyrin (**III.7**) was characterized through appropriate analytical techniques. High-resolution mass spectrometry (HRMS) enabled precise determination of its molecular mass and formula. UV-Vis spectroscopy provided insights into its electronic absorption properties, revealing the presence of conjugated π-systems. NMR spectroscopy elucidated the

chemical environment and connectivity of atoms within **III.7**, offering detailed structural information. X-ray crystallography facilitated the determination of its three-dimensional molecular structure at atomic resolution. Cyclic voltammetry studies provided valuable data on **III.7**'s electrochemical behavior, including redox potentials and reactivity towards electron transfer processes. This multi-faceted approach offered a holistic understanding of **III.7**'s molecular structure and properties, laying the foundation for its potential applications in various fields.

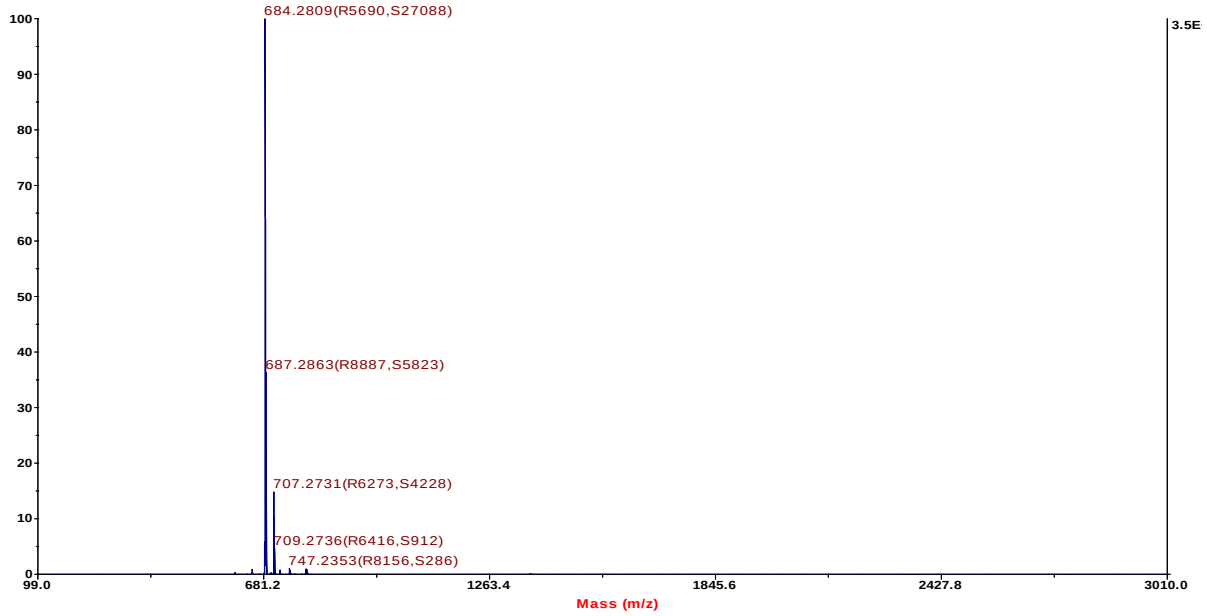

Figure 4 MALDI TOF/TOF mass spectrum of **III.7**(Calculated mass for $C_{42}H_{24}N_2S_4$ is 684.0822).

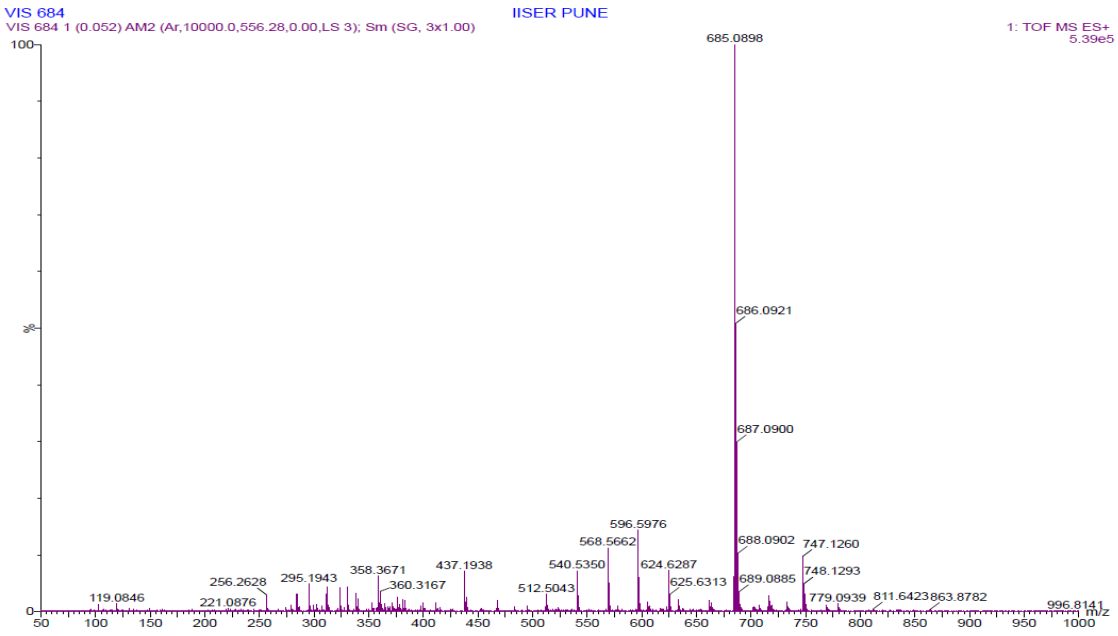

Figure 5 HR-ESI-TOF mass spectrum of of **III.7** in $CHCl_3$/MeOH mixture(Calculated mass for $C_{42}H_{24}N_2S_4$ is

684.0822)..

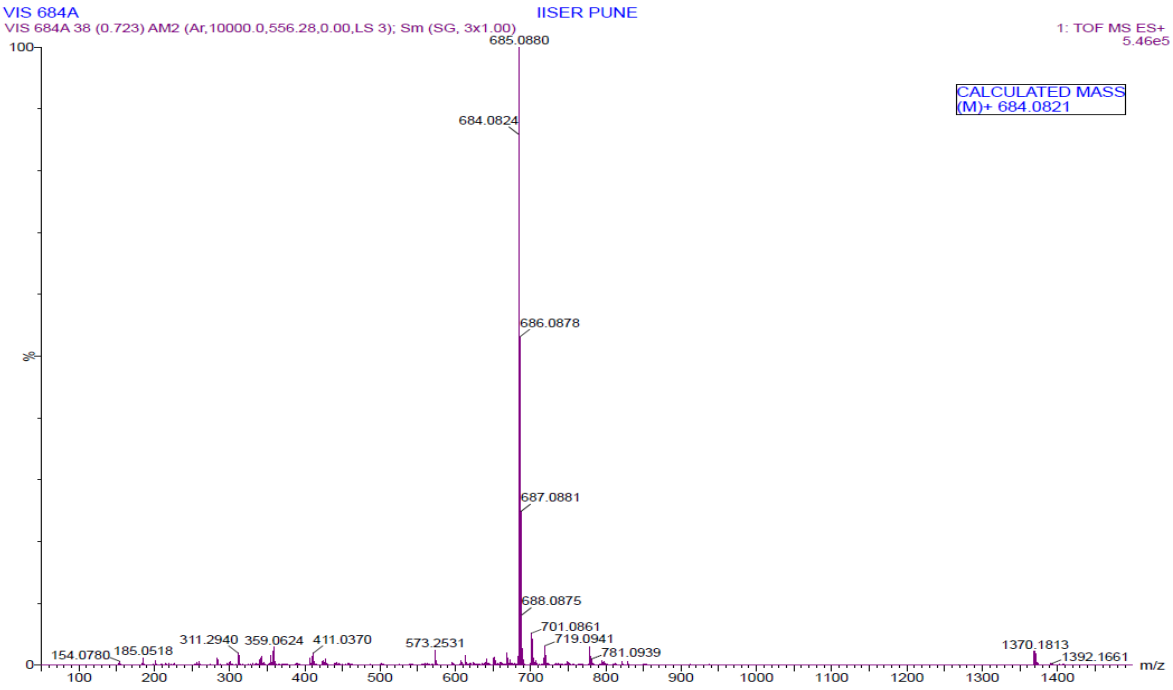

Figure 6 HR-ESI-TOF mass spectrum of **III.7** in $CHCl_3$/ACN mixture(Calculated mass for $C_{42}H_{24}N_2S_4$ is 684.0822)..

NMR characterization

The ^{1}H NMR spectrum of phenanthroline-embedded isoamethyrin **III.7** reveals a reduced number of signals, indicating a higher molecular symmetry for the macrocycle. Four distinct sets of β-CH thiophene protons manifested as doublets at δ 5.97, 6.13, 6.73, and 7.37 ppm. The doublets at δ 5.97 and 7.37 ppm exhibit a coupling constant of 4.2 Hz, while those at δ 6.13 and 6.73 ppm display a coupling constant of 5.6 Hz. These couplings are clearly evident in the ^{1}H-^{1}H COSY spectrum of **III.7.**

Three distinct sets of CH protons from phenanthroline appear as doublets at δ 8.02 and 7.80 ppm with a coupling constant of 8.6 Hz, along with a singlet at 7.34 ppm. Phenyl protons were identified as multiplets within the range δ 7.48-7.23 ppm. These couplings are also distinctly discernible in the ^{1}H-^{1}H COSY spectrum of **III.7**.

Consistent with the molecular structure elucidated through X-ray crystallography, the observed chemical shift values do not align with the anticipated paratropic ring current effect characteristic of 4nπ systems. The estimated Nucleus Independent Chemical Shift (NICS) value of +6.25 ppm for **III.7**

provides further confirmation of moderate paratropic ring current effect, emphasizing the impact of limited global conjugation in the macrocycle.

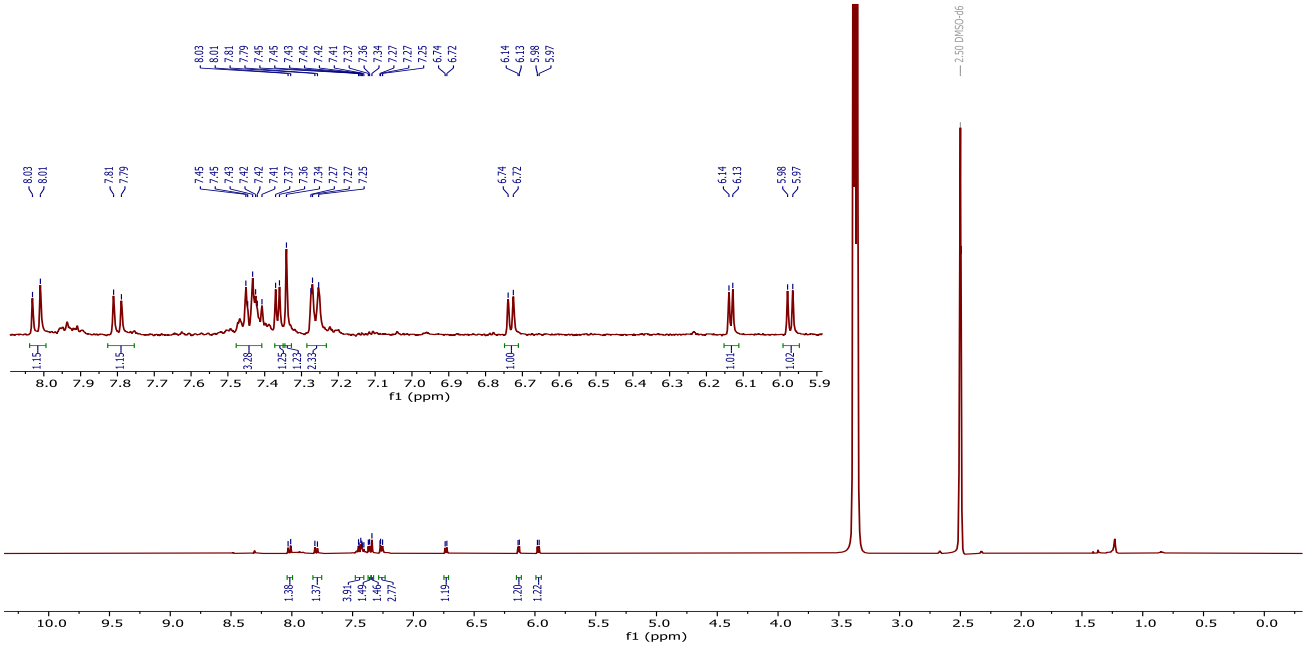

Figure 7 400 MHz ^{1}H NMR spectrum of **III.7** in DMSO-D$_6$**.**

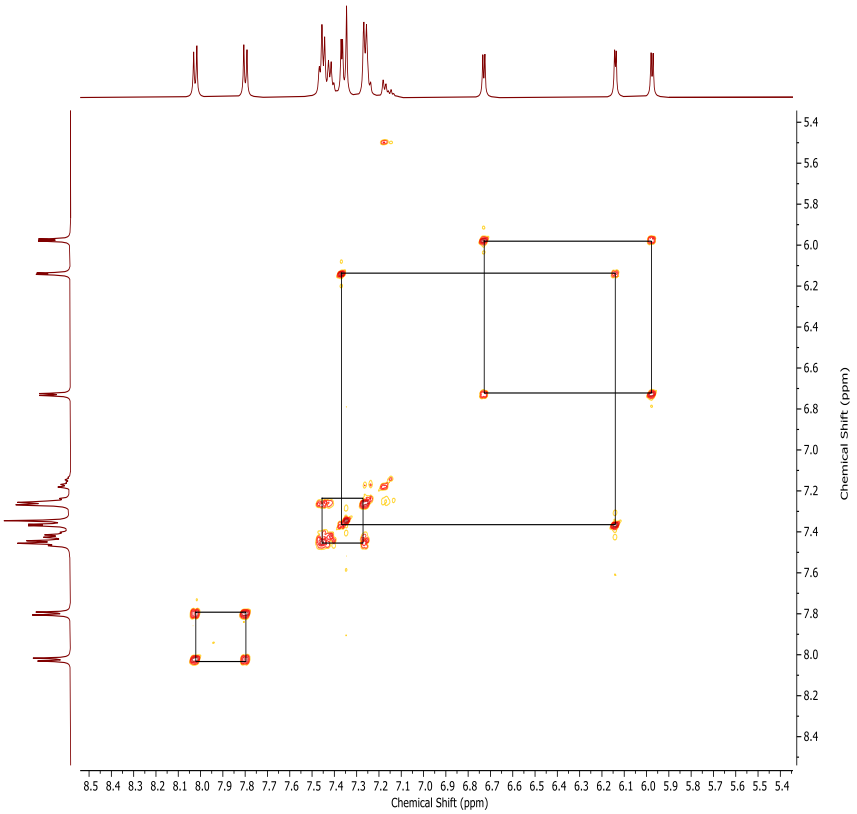

Figure 8 ^{1}H-^{1}H COSY Spectrum of **III.7** in DMSO-D6.

Single crystal X-ray diffraction analysis of phenanthroline-embedded isoamethyrin III.7:

Phenanthroline-embedded isoamethyrin **III.7** was successfully characterized by single-crystal X-ray diffraction analysis, as illustrated in **Fig 9**. Good-quality single crystals were grown through vapor diffusion of either hexane or methanol into the solution of the macrocycle in chloroform. The X-ray diffraction data confirmed a planar structure for the macrocycle, validating the molecular symmetry observed in the ^{1}H NMR spectrum.

The crystal structure analysis revealed a distinctive spatial arrangement within phenanthroline-embedded isoamethyrin **III.7**. Specifically, the thiophene ring and phenanthroline moiety exhibit coplanarity, aligning within the same plane. As expected in typical porphyrinoids, the phenyl rings at the meso positions adopted a nearly orthogonal orientation relative to the mean macrocyclic plane. An intriguing aspect of the crystal structure is the presence of a chloroform molecule nestled at the center of the macrocycle. This finding suggests the occurrence of non-covalent interactions involving the hydrogen atom of chloroform and the nitrogen atoms of the phenanthroline moiety. Which shows N---H bond length varying from 2.297Å to 2.601Å. Such interactions could include hydrogen bonding or other forms of weak intermolecular forces, contributing to the overall stability and three-dimensional architecture of the crystal lattice. The observed non-covalent interactions at the molecular level provide valuable insights into the structural features and intermolecular forces governing the assembly of phenanthroline-embedded isoamethyrin **III.7** in the crystal lattice. These interactions play a crucial role in influencing the overall conformation and stability of the macrocycle in its solid-state structure.

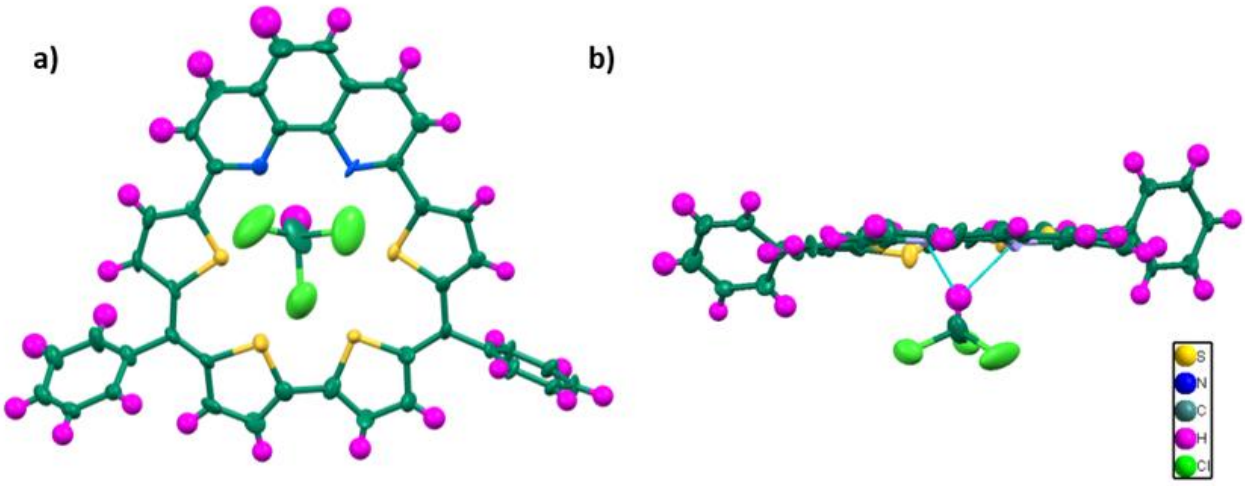

Figure 9 Molecular Structure of **III.7** obtained from $CHCl_3$/Hexane.

Similarly, high-quality single crystals were obtained using a vapor diffusion method, where acetone was introduced into the solution of the respective macrocycles in toluene. X-ray diffraction analysis once again confirmed a nearly planar structure for the macrocycle, as illustrated in **Fig 10**. However, in contrast to chloroform, toluene exhibited weak π-π interactions with the bithiophene unit of the macrocyclic system. This interaction caused the bithiophene unit to protrude slightly from the molecular plane, resulting in a deviation from perfect planar orientation. This deviation suggests the presence of intermolecular forces between the macrocycles and the toluene solvent molecules, influencing the arrangement of the molecular structure in the crystal lattice. Further analysis of these intermolecular interactions could provide insights into the supramolecular assembly and crystal packing of the macrocycles in solid-state structures.

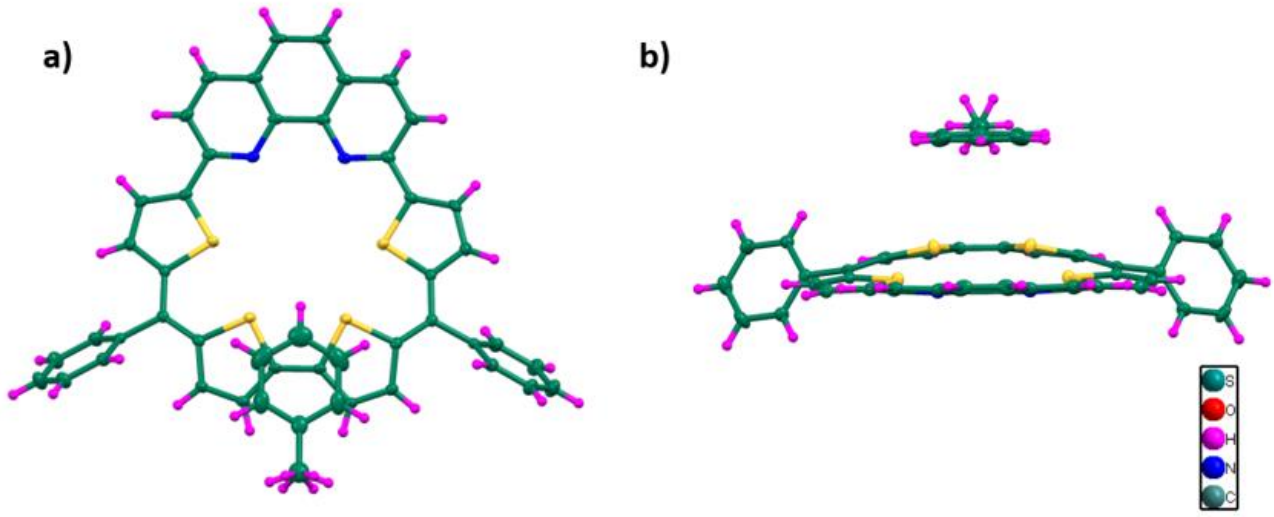

Figure 10 Molecular Structure of **III.7** obtained from Toluene/acetone.

Electronic absorption studies

The UV-Vis absorption spectrum of the 24π phenanthroline-embedded isoamethyrin **III.7**, was recorded in distilled chloroform. The spectrum revealed a prominent high-energy absorption at 421 nm (with a molar absorptivity (ε) value of 16200), accompanied by a low energy absorption peak at 733 nm (with a molar absorptivity (ε) value of 1800) peak, as depicted in **Fig 10.**

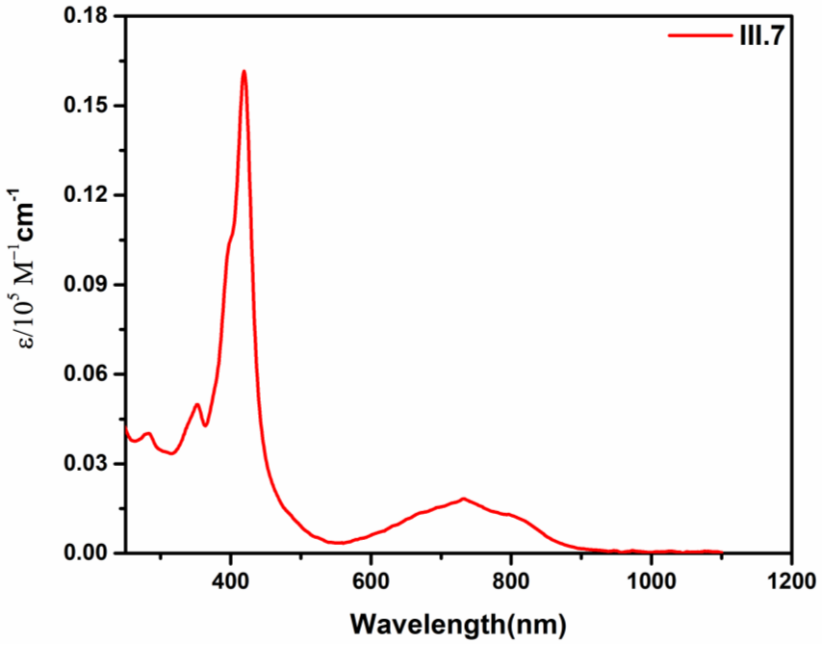

Figure 11 UV-Vis Absorption spectrum of $(7.31*10^{-5}$ molL$^{-1})$ **III.7** in $CHCl_3$.

Cyclic voltammetry studies

Preliminary cyclic voltammetric studies of **III.7** revealed three reduction waves at -1.42 V, -1.20 V, and -0.84 V, along with two oxidation waves at 0.16 V and 0.41 V, as illustrated in Figure 11. Consequently, this indicates the feasibility of utilizing suitable redox reagents to either reduce this 24π antiaromatic system to the 26π aromatic state or oxidize it to the 22π aromatic dication.

Motivated by the electrochemical behavior observed, endeavors were made to chemically synthesize the oxidized 22π aromatic species of **III.7** under varying chemical conditions.

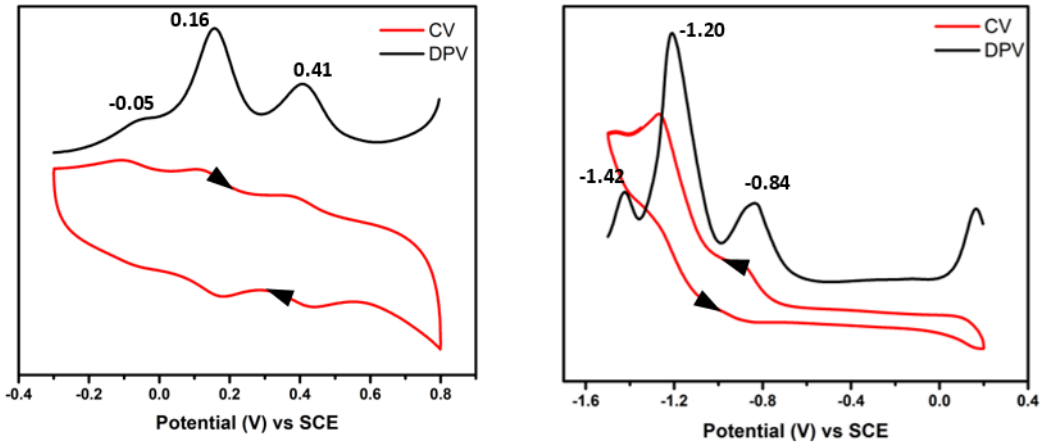

Figure 12 Cyclic voltammogram (CV) and Differential pulse voltammetry (DPV) of **III.7** (oxidation (left) and reduction (right)) in dichloromethane containing 0.1M tetrabutylammonium perchlorate as the supporting electrolyte recorded at 50 mVs^{-1}.

III.A.3 Synthesis and characterization of dication III.8

Synthesis and electronic absorption studies of III.8

Meerwein's salt ($[Et_3O]^+[SbCl_6]^-$) is as a potent one-electron oxidant for π-conjugated molecules and serves as a classic redox reagent for inducing aromaticity switching via electron transfer reactions. Similarly, trifluoroacetic acid (TFA, CF_3COOH) can also serve as an oxidizing agent in lieu of Meerwein's salt ($[Et_3O]^+[SbCl_6]^-$). In anticipation of a two-electron ring oxidation process, **III.7** was subjected to treatment with CF_3COOH in chloroform, as illustrated in **Scheme 2**.

Upon addition of CF_3COOH to **III.7**, an immediate color change was observed, transitioning from light green to greenish-brown. Additionally, the absorption spectrum underwent a notable alteration, with peaks shifting from 421 nm (13000) to 406 nm, 509 nm, 641 nm, and exhibiting low-energy absorption bands at 874 nm (32000) instead of 733 nm (0000).

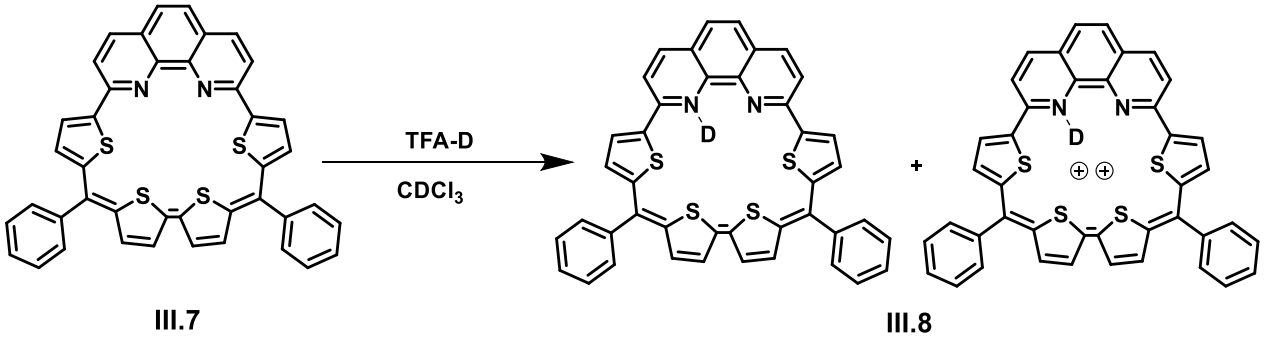

Scheme 2 Synthesis of **III.8** dication from phenanthroline-embedded isoamethyrin(**III.7**).

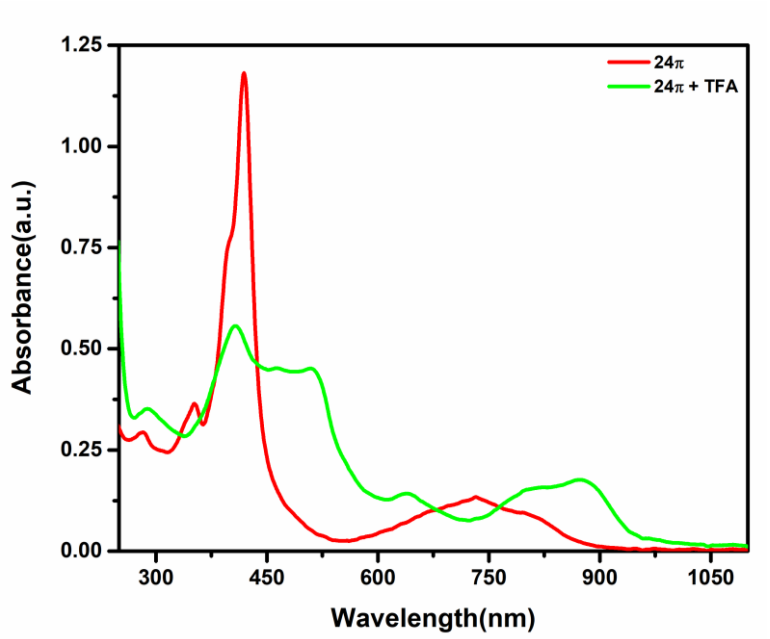

Figure 13 Absorption changes observed for **III.7** (red) upon oxidation to dication **III.8** (green) after addition of TFA in chloroform.

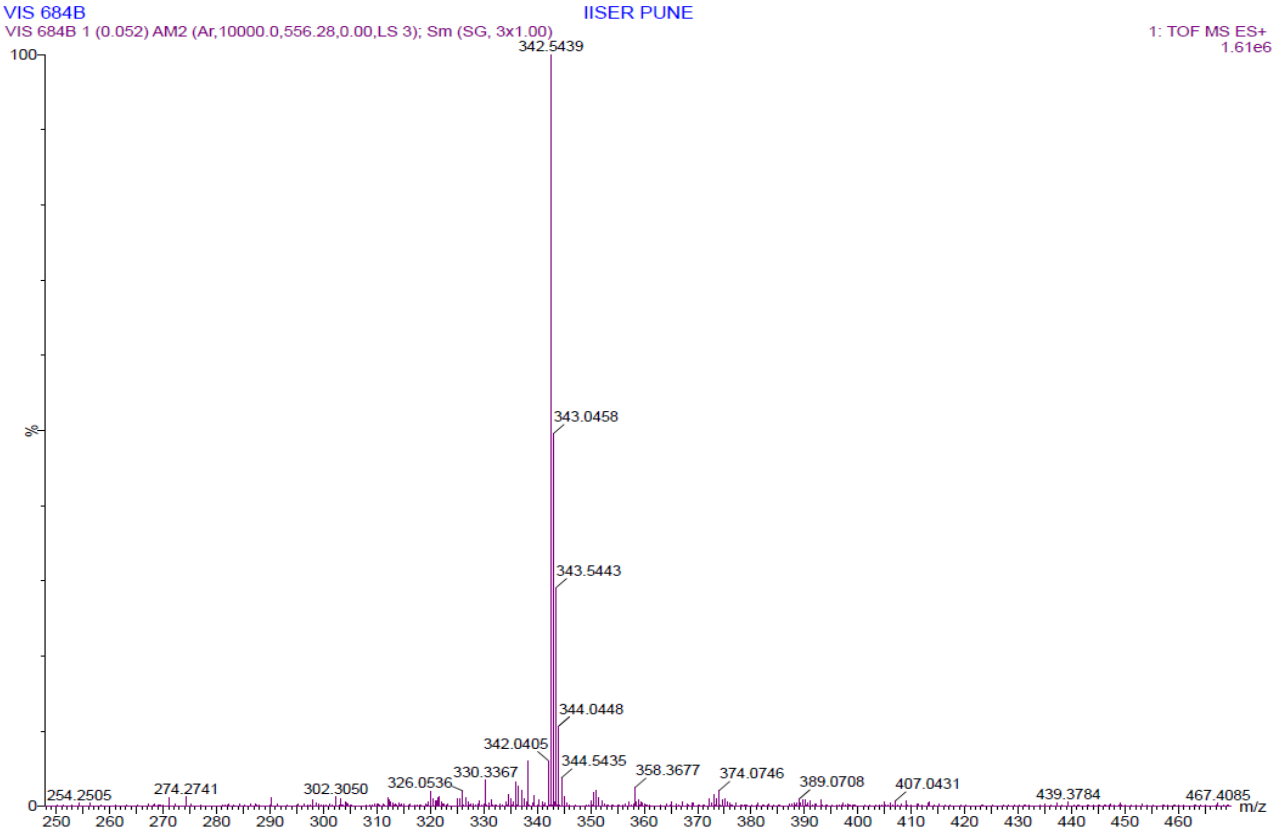

Figure 14 High resolution mass spectrum (HRMS) of dication **III.8**(Calculated mass for $C_{42}H_{24}N_2S_4^{++}$ is 342.5438)..

Structural characterization of dication III.8:

^{1}H NMR Studies of III.8

The ^{1}H NMR spectrum of **III.8** exhibited a more number of signals compared to III.7, suggesting the introduction of asymmetry in the molecule following the addition of trifluoroacetic acid (TFA). This decrease in symmetry can be attributed to the protonation of the phenanthroline moiety in the macrocycle. In the ^{1}H NMR spectrum of **III.8**, each proton corresponding to the macrocycles resonated as an individual signal, leading to an increased number of signals probably arising from the asymmetry through the protonation of the phenanthroline moiety. However, the higher number of signals may result in some overlap, making it challenging to assign specific signals to corresponding protons. Nevertheless, the total number of signals matches the expected number of protons in the macrocycle.

Additionally, an extra signal at δ 6.21 ppm was observed, indicating the protonation of the phenanthroline moiety of the macrocycle at one of its nitrogen atoms. Furthermore, it was noted that signals corresponding to the protonated macrocycle exhibited greater downfield shifts compared to the parent macrocycle **III.7** suggestive of ring current in the macrocycle. The ^{1}H-^{1}H COSY spectrum of **III.8** also shows a greater number of correlations compared to the macrocycle **III.7**, supporting the prediction of emerging asymmetry in the molecule. This increased number of correlations indicates complex interactions and suggests non-uniform electronic distribution, which contributes to the overall asymmetry. This detailed spectral analysis enhances understanding of the difference in structural and electronic properties of **III.8** from **III.7**.

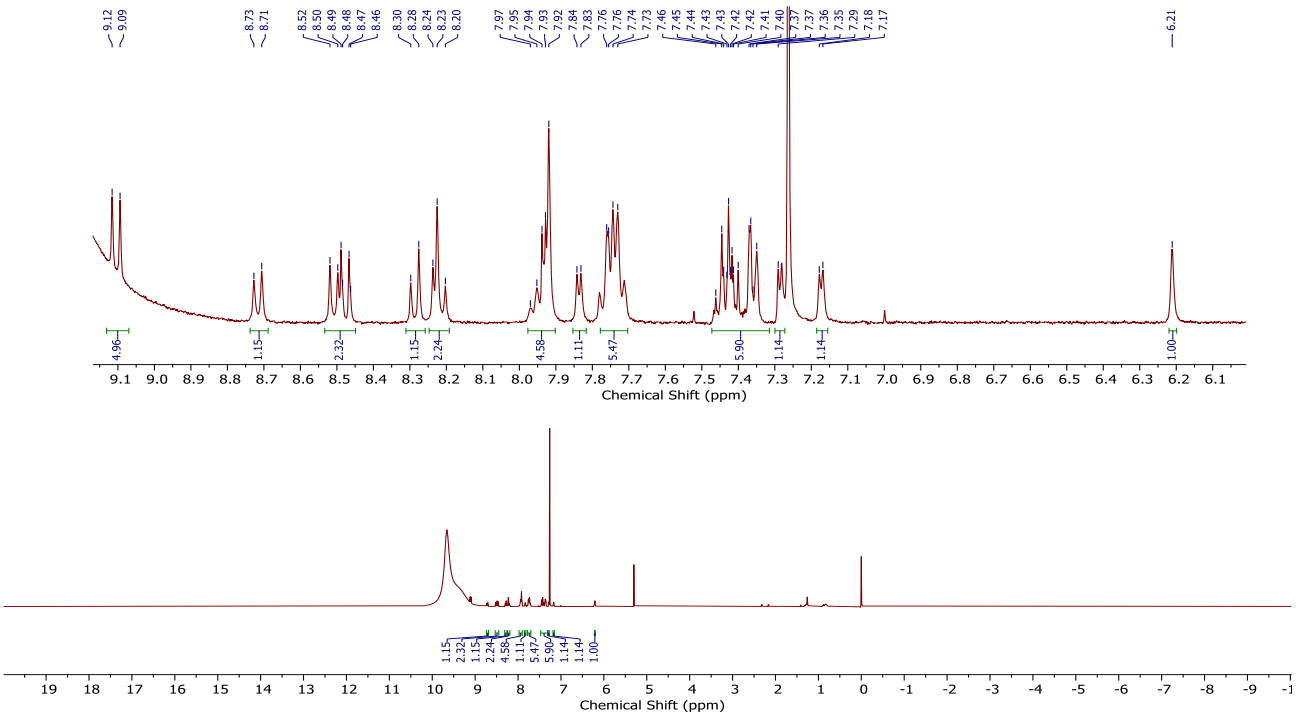

Figure 15 400MHz ^{1}H NMR spectrum of **III.8** in $CDCl_3$.

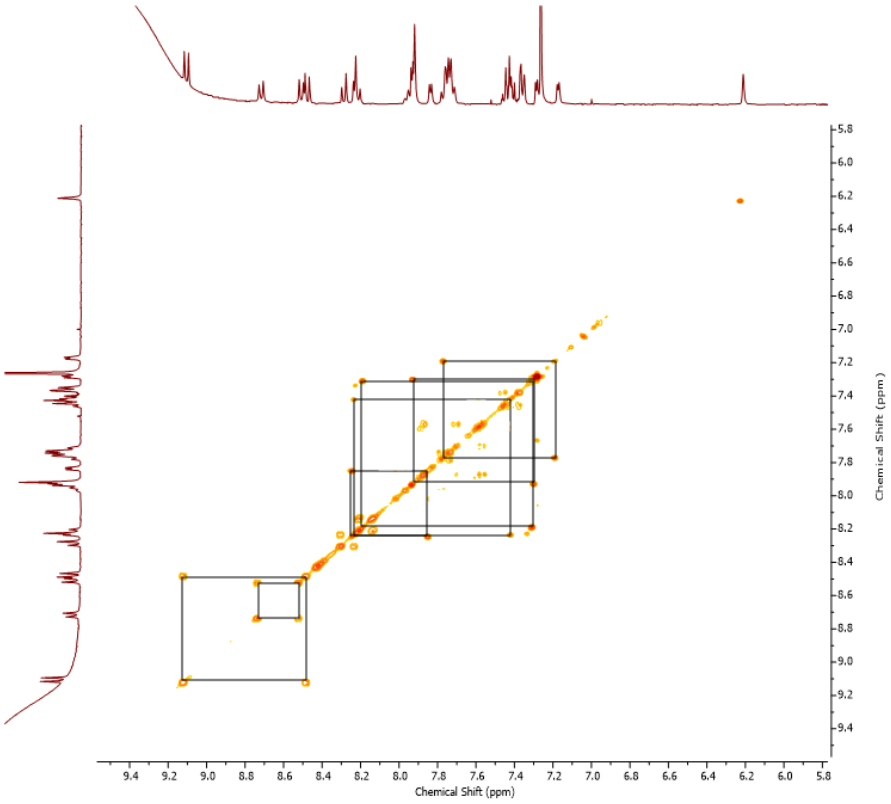

Figure 16 ^{1}H-^{1}H COSY Spectrum of **III.8** in $CDCl_3$**.**

Single crystal X-ray diffraction analysis of oxidized specie III.8 of phenanthroline-embedded isoamethrin III.7:

We have synthesized phenanthroline-embedded pyrrole-based ligands and investigated their protonation behavior with protic acids, specifically HNO_3. Our observations revealed that protonation of the phenanthroline moiety requires two molecules of HNO_3: one NO_3^- ion and another HNO_3 molecule form hydrogen bonds. This dual-molecule requirement for protonation indicates a similar mechanism might be applicable for phenanthroline-embedded macrocyclic systems. Upon attempting protonation of the macrocyclic system, the protonated macrocycle was successfully crystallized in chloroform (with TFA). Single-crystal X-ray diffraction studies of the protonated macrocycle revealed an unexpected planar conformation, as depicted in Fig 16. The crystal structure confirmed the protonation of the phenanthroline moiety, with $[CF_3COO]$- serving as the counter anion.

Interestingly, the crystal structure exhibited a higher number of $[CF_3COO]$- ions than anticipated, with more than four $[CF_3COO]$- ions associated with two macrocycles. This observation suggests that not only does protonation occur, but there is also corroborating evidence of ring oxidation within the macrocycle. The presence of excess counter anions indicates a complex interaction between protonation and oxidation processes in the macrocyclic system. Oxidation was also confirmed with its HRMS spectrum where it showed m/z(2)=342.5439 which is exactly half of the exact mass of **III.7**(**Fig 14**.). This dual behavior of protonation and oxidation highlights the intricate chemical dynamics within phenanthroline-embedded macrocycles.

Furthermore, the crystal structure unveiled π-π stacking interactions between macrocycles, akin to the π-π stacking observed in phenanthroline upon protonation. This observation suggests the presence of intermolecular interactions that contribute to the stabilization and organization of the crystalline lattice.

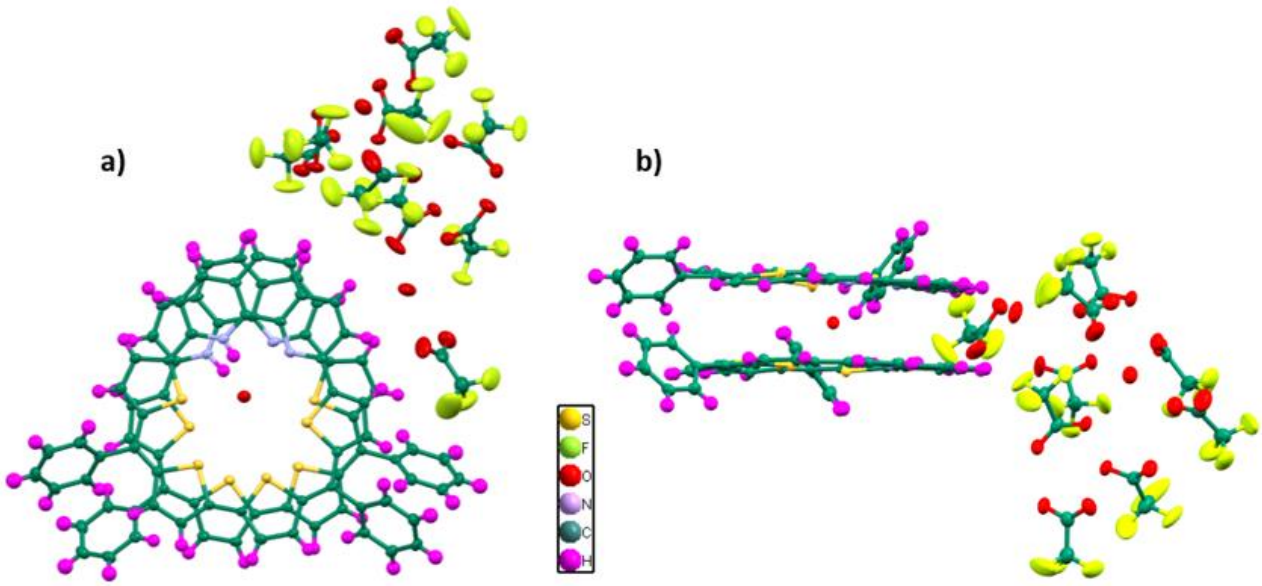

Figure 17 Molecular Structure of **III.8 (III.7+TFA)** in $CDCl_3$**.**

III.A.4 Quantum mechanical calculations:

Nucleus Independent Chemical Shift (NICS)

The aromaticity and anti-aromaticity of molecules **III.7** and **III.8** were assessed through quantum mechanical calculations using the Gaussian09 rev D program. Density Functional Theory (DFT) with Becke's three-parameter hybrid exchange functional (B3LYP) and a 6-31G (d, p) basis set for all atoms was employed. The optimized geometry structures were derived from single-crystal X-ray diffraction analysis. To measure aromaticity/anti-aromaticity, the negative of the calculated magnetic shielding at the center, known as "Nucleus Independent Chemical Shift" (NICS), was utilized. A negative NICS indicates aromatic characteristics, while a positive NICS suggests anti-aromatic features (refer to **Table III.1** for details). The NICS approach, introduced by Schleyer et al., provides a simple magnetic criterion for assessing cyclic conjugated systems when exposed to a magnetic field.

Macrocycle	NICS (0) ppm
III.7	**+6.25**
III.8	**+1.14**

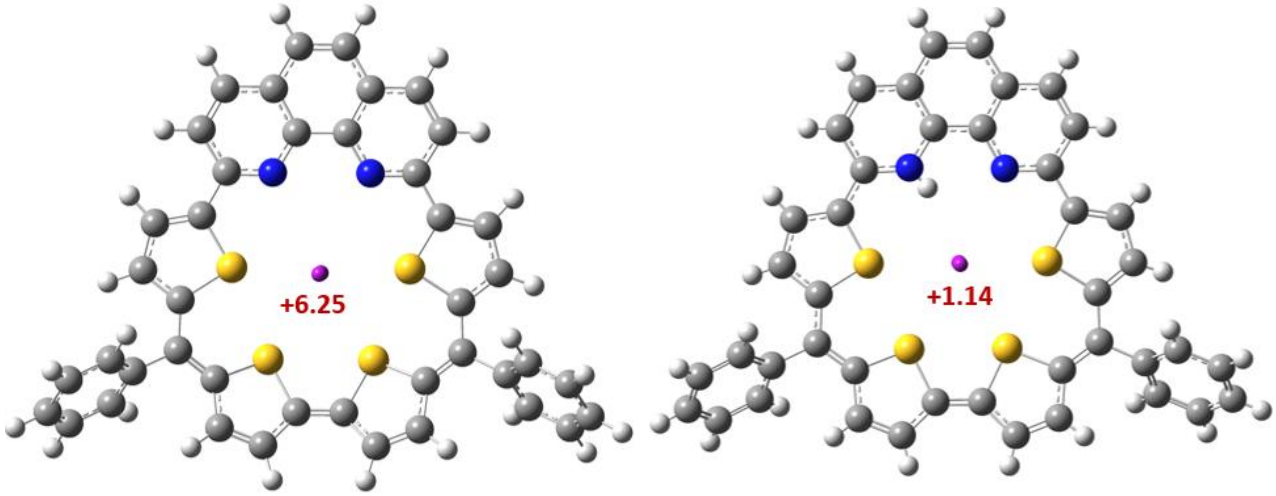

Table III.1: Estimated NICS values for macrocycles **III.7** to **III.8**.

Anisotropy of induced current density (ACID)

The Anisotropy of Induced-Current Density (ACID) emerges as a valuable criterion for assessing ring current effects within aromatic and anti-aromatic systems. This method proves effective in the visualization of the ring current induced by the delocalized π electrons within the macrocyclic structure. The ACID plots not only provide insights into the magnitude but also to the direction of the ring current. These plots are generated when an external magnetic field is applied orthogonally to the mean macrocyclic plane.

Utilizing the Continuously Applying Set of Gauge Transformation (CGST) methods, current density plots are obtained and then visualized using POVRAY 3.7 software for Windows. The ACID plot, depicting the flow of induced current, serves as a powerful tool for representing aromatic and anti-aromatic characteristics. Specifically, a clockwise ring current within the ACID plot signifies the aromatic nature of the molecule, while anti-aromatic ring currents indicate the anti-aromatic nature of the given molecules (**Fig.22**).

Moreover, the ACID plot serves a dual purpose by offering a practical means to discern the pathway of delocalized π electrons within a cyclic conjugated system. The incorporation of arrows in the plot facilitates the determination of the direction in which these π electrons are distributed, adding an additional layer of interpretability to the analysis. This approach, combining theoretical calculations with visual representation, enhances understanding of the electronic structure and aromaticity/anti-aromaticity in cyclic conjugated systems.

From the ACID plot, we observed an anti-clockwise direction of electron flow for **III.7**, indicating its anti-aromatic nature. In contrast, for **III.8,** the electron density is primarily localized around individual

heterocyclic units, rather than being delocalized across the entire macrocycle. This suggests a lack of global conjugation in **III.8**, significantly impacting its electronic properties. The differing electron distribution patterns between **III.7** and **III.8** as we have also observed through its ^{1}H NMR Spectrum, highlight the profound influence of structural modifications on the electronic characteristics of these macrocyclic systems.

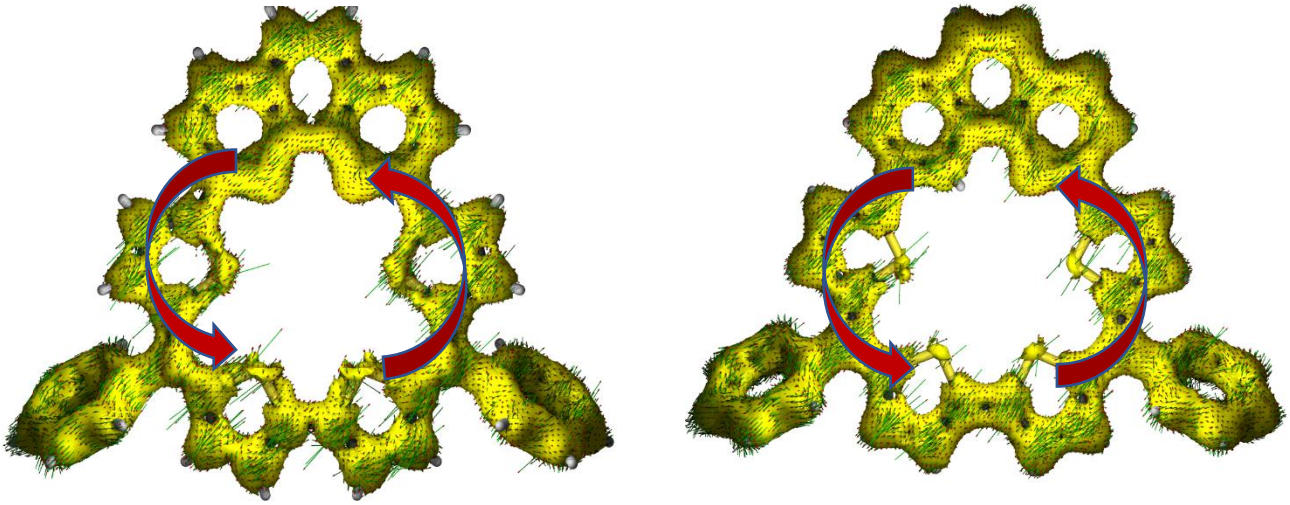

Figure 18 ACID plot for **III.7(Left**) and **III.8 (Right).** At iso value 0.04, an external magnetic field is applied orthogonal to the macrocycle plane.

HOMO-LUMO plots and their band gap for III.7(24π system) and III.8(22π system).

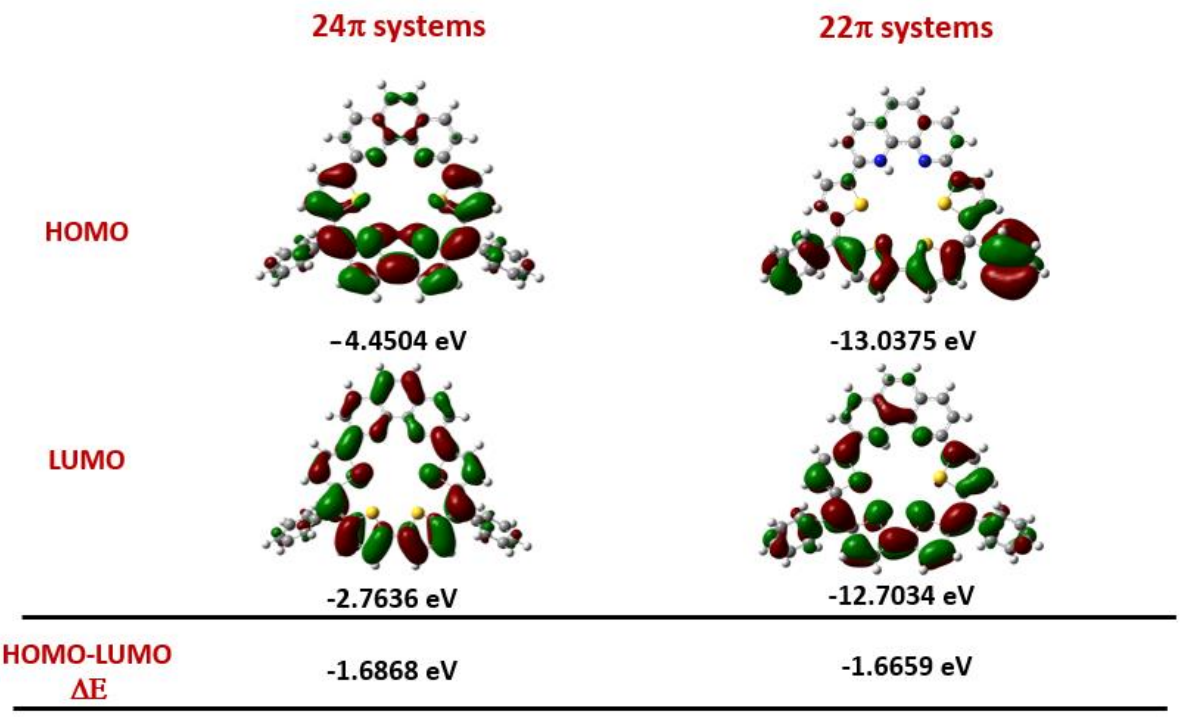

III.A.5 Electron density plots for III.7, III.8 , [III.7]++ and [III.7]+H^+.

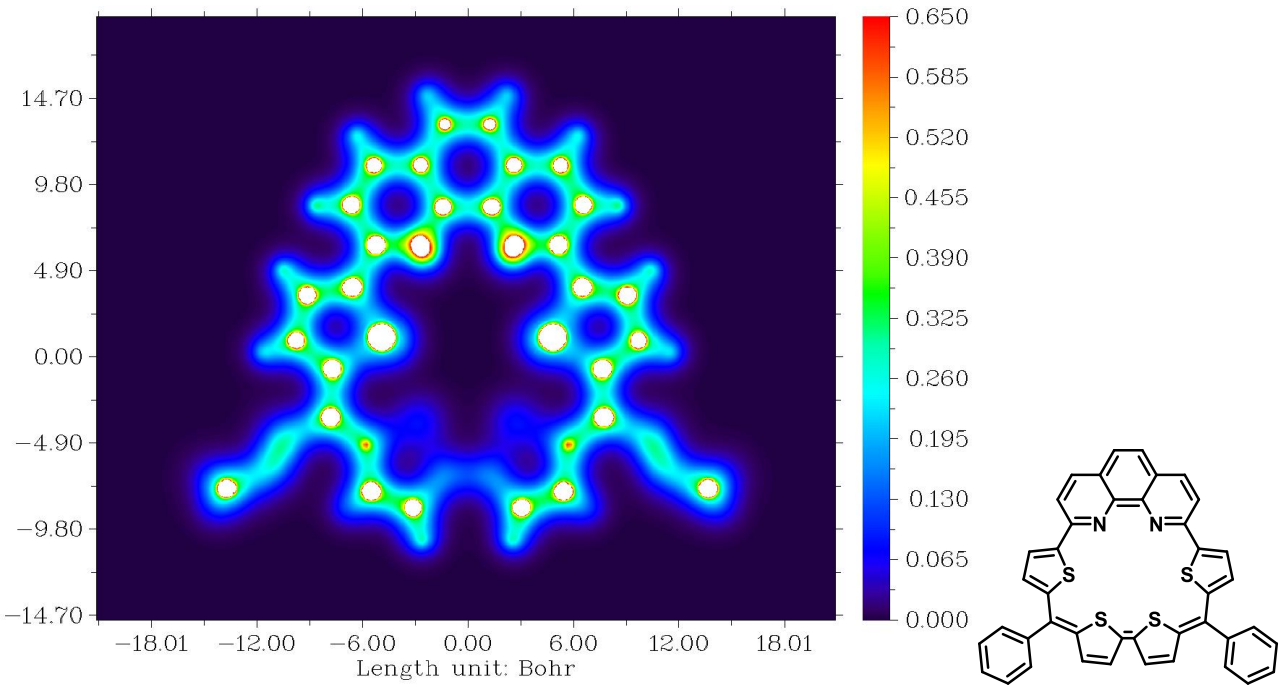

Figure 19 Electron density Plot for **III.7**(24πsystem).(from Crystal Structure) and Chem Draw for **III.7**.

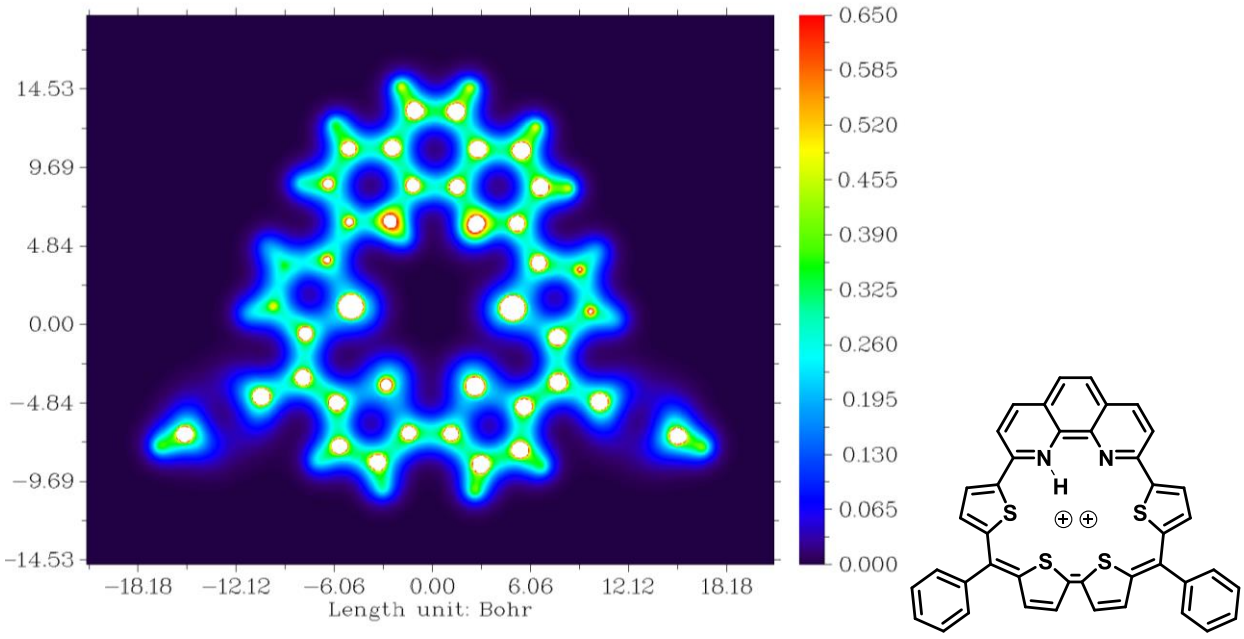

Figure 20 Electron density Plot for **III.8**(22πsystem).(from Crystal Structure) and Chem Draw for **III.8**.

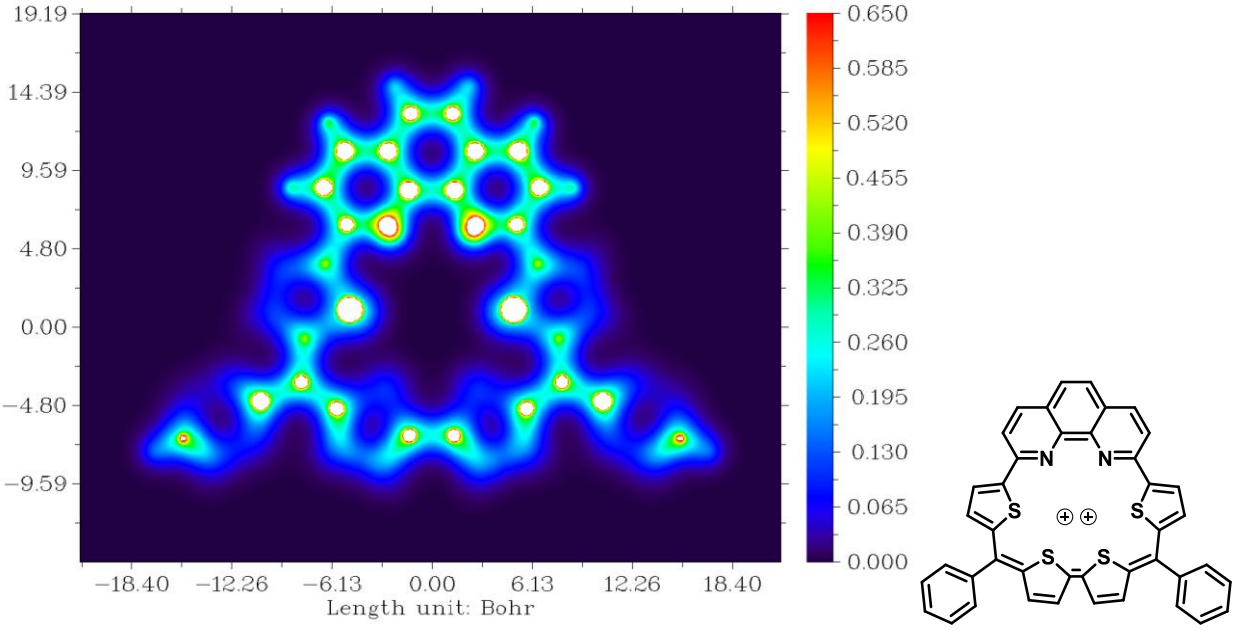

Figure 21 Electron density Plot for [**III.7**]$^{++}$(22πsystem).(from Chem draw structure) and Chem Draw for [**III.7**]$^{++}$.

III.A.6 HOMO-LUMO Energy diagram for III.7, III.8 , [III.7]++ and [III.7]+H^{+}.

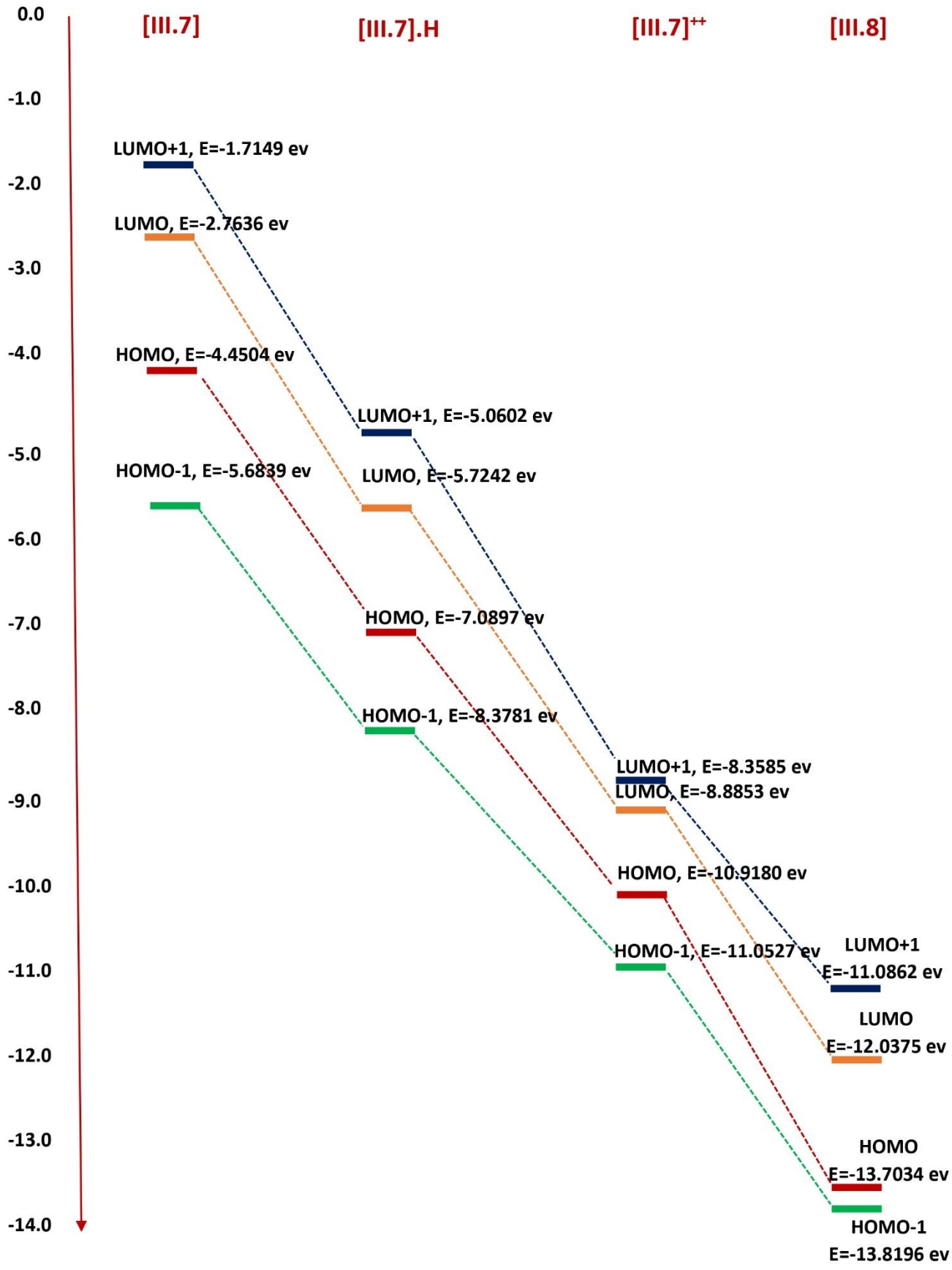

Chapter 3:- Phenanthroline Appended Porphyrinoids

Section-B

Synthesis and characterization of 'phenanthroline-embedded open shell macrocycles'

III.B.1 Introduction:

Aromatic and antiaromatic states denote a distinctive two-electron redox process facilitated by a transient (4n+1) π radical. Despite their potential significance, maintaining open-shell configurations poses a formidable challenge due to their inherently short lifetimes, impeding their isolation and characterization. Following the seminal discovery of the trityl radical, only a handful of other radicals have demonstrated the stability necessary to persist in their radical form.[6] Neutral radicals have garnered considerable attention not only for their intrinsic stability but also for their promising applications in organic radical batteries.[7]

Radicals represent an attractive area of research at the intersection of organic chemistry, materials science, and nanotechnology. These intriguing compounds, characterized by their cyclic structures and unpaired electrons, hold immense potential for applications in diverse fields due to their unique electronic, magnetic, and structural properties.[8] The synthesis, characterization, and exploration of radical macrocycles have captivated the attention of scientists worldwide, driven by both fundamental curiosity and the pursuit of novel materials with tailored functionalities.[9] Radical macrocycles, characterized by their cyclic structures and unpaired electrons, represent a fascinating class of compounds at the forefront of chemistry research. These molecules exhibit unique electronic and magnetic properties, making them promising candidates for applications in various fields.[10]

The synthesis of radical macrocycles presents both challenges and opportunities, as researchers strive to design efficient strategies for the construction and stability of these complex molecular architectures.[11] From traditional synthetic methodologies to innovative approaches inspired by supramolecular chemistry and radical reactions, a wide array of synthetic routes has been developed to access diverse classes of organic radical macrocycles.[12] By carefully controlling reaction conditions and molecular design, chemists can achieve precise control over the size, shape, and electronic structure of these molecules, paving the way for the discovery of new materials and applications.[13]

In 2014, Gopalakrishna et.al. demonstrated a straightforward synthesis pathway for the generation of the most stable organic 25π pentathiophene radical using commercially available precursors.[14] Notably, this radical exhibits properties akin to transition metals, showcasing multiple oxidation states. Both electrochemical and chemical processes, established the amphoteric nature of this radical. Moreover, this milestone was achieved by characterizing the neutral radical along with its oxidized and reduced forms in both solution and solid states, offering valuable insights into their structural and electronic properties. The discovery of such stable organic radicals holds significant promise in various fields, particularly in organic catalysis and the development of organic semiconductors. These radicals are poised to play a pivotal role in advancing catalytic transformations and facilitating the design of novel materials with tailored electronic properties.

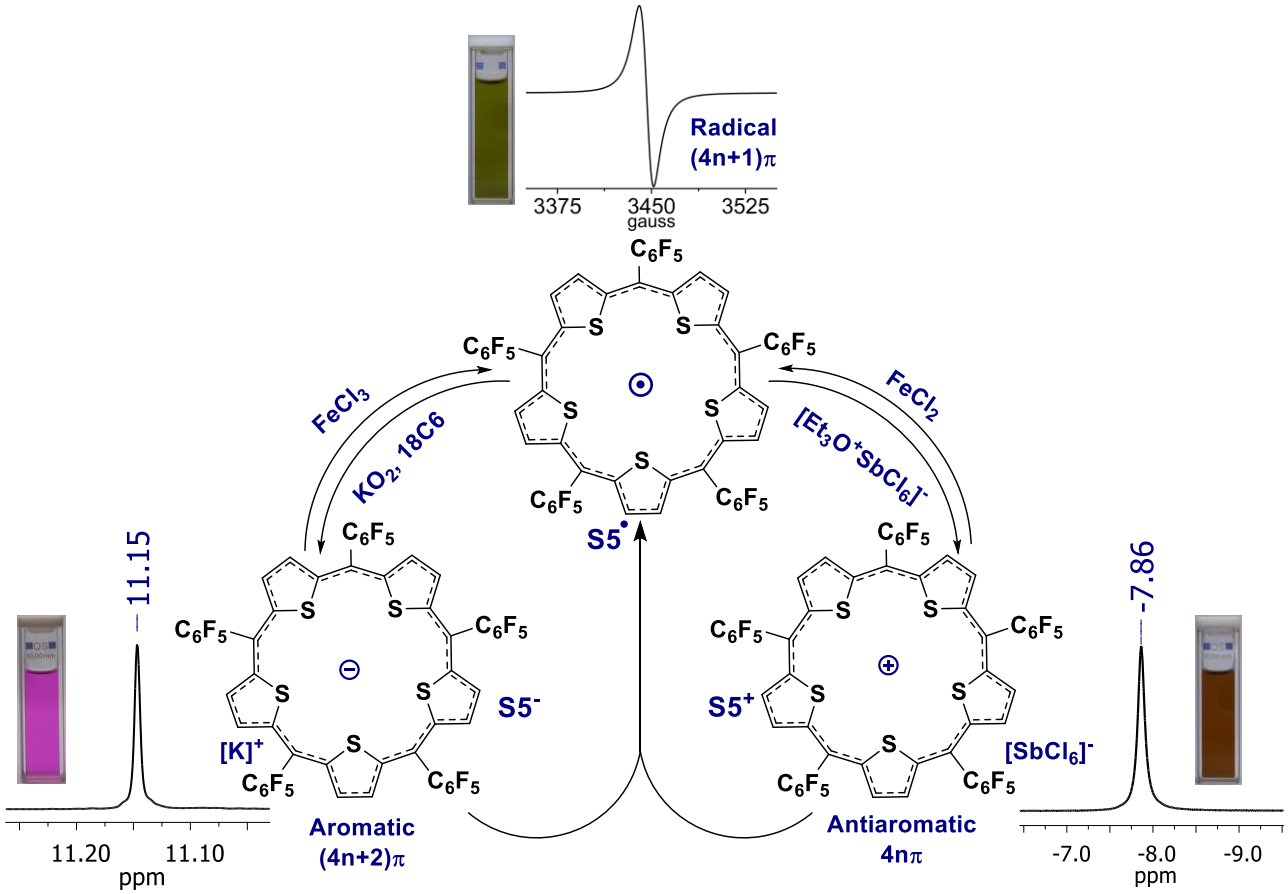

Figure 1 Comproportionation reaction of pentathiophene radical.

III.B.2 Synthesis and characterization of 'phenanthroline-embedded open shell macrocycles' III.9

Synthesis of 'Phenanthroline-embedded open shell macrocycles' III.9.

Based on the above mentioned radical, an attempt was directed towards the synthesis of phenanthroline-embedded open shell macrocycles, a novel molecular architecture integrating phenanthroline within the molecular framework alongside thiophene units. The synthesis of these macrocycles followed a multi-step process akin to the methodology employed for phenanthroline-embedded isoamethrin. In this synthesis approach, 2,9-bis(5-(phenyl(thiophen-2-yl)methyl)thiophen-2-yl)-1,10-phenanthroline was employed as a key precursor for the macrocyclic radical. Unlike the oxidative coupling, this precursor can be cyclized with aryl aldehyde derivatives in the presence of $FeCl_3$ under acidic conditions, leading to the formation of phenanthroline-embedded open-shell macrocycles.

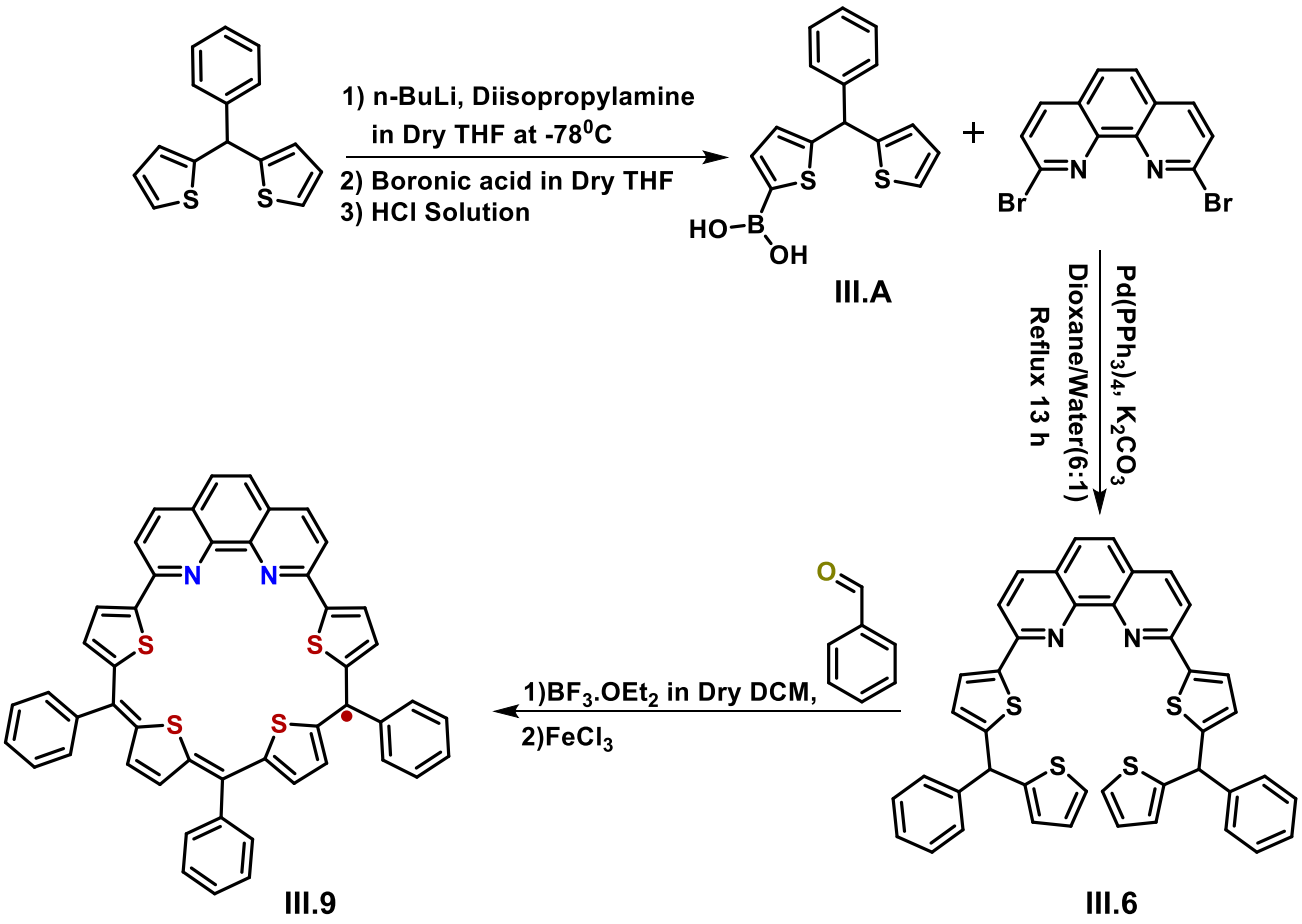

Scheme 1 Synthesis of phenanthroline-embedded open shell macrocycle (**III.9**).

Through this synthetic strategy, it was aimed to engineer a free radical pi conjugated macrocycle, offering new avenues for exploring their electronic and magnetic properties. The precise control over the synthesis process enables us to tailor the molecular structure, paving the way for the investigation of novel materials and their potential applications in various fields of chemistry and materials science.

Structural characterization of 'Phenanthroline-embedded open shell macrocycle' III.9.

An analysis of the reaction mixture by MALDI-TOF/TOF mass spectrometry unveiled the presence of a single macrocycle having four thiophenes and one phenanthroline sub-unit. This macrocycle exhibited a distinctive structural motif featuring three meso carbons, each adorned with a phenyl group substituent.

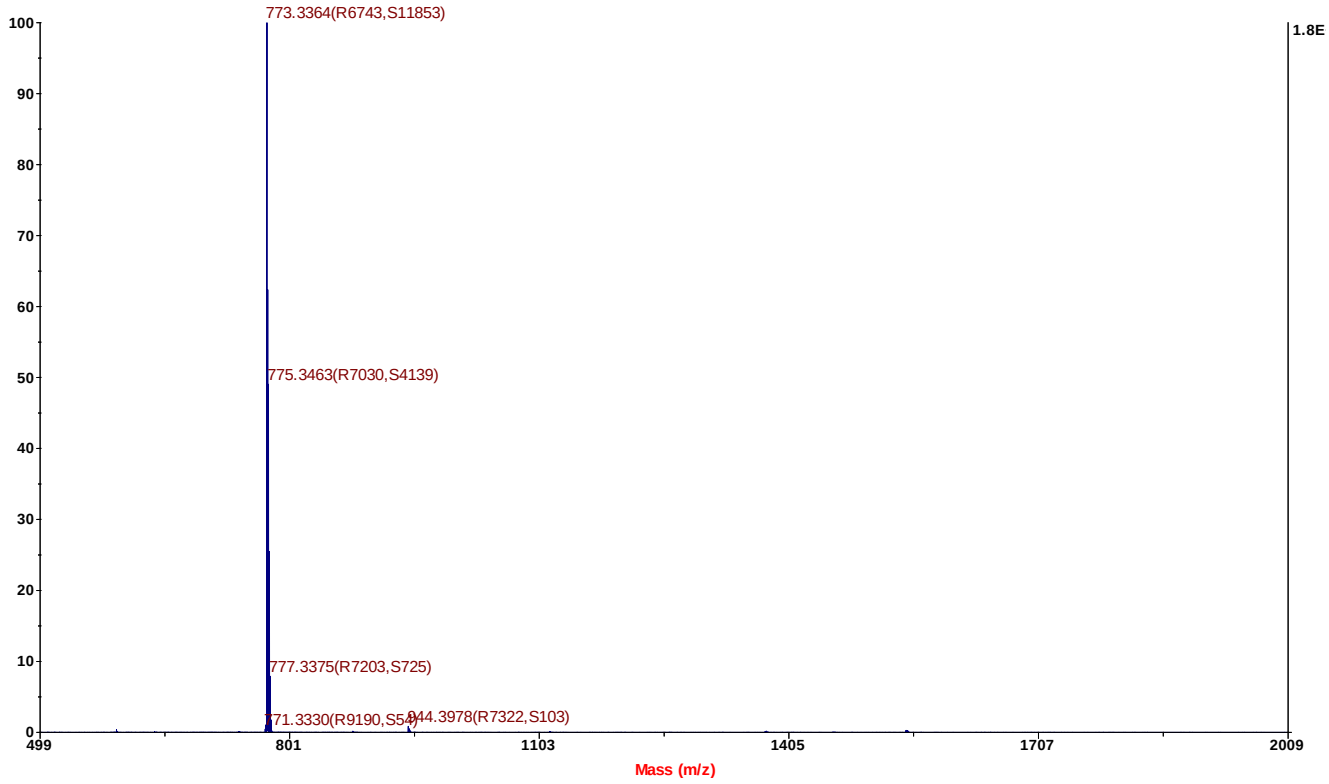

Figure 2 MALDI TOF/TOF mass spectrum of **III.9**(Calculated mass for $C_{49}H_{29}N_2S_4^{\bullet}$ is 773.1214).

After routine workup, column chromatographic separation of the reaction mixture led to the isolation of individual macrocycles. A dark pink colored fraction that eluted with CH_2Cl_2 / Petroleum ether (10:1) displayed a broad absorption at 524 nm (ε = 10,700) and another high energy band at 354 nm (ε = 25,200). It corresponded to an m/z value of 773.1212 in its high-resolution mass spectra (**Figure 2.**). Its ^{1}H NMR spectrum did not display any signal corresponding to the macrocycle, either at room temperature or at low temperature. Electron Paramagnetic Resonance (EPR) spectrum recorded at

room temperature and at 100 K (Figure-II.3) displayed a singlet with g = 2.0018, characteristic of organic free radical due to an unpaired electron (S=1/2). It was found to be stable even upon exposure to ambient atmosphere for several months.

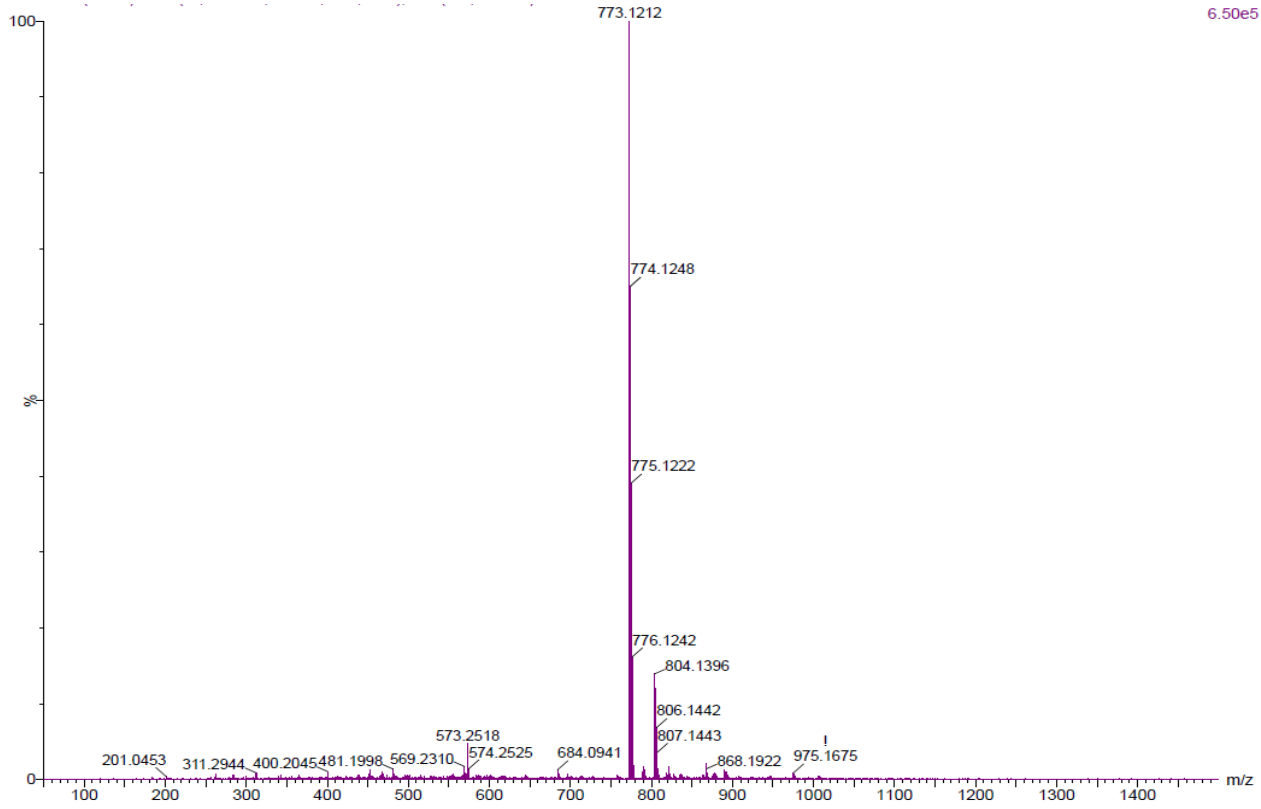

Figure 3 High resolution mass spectrum (HRMS) of **III.9**(Calculated mass for $C_{49}H_{29}N_2S_4^{\bullet}$ is 773.1214)**.**

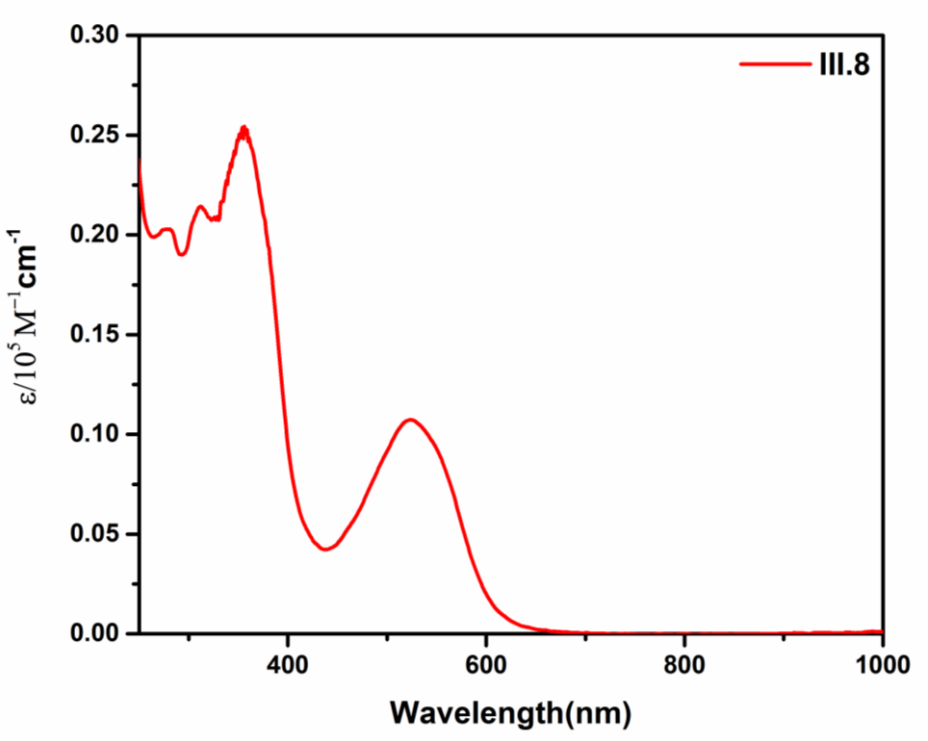

Figure 4 UV-Vis Absorption spectrum of ($6.47*10^{-5}$molL^{-1}) **III.9** in $CHCl_3$.

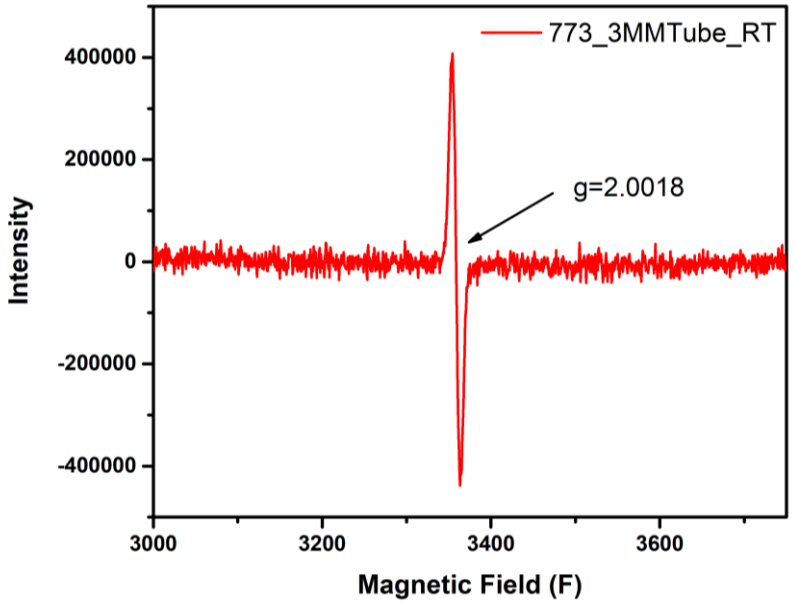

Figure 5 EPR spectra of **III.9** at 298 K in the solid state.

Single crystal X-ray diffraction analysis of phenanthroline-embedded open-shell macrocycle III.9:

To ascertain the precise molecular structure of III.9, high-quality single crystals were cultivated using a solvent diffusion method. These crystals exhibited monoclinic symmetry with the P 21/n space group, revealing a planar conformation reminiscent of the S5 radical. Notably, the sulfur and nitrogen atoms

originating from the phenanthroline and thiophene units, respectively, converged towards the center of the macrocycle.

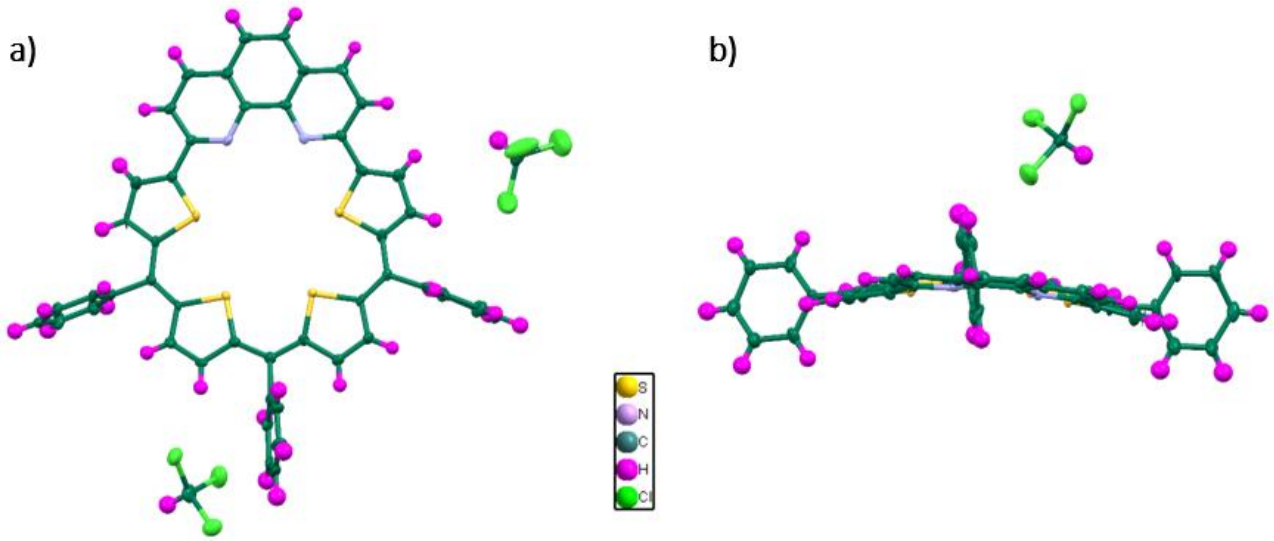

Figure 6 Molecular structure of **III.9** top view (left) and side view (right) phenyl rings are orthogonal to the plane of macrocycle with $CHCl_3$ as a solvent.

This arrangement underscored the efficient delocalization of π-electrons, enhancing the stability of the radical, akin to the S5 radical species. Furthermore, the near orthogonal alignment of the pentafluorophenyl rings relative to the macrocycle's plane in **III.9** facilitated steric hindrance, thereby impeding π stacking interactions. This steric hindrance mechanism mitigated potential intermolecular interactions involving the unpaired electrons. With a formal count of 25 π electrons distributed along its conjugated pathway, III.9 was unequivocally classified as a radical species as S5.

III.B.3 Quantum mechanical calculations:

Spin density distribution

Unrestricted DFT calculations (UB3LYP/ 6-31G (d,p)) were performed to understand the unusual high stability of this open-shell species, **III.9**. The calculations implied the unpaired electron density to be encompassed over the cyclic framework of **III.9** (**Fig 7.**)

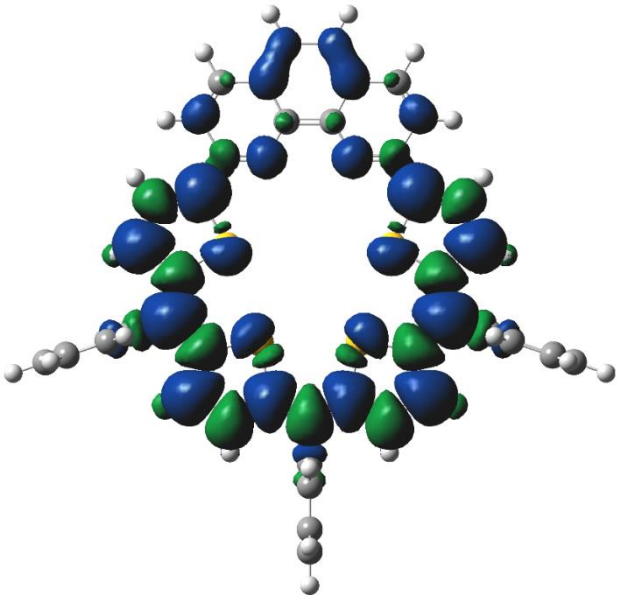

Figure 7 Spin density distribution of **III.9** calculated at UB3LYP/6-31G (d,p).

Nucleus Independent Chemical Shift (NICS) and Anisotropy of induced current density (ACID)

NICS values were obtained with gauge independent atomic orbital (GIAO) method based on the optimized geometries. The global ring centers for the NICS (0) values were designated at the non-weighted mean centers of the macrocycles. Despite its radical nature, a positive NICS (0) value of +2.35 ppm was estimated for III.9, suggesting the weak delocalized nature of unpaired electrons.

The Anisotropy of the Current-Induced Density (ACID) was also plotted to visualize the ring current due to delocalized π electrons which clearly indicates that pi electrons are weakly globally delocalized.

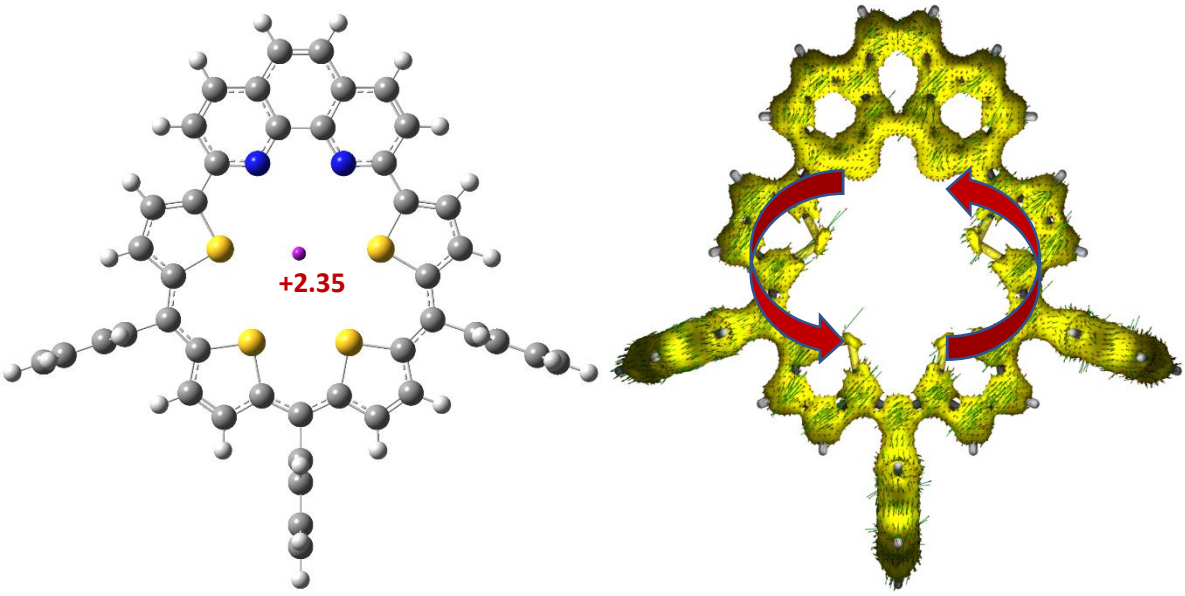

Figure 8 NICS calculation (on the left) and ACID plot (on the right) of **III.9.**

Cyclic voltammetry studies

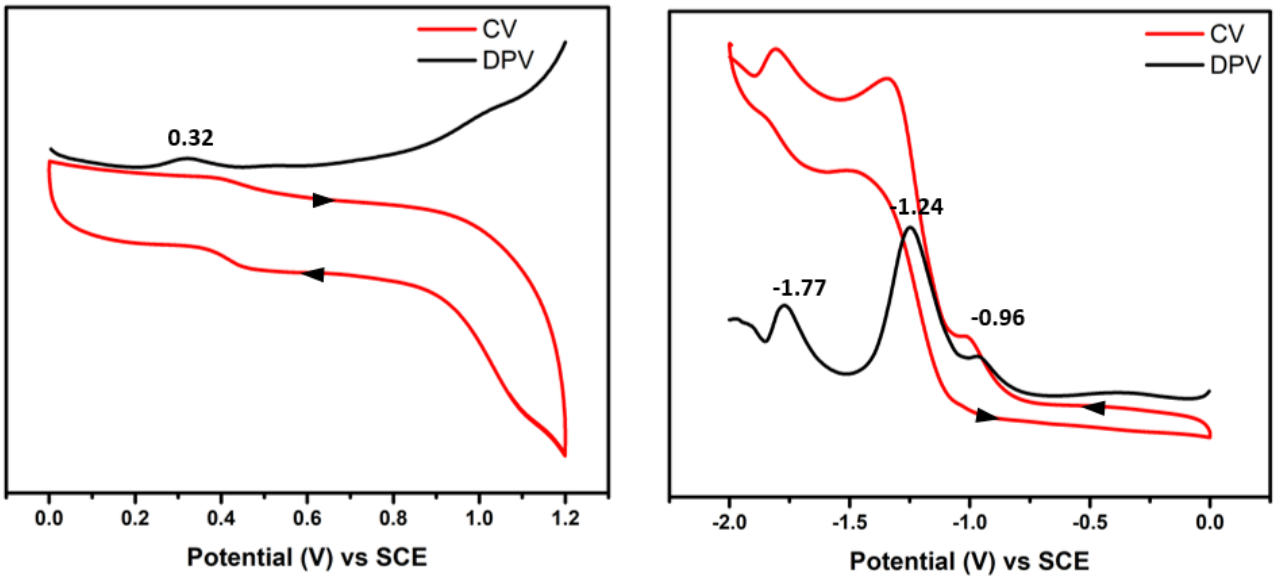

Figure 9 Cyclic voltammogram (CV) and Differential pulse voltammetry (DPV) of **III.9** (oxidation on the left and reduction on the right) in dichloromethane containing 0.1M tetrabutylammonium perchlorate as the supporting electrolyte recorded at 50 mVs^{-1}.

Cyclic voltammetric studies conducted on III.9 exhibited three reduction waves at -1.77 V, -1.24 V, and -0.96 V, analogous to those observed for III.7, accompanied by one oxidation wave at 0.32 V, as depicted in Fig 10. These findings suggest the potential for employing appropriate redox reagents to either reduce the 25π radical system to the 26π aromatic anionic state or oxidize it to the 24π antiaromatic cationic species.

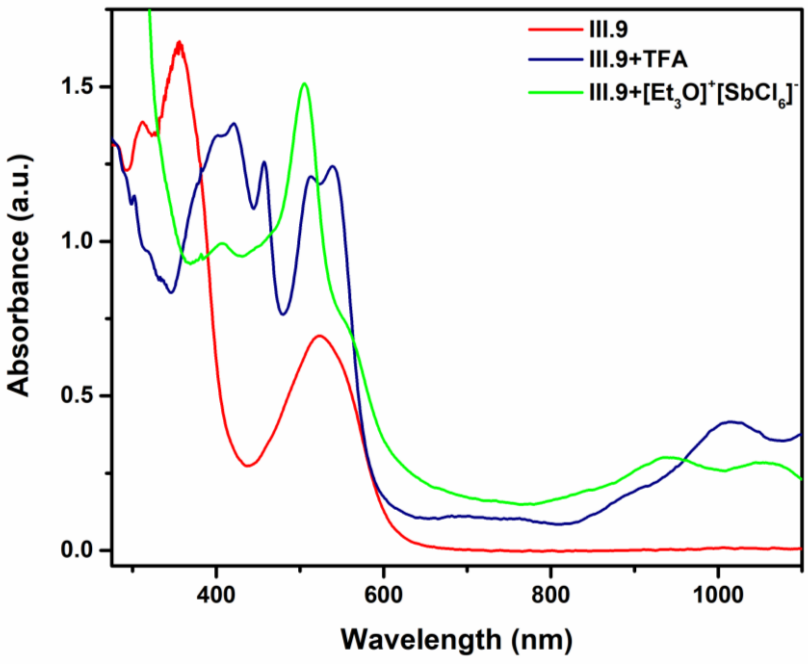

Figure 10 UV-Vis Absorption spectrum of oxidation of **III.9** in $CHCl_3$.

Chemically we also tried to observe the oxidation with different oxidizing agents using UV-Vis spectroscopy, where it shows a clear change in its absorption spectra.

III.B.4 Synthesis and characterization of 'phenanthroline-embedded open shell macrocycle' III.11

Synthesis of 'Phenanthroline-embedded open shell macrocycles' III.11.

Similar synthetic methodology was employed for the synthesis of a Phenanthroline-embedded diradical molecule, akin to the approach used for phenanthroline-embedded open shell macrocycle **III.9**. The precursor, 2,9-bis(5-(phenyl(thiophen-2-yl)methyl)thiophen-2-yl)-1,10-phenanthroline, was cyclized with terephthalaldehyde in the presence of $FeCl_3$ under acidic conditions, resulting in the formation of phenanthroline-embedded diradical macrocycles. However, analysis of the MALDI TOF/TOF mass spectrum revealed an observed mass of m/z 801.6758 instead of m/z 786.1296, indicating that the condensation reaction involved only one aldehyde group of terephthalaldehyde while the other remained unreacted, as depicted in **Scheme 2**.

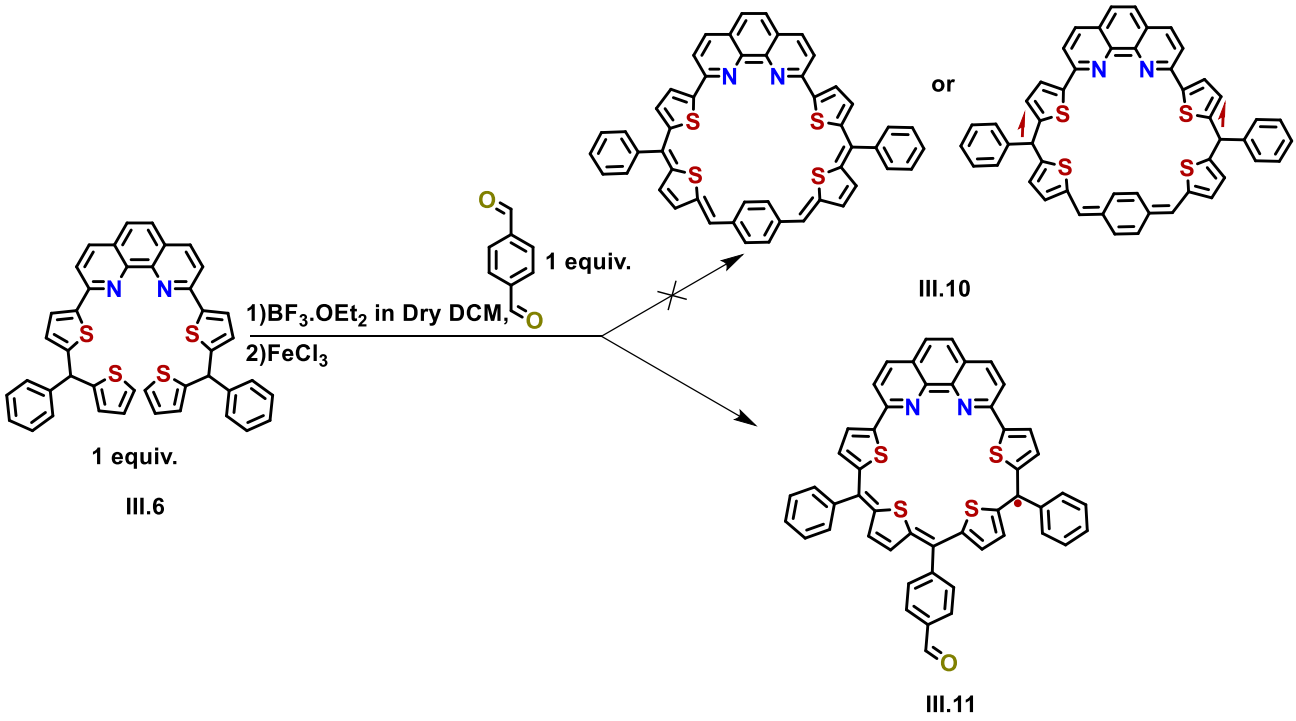

Scheme 2 Synthesis of phenanthroline-embedded open shell macrocycle (**III.11**).

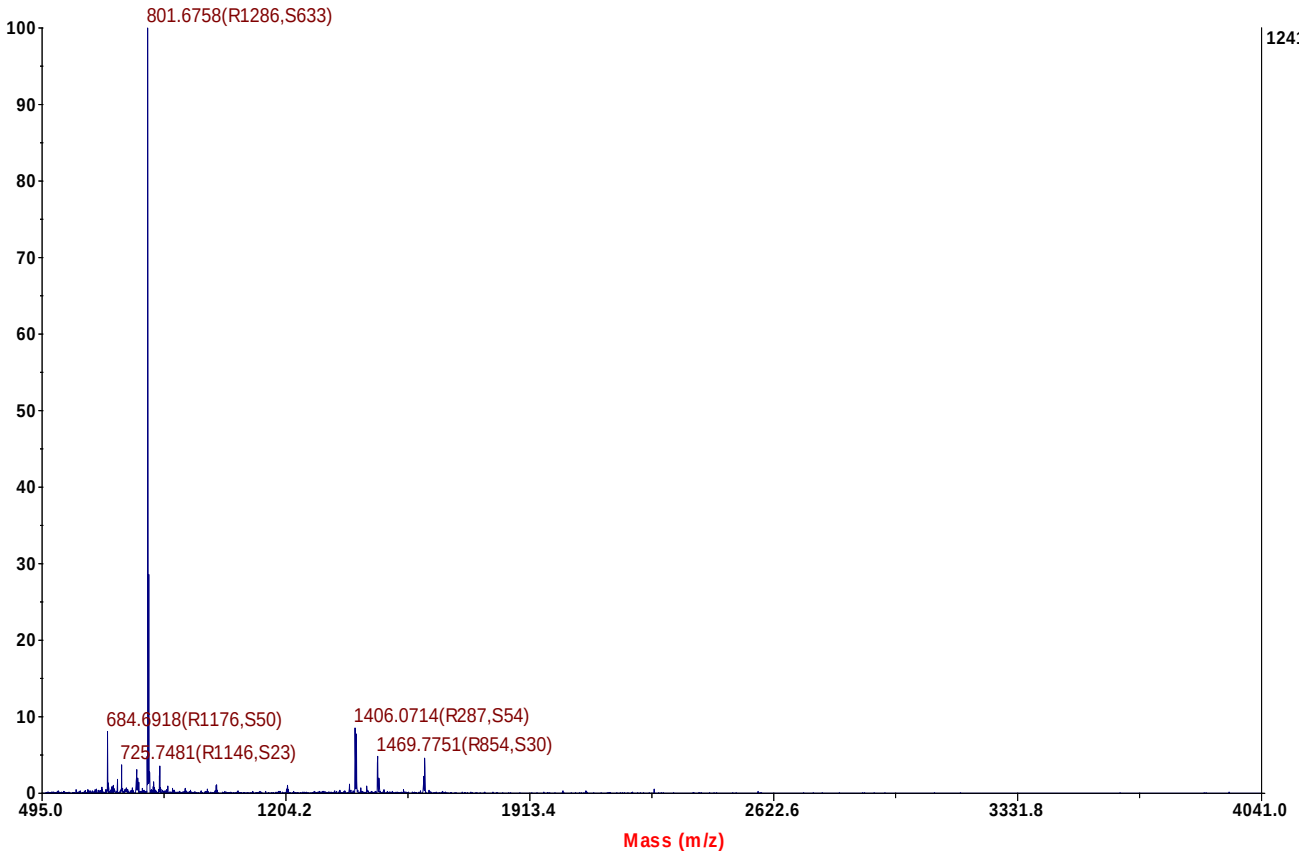

Figure 11 MALDI TOF/TOF mass spectrum of **III.11**(Calculated mass for $C_{50}H_{29}N_2OS_4^{\bullet}$ is 801.1163)..

This observation suggests that altering the stoichiometry of 2,9-bis(5-(phenyl(thiophen-2-yl)methyl)thiophen-2-yl)-1,10-phenanthroline relative to terephthalaldehyde could potentially yield a phenanthroline-embedded open shell dimer molecule (**III.12**), as depicted in **Scheme 3**, which would function as a 'biradical' (refer to **Fig 13**.). This hypothesis was substantiated by the presence of a less intense peak with a mass of m/z 1469.3519, alongside the dominant peak at m/z 801.6355 corresponding to **III.11** (see **Fig 12**.).

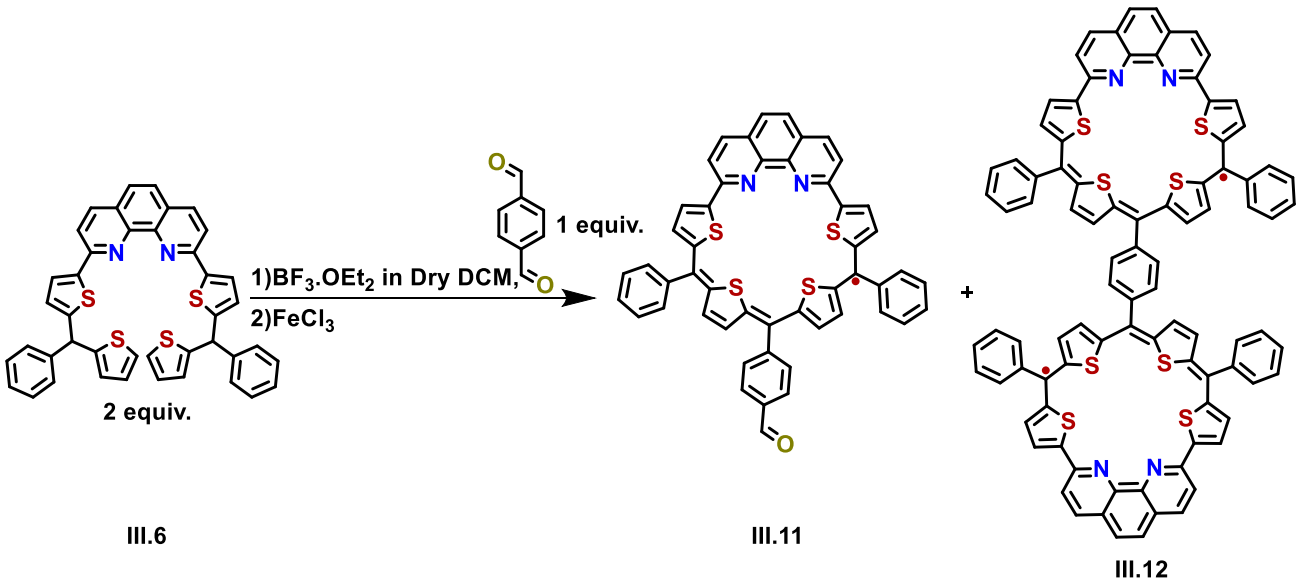

Scheme 3 Synthesis of phenanthroline-embedded open shell macrocycle (**III.12**).

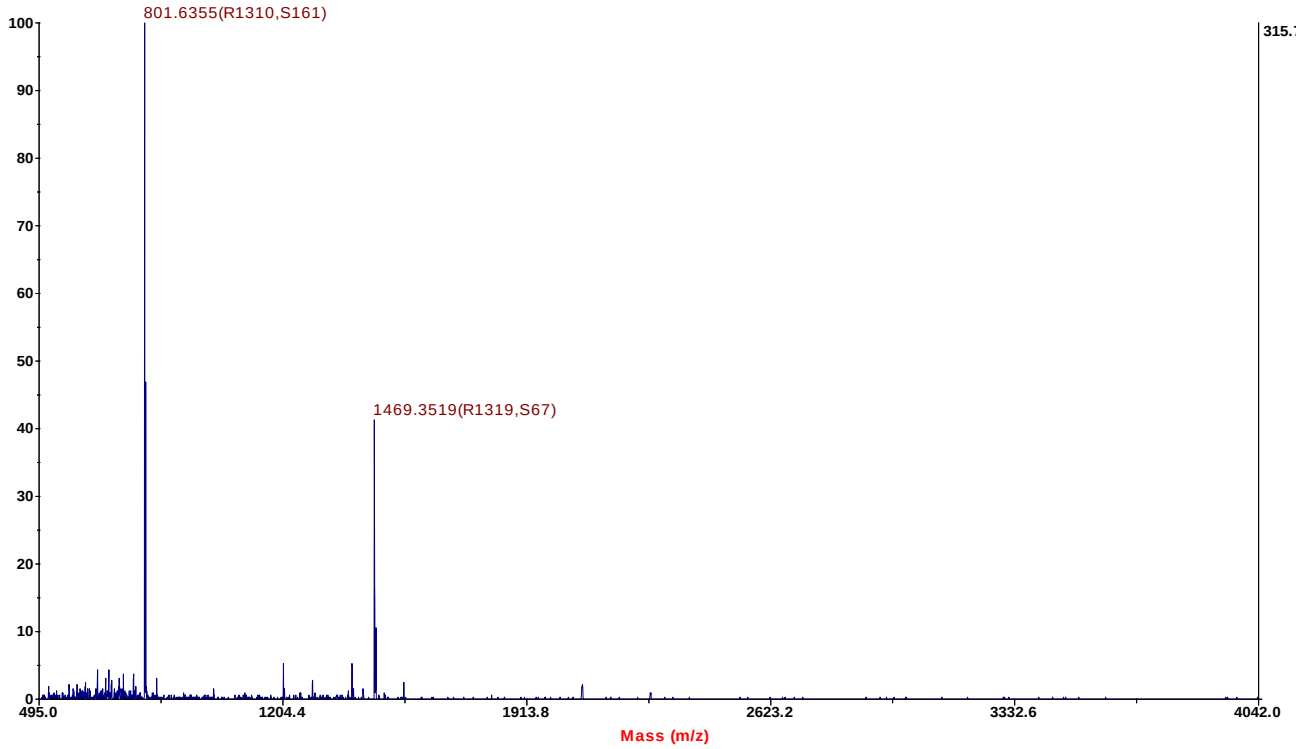

Figure 12 MALDI TOF/TOF mass spectrum of **III.12**(Calculated mass for $C_{92}H_{52}N_4S_8^{2\bullet}$ is 1468.1958).

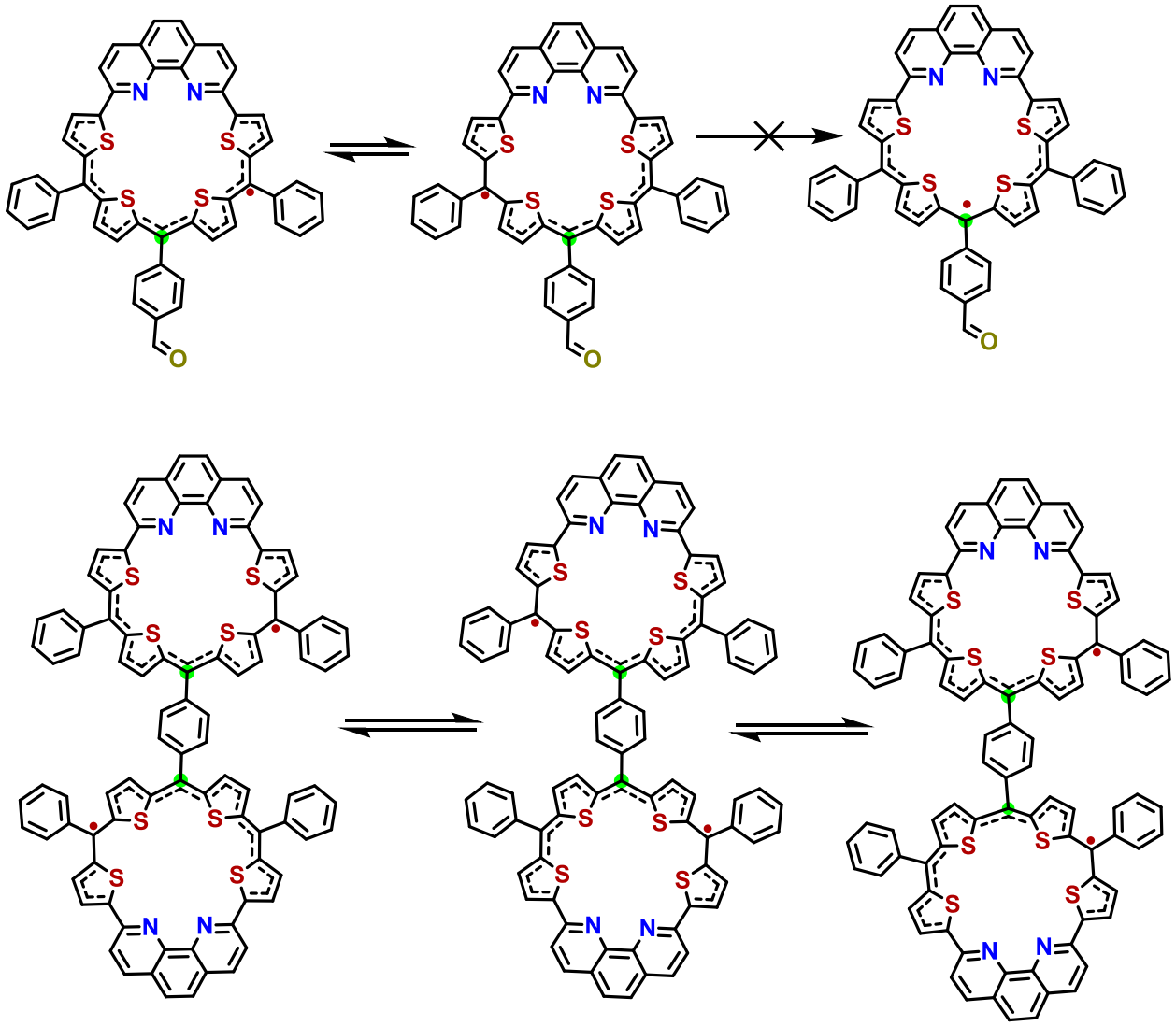

Figure 13 Canonical structures confirms the biradical nature of **III.12**.

Conclusions

The exploration of Phenanthroline-embedded porphyrinoids represents a significant step forward in the field of synthetic chemistry, offering not only fundamental insights into the molecular design but also promising avenues for the development of novel materials. Our thorough analytical investigations confirm the observation of a weak paratropic ring current in the phenanthroline-appended porphyrinoid, attributed to the limited global conjugation within the phenanthroline moiety. Quantum chemical calculations further bolster this finding, supporting the characterization of the isoamethrin (**III.7**) and phenanthroline-embedded radical (**III.9**) as weakly antiaromatic.

The synthesis and characterization of Phenanthroline-embedded porphyrinoids offer invaluable insights into the intricate structure-property relationships within these compounds. Techniques such as

X-ray crystallography, NMR spectroscopy, UV-Vis spectroscopy, and cyclic voltammetry have collectively provided a comprehensive understanding of their molecular architecture and inherent properties. By leveraging these analytical techniques, researchers gain a deeper understanding of how structural modifications, such as the integration of phenanthroline, influence the electronic and chemical behavior of porphyrinoid systems. Such insights not only contribute to our fundamental understanding of molecular design but also pave the way for the rational development of tailored materials with targeted functionalities, spanning applications in catalysis, sensing, and molecular electronics.

Moving forward, our continued endeavors are focused on achieving the synthesis of the elusive Phenanthroline-embedded porphyrinoids, leveraging the knowledge and insights acquired from this research endeavor. We anticipate that the outcomes of our investigations will significantly enhance the understanding of phenanthroline-embedded isoamethrin and radical chemistry, shedding light on its structural intricacies and reactivity patterns. These findings hold promise to catalyze further advancements in the field of macrocyclic porphyrinoids, offering new avenues for exploration and innovation.

Experimental Section

Materials and Synthesis methods:

All reactions utilizing air- or moisture-sensitive reagents were carried out in heating oven-dried glassware under a nitrogen atmosphere unless otherwise stated. Anhydrous tetrahydrofuran (THF) was distilled from sodium-benzophenone; dry Dioxane and Nitromethane were purchased at the highest commercial quality. Reagents were purchased at the highest commercial quality and used without further purification unless otherwise stated. Reactions were magnetically stirred and monitored by thin layer chromatography (TLC) with 0.15–0.2 mm pre-coated silica gel (10–40 μm) plates, using UV light as the visualizing agent. Column chromatography was performed with silica gel (100-200 as well as 230–340 mesh), Basic Al_2O_3 and size exclusion column chromatography for purification of precursor and target molecules (Macrocycles). NMR spectrum were recorded on Bruker 400 spectrometers and were calibrated using residual undeuterated solvent as an internal reference

(DMSO-D_6 ^{1}H NMR δ = 2.5 ppm) The following abbreviations were used to explain multiplicities: s = singlet, d = doublet, t = triplet, q = quartet, m = multiplet, br = broad.

Synthesis of (5-(phenyl(thiophen-2-yl)methyl)thiophen-2-yl)boronic acid (III.A)

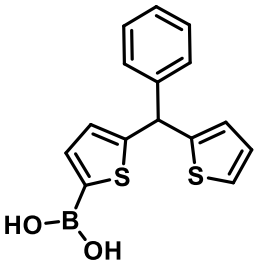

Lithium diisopropylamine (LDA) was prepared by the addition of n-BuLi (1.6 M in hexanes, 0.0023 mol) to a solution of diisopropylamine (218 mg , 0.0023 mol) in 25 mL of anhydrous THF (-78°C to room temperature).Thiophene DPM (0.65 ml, 0.002 mol) was dissolved in dry THF and was added to the LDA prepared, dropwise at −78 °C under an inert atmosphere. The solution was then stirred for 1.5 h at −78 °C. Boronic acid(608 mg, 0.006 mol) was added and the reaction mixture was stirred overnight at room temperature. The reaction was quenched with a 1 M HCl solution, dichloromethane was added and the organic phase was washed with water (2×), dried over anhydrous $MgSO_4$, and filtered. The solvent was removed under reduced pressure and the crude product III.7 was obtained as a brown sticky solid (75%).

Synthesis of 2,9-bis(5-(phenyl(thiophen-2-yl)methyl)thiophen-2-yl)-1,10-phenanthroline (III.6)

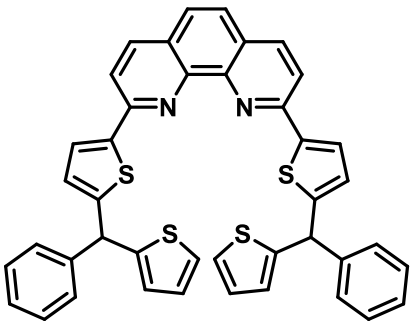

Took 2,9-dibromo-1,10-Phenanthroline(250 mg, 0.7 mmol) in an oven-dried slank tube followed by the addition of III.A (2.1 mmol) and K_2CO_3(3 mmol) at room temperature. Then added 30 ml of Dry 1,4-Dioxane and 6 ml of water(in 6:1 ratio) and purged for 1/2h with N_2 gas. After that added $Pd(PPh_3)_4$ and again purged for 1/2h with N_2 gas and refluxed for 13-15h. Then quenched the reaction with water and after evaporation under reduced pressure extracted with CH_2Cl_2 and dried over Na_2SO_4 and after evaporation under reduced pressure the crude product was purified by Column chromatography (basic Al_2O_3, n-hexane : ethyl acetate, 4:1) (85%).

^{1}H NMR (400 MHz, $CDCl_3$), δ (ppm): 8.15 (d, *J* = 8.4 Hz, 2H), 7.89 (d, *J* = 8.4 Hz, 2H), 7.68 (d, *J* = 3.8 Hz, 2H), 7.66 (s, 2H), 7.42 – 7.36 (m, 4H), 7.31 (td, *J* = 7.2, 1.3 Hz, 4H), 7.19 (dd, *J* = 4.6, 1.7 Hz, 2H), 6.94 – 6.89 (m, 6H), 5.92 (s, 2H).

Synthesis of Phenanthroline-embedded isoamethrin (III.7)

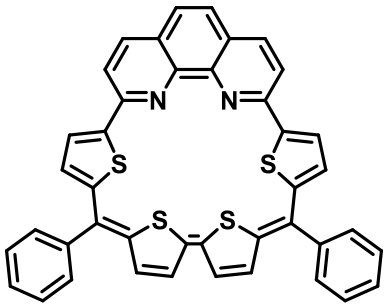

In a two-neck 50 ml oven-dried RB flask added III.6 (30 mg) purged with N_2 gas. 30 ml of CH_2Cl_2 and CH_3NO_2(1:1) then added TFA(0.2-0.3 ml) and stirred for 1/2h and then added $FeCl_3$(4 eq)continued stirring for 1/2 h. MALDI suggest the formation of 3. After evaporation under reduced pressure, the crude product was purified by Column chromatography (basic Al_2O_3, n-hexane : DCM, 1:1) as a purple coloured solid as a pure product (10%).

^{1}H NMR (400 MHz, DMSO-D_6), δ (ppm): 8.02 (d, *J* = 8.6 Hz, 1H), 7.80 (d, *J* = 8.5 Hz, 1H), 7.48 – 7.41 (m, 3H), 7.37 (d, *J* = 4.2 Hz, 1H), 7.34 (s, 1H), 7.29 – 7.23 (m, 2H), 6.73 (d, *J* = 5.7 Hz, 1H), 6.13 (d, *J* = 4.2 Hz, 1H), 5.97 (d, *J* = 5.6 Hz, 1H);

UV-Vis λmax (nm) (ε) Lmol-1cm-1 (in CH_2C1_2) ε; 421(16200), 733(1800)

MALDI TOF/TOF mass spectra calculated for $C_{42}H_{24}N_2S_4$ is 684.0822, found 684.2809.

HR-MS (ESI-TOF): m/z=685.0880(found [M]+H)(Calculated mass for $C_{42}H_{24}N_2S_4$ is 684.0822).

Crystal data: $C_{42}H_{24}S_4N_2$, $CHCl_3$ Orthorhombic, space group Pca21, a = 22.618(4), b = 18.794(4), c = 17.346(3)Å, α = 90, β = 90, γ= 90. V = 7374(2)$Å^3$, Z = 8, T=150(2) K, D_{calcd} = 1.449 g cm^{-3}, R_1 = 0.1203(6490), Rw (all data) = 0.2949(3388), GOF = 1.203.

Synthesis of oxidized Phenanthroline-embedded isoamethrin (III.8)

In an oven-dried NMR tube added approx 5mg of III.7 then added $CDCl_3$ to the NMR tube and dissolved it properly and after that added few drops of TFA then observed a significant color change which converts from light green to dark green solution and after solidifying it gives dark green colored crystals in quantitative yield.

^{1}H NMR (400 MHz, $CDCl_3$), δ (ppm): 9.10 (d, *J* = 8.7 Hz, 1H), 8.72 (d, *J* = 8.6 Hz, 1H), 8.53 – 8.45 (m, 2H), 8.29 (d, *J* = 8.9 Hz, 1H), 8.25 – 8.19 (m, 2H), 7.98 – 7.90 (m, 4H), 7.84 (d, *J* = 4.4 Hz, 1H), 7.75 (dd, *J* = 8.4, 3.7 Hz, 5H), 7.47 – 7.31 (m, 5H), 7.29 (s, 1H), 7.17 (d, *J* = 3.9 Hz, 1H), 6.21 (s, 1H).;

UV-vis λmax (nm) (ε) $Lmol^{-1}cm^{-1}$ (in CH_2C1_2): 406(7600), 511(5200), 804(2100) and 874(2300).

HR-MS (ESI-TOF): m/z=342.5439 (found [M]+H/2)(Calculated mass for $C_{42}H_{24}N_2S_4^{++}$ is 342.5440).

Crystal data: 2($C_{42}H_{24}S_4N_2$), 9($C_2F_3O_2$), 3(O) Triclinic, space group P -1, a = 14.290(3), b = 19.005(4), c = 20.700(4)Å, α = 113.699(5), β = 95.389(6), γ= 96.276(6). V = 5057.8(18)$Å^3$, Z = 2, T=150(2) K, D_{calcd} = 1.599 g cm^{-3}, R_1 = 0.0776 (9816), Rw (all data) = 0.2318(23216), GOF = 0.976.

Synthesis of Phenanthroline-embedded open-shell macrocycle(III.9)

In a two-neck 50 ml oven-dried RB flask added III.6 (30 mg) and benzaldehyde(1 equiv.) purged with N_2. 30 ml of dry CH_2Cl_2 then added $BF_3.OEt_2$(0.1-0.3 equiv.) then added $FeCl_3$(10-15 equiv.) continued stirring for 1/2 h. MALDI suggests the formation of III.9. After evaporation under reduced pressure, the crude product was purified by Column chromatography (basic Al_2O_3, n-hexane : DCM, 1:1) as a purple-colored solid as a pure product (10%).

UV-vis λmax (nm) (ε) $Lmol^{-1}cm^{-1}$ (in CH_2C1_2); 313(2100), 355(2600) and 522(1100).

MALDI TOF/TOF mass spectra calculated for $C_{49}H_{29}N_2S_4^{\bullet}$ is 773.1214, found 773.3364.

HR-MS (ESI-TOF): m/z=773.1212(found [M]+)(Calculated mass for $C_{49}H_{29}N_2S_4^{\bullet}$ is 773.1214).

Crystal data: $C_{51}H_{31}Cl_7N_2S_4$, Monoclinic, space group P 21/n, a = 9.0597(15), b = 21.588(4), c = 24.609(4)Å, α = 90, β = 90.485(6), γ= 90. V = 4812.9(14)$Å^3$, Z = 4, T=150(2) K, D_{calcd} = 1.447 g cm^{-3}, R_1 = 0.1671 (4482), Rw (all data) = 0.4149(5308), GOF = 1.319.

Synthesis of Phenanthroline-embedded open-shell macrocycle(III.11)

In a two-neck 50 ml oven-dried RB flask added III.6 (30 mg) and terephthalaldehyde (1 equiv.) purged with N_2. 30 ml of dry CH_2Cl_2 then added $BF_3.OEt_2$(0.1-0.3 equiv.) then added $FeCl_3$(10-15 equiv.) continued stirring for 1/2 h. MALDI suggests the formation of III.11. After evaporation under reduced pressure, the crude product was purified by Column chromatography (basic Al_2O_3, n-hexane : DCM, 1:1) as a purple-colored solid as a pure product (<5%).

MALDI TOF/TOF mass spectra calculated for $C_{50}H_{29}N_2OS_4^{\bullet}$ is 801.1163, found 801.6758.

Synthesis of Phenanthroline-embedded open-shell dimer (III.12)

In a two-neck 50 ml oven-dried RB flask added **III.6** (30 mg) and terephthalaldehyde (0.5 equiv.) purged with N_2 gas. 30 ml of dry CH_2Cl_2 then added $BF_3.OEt_2$(0.1-0.3 equiv.) then added $FeCl_3$(10-15 equiv.) continued stirring for 1/2 h. MALDI suggests the formation of **III.12**. After evaporation under reduced pressure, the crude product was purified by Column chromatography (basic Al_2O_3, n-hexane : DCM, 1:1) as a purple-colored solid as a pure product (<1%).

MALDI TOF/TOF mass spectra calculated for $C_{92}H_{52}N_4S_8^{2\bullet}$ is1468.1958, found 1469.3519.

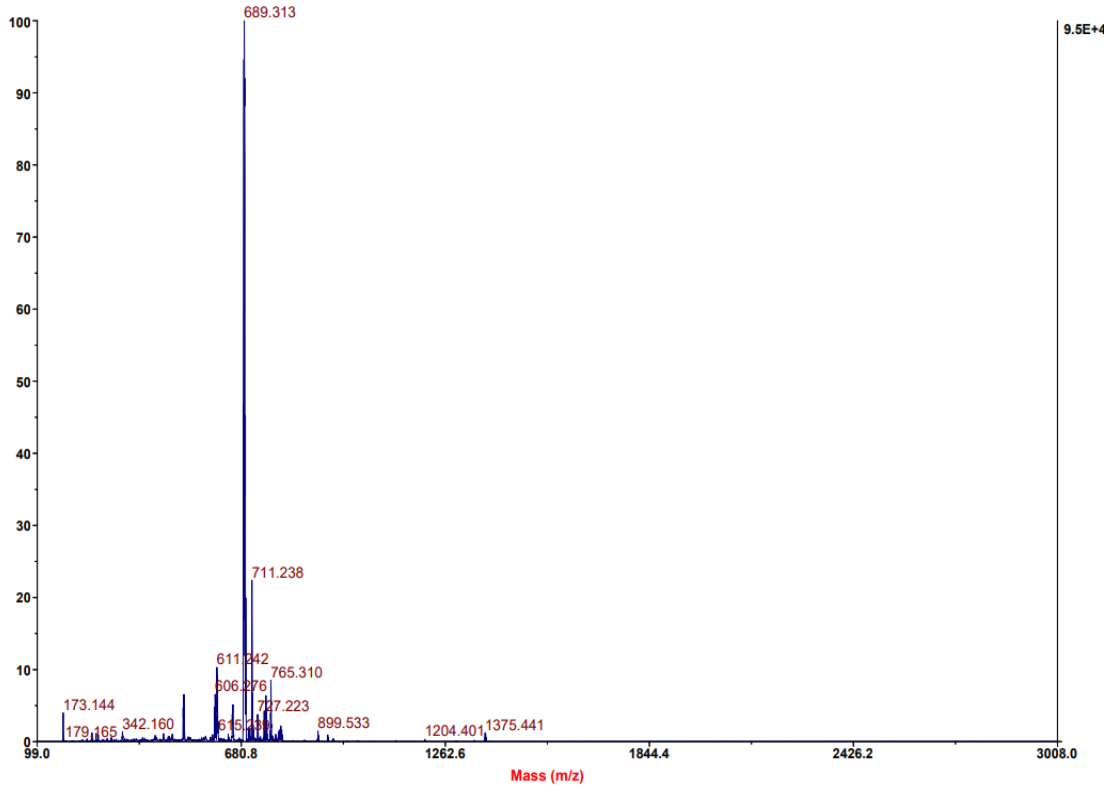

Figure 14 MALDI TOF/TOF mass spectrum of **III.6** (Calculated mass for $C_{42}H_{28}N_2S_4$ is 688.1135).

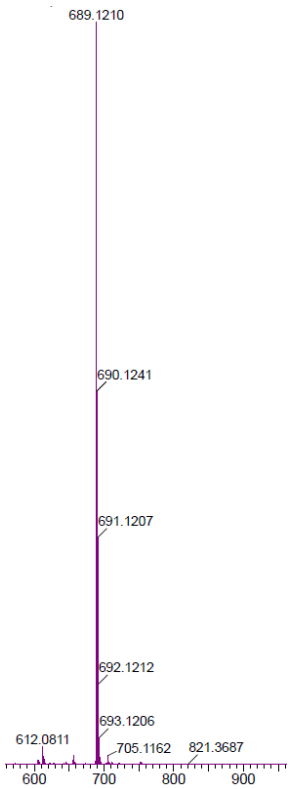

Figure 15 HRMS mass spectrum of **III.6**(Calculated mass for $C_{42}H_{28}N_2S_4$ is 688.1135)**.**

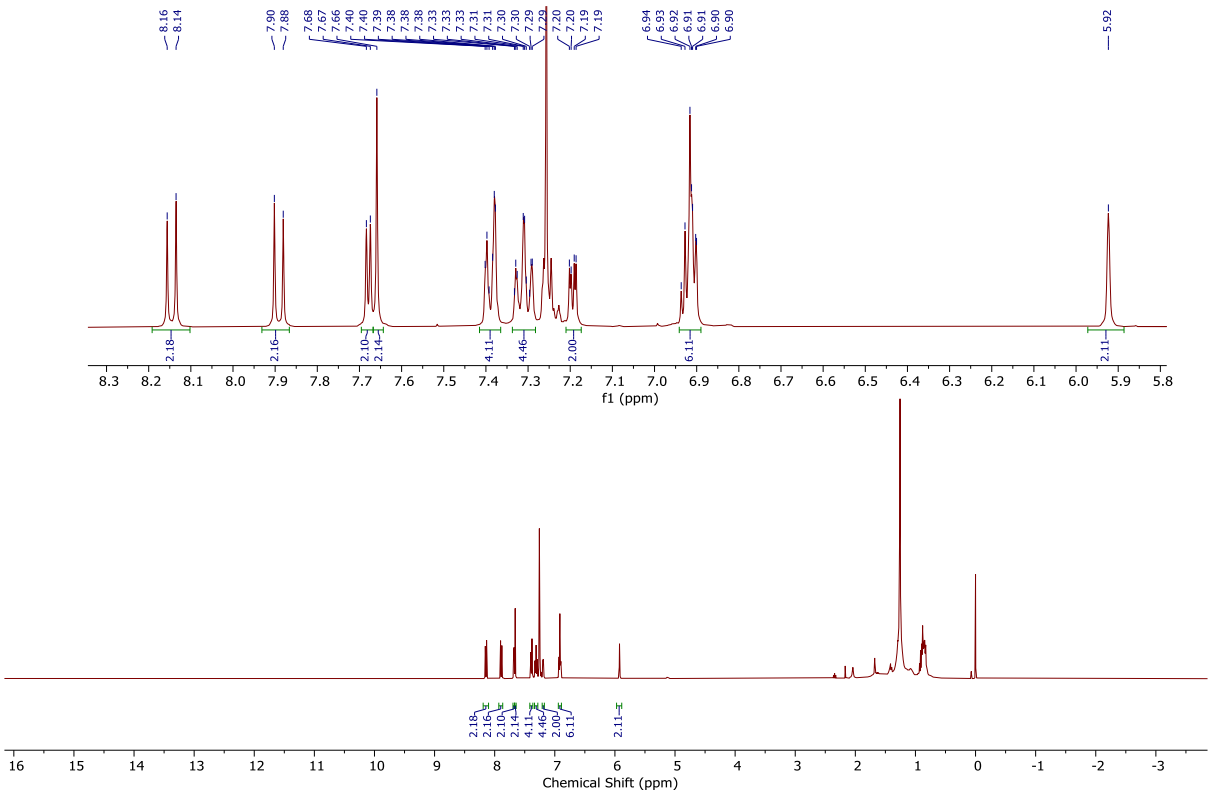

Figure 16 ^{1}H NMR spectrum of **III.6** in $CDCl_3$.

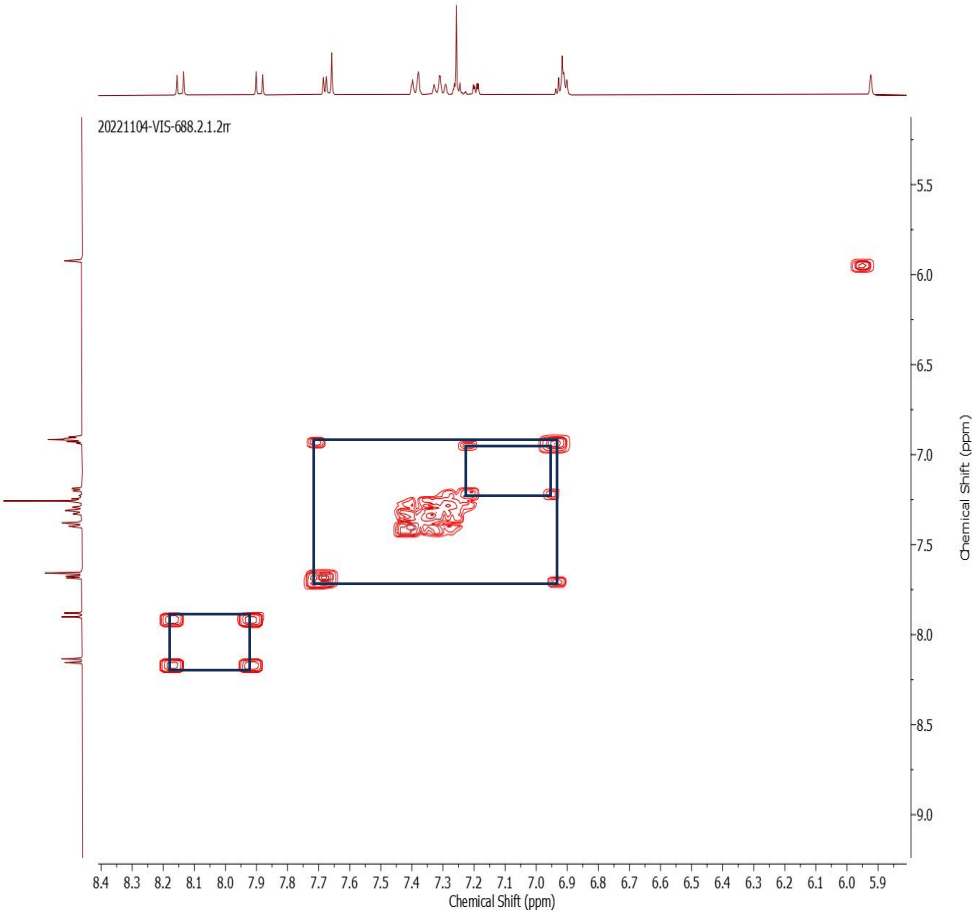

Figure 17 ^{1}H-^{1}H COSY Spectrum of **III.6** in $CDCl_3$**.**

References

(1) Gianluca Accorsi, Andrea Listorti, K. Yoosaf and Nicola Armaroli, *Chem. Soc. Rev.*, 2009, **38**, 1690–1700.

(2) M. J. Crossley, P. L. Burn, S. J. Langford and J. K. Prashar, *J. Chem. Soc., Chem. Comm.*, 1995, 1921-1923.

(3) Jean-Pierre Sauvage, *Acc. Chem. Res.*, 1990, **23**(10), 319-327.

(4) Masatoshi Ishida, Yoshinori Naruta, and Fumito Tani, *Angew. Chem. Int. Ed.*, 2010, **49**, 91 – 94.

(5) Hassan Norouzi-Arasi, Wojciech Pisula, Alexey Mavrinskiy, Xinliang Feng, and Klaus Mullen., *Chem. Asian J.*, 2011, **6**, 367 – 371.

(6) M. Gomberg, *J. Am. Chem. Soc.* 1900, **22**, 757; b) K. Goto, T.Kubo, K. Yamamoto, K. Nakasuji, K. Sato, D. Shiomi, T. Takui,M. Kubota, T. Kobayashi, K. Yakusi, J. Ouyang, J. *Am. Chem.Soc.* 1999, **121**, 1619; c) A. Rajca, J. Wongsriratanakul, S. Rajca, *Science.*, 2001, **294**, 1503; d) M. E. Itkis, X. Chi, A. W. Cordes,R. C. Haddon, *Science*., 2002, **296**, 1443; e) R. G. Hicks, *Org. Biomol. Chem.* 2007, **5**, 1321; f) Y. Morita, S. Nishida, Stable Radicals, Wiley, Hoboken, 2010, p. 81.

(7) Y. Morita, S. Nishida, T. Murata, M. Moriguchi, A. Ueda, M.Satoh, K. Arifuku, K. Sato, T. Takui, *Nat. Mater.*, 2011, **10**, 947.

(8) J. Doe, *Chem. Rev.*, 2021, **121**, 7890–7901.

(9) A. Smith and B. Johnson, *Acc. Chem. Res.*, 2020, **53**, 1543–1554.

(10) C. Brown, Radical Chemistry: Applications and Advances, Wiley, 2019, ch. 5, pp. 112–145.

(11) J. Doe and M. Smith, *J. Org. Chem.*, 2021, **86**, 2345–2357.

(12) A. Brown, *Chem. Soc. Rev.*, 2020, **49**, 678–690.

(13) B. Johnson, *Advances in Radical Chemistry*, Springer, 2019, pp. 123–145.

(14) Tullimilli Y. Gopalakrishna, J. Sreedhar Reddy, and Venkataramanarao G. Anand, *Angew. Chem. Int. Ed.*, 2014, **53**, 10984 –10987.

Chapter 4:- Aromatic Expanded Porphyrinoids

Section-A
Synthesis and characterization of Aromatic Expanded Porphyrinoids: Behaving like Molecular Absorber(Sponge)

IV.A.1 Introduction:

Porphyrinoids have captivated the interest of chemists, physicists, and materials scientists for decades due to their remarkable structural, electronic, and functional properties. Derived from the parent compound porphyrin, which serves as the core structure of important biological molecules such as heme, chlorophyll, and vitamin B12, porphyrinoids exhibit a wide range of structural variations and chemical functionalities. This versatility has paved the way for their utilization in a diverse array of applications, ranging from catalysis and sensing to photovoltaics and medicine.

The unique electronic properties of porphyrinoids stem from their aromaticity and conjugated π-systems, which endow them with a host of intriguing characteristics, including strong absorption in the visible region, high thermal and chemical stability, and facile redox chemistry. These features have rendered porphyrinoids indispensable in fields such as molecular electronics, where they serve as building blocks for organic semiconductors and optoelectronic devices, as well as in catalysis, where they act as versatile catalysts for a variety of chemical transformations.

Among the diverse array of porphyrinoids, aromatic expanded porphyrinoids occupy a special niche, distinguished by their unique structural motifs and extended π-conjugated frameworks. These molecules, which feature additional aromatic rings fused to the traditional porphyrin core, exhibit enhanced delocalization of π-electrons and altered electronic properties compared to their classical counterparts. The exploration of aromatic expanded porphyrinoids has thus emerged as a burgeoning field of research, driven by the quest for novel materials with tailored electronic and optical properties.

In recent years, significant strides have been made in the synthesis, characterization, and application of aromatic expanded porphyrinoids, fuelled by advances in organic synthesis, spectroscopy, and computational chemistry. These developments have not only expanded our understanding of the structural diversity and reactivity of these compounds but have also unlocked new avenues for their utilization in various technological and scientific domains.

This chapter aims to provide a comprehensive overview of aromatic expanded porphyrinoids, encompassing their synthesis, structural characterization, physical and chemical properties, as well as their emerging applications. Synthesis and analysis of a wide range of aromatic expanded porphyrinoids, will aid to elucidate the underlying principles governing their behavior and explore their potential in fields such as molecular electronics, catalysis, and biomedicine.

Subsequent sections will describe the synthetic methodologies employed for the preparation of aromatic expanded porphyrinoids, discussing both traditional approaches and recent advances. Further, the structural features and spectroscopic characteristics of these compounds will provide insights into their electronic structure and optical properties. Their physical and chemical properties, including redox behavior, and reactivity towards various substrates will be detailed.

The pioneering discovery of sapphyrin[1] by R. B. Woodward marked the inception of expanded porphyrin chemistry. In 1990, Sessler and collaborators unveiled Sapphyrin **IV.1**[2], showcasing the potential of expanded porphyrins in diverse applications such as anion recognition, aromaticity, photodynamic therapy (PDT), and magnetic resonance imaging (MRI) contrast agents.[3,4,5] This seminal work paved the way for subsequent advancements in the field. Additionally, the same group introduced "Turcasarin," a decapyrrolic macrocycle with a unique "figure-of-eight" conformation, increasing the structural diversity of expanded porphyrins.[6]

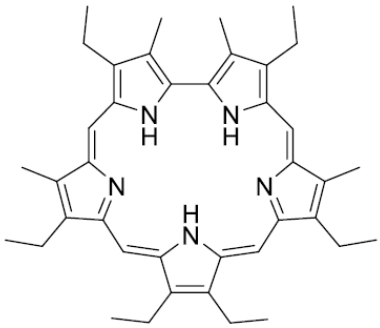

IV.1

Figure 1 Sapphyrin serves as a prominent example of an expanded porphyrin.

In a scientific context, Sessler and Seidel established a precise definition of expanded porphyrins, classifying them as macrocycles that integrate pyrrole, thiophene, furan, or other heterocyclic subunits. These subunits are interconnected either directly or through spacer atoms, ensuring the presence of a minimum of 17 atoms within the internal ring pathway.[7] Moreover, Osuka and collaborators serendipitously uncovered a series of expanded porphyrins featuring meso pentafluorophenyl substitutions while synthesizing tetrakis(pentafluorophenyl)porphyrin. This unexpected finding not only diversified the structural landscape of porphyrin derivatives but also highlighted the potential for serendipitous discoveries within scientific research endeavors.[8,,9,10]

From this reaction, a range of higher-membered macrocycles emerged, including pentaphyrin (**IV.3**), hexaphyrin (**IV.4**), heptaphyrin (**IV.5**), octaphyrin (**IV.6**), and larger analogs. In comparison to porphyrin, these macrocycles contain an increasing number of heterocyclic rings, resulting in enhanced conformational flexibility. As a consequence, they tend to adopt a twisted conformation, which ultimately leads to a loss of aromaticity or antiaromaticity due to their unique structural arrangement.

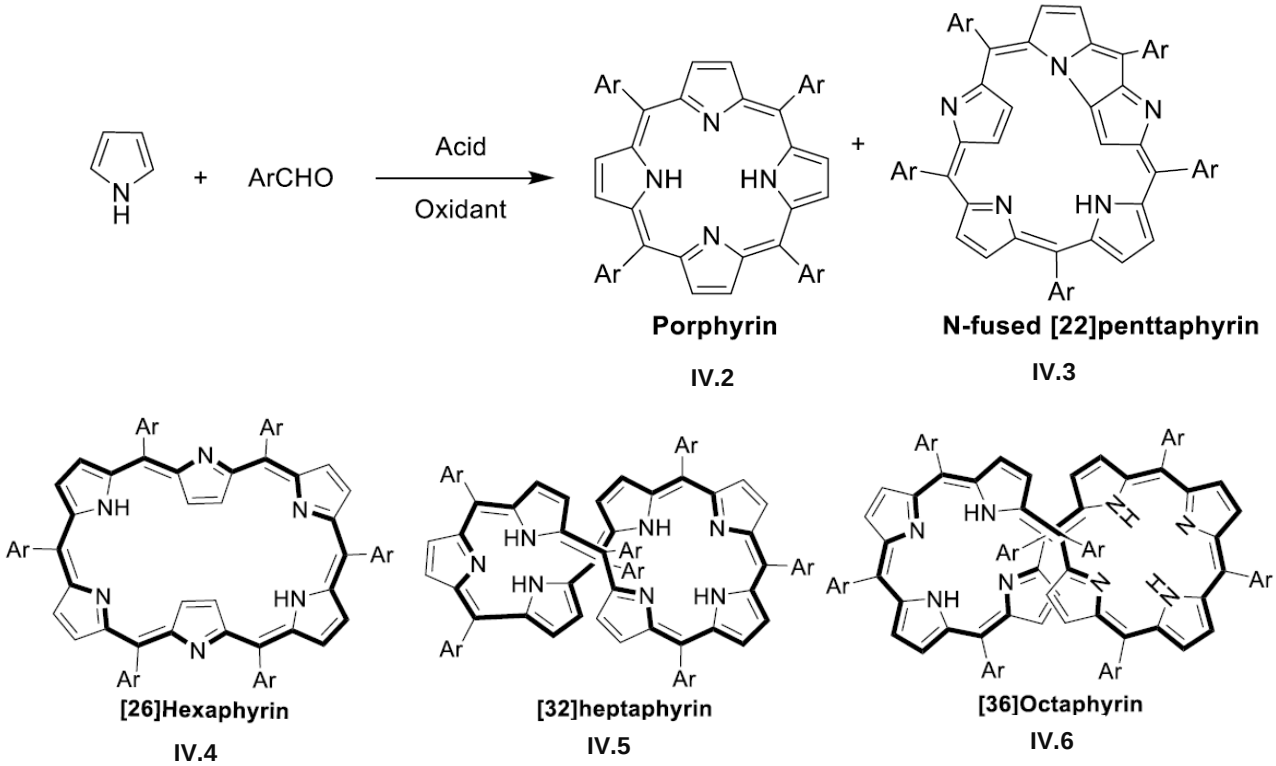

Figure 2 One pot synthesis of meso-aryl substituted porphyrin and expanded porphyrinoids.

In 2008, report on the synthesis of electron-deficient pentafluorophenyl-substituted meso carbons, resulted in the formation of air-stable 20π isophlorins **IV.7** and **IV.8**. Their structural configuration was found to be contingent upon the heteroatoms present within the macrocycle's core. Specifically, the tetraoxaisophlorin **IV.7** exhibits a flat square conformation, whereas compound **IV.8** adopts a flat rectangle shape, despite both possessing a formal count of 20π electrons. This difference can be attributed to the presence of two bulky sulfur atoms at the center, which occupy additional space and consequently push the two oxygen atoms away from the center.[11]

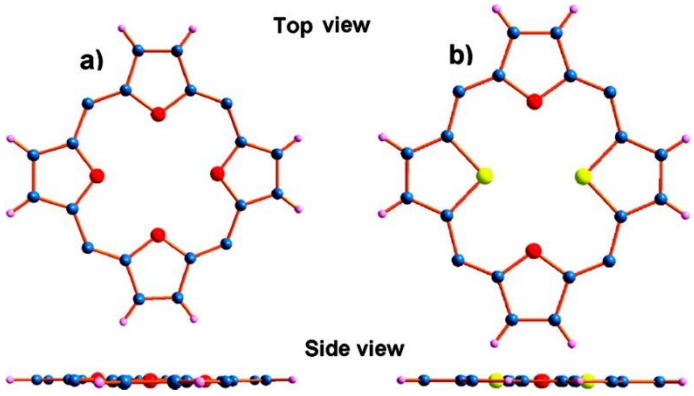

Figure 3 Structural diversity in 20π macrocyclic systems, **IV.7(a)** and **IV.8(b)**.

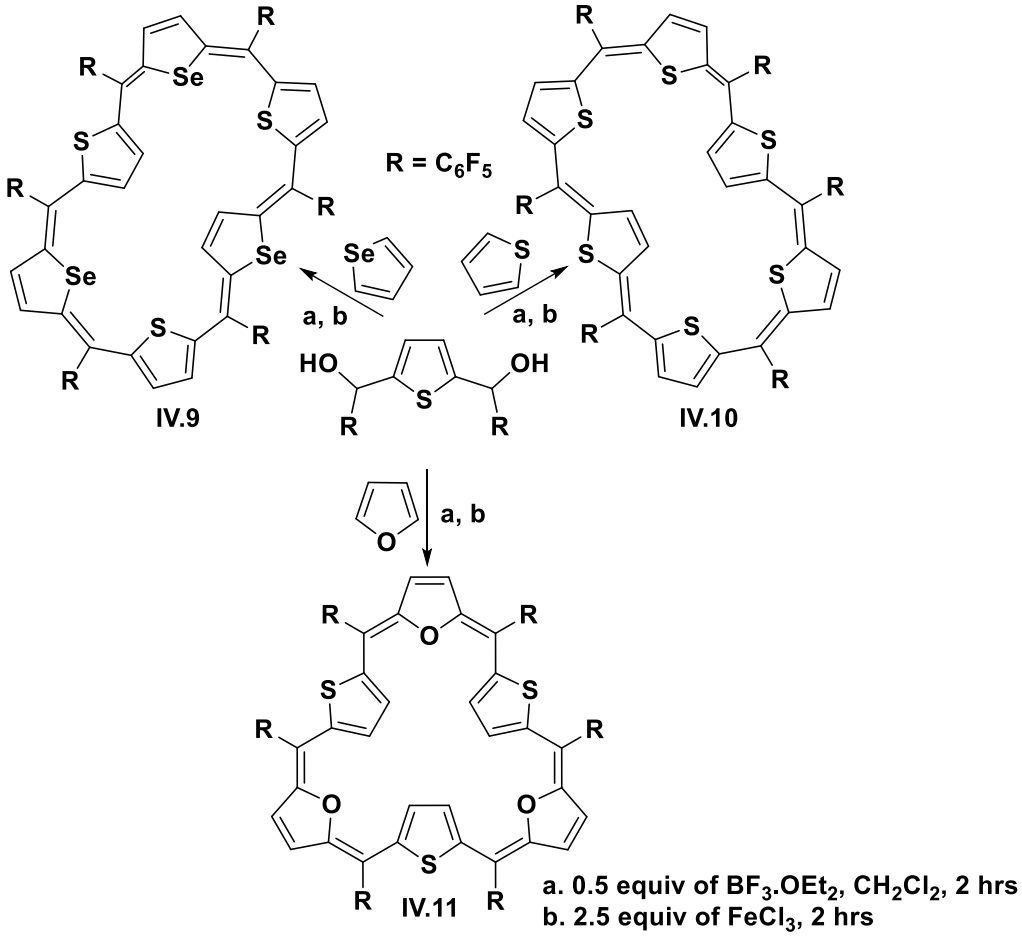

Figure 4 Structural diversity in 30π macrocyclic system due to Core-modification.

Similarly, the influence of core modification in hexapyrin **IV.4** was evaluated by replacing nitrogen with a combination of various chalcogens. From **Figure 4**, it is evident that the macrocycle adopts two distinct geometries: one exhibiting a rectangular shape, where the diol undergoes condensation with thiophene and selenophene, and the other displaying a triangular configuration, wherein the diol undergoes condensation with furan.[12]

IV.A.2 Synthesis and characterization of Aromatic Expanded Porphyrinoids' IV.12.

'Synthesis of Aromatic Expanded Porphyrinoids' IV.12.

To explore additional factors contributing to structural diversity in these macrocycles, β-substituted thiophene was employed by condensing with an appropriate diol. This investigation provided valuable insights into the interplay between chemical modifications and resulting structural diversity in these systems.

The synthesis of 30π expanded porphyrinoid **IV.12** involved an acid-mediated condensation reaction between 3,4-diphenylthiophene and thiophene-2,5-diylbis((perfluorophenyl)methanol) under inert conditions, followed by oxidation in ambient air (**Scheme 1**). Purification of the expected product was achieved via silica gel column chromatography, yielding an orange-brown-colored band in 10% yields.

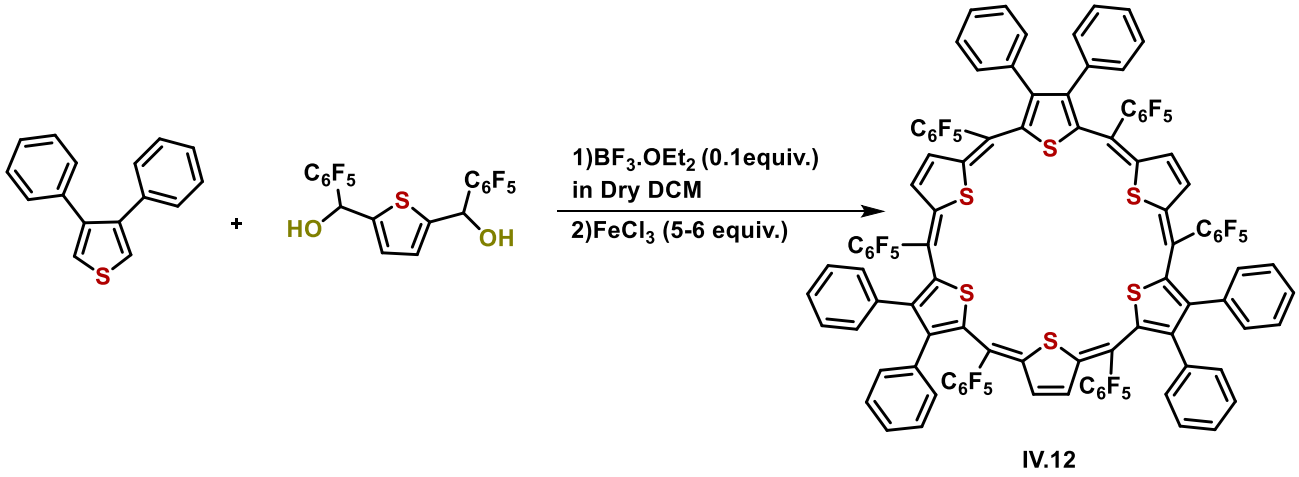

Scheme 1 Synthesis of 30π Expanded prophyrinoid, **IV.12**.

Structural characterization of Aromatic Expanded Porphyrinoid IV.12.

Aromatic expanded porphyrinoid **IV.12**, was characterized through a diverse range of analytical techniques. High-resolution mass spectrometry (HRMS) accurately confirmed its exact molecular mass and composition. UV-Vis spectroscopy unveiled its electronic absorption properties, highlighting the weak interacting p orbitals that are responsible for global conjugation. NMR spectroscopy provided insights into the chemical environment and connectivity of atoms within **IV.12**, offering detailed structural information. X-ray crystallography facilitated the determination of its three-dimensional molecular structure at atomic resolution.

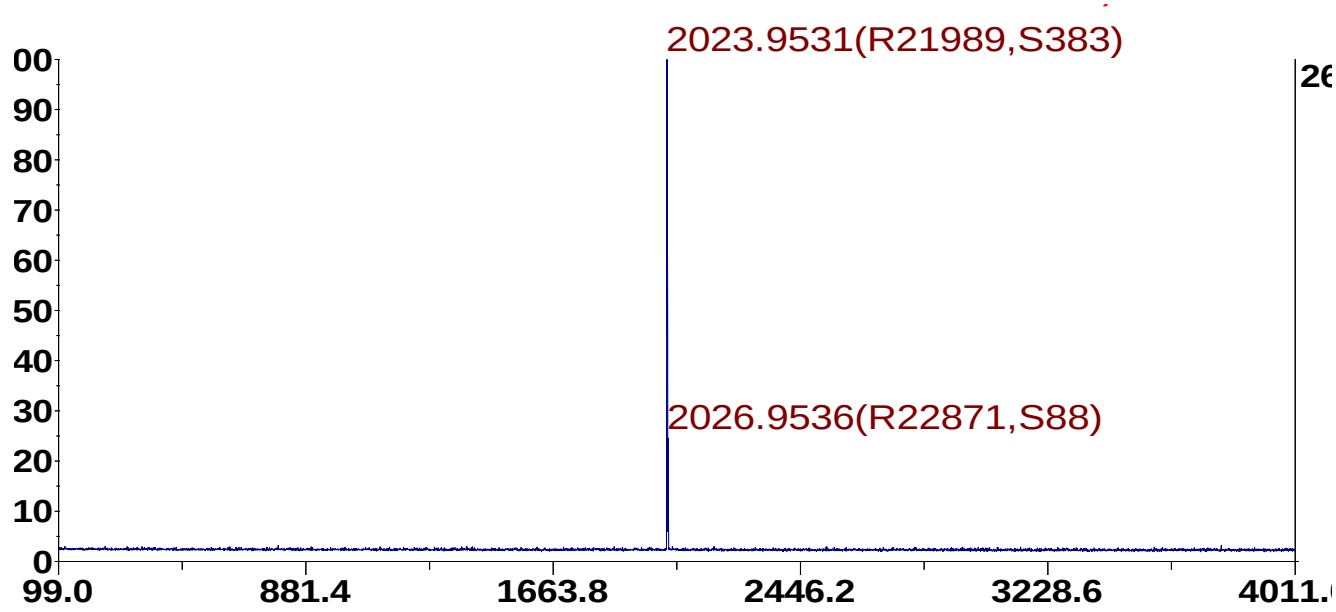

Figure 5 MALDI TOF/TOF mass spectrum of **IV.12**(Calculated mass for $C_{102}H_{36}F_{30}S_6$ is 2022.8963).

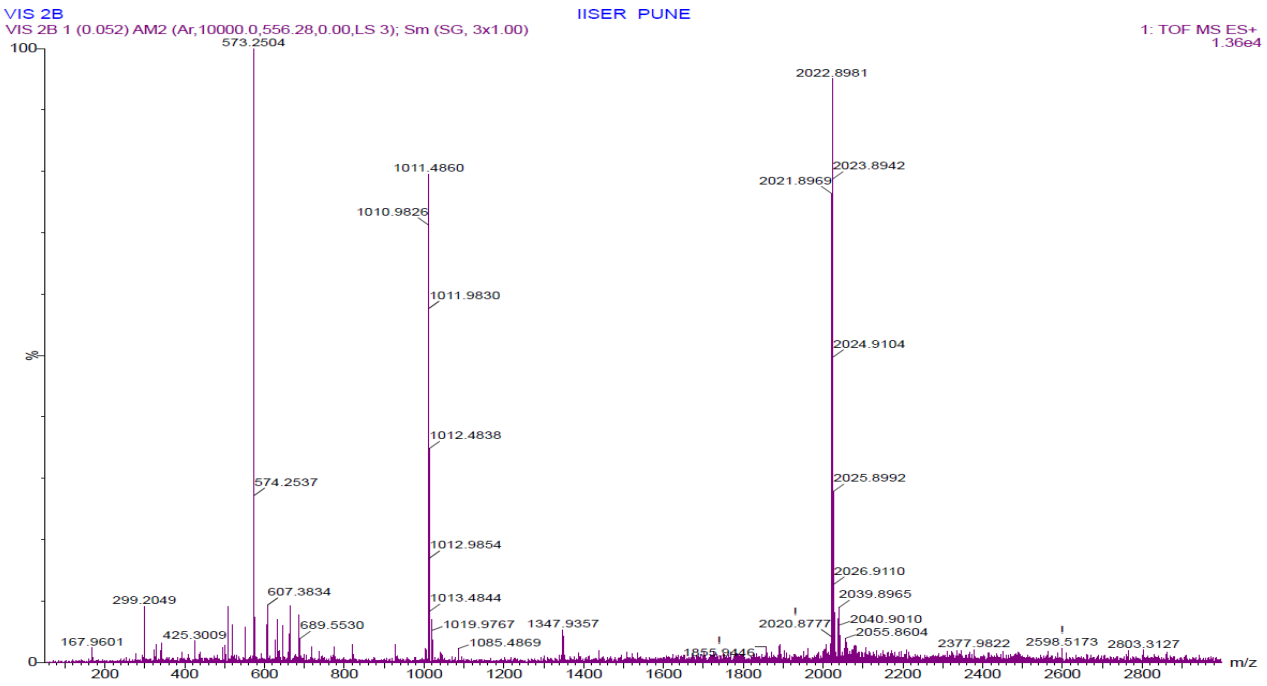

Figure 6 HR-ESI-TOF mass spectrum of of **IV.12**(Calculated mass for $C_{102}H_{36}F_{30}S_6$ is 2022.8963).

NMR characterization

The ^{1}H NMR spectrum of Aromatic expanded porphyrinoid **IV.12**, revealed a reduced number of signals, indicating potential higher molecular symmetry. Only one set of β-CH thiophene protons manifested as singlet at δ 7.15 ppm. Phenyl protons were identified as multiplets within the ranges of δ 7.08-6.95 and 6.94-6.85 ppm.

Consistent with the molecular structure elucidated through X-ray crystallography, the observed chemical shift values do not align with the anticipated diatropic ring current effect characteristic of (4n+2)π systems. The estimated Nucleus Independent Chemical Shift (NICS) value of -0.69 ppm for **IV.12** provides further confirmation of the weak ring current, emphasizing the impact of limited global conjugation in the molecule.

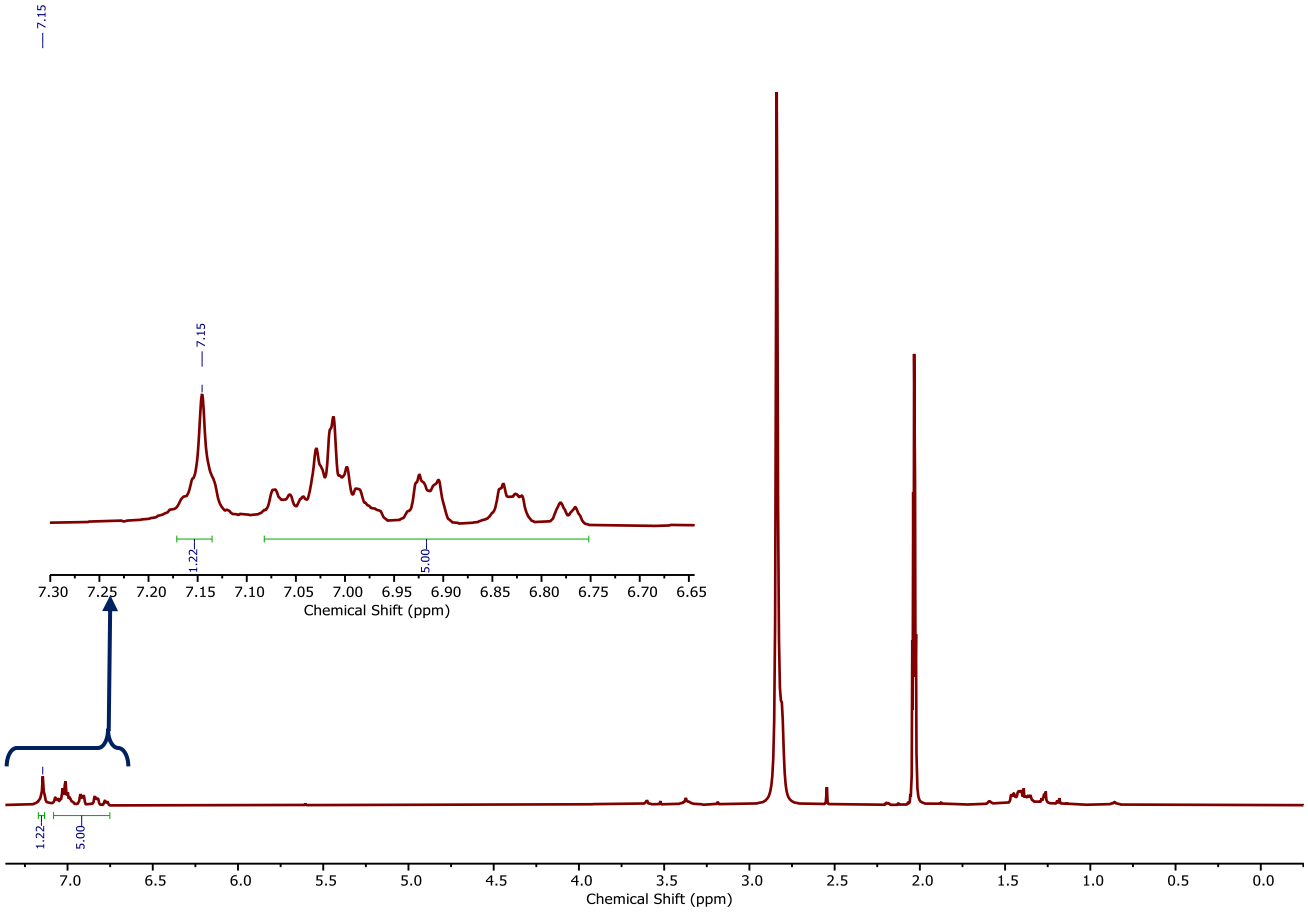

Figure 7 400 MHz ^{1}H NMR spectrum of **IV.12** in Acetone-D_6 at room temperature**.**

Single crystal X-ray diffraction analysis Aromatic Expanded Porphyrinoid' IV.12:

Aromatic expanded porphyrinoid **IV.12**, successfully characterise via single-crystal X-ray diffraction analysis, as illustrated in **Fig 8**. High-quality crystals were achieved through vapor diffusion of either hexane or methanol into the solution of the respective macrocycles in THF. The X-ray diffraction data confirmed a bowl-shaped structure for the macrocycle, validating the molecular symmetry observed in the ^{1}H NMR spectrum. Upon analysis of the single crystal structure, it becomes apparent that the molecule adopts a triangular structure, contrary to the previously discussed rectangular structure for **IV.10**. Specifically, the observed inverted thiophene moiety belongs to the diol. This updated

observation underscores the significance of β-substitution in refining the comprehension of the alteration in molecular geometry and structure.

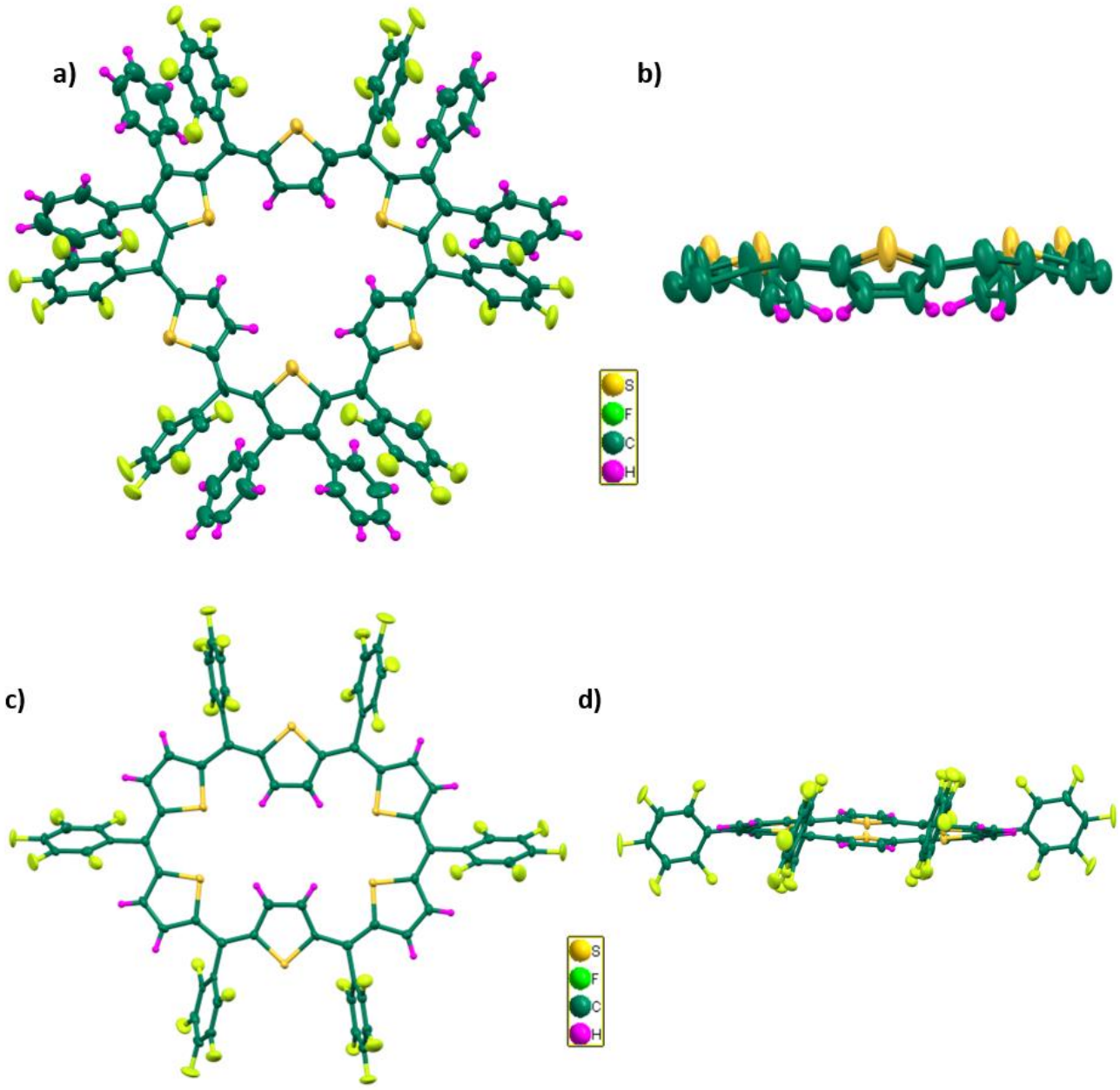

Figure 8 Molecular Structure of **IV.12 (a, b)** and **IV.10 (c, d)**.

Aromatic Expanded Porphyrinoid IV.12 acting as 'Molecular Sponge'

In addition to this structural feature, a remarkable observation was made regarding the presence of solvent molecules (THF) embedded within the crystal lattice. A total of nine solvent molecules were identified and arranged systematically within the molecular framework. Specifically, three solvent molecules were situated at the periphery of the molecule, oriented perpendicular to the molecular plane. Another three solvent molecules were positioned at the inner periphery of the molecule, oriented

parallel to the molecular plane. Intriguingly, the remaining three solvent molecules were nestled within the core of the macrocycle. This findind highlights the molecular geometry and solvent trapping, underscoring the versatility of the molecule's structural architecture.

Upon immersing the crystal into chloroform solvent, an intriguing phenomenon was observed: all the THF molecules embedded within the molecule were replaced by an equal number of chloroform molecules. Furthermore, a meticulous single crystal analysis revealed a strikingly similar arrangement of solvent molecules, akin to the previous arrangement observed with THF. This observation strongly suggests a molecular sponge-like behavior exhibited by the molecule, wherein it readily absorbs and retains solvent molecules within its structure. Moreover, the dominance of chloroform as a solvent over THF became apparent, as evidenced by its ability to effectively replace the THF molecules within the crystal lattice. This analysis sheds light on the dynamic solvent interactions and highlights the molecule's remarkable capability to adapt to different solvent environments.

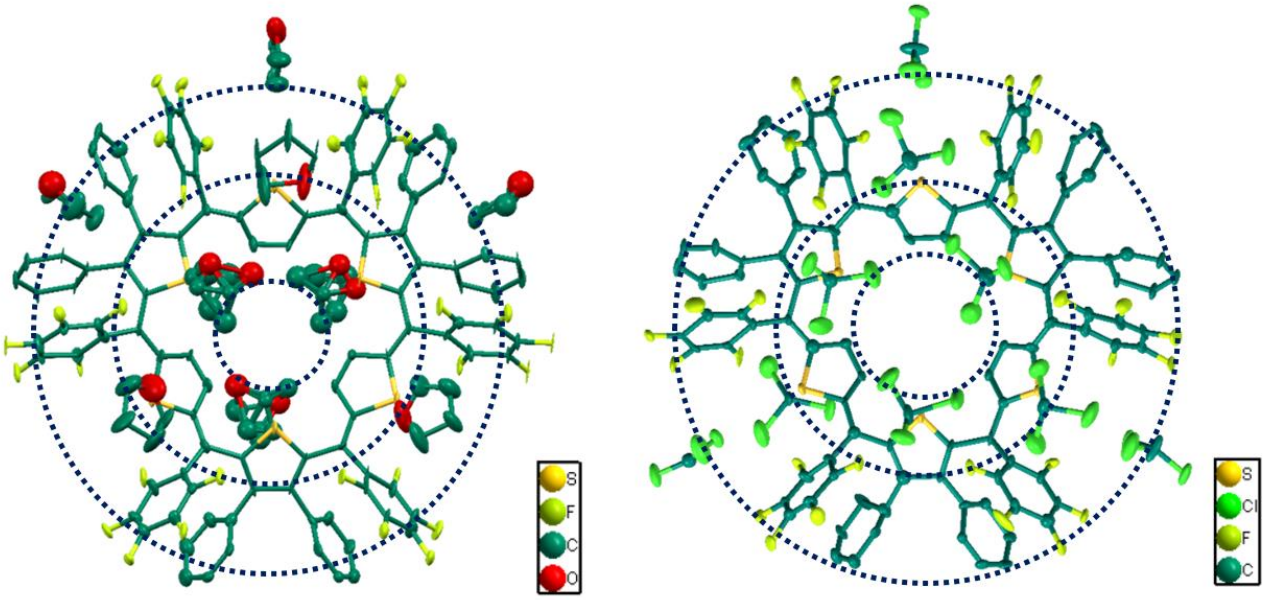

Fig 9. Molecular Structure of **IV.12** with THF(left) and Chloroform(right) (Hydrogens omitted for clarity).

Electronic absorption studies

The UV-Vis absorption spectrum of the 30π Aromatic Expanded Porphyrinoid **IV.12** was measured in dry toluene. Analysis of the spectrum revealed a significant and broad absorption peak at 454 nm, exhibiting a high molar absorbance value of 15200, as shown in **Fig 10**. This pronounced absorption peak indicates the presence of electronic transitions within the molecule, suggesting a level of conjugation between the heterocyclic units. However, the broadness of the peak proposes a relatively weak conjugation, potentially due to steric hindrance within the molecular framework.

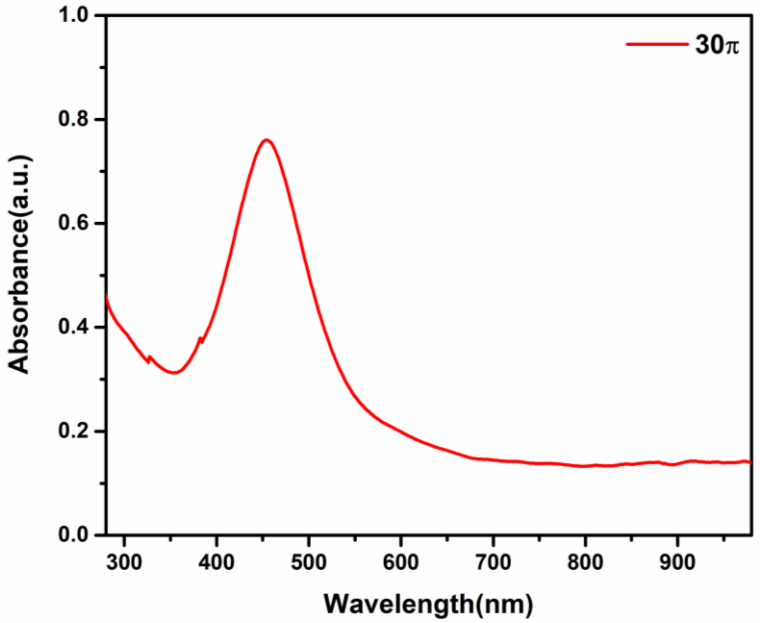

Figure 10 UV-Vis Absorption Spectrum of **IV.12 (0.49 g/L)**.

IV.A.3 Synthesis and characterization of 20π isophlorin IV.13.

Synthesis 20π isophlorin IV.13.

In the same reaction, another 20π porphyrin analogue **IV.13**, was initially confirmed through MALDI TOF/TOF mass spectrometry. Subsequently, purification of the anticipated product was accomplished using silica gel column chromatography, resulting in the isolation of a dark orange-colored band. The yield of the purified product was estimated to be 5%.

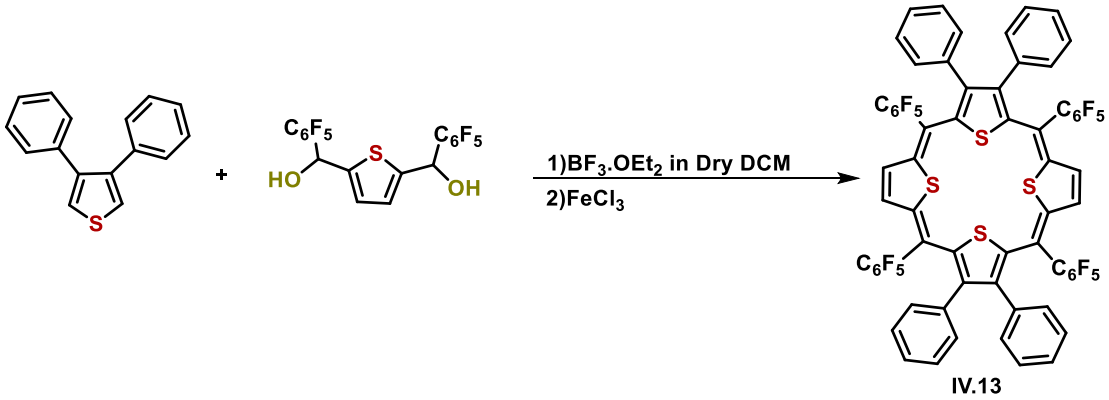

Scheme 2 Synthesis of Expanded prophyrinoid, **IV.13**.

Structural characterization of 20π isophlorin IV.13.

Porphyrin analogue **IV.13**, was characterized through a diverse range of analytical techniques. High-resolution mass spectrometry (HRMS) accurately determined its actual molecular mass and chemical

composition. UV-Vis spectroscopy unveiled its electronic absorption properties, highlighting the weak interacting p orbitals that are responsible for global conjugation. NMR spectroscopy provided insights into the chemical environment and connectivity of atoms within **IV.13**, offering detailed structural information. X-ray crystallography facilitated the determination of its three-dimensional molecular structure at atomic resolution.

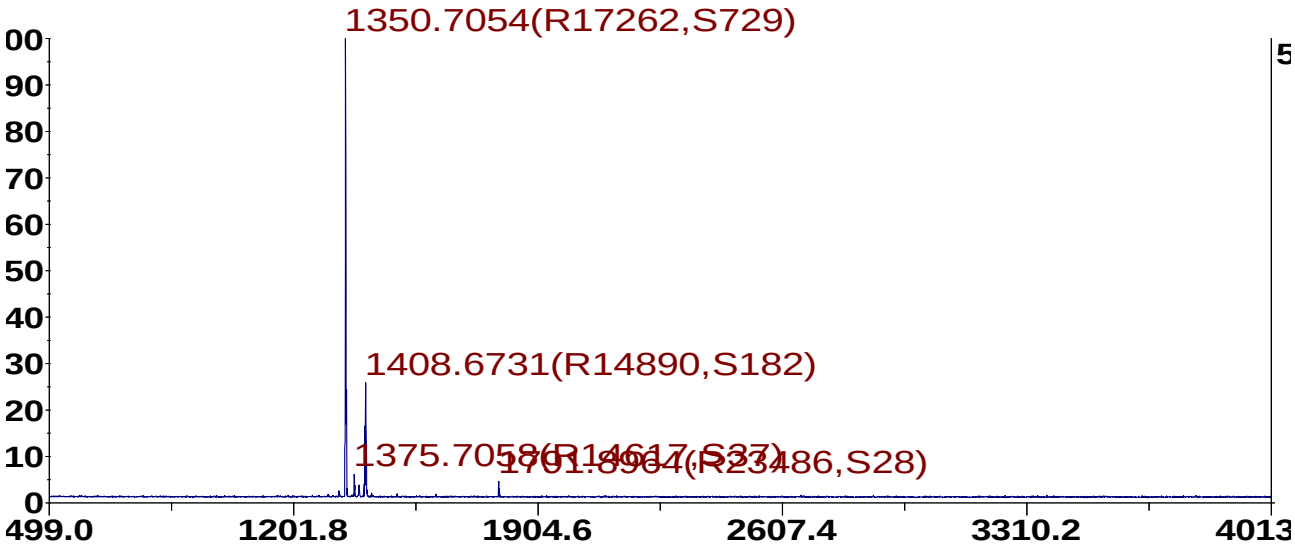

Figure 11 MALDI TOF/TOF mass spectrum of **IV.13**(Calculated mass for $C_{68}H_{24}F_{20}S_4$ is 1348.9541).

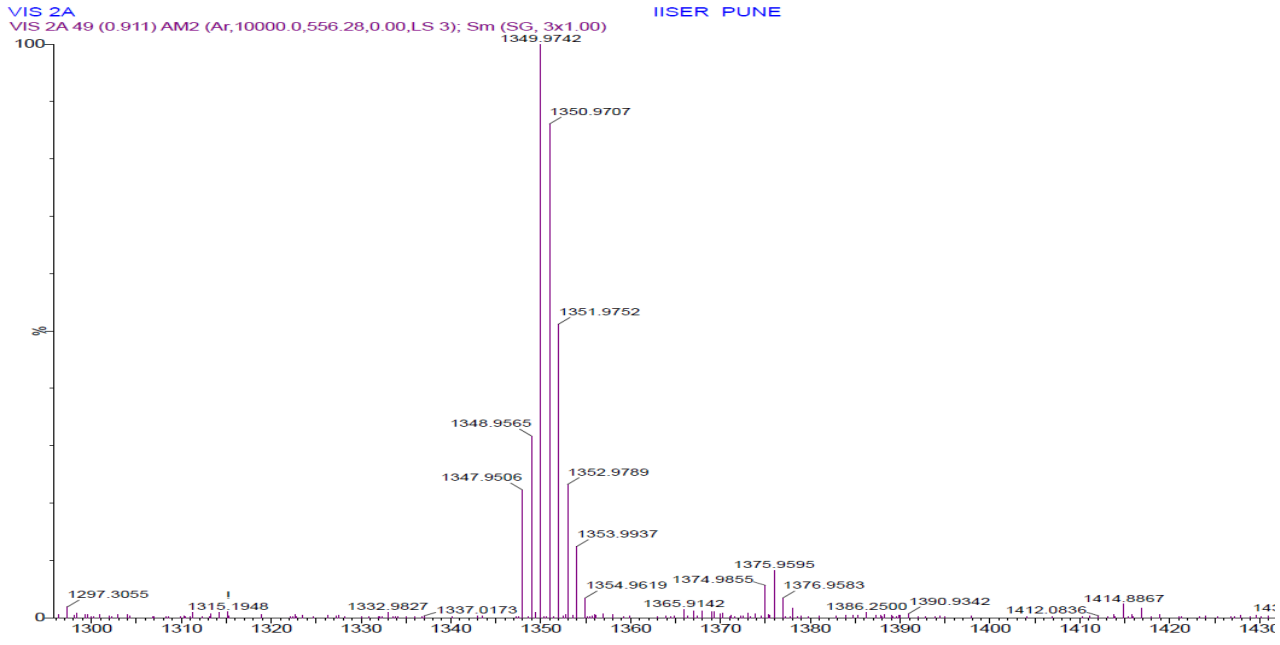

Figure 12 HR-ESI-TOF mass spectrum of of **IV.13**(Calculated mass for $C_{68}H_{24}F_{20}S_4$ is 1348.9541).

NMR characterization

The ^{1}H NMR spectrum of 20π isophlorin **IV.13**, shows a reduced number of signals similar to the aromatic expanded porphyrinoid **IV.13**, indicating potential higher molecular symmetry. Only one set of β-CH thiophene protons manifested as singlet at δ 6.62 ppm which is slightly upfield shifted in comparision to the aromatic expanded porphyrinoid **IV.12**. Phenyl protons were identified as multiplets within the ranges of δ 7.09-6.95 and 6.98-6.92 ppm.

Consistent with the molecular structure elucidated through X-ray crystallography, the observed chemical shift values do not align with the anticipated paratropic ring current effect characteristic of 4nπ systems. The estimated Nucleus Independent Chemical Shift (NICS) value of +1.83 ppm for **IV.13** further confirmed weak ring current, emphasizing the impact of limited global conjugation in the molecule.

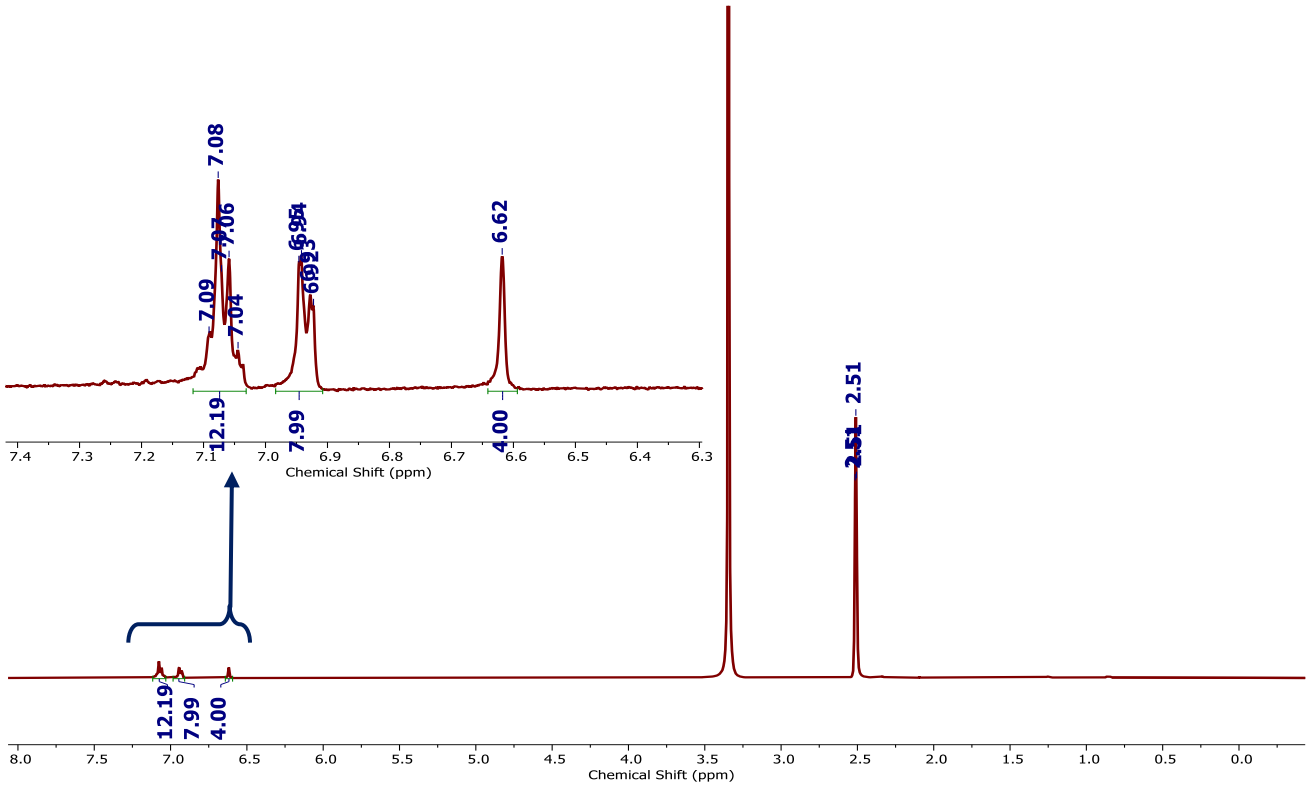

Figure 13 ^{1}H NMR spectrum of **IV.13** in DMSO-D_6.

Single crystal X-ray diffraction analysis 20π isophlorin IV.13:

The characterization of 20π isophlorin **IV.13** through single-crystal X-ray diffraction analysis provided detailed insights into its molecular structure. This analysis was crucial for understanding the geometric arrangement of the molecule in three-dimensional space. The production of high-quality crystals was achieved through vapor diffusion of either hexane or methanol into the solution of the macrocycle in

THF, following a procedure similar to that used for macrocycle **IV.12**. This method ensured the formation of well-defined crystals suitable for X-ray diffraction analysis.

The X-ray diffraction data confirmed the presence of a butterfly-shaped structure for the macrocycle, consistent with the molecular symmetry observed in the ^{1}H NMR spectrum.

Further analysis of the single crystal structure revealed specific details about the molecular conformation of **IV.13**. It was observed that the molecule adopts a square-type structure, with two diagonal thiophenes lying in the same plane, while the other diagonal thiophenes are positioned out of the plane. This arrangement provided valuable insights into the spatial orientation of the molecular components and their interactions within the macrocycle.

Notably, unlike macrocycle **IV.12**, 20π isophlorin **IV.13** did not display molecular sponge behavior. This observation was based on the detection of only one THF molecule at the center of the macrocycle, indicating a distinctly different or poor solvent interaction pattern in the crystal lattice compared to **IV.12**. Understanding these differences in solvent behavior between the two macrocycles contributes to our knowledge of their chemical properties and potential applications in various fields.

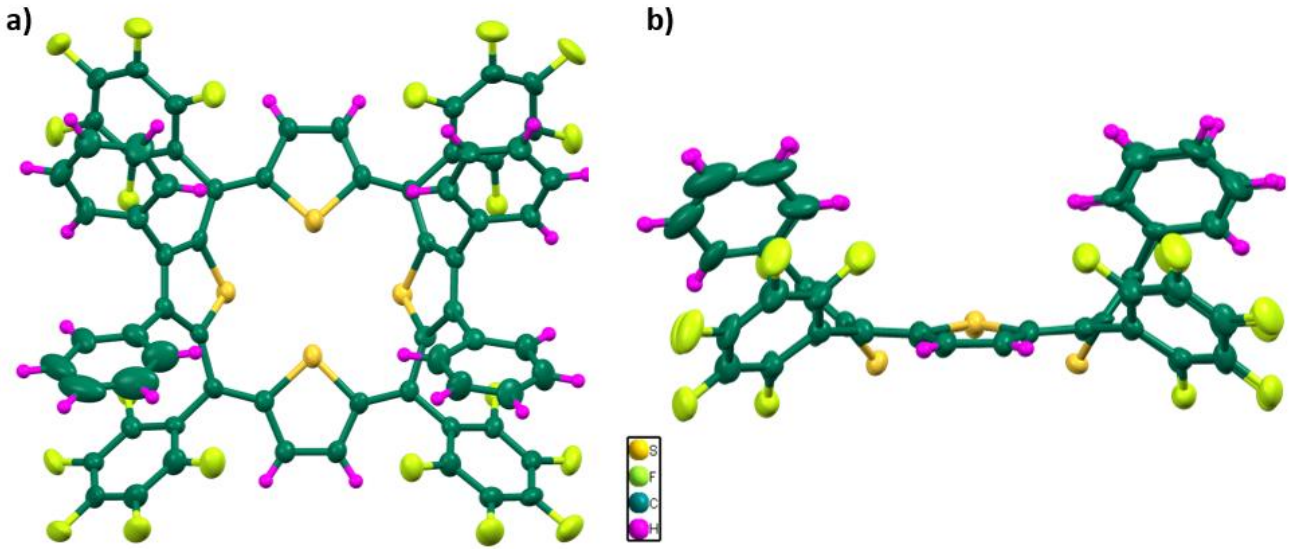

Figure 14 Molecular Structure of **IV.13** in THF (solvent molecules omitted for clarity).

Electronic absorption studies

The UV-Vis absorption spectrum of the 20π isophlorin **IV.13** was meticulously recorded in distilled chloroform. Upon analysis, the spectrum revealed two prominent high-energy absorption peaks: one observed at 433 nm (with a considerable molar absorbance value of 24500), and the other detected at 368 nm, (also with a significant molar absorbance value of 15800), as depicted in **Fig 15**.

These distinct absorption peaks indicate the occurrence of electronic transitions within the molecule, suggesting the presence of conjugation between the heterocyclic units.

However, the presence of multiple high-energy absorption peaks suggests a complex electronic structure for **IV.13**. This complexity may arise from various factors such as steric hindrance, electronic interactions within the molecular framework, or even the influence of solvent polarity. The feeble conjugation between the heterocyclic units, inferred from the UV-Vis spectrum, implies a delicate balance of electronic effects within the molecule.

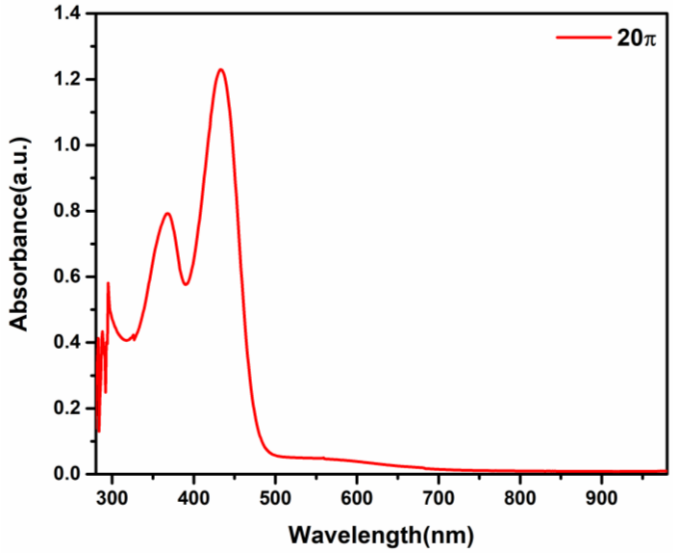

Figure 15 UV-Vis Absorption Spectrum of **IV.13** (0.50 g/L).

IVA.4 Quantum mechanical calculations:

Nucleus Independent Chemical Shift (NICS)

The estimated Nucleus Independent Chemical Shift (NICS) values for **IV.12** and **IV.13** are -0.69 and +1.83 ppm, respectively. These values further confirm the presence of a weak ring current in both molecules, underscoring the impact of limited global conjugation within the molecular framework. The positive NICS value for **IV.13** suggests a slightly stronger ring current compared to **IV.12**, indicating differences in the aromaticity of the respective macrocycles. This observation highlights the subtle variations in molecular structure and electronic properties between **IV.12** and **IV.13**.

Upon comparing the NICS values of **IV.12** with **IV.10**, a notable difference was observed. **IV.10** exhibited a significantly higher NICS value of -15.05 ppm, indicating a strong aromatic behavior. This observation was further corroborated by the analysis of its ^{1}H-NMR spectra, which also revealed characteristic features associated with aromatic compounds. The high NICS value and distinct spectral characteristics provide compelling evidence of the pronounced aromaticity of **IV.10**.

Macrocycle	NICS (0) ppm
IV.10	-15.05
IV.12	-0.69
IV.13	+1.83

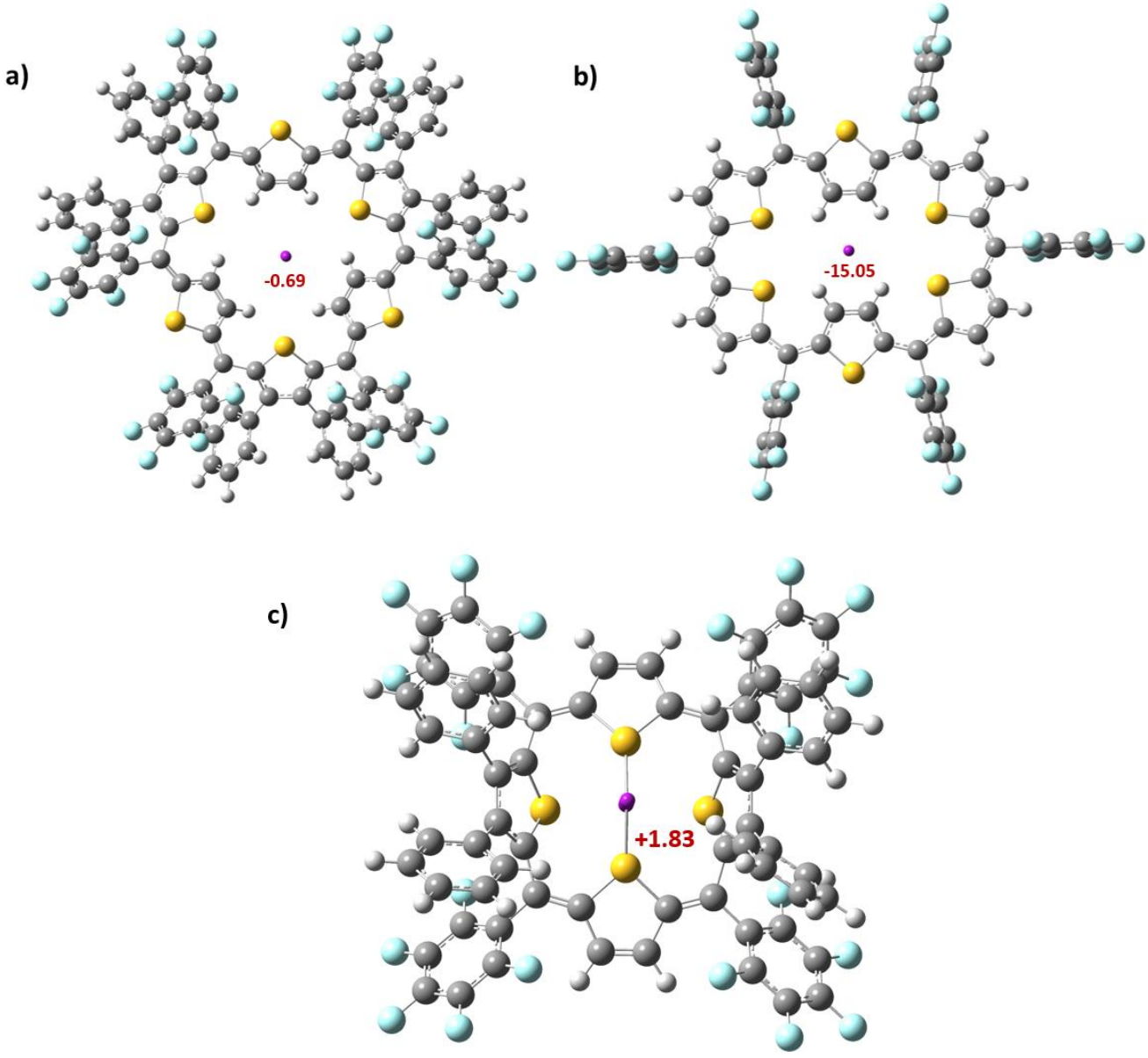

Table IV.1: Estimated NICS values for macrocycles **IV.10 (b), IV.12 (a)** and **IV.13 (c)**.

Anisotropy of induced current density (ACID)

The ACID plots further confirm the influence of limited global conjugation within the molecular framework. In these plots, it is evident that the majority of electron density is localized around the individual heterocyclic rings. This localization indicates a restricted delocalization of π-electrons throughout the molecule, highlighting the impact of limited global conjugation. The observed electron

density distribution underscores the importance of understanding the spatial distribution of electron density within the molecule, providing insights into its electronic structure and aromatic behavior.

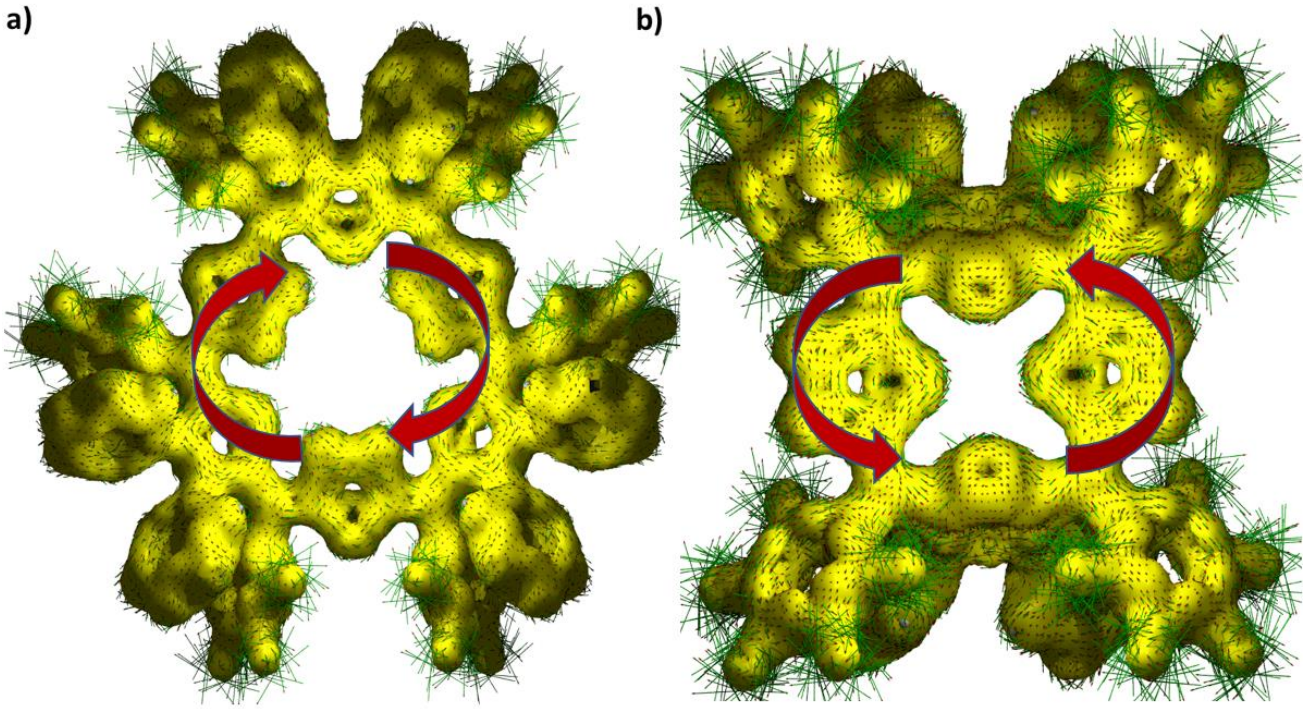

Figure 16 ACID plot for **IV.12(a**) and **IV.13 (b).** At iso value 0.04, an external magnetic field is applied orthogonal to the macrocycle plane.

Conclusions

In conclusion, the synthesis and characterization of aromatic expanded porphyrinoids provide valuable insights into their structural diversity, electronic properties, and potential applications. A comprehensive exploration of various synthetic methodologies and analytical techniques, revealed molecular architecture dependent solid state behavior of these intriguing macrocycles.

The investigation of aromatic expanded porphyrinoids show the significance of core modifications, β-substitution, and solvent interactions in influencing their structural diversity and behavior. From the observation of distinct geometries to the characterization of solvent absorption behavior, these studies have shed light on the dynamic nature of these molecules with respect to solvent specific adsorption in the crystalline state.

Furthermore, quantum mechanical calculations, such as Nucleus Independent Chemical Shift (NICS) analysis and Anisotropy of induced current density (ACID) plots, have been useful to estimate their evaluate aromatic and electronic structure of aromatic expanded porphyrinoids. These calculations

have highlight limited global conjugation and the distribution of electron density within the macrocycles.

Chapter 4:- Aromatic Expanded Porphyrinoids

Section-B
Synthesis and characterization of Ethylene Bridged Aromatic Expanded Porphyrinoids

IV.B.1 Introduction:

As highlighted in the introduction of Chapter 4A, the macrocycles possess a greater number of heterocyclic rings compared to porphyrins, This increased ring count contributes to their heightened conformational flexibility. Consequently, they often adopt twisted conformations, deviating from typical topology of porphyrins resulting in the loss of aromaticity or antiaromaticity inherent to majority of expanded porphyrinoids.

Vogel and co-workers[13]serendipitously discovered a twisted octapyrrole, **IV.18**, in their endeavor to synthesize a structural isomer of porphyrin, **IV.16** (Scheme 1). Unexpectedly, their synthesis yielded a macrocycle comprising eight pyrrole rings instead of the anticipated tetrapyrrole macrocycle. Employing conventional MacDonald-type condensation conditions, they condensed a bipyrrole dialdehyde, **IV.14**, with a dipyrrylethane dicarboxylic acid, **IV.15**, catalyzed by perchloric acid.

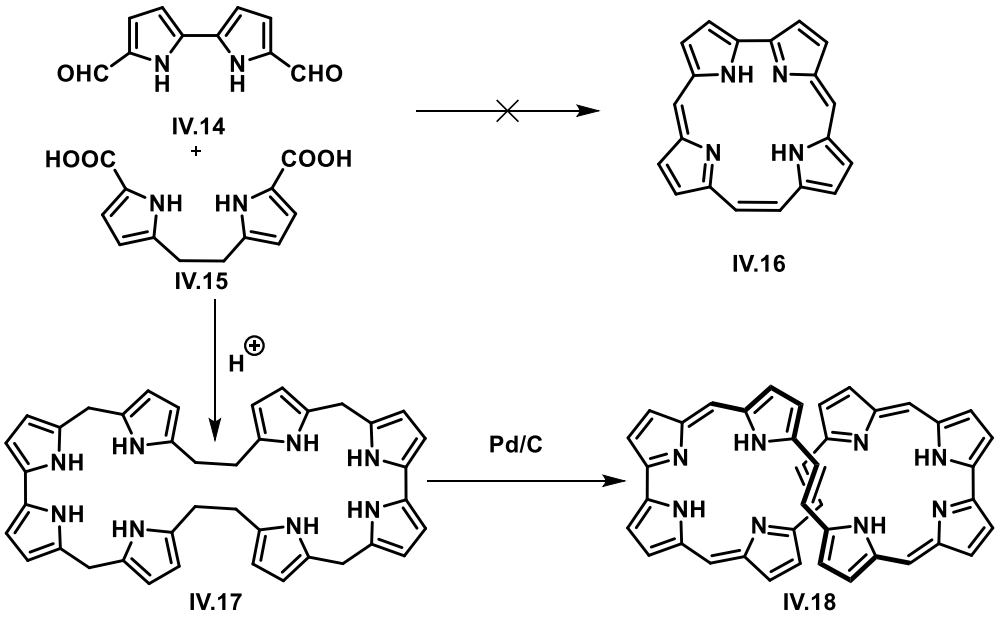

Scheme 1: Synthesis of the octapyrrolic macrocycle **IV.18**. The 3, 4-diethyl substituents of the pyrrole rings are omitted for clarity.

Primarily, **IV.17** was identified as a partially oxidized product. Subsequent thermal dehydrogenation of **IV.17** in the presence of 10% Palladium on carbon (Pd/C) resulted in the formation of the fully conjugated octaphyrin, **IV.18**. Upon treatment with perchloric acid and 10% hydrochloric acid, the octaphyrin yielded either the tetrakis(hydroperchlorate) or the tetrakis(hydrochloride), respectively. Surprisingly, the ^{1}H NMR spectrum of octaphyrin **IV.18** did not display significant paratropic ring current effects, contrary to expectations for a 36π anti-aromatic macrocycle. Single-crystal X-ray diffraction analysis of the dichloride and perchlorate salts unveiled the non-planar structure of **IV.18**, with both salts exhibiting a twisted configuration resembling a figure-of-eight topology. This non-planar conformation was attributed to deprotonation in the case of the dichloride salt and tetraprotonation in the perchlorate salt. Exploring the structural characteristics of octaphyrin, investigations focused on the impact of meso carbons on the macrocycle's topology.[13a,13b] To this end, bipyrrole dialdehyde **IV.14** was reacted with dipyrromethane dicarboxylic acid **IV.19** under conditions akin to those employed for the synthesis of **IV.21** (**Scheme 2**).

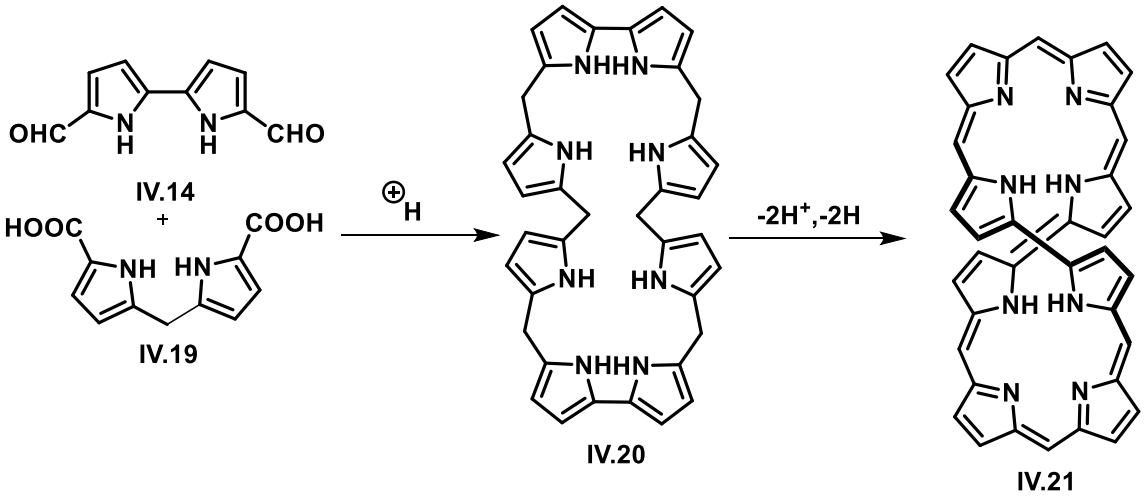

Scheme 2. Synthesis of the octapyrrolic macrocycle. 3, 4-diethy1 substituents of the pyrrole rings are omitted for clarity.

The synthesis process led to the formation of a 34π octaphyrin **IV.21**, which was favored over the production of the tetrapyrrolic corrole. With a formal count of 34π electrons, **IV.21** was anticipated to exhibit diatropic ring current effects in its ^{1}H NMR spectrum, characteristic of an aromatic macrocycle. However, contrary to expectations, similar to the 36π octaphyrin, **IV.21** did not show significant diatropic ring current effects. This absence hinted at a non-planar structure for **IV.21**, a hypothesis that was later confirmed through single-crystal X-ray diffraction analysis.

Chandrashekar and co-workers have explorated the synthesis of expanded porphyrins, by substituting the pyrrole rings of the macrocycle with other heterocycles, such as thiophene, within an octaphyrin framework. Their endeavor involved the synthesis of a core-modified octaphyrin, termed

dithiatetrapyrrane **IV.22**. This compound can be condensed with aryl aldehyde under acid-catalyzed conditions, followed by oxidation with chloranil, leading to the formation of a 34π octaphyrin, **IV.23** (**Scheme 3**).[14]

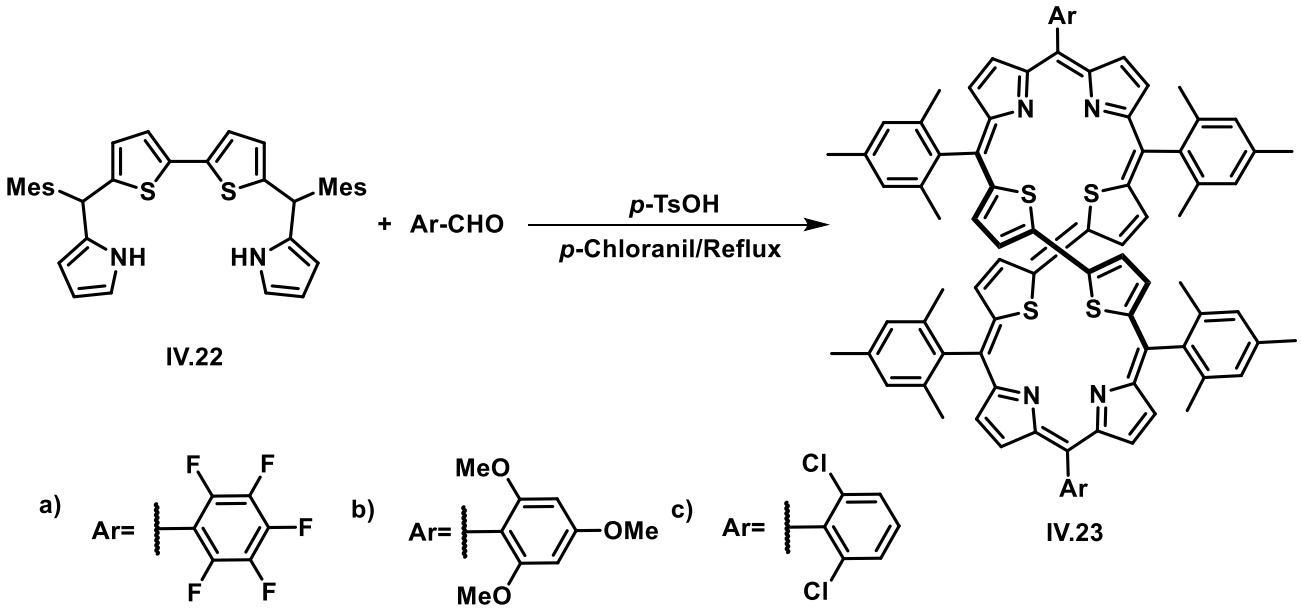

Scheme 3. Synthesis of core-modified octaphyrin.

Spectroscopic analysis and examination through single-crystal X-ray diffraction confirmed a twisted conformation for the 34π octaphyrin **IV.23**. Despite the adjacent thiophene units being arranged in an anti-parallel manner, **IV.23** couldn't maintain a flat structure. This observation suggested that the additional meso carbons expand the volume of the macrocyclic core, creating pockets reminiscent of those found in a corrole.

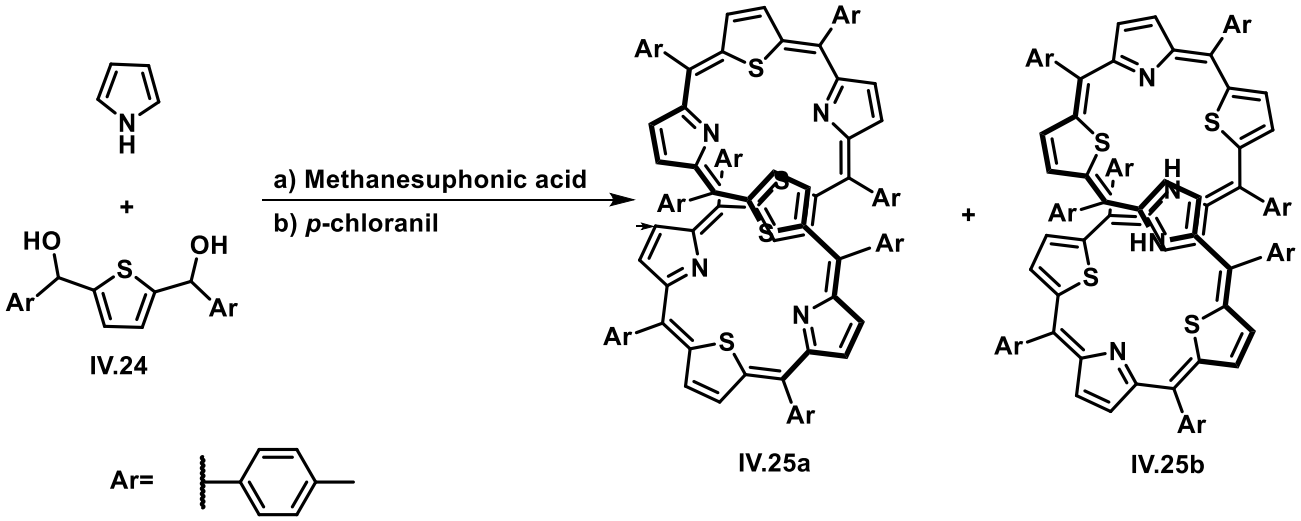

Scheme 4. Synthesis of 36π and 38π core-modified tetrathiaoctaphyrins.

Latos and colleagues also contributed to this field by reporting two core-modified octaphyrins[15], comprising four pyrroles and four thiophene units with eight meso positions. These compounds were synthesized through the reaction of pyrrole and thiophene diol under acidic conditions (**Scheme 4**). Two different tetrathiaoctaphyrins, **IV.25a-b**, with a difference of two mass units, were isolated from this reaction. While macrocycle **IV.25a** corresponded to a 36π octaphyrin, **IV.25b** represented a 38π macrocycle. Despite only two protons differing between the two macrocycles, this variance significantly influenced their electronic properties. Moreover, they were found to be interconvertible through a reversible two-electron redox process. Specifically, the 36π octaphyrin, **IV.25a,** could be quantitatively dihydrogenated to the 38π octaphyrin, **IV.25b**, using reducing agents like sodium borohydride or sodium hyposulfite. Conversely, tetrathiaoctaphyrin **IV.25b** could be quantitatively dehydrogenated to 36π octaphyrin **IV.25a** upon oxidation by *p*-chloranil. Such interconvertible systems exemplify typical proton-coupled electron transfer reactions in organic molecules. Detailed NMR analyses and computational calculations concluded that both **IV.25a** and **IV.25b** adopted a figure-of-eight configuration rather than a planar structure. The ^{1}H NMR spectrum showed no significant diatropic ring current effects for **IV.25b**, while only marginal paratropic ring current effects were observed for **IV.25a**. Despite their similar structural characteristics, variable temperature NMR spectroscopy revealed fluxional behavior for **IV.25a**, which could exist in two different conformations with a twisted topology. The estimated interconversion energy, based on the probable reaction mechanism for the transformation, was 63.6±3.0 kJmol^{-1}.

Anand and co-workers synthesized octaphyrin with four thiophene and four furan rings.[16] This macrocycles lack amine-imine conversion due to the presence of divalent chalcogen atoms in both the heterocyclic rings. Notably, **IV.26** comprises 40π electrons and is anticipated to display antiaromatic characteristics.

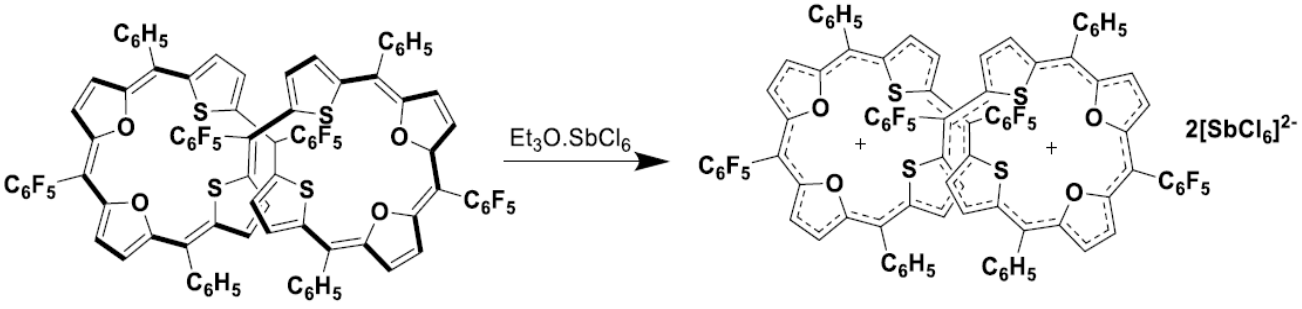

IV.26 **IV.27**

Scheme 5. Two electron oxidation of 40π isophlorin.

In the ^{1}H NMR analysis, no significant paratropic chemical shifts were observed, and signals were detected within the 5.0 to 9.0 ppm region. The absence of pronounced shifts corresponds to the non-

planar structural nature of the macrocycle, indicating a lack of extensive aromaticity. Furthermore, single-crystal X-ray diffraction analysis confirmed a figure-of-eight conformation for the macrocycle. This conformation, consistent with the NMR findings, reflects the flexible and twisted geometry of the macrocycle. Moreover, the estimated NICS (Nucleus Independent Chemical Shift) value of 3.5 ppm for **IV.26** was also in support of the analyzed antiaromatic characteristics. This finding contrasts with the expectations based on its structural composition. Additionally, **IV.26** demonstrated potential for two-electron ring oxidation to the 38π dicationic octaphyrin **IV.27** using Meerwein salt. However, despite this transformation, there remains an absence of diatropic ring current in the NMR spectra. This collective evidence supports the conclusion that both **IV.26** and **IV.27** deviate from traditional aromatic or antiaromatic behavior due to their flexible and dynamic structures. Instead, they exhibit a loss of planarity induced by their inherent flexibility, leading to their classification as non-antiaromatic and non-aromatic octaphyrins, respectively. This characterization highlights the intricate interplay between molecular structure and electronic properties in expanded porphyrinoids.

IV.B.2 Synthesis and characterization of Ethylene Bridged Aromatic Expanded Porphyrinoids IV.30.

Synthesis of Ethylene Bridged Aromatic Expanded Porphyrinoids IV.30.

Based on the above observations, research was focused on the synthesis ethylene-bridged core-modified radical molecules, a novel molecular architecture integrating ethylene bridges within the molecular framework alongside thiophene units. The synthesis of this macrocycle followed a multi-step process similar to the methodology employed for Ethylene Bridged Aromatic Expanded Porphyrinoids. In this the precursor molecules (E)-1,2-di(thiophen-2-yl)ethene and ((phenylmethylene)bis(thiophene-5,2-diyl))bis((perfluorophenyl)methanol) were employed as the key precursors. They were condensed in the presence of $FeCl_3$ under acidic conditions, with the intended goal of producing ethylene-bridged core-modified radical macrocycle.

However, contrary to expectations, the cyclization reaction resulted in the formation of Ethylene Bridged Aromatic Expanded Porphyrinoids(42π) **IV.31** instead of the targeted ethylene-bridged core-modified radical molecules **IV.30**. This unexpected outcome suggests the influence of reaction conditions and precursor reactivity on the final product formation(**Scheme 6**).

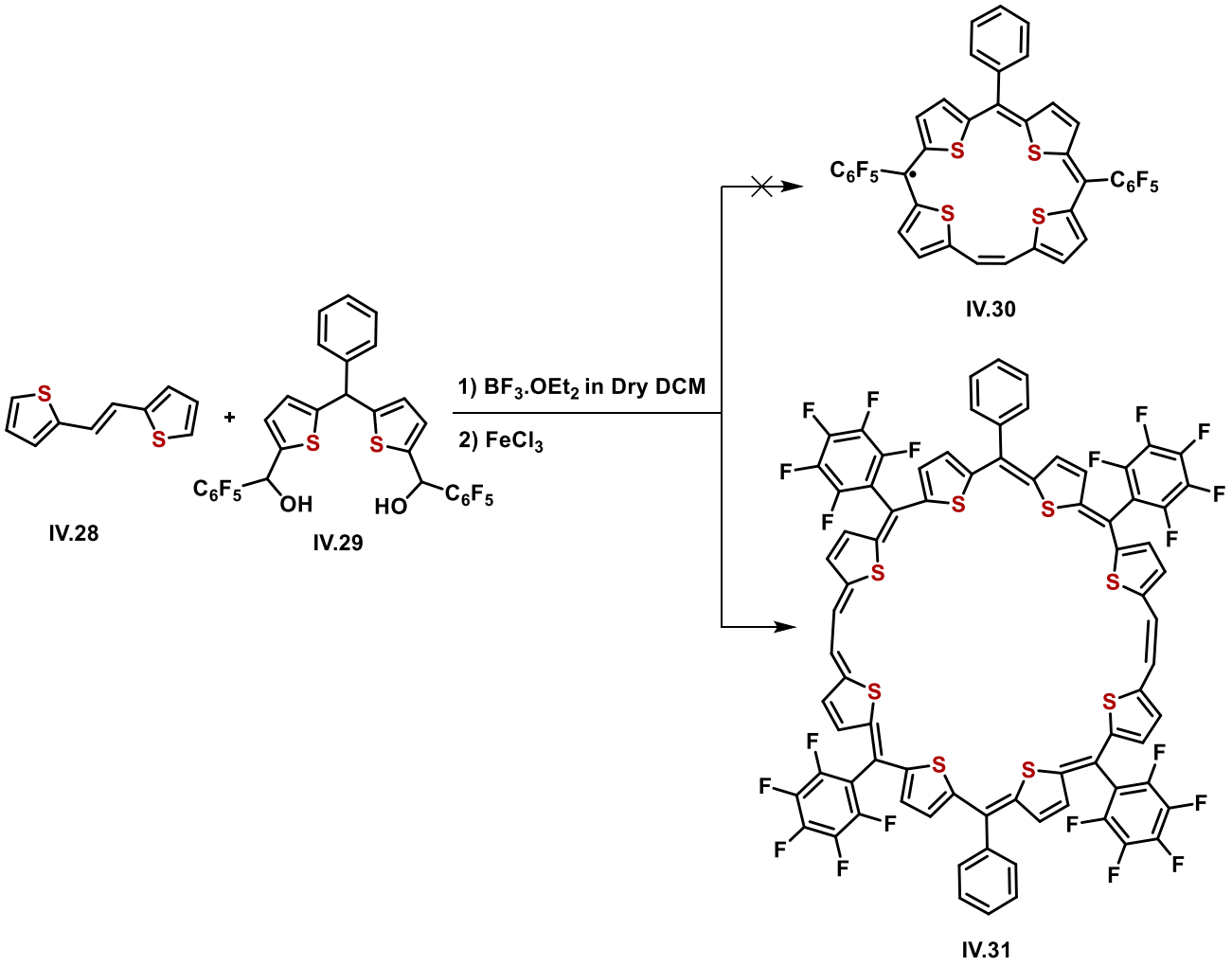

Scheme 6. Synthesis of Ethylene Bridged Aromatic Expanded Porphyrinoid **IV.31**.

Structural characterization of 'Ethylene Bridged Aromatic Expanded Porphyrinoid' IV.31.

Ethylene Bridged Aromatic Expanded Porphyrinoid (**IV.31**) was initially identified using MALDI TOF/TOF spectrum, providing insights into its molecular mass and composition. However, to ensure its purity and precise molecular composition, High-Resolution Mass Spectrometry (HRMS) was employed to confirm the exact mass corresponding to the macrocyclic structure of **IV.31**. This multi-step validation process not only confirmed the identity of **IV.31** but also provided crucial information regarding its molecular characteristics.

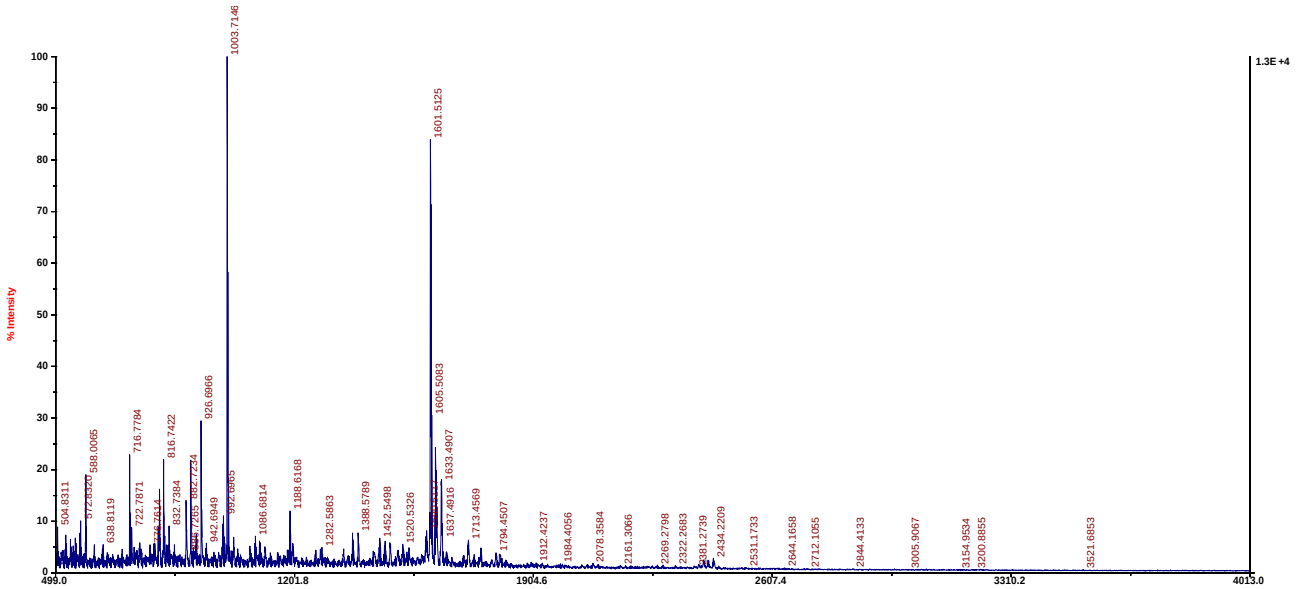

Figure 1 MALDI TOF/TOF mass spectrum of **IV.31**(Calculated mass for $C_{78}H_{30}F_{20}S_8$ is 1601.9794).

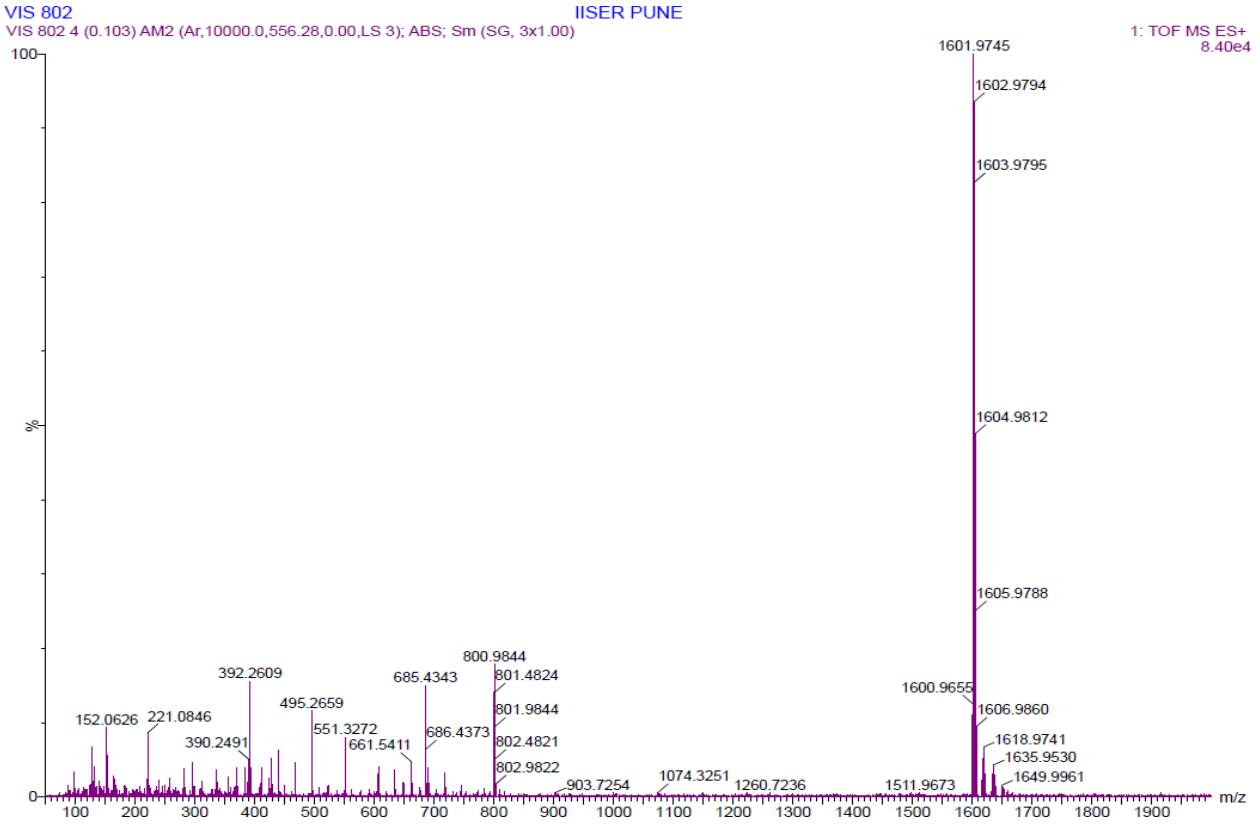

Figure 2 HR-ESI-TOF mass spectrum of **IV.31** in $CHCl_3$/MeOH mixture(Calculated mass for $C_{78}H_{30}F_{20}S_8$ is 1601.9794).

NMR characterization

The ^{1}H NMR spectrum of Ethylene Bridged Aromatic Expanded Porphyrinoid (**IV.31**) exhibited a

complex pattern with an increased number of signals, suggesting the presence of structural isomers within the sample. Upon detailed analysis, it could be envisaged that the sample comprised of two distinct inseperable molecules with identical molecular masses but differing in their structural configurations. It can be proposed that, one molecule adopts a cis-confirmation of the ethylene bridge, while the other adopts a trans-confirmation.

The possible presence of these isomeric forms highlights the structural flexibility and dynamic nature of Ethylene Bridged Aromatic Expanded Porphyrinoid (**IV.31**). The ability of the molecule to exist in multiple conformations has implications for its chemical reactivity, electronic properties, and potential applications in various fields, ranging from materials science to catalysis and molecular electronics. Further investigations into the synthesis and characterization of these isomers are essential for a comprehensive understanding of their properties and behavior.

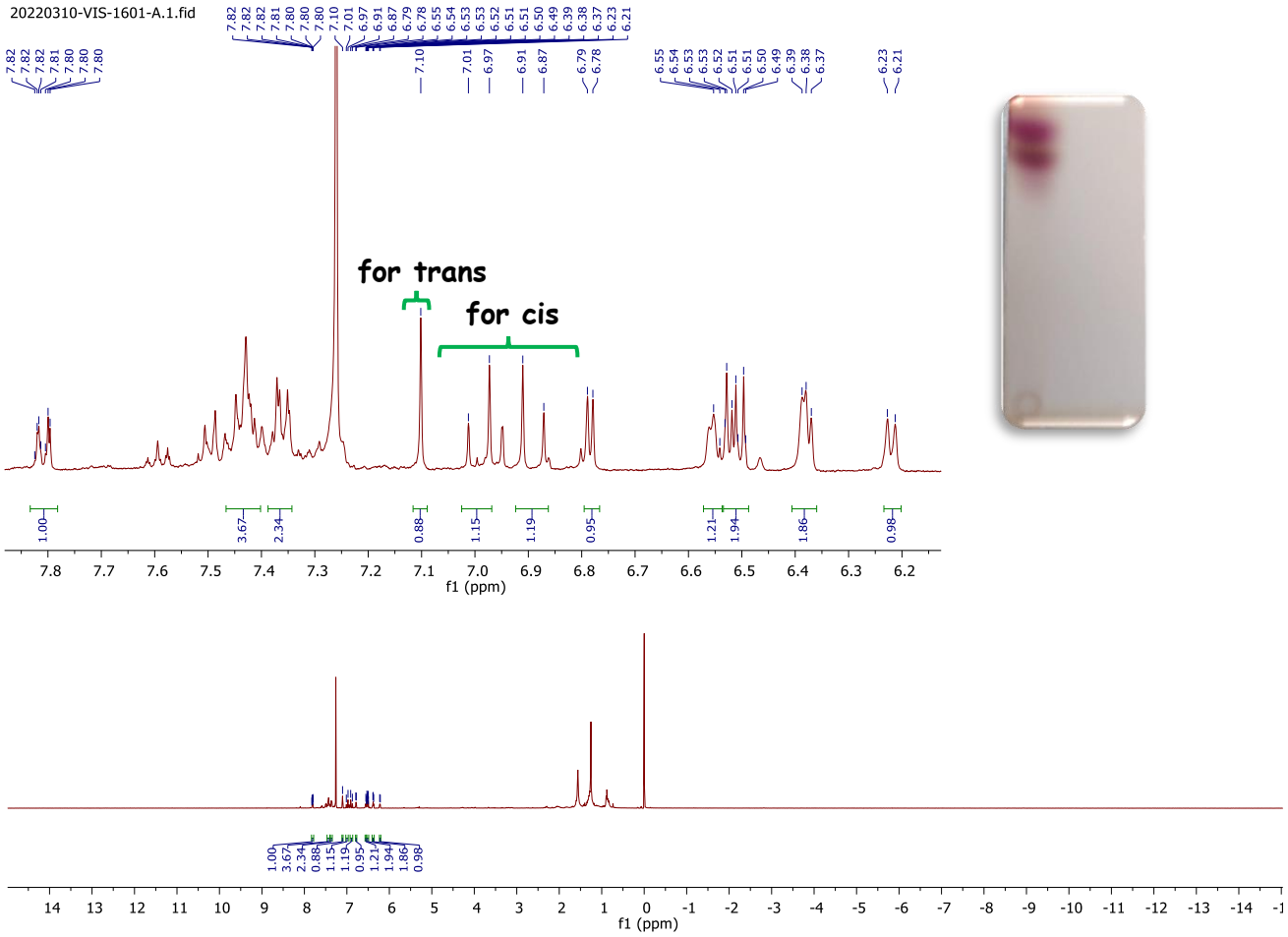

Figure 3 ^{1}H NMR spectrum of **IV.31** in $CDCl_3$.

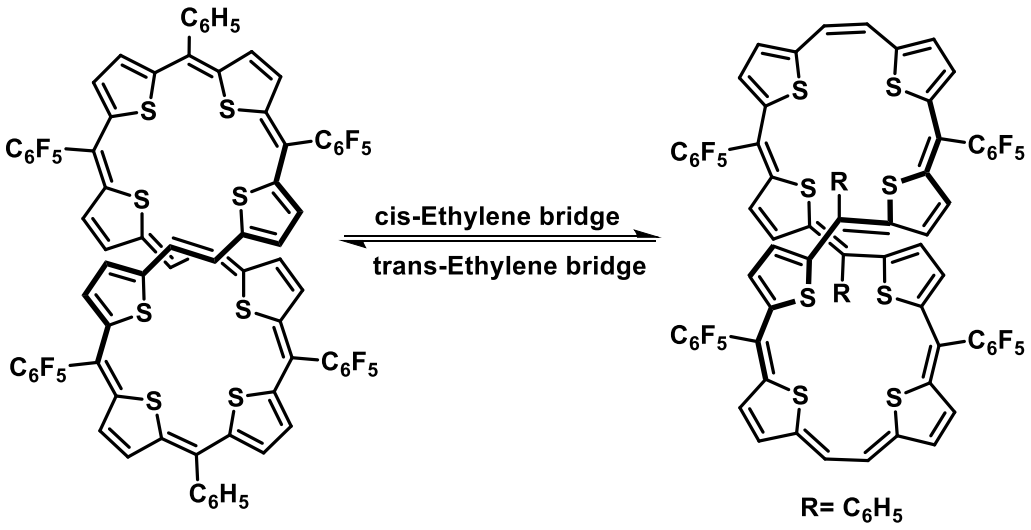

Figure 4 Plausible Isomeric Structures of **IV.31.**

Unfortunately, characterization of the Ethylene Bridged Aromatic Expanded Porphyrinoid (**IV.31**) was seriously limited by purification process.

As a result, we were unable to employ techniques such as cyclic voltammetry (CV), UV-Vis spectroscopy, and X-ray crystallography to further elucidate the molecular structure and properties of **IV.31**.

Despite these challenges, the initial confirmation of **IV.31** through MALDI TOF/TOF and HRMS spectrometry represents a crucial step in the characterization process, providing essential information about its molecular mass and formula. Moving forward, resolving the purification issues will be paramount for enabling comprehensive characterization using a broader range of analytical techniques, thereby advancing our understanding of **IV.31** and its potential utility in various fields of research.

IVB.3 Quantum mechanical calculations:

Since obtaining the crystal structure of molecule **IV.31** proved challenging, alternative methods were explored to gain insights into its structural characteristics and aromaticity. Therefore Quantum chemical calculations were employed to obtain the energy optimized structure. It revealed a non-planar "U" shaped geometry. This observation is indicative of its non-aromatic behavior, a hypothesis corroborated by the ^{1}H-NMR spectra analysis. Notably, despite its 42π (4n+2π) system, the macrocycle exhibited no diatropic ring current effect in the ^{1}H-NMR spectra. This absence of ring current effects further supports the non-aromatic nature of molecule **IV.31**.

The adoption of a non-planar "U" shaped geometry, as revealed by energy optimization, underscores the deviation from the expected planarity characteristic of aromatic systems. The absence of diatropic ring current effects in the ^{1}H-NMR spectra is consistent with the non-aromatic behavior observed in

other structural and spectroscopic analyses. These findings collectively highlight the unconventional electronic structure of molecule **IV.31**, challenging traditional aromaticity paradigms and emphasizing the importance of alternative structural characterization methods in elucidating complex molecular systems.

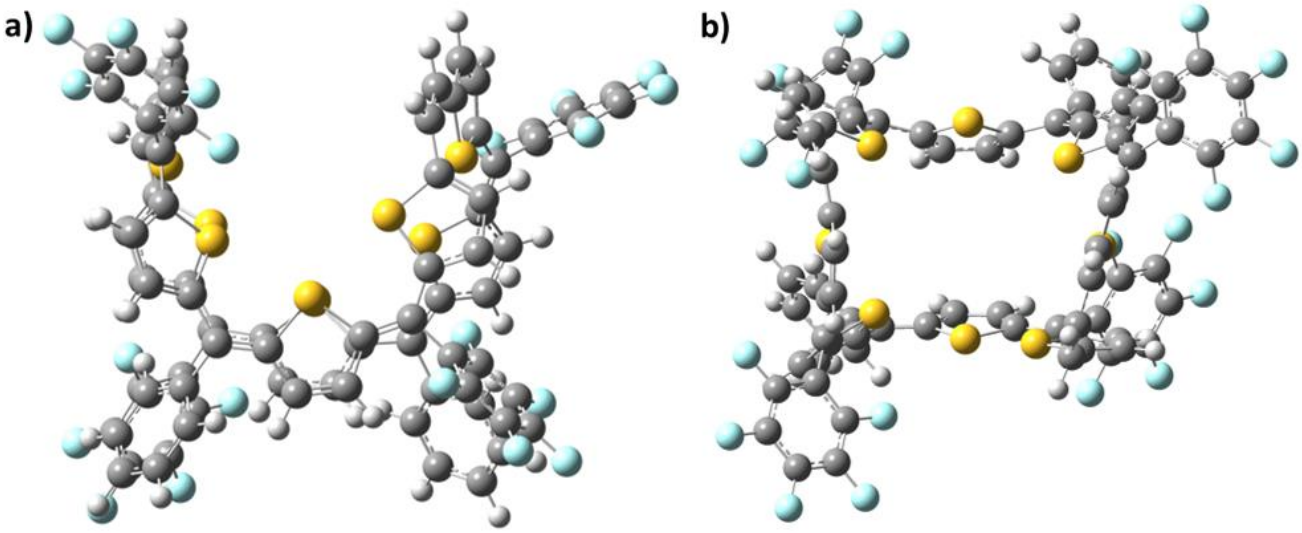

Figure 5 Energy Optimized ChemDraw Structure of **IV.31(a)** from the side and **(b)** from the top.

Nucleus Independent Chemical Shift (NICS)

The nucleus-independent chemical shift (NICS) value also lent support to the observed non-aromatic behavior of the macrocycle. An estimated NICS value **IV.31** is recorded -0.85, indicated the absence of any discernible ring current effect. The simulated NICS values, comprising zero at the external nuclei and negative values within, affirm the non-aromaticity of the molecule. It can be inferred that **IV.31** is predominantly non-aromatic.

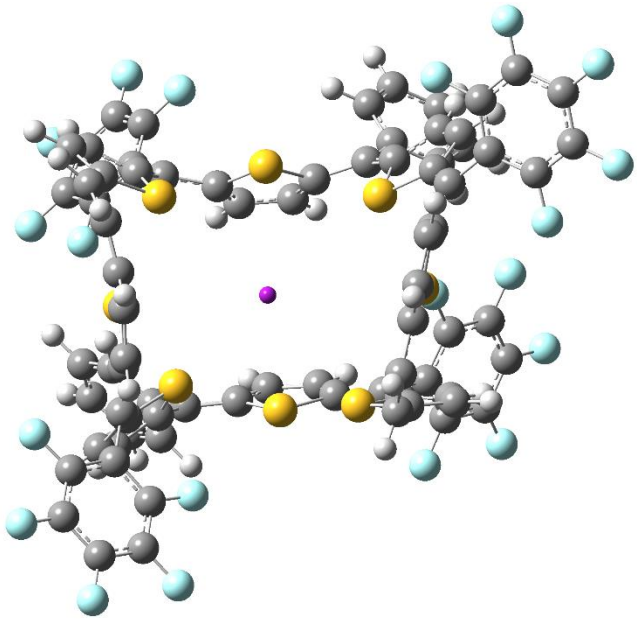

Figure 6 The estimated NICS value is -0.85 for macrocycle **IV.31.**

Anisotropy of induced current density (ACID)

The absence of widespread delocalization of electron density across the molecule's framework suggests a lack of aromaticity. Further the ACID plot serves as an additional evidence supporting the molecule's non-aromatic character, emphasizing the energy optimized electronic structure in elucidating the aromaticity properties of this macrocycle.

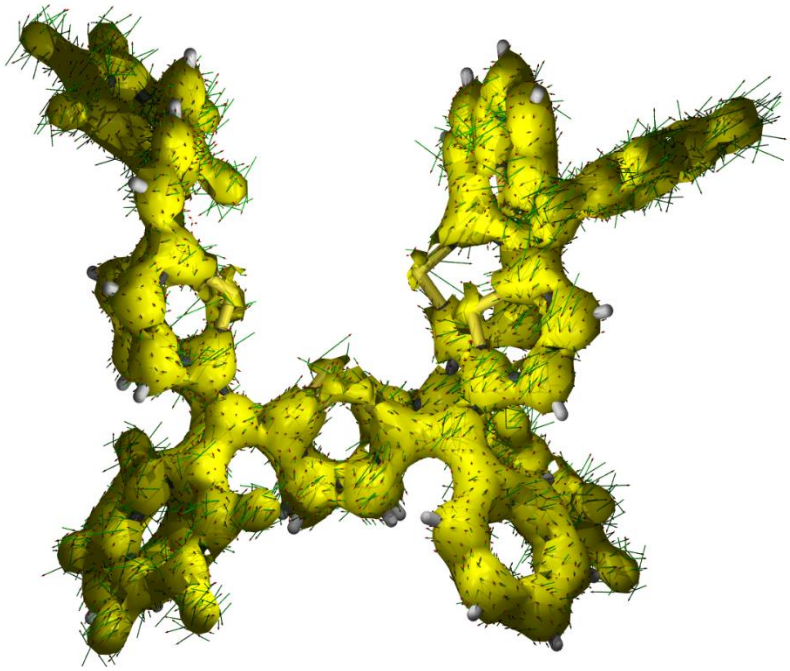

Figure 7 ACID plot for **IV.31**.

Conclusions

In conclusion, an attempt was aimed to synthesize ethylene-bridged core-modified radical macrocycle, integrating ethylene bridges within the molecular framework alongside thiophene units. However, it resulted in the unexpected formation of Ethylene Bridged Aromatic Expanded Porphyrinoids (42π) instead of the targeted radical macrocycle. This outcome underscores the influence of reaction conditions and precursor reactivity on product formation. Further investigation into the underlying mechanistic pathways and structural preferences is warranted to understand this intriguing observation better, Despite challenges in obtaining Ethylene Bridged Aromatic Expanded Porphyrinoid (**IV.31**) in its purest form, high-resolution mass spectrometry (HRMS) and NMR spectroscopy were employed for characterizing the isolated species. The possible presence of isomeric forms of **IV.31** highlights its structural dynamics in the solution state.

While purification challenges hindered additional characterizations using techniques such as cyclic voltammetry (CV) and UV-Vis spectroscopy, initial confirmation through MALDI TOF/TOF and HRMS spectrometry provided essential identification data. Resolving purification issues will be crucial for enabling comprehensive characterization, thereby advancing the understanding of **IV.31** and its potential utility. Furthermore, quantum mechanical calculations revealed a non-aromatic behavior of **IV.31**, supported by the absence of diatropic ring current effects in the ^{1}H-NMR spectra and the NICS value. The ACID plot further corroborated the molecule's non-aromatic character, emphasizing the importance of comprehensive electronic structure analysis in elucidating aromaticity properties.

Experimental Section

Materials and Synthesis Methods:

Dichloromethane (CH_2Cl_2) was dried by refluxing and distillation over P_2O_5. Commercially available thiophene was freshly distilled before use. Other reagents and solvents were of commercial reagent grade and were used without further purification. Column chromatography was performed using basic alumina and silica in glass columns. ^{1}H-NMR spectra were recorded on a Bruker 400 MHz spectrometer, with chemical shifts reported on the delta scale in ppm relative to $CHCl_3$ (7.28) or CD_2Cl_2 (δ = 5.51). Electronic spectra were measured on a Perkin-Elmer λ-35 UV-Vis spectrophotometer and Shimadzu UV3600 UV/Vis/NIR spectrophotometer in an optical quartz cuvette with a 10 mm path length. High-resolution mass spectrometry (HRMS) was conducted using a WATERS G2 Synapt Mass Spectrometer. Single-crystal diffraction analysis data were collected at 100K with a BRUKER KAPPA APEX II CCD Duo diffractometer, operated at 1500 W power (50 kV, 30 mA), using graphite monochromatic Mo Kα radiation (λ = 0.71073 Å). In cases involving disordered solvent molecules,

contributions to the scattering arising from these disordered solvents in the crystal were removed using the utility SQUEEZE in the PLATON software package.

Quantum mechanical calculations were performed with the Gaussian09 rev D program suite using a High-Performance Computing Cluster facility of IISER PUNE. All calculations were carried out by Density functional theory (DFT) with Becke's three-parameter hybrid exchange functional and the Lee-Yang-Parr correlation functional (B3LYP) and 6-31G(d, p) basis set for all the atoms were employed in the calculations. The molecular structures obtained from single-crystal analysis were used to obtain the geometry-optimized structures. To simulate the steady-state absorption spectra, the time-dependent TD-DFT calculations were employed on the optimized structures. Molecular orbital contributions were determined using GaussSum 2.2.Program package. The global ring centers for the NICS (0) values were designated at the non-weighted mean centers of the macrocycles. The NICS (0) value was obtained with the gauge gauge-independent atomic orbital (GIAO) method based on the optimized geometries.

Synthesis Aromatic Expanded Porphyrinoid IV.12.

flame-dried 500-mL two neck round-bottomed flask was charged with 3,4-diphenylthiophene (1equiv.), and thiophene-2,5-diylbis((perfluorophenyl)methanol) (1.3equiv.), in 200 mL of anhydrous dichloromethane under nitrogen atmosphere and degassed with nitrogen for further ten minutes. $BF_3.OEt_2$ (0.37equiv.) was added in the dark using a syringe, and the resulting solution was stirred for one to two hours under an inert atmosphere. After adding $FeCl_3$ (approx. 5-6 mmol), the reaction mixture was opened to air and stirred for two more hours. A few drops of triethylamine were added and passed through a short pad of basic alumina. This mixture was concentrated and further purified by basic alumina column chromatography using CH_2Cl_2/Hexane as eluent. **IV.12** obtained in 10% yield as an orange-brown-colored band.

^{1}H NMR (400 MHz, Acetone-D_6), δ (ppm): 7.15 (s, 6H), 7.08 – 6.75 (m, 30H).

UV-Vis λmax (nm) (ε) $Lmol^{-1}cm^{-1}$ (in Toluene) 454(15200);

MALDI TOF/TOF mass spectra calculated for $C_{102}H_{36}F_{30}S_6$ is 2022.8963, found 2023.9531.

HR-MS (ESI-TOF): m/z=2022.8981(found $[M]^+$)(Calculated mass for $C_{102}H_{36}F_{30}S_6$ is 2022.8963).

Crystal data: $C_{102}H_{36}F_{30}S_6$, Triclinic, space group P1, a =9.160, b = 19.951, c = 19.977(3)Å, α = 117.562˚, β = 98.759˚, γ= 98.841˚. V = 3092.25Å^3, Z = 8, T=150(2) K, D_{calcd} = 1.449 g cm^{-3}, R_1 = 0.1203(6490), Rw (all data) = 0.2949(3388), GOF = 1.203.

Synthesis of 20π isophlorin IV.13.

In the same reaction for the synthesis of **IV.12,** we observed the presence of **IV.13** which was further purified by basic alumina column chromatography using CH_2Cl_2/Hexane as an eluent. **IV.1** obtained in 5% yield as an orange-colored band.

^{1}H NMR (400 MHz, DMSO-D_6), δ (ppm): 7.09-7.04 (m, 12H), 6.99 – 6.92 (m, 8H), 6.62(s, 4H).

UV-Vis λmax (nm) (ε) $Lmol^{-1}cm^{-1}$ (in MeOH); 433(24500) and 368(15800);

MALDI TOF/TOF mass spectra calculated for $C_{68}H_{24}F_{20}S_4$ is 1348.9541, found 1350.7054.

HR-MS (ESI-TOF): m/z=1349.9742(found $[M]^+H$)(Calculated mass for $C_{68}H_{24}F_{20}S_4$ is 1348.9541).

Crystal data: $C_{68}H_{24}F_{20}S_4$, Monoclinic, space group C *2c*, a = 22.310(4), b = 21.813(4), c = 28.840(3)Å, α = 90, β = 111.42, γ= 90. V = 13066(15)$Å^3$, Z = 8, T=150(2) K, D_{calcd} = 1.372 g cm^{-3}, R_1 = 0.1124(3727), Rw (all data) = 0.3919(15029), GOF = 0.955.

Synthesis of Ethylene Bridge Aromatic Expanded Porphyrinoid IV.31.

In a flame-dried 500-mL two-neck round-bottomed flask, 1,2-di(thiophen-2-yl)ethene (1 equiv.) and ((phenylmethylene)bis(thiophene-5,2-diyl))bis((perfluorophenyl)methanol) (1.3 equiv.) were dissolved in 200 mL of anhydrous dichloromethane under a nitrogen atmosphere and degassed with nitrogen for an additional ten minutes. $BF_3.OEt_2$ (0.37 equiv.) was cautiously added using a syringe in the absence of light, and the resulting solution was stirred for one to two hours under an inert atmosphere. After the addition of $FeCl_3$ (approximately 4.5 mmol), the reaction mixture was exposed to air and stirred for another two hours, and the mixture was passed through a short pad of basic alumina. The resulting mixture was concentrated and further purified via basic alumina as well as silica column chromatography, using CH_2Cl_2/Hexane as the eluent. Upon conducting column chromatography, we observed the presence of two distinct pink-colored bands that moved together throughout the chromatographic process. This phenomenon was evident and pronounced in the thin-layer chromatography (TLC), where two separate pink-colored spots appeared adjacently and were inseparable during the chromatographic separation. Despite our efforts, the chromatographic technique failed to resolve these two components, indicating their close similarity in polarity and/or composition. This observation raised intriguing questions about the nature of these components and their potential isomeric or diastereomeric relationship.

MALDI TOF/TOF mass spectra calculated for $C_{78}H_{30}F_{20}S_8$ is 1601.9794, found 1601.5125.

HR-MS (ESI-TOF): m/z=1601.9745 (found $[M]^+$)(Calculated mass for $C_{78}H_{30}F_{20}S_8$ is 1601.9794).

References

(1) V. J. Bauer, D. L. J. Clive. D.Dolphin, J. B. Paine, F. L. Harris, M. M. King, J. Loder, S. W. C. Wang, R. B. Woodward, *J. Am. Chem. Soc.* 1983, **105**, 6429-6436.

(2) J. L Sessler, M. J, Cyr, V Lynch, E. McGhee, J. A Ibers *J. Am. Chem. Soc.* 1990, **112**, 2810−2813

(3) S. W Young, F. Qing, A. Harriman, J. L Sessler, W. C Dow, T. D Mody, G. W Hemmi, Y. Hao, R. A Miller, *Proc. Natl. Acad. Sci. U. S. A.* 1996, **93**, 6610−6615.

(4) J. L Sessler, N. A Tvermoes, D. M. Guldi, T. D. Mody, W. E. Allen, *J. Phys. Chem.,* 1999, **103**, 787−794.

(5) J. L Sessler, R. A. Miller, *Biochem.Pharmacol.,* 2000, **59**, 733−739.

(6) J. L. Sessler, S. J. Weghorn, V. Lynch, M. R. Johnson, *Angew. Chem.*, 1994, **106**, 1572-1575; Angew. Chem. Int. Ed. 1994, 33, 1509-1512.

(7) J. L Sessler, D. Seidel., *Angew. Chem., Int. Ed.,* 2003, **42**, 5134−5175.

(8) J. Y. Shin, H. Furuta, K. Yoza, S. Igarashi, A Osuka, *J. Am. Chem. Soc.*, 2001, **123**, 7190−7191.

(9) A. Osuka. *Chem. Rev.* 2015, **15**, 143−159.

(10) S. Shimizu, A. Osuka *J. Porphyrins Phthalocyanines.,* 2004, **08**, 175−181.

(11) J. Sreedhar Reddy, and Venkataramanarao G. Anand, *J. Am. Chem. Soc.,* 2008,**130**, 3718-3719

(12) J. Sreedhar Reddy, and Venkataramanarao G. Anand, *J. Am. Chem. Soc.,* 2009, **131**(42), 15433-15439.

(13) a) E. Vogel, M. Broring, J. Fink, D. Rosen, H. Schmickler, J. Lex, K. W. K. Chan, Y.-D. Wu, D. A. Plattner, M. Nendel, K. N. Houk, *Angew. Chem.* 1995, **107**, 2705-2709; *Angew. Chem., Int. Ed.* 1995, **34**, 2511-2514; b) M. Broring, J. Jendrny, L. Zander, H. Schmickler, J. Lex, Y.-D. Wu, M. Nendel, J. Chen, D. A. Plattner, K. N. Houk, E. Vogel, *Angew. Chem.* 1995, **107,** 2709-2711; *Angew. Chem. Int. Ed.* 1995, **34**, 2515-2517.

(14) H. Rath, J. Sankar, V. PrabhuRaja, T. K. Chandrashekar, B. S. Joshi, R. Roy, *Chem. Commun.* 2005, 3343-3345

(15) N. Sprutta, L. Latos-Grazynski, *Chem. Eur. J.* 2001, **7,** 5099-5112.

(16) P. Gupta, V.G. Anand *J. Chem. Sci.* 2016, **128**(11)**,** 1703–1707

Summary of the Thesis

This thesis has explored the intricate world of "confused systems" in porphyrins, revealing the profound impact of structural modifications on the properties and applications of these macrocyclic compounds. The research journey began with foundational work on porphyrin isomers, which set the stage for investigating core-modified porphyrins, including carbaporphyrins and porphycenes, known for their unique electronic and photophysical behaviors. A key highlight of this research was the synthesis and detailed characterization of N-confused tetraphenylporphyrin, alongside the exploration of novel macrocyclic compounds such as SeC-DPDTPH. These studies provided valuable insights into macrocycle formation, aromaticity, and the effects of heteroatom incorporation on stability and coordination chemistry.

The synthesis of stable macrocyclic radicals, expanded porphyrins, and various other macrocyclic compounds with diverse electronic properties marked significant advancements. Among these, the creation of α-cyclo[n]thiophenes and novel methods for electronic modulation through protonation emerged as notable contributions. The research also ventured into the synthesis of Phenanthroline-embedded porphyrinoids, showcasing protonation-induced magnetization, thus paving the way for innovative molecular devices and switches. In particular, the study of expanded porphycenes composed entirely of confused heterocyclic units has pushed the boundaries of what is known about porphyrinoid chemistry. The demonstration of the lack of aromaticity in tetra S-confused porphyrinoids, attributed to cross-conjugation from the 2,4-connectivity of heterocyclic units, represents a groundbreaking finding. Quantum chemical calculations further solidified these observations, pointing towards a cross-conjugated π-network in the studied porphycene.

The exploration of Phenanthroline-embedded porphyrinoids added another layer of understanding, confirming weak antiaromaticity through analytical and computational methods. These findings underscore the intricate relationship between structural modifications and the electronic properties of macrocycles, offering pathways for the rational design of materials with tailored functionalities. Despite challenges in the synthesis and purification of certain targeted compounds, such as the Ethylene Bridged Aromatic Expanded Porphyrinoid (**IV.31**), the research has significantly advanced the understanding of these complex systems. The unexpected formation of non-aromatic species highlights the delicate interplay of reaction conditions and precursor reactivity in determining product outcomes. Looking ahead, this work opens up promising avenues for further exploration, particularly in the synthesis of hypothetical hyper-confused tetra-pyrrolic porphyrins and other novel

porphyrinoids with distinct electronic properties. The insights gained from this research not only enhance our understanding of porphycene chemistry but also hold the potential to drive innovations in materials science, catalysis, and molecular electronics.

In conclusion, this thesis represents a significant step forward in the study of porphyrinoids, expanding both the theoretical and practical knowledge of these fascinating macrocycles. The findings presented herein are expected to inspire continued research and development in the field, contributing to the broader scientific endeavor of designing advanced molecular systems with tailored properties for a wide range of applications.